THE FORMULATION AND EVALUATION OF ALTERNATIVE AUTOMATED REFUSE ACCUMULATION SYSTEMS

A THESIS

Presented to

The Faculty of the Division of Graduate

Studies and Research

By

William Edward Pugh, III

In Partial Fulfillment

of the Requirements for the Degree

Doctor of Philosophy

in the School of Mechanical Engineering

Georgia Institute of Technology

July, 1974

THE FORMULATION AND EVALUATION OF ALTERNATIVE AUTOMATED REFUSE ACCUMULATION SYSTEMS

Approved:

S. L. Dickerson, Chairman

R. B. Evans

J. C. Snyder

T. E. Stelson

G. J. Thuesen

W. M. Williams

Date approved by Chairman: 5/30/74

ACKNOWLEDGEMENTS

I would like to thank my thesis advisor, Dr. S. L. Dickerson, for the advice and guidance he provided throughout this work. The members of the reading committee, Drs. R. B. Evans, J. C. Snyder, T. E. Stelson, G. J. Thuesen and W. M. Williams provided useful suggestions in formulating the scope and nature of the investigation and in the preparation of the final draft.

Appreciation is also due to the National Aeronautics and Space Administration who supported this work with a Design Traineeship and to the Georgia Tech Engineering Experiment Station where the author was employed as a Research Assistant.

Finally, I would like to thank my wife for her help and understanding during the years of my graduate study.

TABLE OF CONTENTS

TABLE OF CONTENTS (Continued)

TABLE OF CONTENTS (Continued)

TABLE OF CONTENTS (Concluded)

LIST OF TABLES

LIST OF TABLES (Continued)

LIST OF ILLUSTRATIONS

LIST OF ILLUSTRATIONS (Continued)

LIST OF ILLUSTRATIONS (Continued)

LIST OF ILLUSTRATIONS (Concluded)

SUMMARY

The primary objective of this investigation was to evaluate the feasibility and expected performance of automated refuse collection vehicles capable of one-man operation. Significantly, it was not assumed that the pick up operation would be conducted with the vehicle at rest and the operator's strategy and physical limitations were included in the evaluation of expected performance. A second objective was to demonstrate, as a design methodology, a rational approach to alternative formulation for the various subsystems of the refuse accumulator (the device which conveys the refuse from the curb to the collection vehicle) beginning with subsystem definitions relating to functional requirements. Thirdly, it was sought to show the potential utility of state of the art technology in an area where little technical expertise has been employed.

Alternative subsystems were formulated from an investigation of the physical parameters of the system and its operating environment available to the designer to aid in performing the required functions. The kinematic portion of the accumulator mechanism was formulated by a systematic analysis of the applicable class of kinematic chains.

A mathematical model of the entire system was constructed from analyses of the road roughness disturbance to the collection vehicle, the vehicle dynamics, accumulator control system response and kinematic chain dynamics, and the control strategy and physical limitations of the human operator.

To assure realizability of the alternative formulated, a prototype accumulator linkage was designed and the dynamic characteristics of a commercially available refuse collection vehicle were determined. Roadway roughness statistics were based on experimental data and humanly possible operator responses were demonstrated.

The mathematical model was adapted to computer simulation and the stochastic nature of the model accommodated by the application of the concept of expectation to the random variables in the system response.

It was concluded that non-stop automated refuse collection is feasible at speeds up to one half mile per hour using conventional truck chassis without special ride augmentation systems. The man-machine interface most readily adaptable to automated refuse collection was determined to be a master-slave system and the most important feature of the grappling device was found to be its positional tolerance. The desirable dynamic characteristics of the kinematic chains were found to vary with the attainable rigidity of the alternative.

Automated refuse accumulators may be expected to reduce the total collection time required on the order of 50 percent of that of the most cost effective manual system. For this reason it is likely that the system will be economically superior to conventional collection systems. As the reduction in collection time is not entirely dependent on the ability of the device to operate with the vehicle in motion, the economic applicability of this system to urban as well as suburban areas is indicated.

CHAPTER I

INTRODUCTION

Motivation

In the United States and other industrial nations, development of the technology necessary to permit economical management of solid wastes in a manner which insures the protection of environmental quality is urgently needed. Richard D. Vaughan, Director of the Bureau of Solid Waste Management, reported in 1969 that approximately 800 million pounds of solid wastes were generated in the United States each day, that 4.5 billion dollars were spent annually for the collection and disposal of this material and that 75 percent of this cost was attributable to the collection process (1).

Most of the research being done in solid waste management is directed to the problem of disposal, while the more costly problem of collection has received little technical attention. A comparison of techniques used in the first quarter of this century with those of today reveals that very little change has occurred in basic concepts applied to the collection problem. (Compare references 2 and 3.) Over the same period, however, the per capita volumetric production of solid wastes has increased dramatically (4). This disparity between the growing magnitude of the collection problem and the slow development of new techniques to solve it has resulted in today's condition of high costs and poor service.

The current practice in solid waste collection relies heavily on human labor

with little mechanization to reduce the effort, unpleasantness and hazards associated with the task of manually lifting, transporting and dumping heavy containers of the obnoxious potentially pathogenic material (4). As a result, municipalities are finding it increasingly difficult to hire the large numbers of sanitation workers required to collect the wastes produced, and dissatisfaction among those workers that can be hired runs high, as is attested to by the frequent sanitation strikes which threaten public health and inconvenience urban populations. This dissatisfaction among refuse collection workers is not without cause. Not only is their task an unpleasant one of low prestige, but the injury frequency rate* for this group is the third highest among all industries for which data is maintained by the Bureau of Labor Statistics, exceeded only by lead-zinc mining and fire fighting, and is 326 percent of the average for all manufacturing trades. The injury severity** for this group is also high at 217 percent of the average for the manufacturing trades (5). At the same time, salaries paid collection workers are notoriously low.

The extremely high cost of collection (3.4 billion dollars in 1969, by Mr. Vaughan's figures) coupled with the relatively low technology which has been applied to this task at present, make the probability for substantial savings from the wise application of modern technology to solid waste collection quite high. The high injury frequency and severity rates among collection workers also indicate the need for improvements in collection technology.

---

*The injury frequency rate is the number of disabling work injuries per million employee-hours of exposure (5).

**The injury severity rate is the number of days of disability resulting from disabling work injuries per million employee-hours of exposure (5).

Review of Current Efforts in Solid Waste Collection

The current research effort in solid waste collection may be broadly classified as being directed either to improved administrative methods or to new collection technology. Most of the formal research applied to refuse collection has been of the former class: directed to improving routing methods, developing preventive maintenance scheduling and employee incentive programs, determining optimum crew size and so on (6). The rather large amount of information available in this area is in part due to the great similarity between refuse collection and other industrial management problems. For example, the collection problem is the inverse of the traveling salesman and postman problems since collection can be thought of as inverse distribution (7). Of course, maintenance scheduling has been studied extensively for application to industry and the techniques developed there are being applied to refuse collection. The effects of crew size and truck capacity on collection costs have been investigated. Of particular interest is the work of Stone (8), who found the most economical crew size for curbside pick-up to be a single driver-loader. While most of the work which has been done was based on systems incorporating conventional collection equipment, the results could be readily applied to systems using more innovative technology.

The development of new collection technology has progressed in a far less formal manner. Proposals for "futuristic" water-born or pneumatic collection systems have been advanced. These systems of course would require extensive modification to existing pavements and structures for installation and for this reason have not been well received as solutions to current collection problems.

Research has also been carried out to determine the feasibility of mechanical refuse pick-up. Through Demonstration Grants funded by the United States Department of Health, Education and Welfare a few prototype mechanical collection units have been produced and tested (9) and the characteristics of these units are summarized in Appendix I. Gulf Oil Corporation, in an effort to make their line of disposable plastic containers more attractive to municipalities, developed a machine called the MBR, or Mechanical Bag Retriever, which is a one-man-crew, semi-automated collection unit (10), and American Can has built a "Litter Gulper" designed to rake litter from roadways. Such developments are certainly potentially useful both in reducing solid waste collection costs and in avoiding injuries among sanitation workers.

Objectives

One objective of this investigation was to evaluate the feasibility and expected performance of automated refuse collection vehicles capable of one-man operation. Significantly, it was not assumed that the pick-up operation would be conducted with the vehicle at rest, and the characteristics of the operator's strategy and physical limitations were included in the evaluation of expected performance. A second objective was to demonstrate, as a design methodology, a rational approach to alternative formulation for the various subsystems of the refuse accumulator, beginning with subsystem definitions relating to functional requirements. Thirdly, it was sought to show the potential utility of state-of-the-art technology in an area where little technical expertise has been employed.

CHAPTER II

PRELIMINARY DESIGN CONSIDERATIONS

Functional Description of a Refuse Accumulator

The term "refuse accumulator" has been coined to describe a device which in some way moves refuse from its pick up point to the collection vehicle and, if necessary, returns the container. A functional description of the device and its relationship to the collection function in a solid waste management system is shown within the darkened blocks in Figure 1. The refuse accumulator must move into position near the refuse pick up point (locate) and bring the refuse container into its possession (capture). These two operations complete the "secure container" function of the device. The "convey" function is shown in the Figure to have two subfunctions, "support" and "guide." These functions require that the device be capable of exerting the forces necessary to convey the refuse container to the vehicle (support) along a controlled path (guide). At this point the refuse must be transferred from the accumulator to the storage body of the collection vehicle. This is accomplished by freeing the refuse from the confines of its container (free) and depositing it into the vehicle (deposit). Where non-disposable refuse containers are used, the accumulator must also have the capability of returning the container to the pick up point (replace). The mechanical capabilities required in the performance of this last function are inherent in devices which meet the other functional requirements of the system.

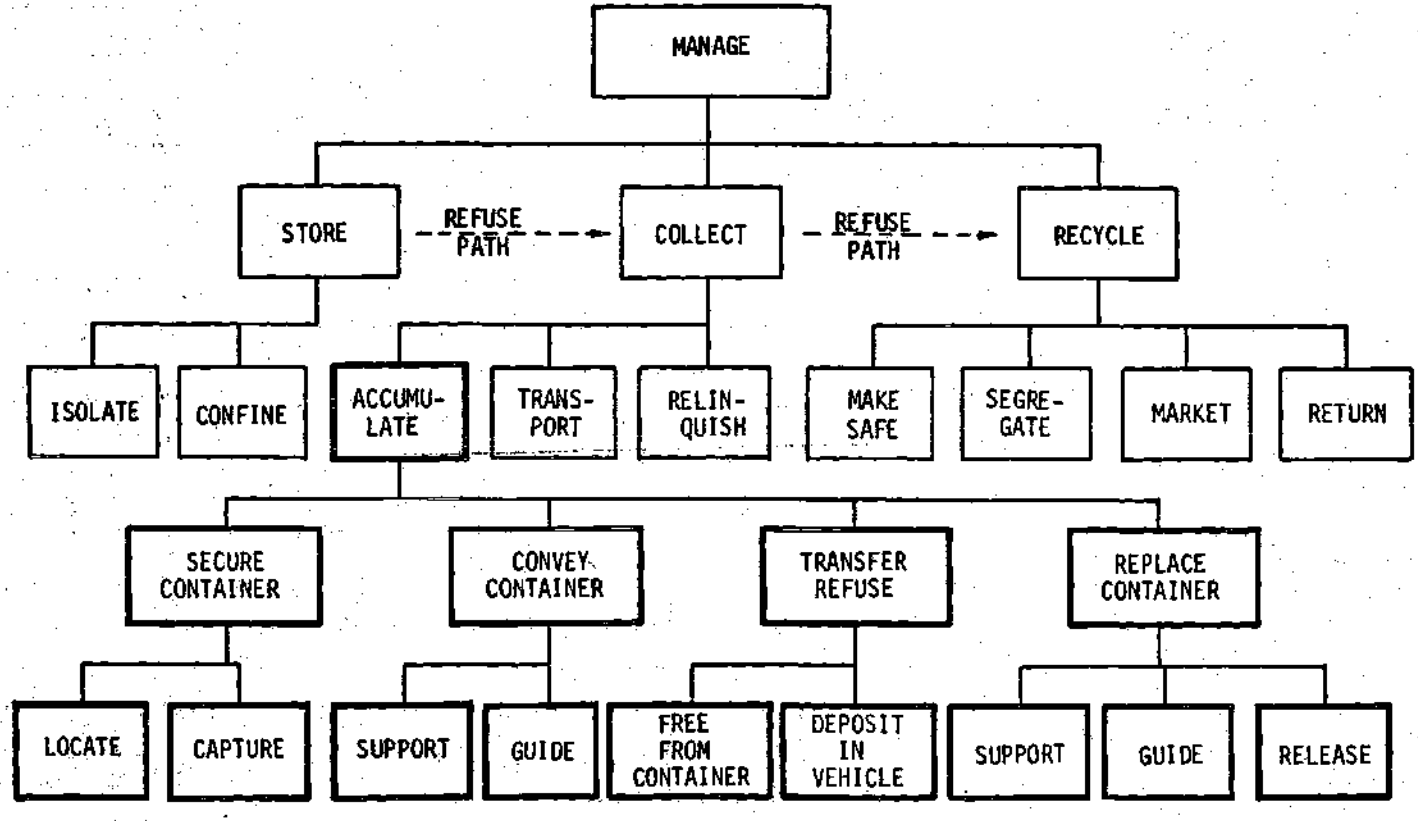

Figure 1. Functional Description of Refuse Accumulation

The Operating Environment

The design of a refuse accumulator which fulfills these functional requirements is influenced by the parameters of its operating environment enumerated in Table 1.

The influence of each parameter in Table 1 on the accumulator design must be analyzed. Storage alternatives must be selected with due regard to their principal functions (isolation and confinement) and cost. Additionally, the appearance of the devices becomes important when large numbers of them are exposed to public view over extended periods, as is the case when the curb side pick up alternative is selected. Experience has shown that the use of containers which chemically and biologically isolate waste from the environment, physically confine it for ready collection, and present a reasonably acceptable appearance, can only be insured when standardized containers are required. The use of functional containers is most important to public health, a fact amply substantiated in references 11 and 12. For these reasons, it was initially assumed that the accumulator alternatives should be compatible with rigid and/or flexible standardized containers. (Compatibility with some non-standard containers resulted from this approach, but compatibility with non-standard containers was not a design objective.)

The pick-up point alternative has a great influence on the basic nature of compatible accumulator designs. The most important characteristics of the pick up point location are its visibility and distance from the path of possible transportation alternatives. For small distances, as is the case for curb side pick up, a mechanical linkage may be used to satisfy the "convey" function of the accumulator.

Table 1. Environmental Parameters Which Affect Accumulator Design

• Storage Alternative
• Pick Up Point Alternative
• Transportation Alternative
• Collection Area Characteristics
refuse bulk density
refuse generation rate
topography
roadway specifications
vertical clearance
traffic conditions
obstacles
distance between pick up points
• Recycling Alternative

The problem of "locating" the refuse container and "capturing" it may be left to the collection device operator. For intermediate distances, corresponding to pick up points at the sides of buildings or other distant places in view of the operator, the "convey" function may require a remote intermediate vehicle. Again the "location" and "capture" of the refuse may be accomplished by the operator of the collection device, possibly through an electromagnetic link. For large

distances and zero visibility, corresponding to back yard pick up, an intermediate vehicle would be required to fill the "convey" function and the "locate" and "capture" functions as well. Such a device would be quite sophisticated and might be considered a third generation accumulation alternative. Since the requirements for accumulators compatible with each of the three classes of pick up points are very different, the formulation of alternative accumulators compatible with each pick up point class is a distinctly different problem.

The requirement that the collection system be compatible with existing urban design restricts the transportation alternatives to land vehicles of rather conventional characteristics. Questions of vehicle capacity, power source and compaction or processing capability have little bearing on accumulator design. The vehicle must meet statutory weight and dimension requirements, it must be compatible with the roadway, topography, vertical clearance and traffic conditions of the collection area, and it must be capable of providing energy requirements to the accumulation device. Compatible accumulator alternatives of course occupy as little of the gross vehicle weight and allowable volume as possible, must be capable of conveying refuse to a loading point on the vehicle, and have energy requirements suitable to mobile operation. The accumulator must also be capable of assuming a position which allows safe operation of the vehicle between the collection area and the recycling point.

Collection area characteristics are also important to the accumulator design. The refuse bulk density and generation rate influence the power requirements of the accumulator, the load capacity of the conveyance alternatives, and

the volume requirements for the "capture" function. The topographic, roadway, and vertical clearance characteristics of the collection area influence the possible location of pick up points relative to the transportation vehicle. Special traffic conditions may place additional requirements on the accumulation device. High traffic flow rates might limit an accumulator otherwise capable of functioning equally well from both sides of the transportation vehicle to operation along the right curb, and one way streets in a collection area could make accumulation capability from the left curb mandatory. In most collection areas a high degree of obstacle avoidance capability would be a desirable feature for refuse accumulation mechanisms.

The recycle alternative which would influence the accumulator design considerations is salvage and marketing which includes some on site segregation. Since this practice is not common at present, the thesis investigation was limited to accumulation alternatives for mixed collection, noting that the accumulators so designed would be adaptable to segregated collection if the storage and transportation equipment were properly modified.

Some additional assumptions which limit the scope of the investigation were necessary to facilitate incremental improvement in the existing system of refuse collection for suburban residential areas. First it was decided to investigate only systems designed for curb side pick up. More specifically, admissible pick up points were assumed to be visible from the collection vehicle and within the range of a direct mechanical linkage to it. This mode of refuse collection service is by far the most prevalent nation wide.

The storage alternative which is most readily adaptable to automated collection is the disposable standardized container in the form of a plastic or heavy paper bag. The most significant characteristic of systems incorporating disposable containers is the elimination of the necessity to return containers to the curb after pick up is made, with the attendant reduction in pick up cycle time. The use of standardized disposable containers was therefore assumed.

In the next chapter the subsystems required to execute the functions of a refuse accumulator are identified and alternative design solutions formulated.

CHAPTER III

ALTERNATIVE DESIGN FORMULATION

Subsystem Identification

The functional description of the refuse accumulator as shown in Figure 1 leads to the definition of three subsystems shown schematically in Figure 2. The capture subsystem is that portion of the mechanism which accomplishes the task of bringing the refuse and storage unit within the physical control of the refuse accumulator. The convey subsystem is that portion of the mechanism which applies the forces necessary to "support" and "guide" the refuse under the direction of the operator. Finally, the control subsystem, of which the human operator is an integral part, directs the mechanism along a path and facilitates the performance of the "locate," "guide," "transfer," and if necessary "replace" functions of the refuse accumulator. Also shown in Figure 2 are the storage and transportation systems, important to the accumulator's operation as they directly interface with it. A particular refuse accumulator alternative is defined when specific alternative capture, convey, and control subsystems are coupled.

Capture Subsystem Formulation

The capture function must be performed by taking advantage of the physical characteristics of the refuse container unit and its environment. Those characteristics which might be useful in performing this task are listed in Table 2.

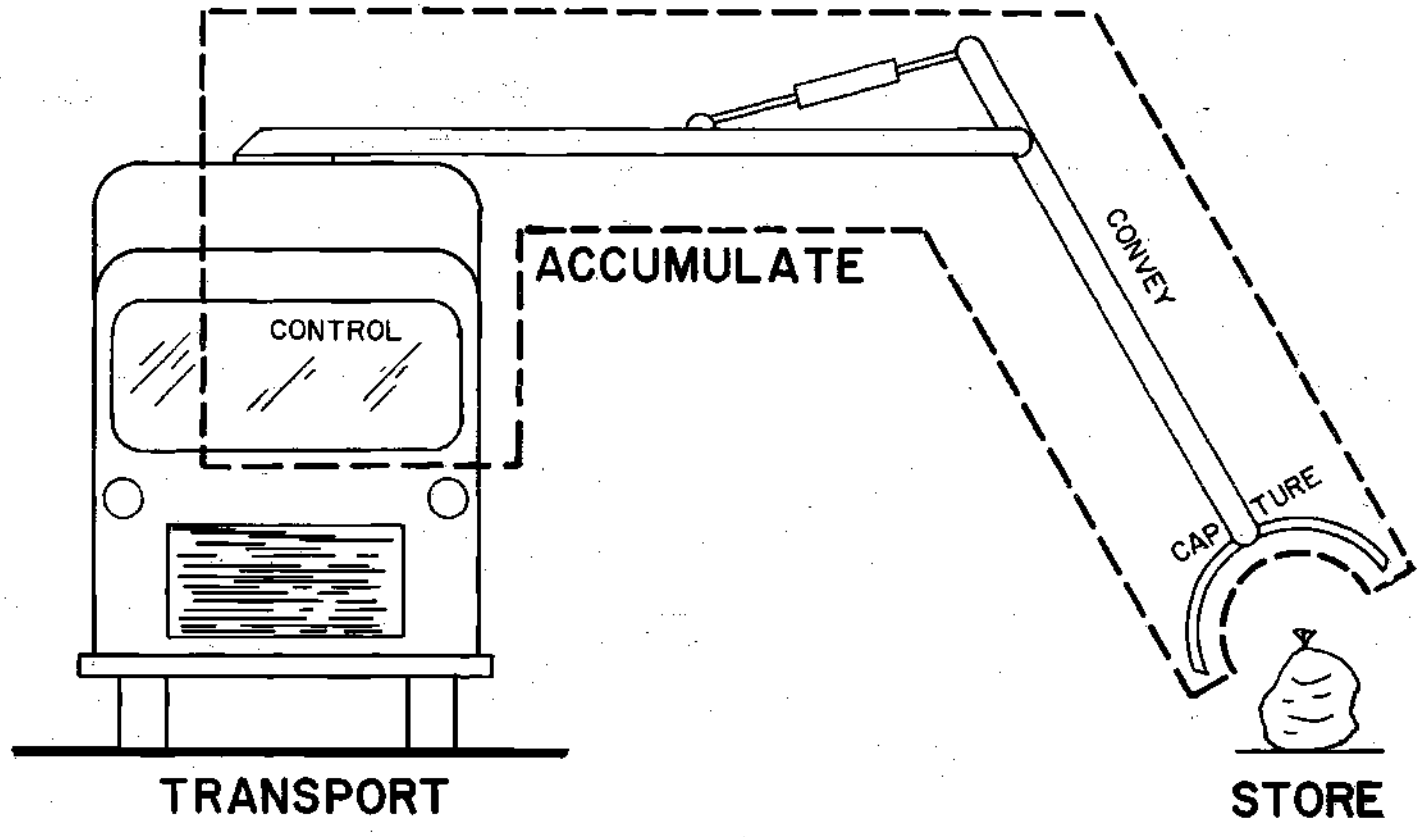

Figure 2. Schematic of Refuse Accumulator and Subsystems

Table 2. Physical Characteristics Potentially Useful in Performing the Capture Function

• Refuse Container Unit	
	Mass
	Flexibility/Rigidity
	Compressive Strength
	Magnetic Permeability
• Environment	
	Surrounding Fluid (air)
	Gravitational Field
	Friction

The alternative "capture" mechanisms formulated and the refuse environment characteristics employed by each are given in Table 3. The engage mechanism differs from the grasp mechanism in that it requires a coupling attached to a standardized container for operation while the grasp mechanism does not.

The vacuum mechanism has potential benefits unique among the capture alternatives but it also has the potential for unique environmental hazards. Among the benefits could be the ability to sweep up refuse scattered by spillage and to perform auxiliary functions such as street cleaning and leaf collection. The potential hazards associated with this capture mechanism include the emission of pathogens and foul odor where raw refuse is exposed to the air flow (and hence wherever

Table 3. Capture Mechanisms and Employed Physical Characteristics

• Vacuum	
	Surrounding fluid
• Scoop	
	Mass
	Gravitational field
	Friction
• Grasp	
	Mass
	Gravitational field
	Friction
	Compressive strength
	Flexibility/rigidity
	Magnetic permeability
• Engage	
	Mass
	Gravitational field
	Friction
	Rigidity

damaged refuse containers may be encountered) and the considerable noise associated with blowers of high volumetric capacity. Solutions to these problems, such as filtering, disinfecting and muffling the blower exhaust would have to be found if the vacuum mechanism were employed.

Convey Subsystem Formulation

The types of convey subsystems which may be formulated can be classified as those which are batch operated and those which operate continuously. By batch operation it is meant that the collection vehicle moves from pick up point to pick up point, stopping at each for the accumulator to function. In the continuous operation alternatives it would not be necessary for the vehicle to stop to allow accumulation to take place.

While these two classes of alternatives may appear to be very different, they must rely on basic mechanical chains for their operation. The functions of guiding these units to the refuse pick up point and of conveying refuse to the truck can be characterized by the need to control some finite number of degrees of freedom of the system, usually three.

Reuleaux (13) defined six basic kinematic pairs, enumerated in Table 4, which describe the simplest types of relative motion possible between two bodies in a kinematic chain. Also shown in the table are the kinematic symbols associated with Reuleaux's pairs and the number of degrees of freedom allowed by each.

Alternative convey mechanisms can be formulated as open kinematic chains by the following procedure. First for any alternative capture mechanism and batch/continuous convey classification, the number of degrees of freedom, N, up to three, required for the convey subsystem must be determined and a decision made as to whether the device should be a planar or spatial chain. The chains available with N degrees of freedom can then be generated in a formal manner:

1. Let a chain be defined by a series of kinematic pair symbols, progressing

Table 4. Reuleaux's Simple Kinematic Pairs

Pair Name	Symbol	Sketch	Freedoms
Revolute	R	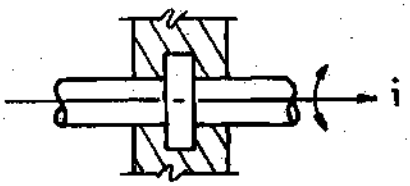	1
Prismatic	P	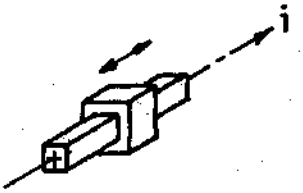	1
Screw	S	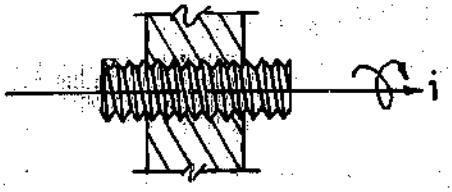	1
Cylindric	C	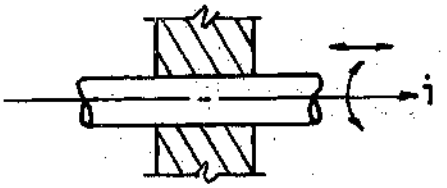	2
Flat	F	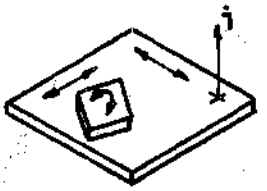	3
Sphere	G (Global)	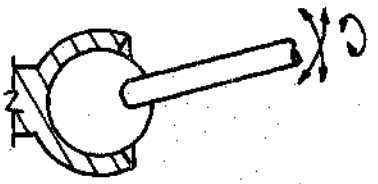	3

left to right from the ground (mounting) pair to the last link and let subscript $i = 1, 2, 3$ indicate pair axes, as shown in Table 4, where $\bar{1}\,\bar{2}\,\bar{3}$ form the right hand orthogonal set shown in Figure 3. (For each succeeding pair beyond the ground pair, these axes would be fixed in the link closest to ground.)

2. Eliminate from Table 4 pairs with motions not useful in the application, in particular the screw, flat and global pairs.

3. Enumerate all possible pair groups of remaining pairs whose freedom sum to N, the number of degrees of freedom desired. For example, $R_i R_i R_i$, $R_i P_i P_i$ and $C_i P_i$ are three degree of freedom chains.

4. For $i = 1, 2, 3$ find all possible subscript and position permutations for each combination of pairs, with the exception of the ground link, where only R_1 or P_1 need be considered. Resulting chains may be located in any orientation in the vehicle.

5. Examine resulting chains and eliminate those which are or are not planar, depending on design requirements, and those with redundant prismatic pairs (two successive prismatic pairs along the same axis).

From this list of potentially useful kinematic chains,* alternatives for the convey subsystem must be selected using such additional criteria as the ability of the chain to assume a safe traveling position, to convey refuse to a loading

---

*It should perhaps be pointed out that chains including cylindric (C) pairs can be formed from prismatic (P) and revolute (R) pairs, since $C_i = P_i R_i$ kinematically. Thus the set of chains including cylindric pairs is a subset of the set containing revolute and prismatic pairs.

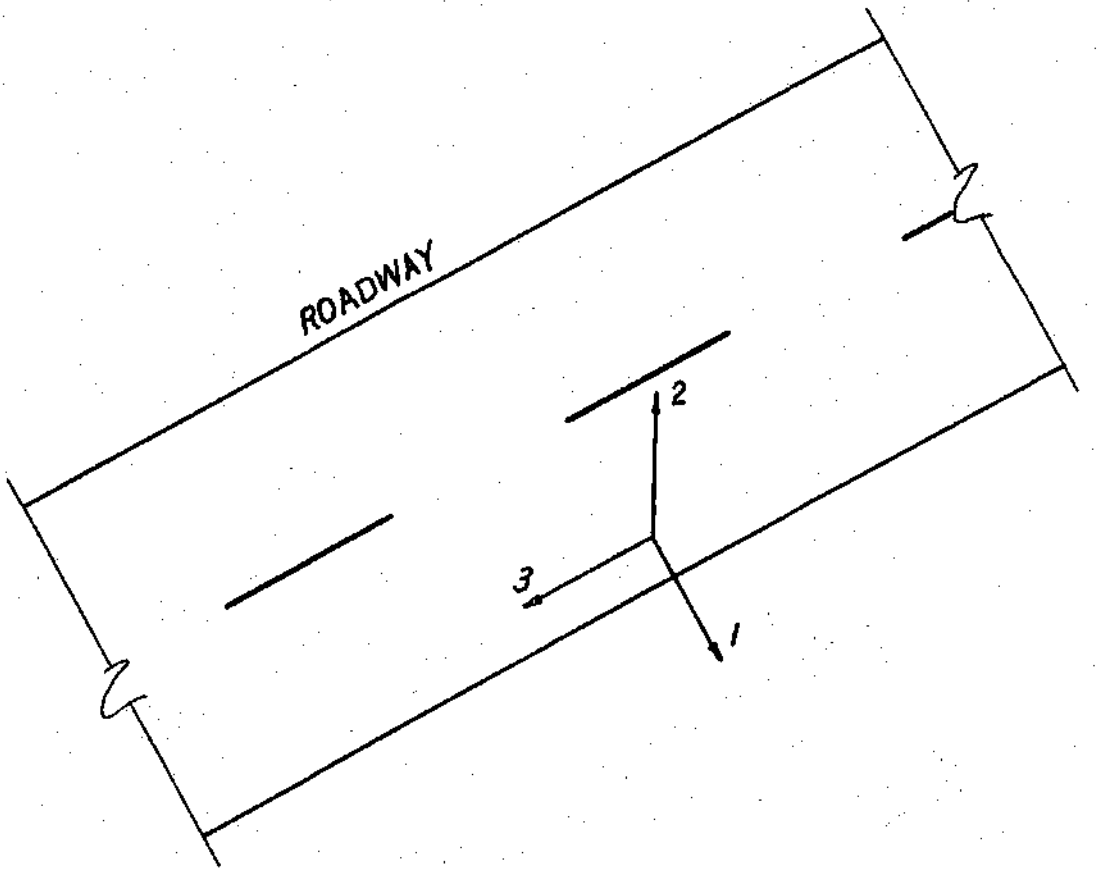

Figure 3. Orientation of Ground Coordinates

point on the vehicle, and to avoid collection area obstacles.

There may be some advantage in considering redundant freedom chains (those with more freedoms than absolutely necessary to reach required points in space) because of their greater obstacle avoidance capability. This option further complicates the design situation; however, and it is felt that redundancies should be left as a second generation design problem, after basic questions of system feasibility have been answered. Also, the capability of the collection vehicle to move along the roadway adds one additional degree of freedom to the system and therefore provides an obstacle avoidance capability.

The result of this kinematic chain generation procedure is given in detail in Appendix II for N=3 (three degree of freedom chains). Consideration of adaptability to the refuse accumulation task of each chain so generated resulted in the selection of five alternatives which, in the author's view, have the greatest likelihood of successful implementation. These convey chains are derived from only three kinematic solutions, the two additional alternatives being the result of contracting one of the link lengths to zero. Table 5 enumerates these most likely convey subsystem alternatives in order of expected desirability.

The Control Subsystem

The detailed design of a control system to convert operator inputs to refuse accumulator response is a straight forward process when the mechanical details of the accumulator and the man-machine interface are known. For low inertia manipulators of the type being considered for this application, it is not at all unreasonable to require that the limiting factors on the system frequency response

Table 5. Primary Convey Subsystem Alternatives

Chain	Modification	Sketch	Alternative Designation
$R_1R_2P_3$	rotated 90°	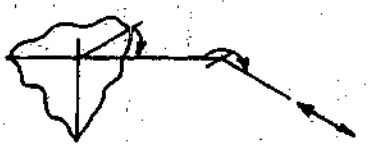	1
$R_1R_2P_3$	rotated 90° first link contracted	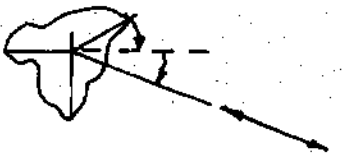	2
$R_1P_3R_2$	rotated 90°	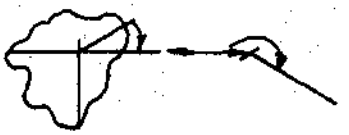	3
$R_1R_2R_2$	rotated 90°	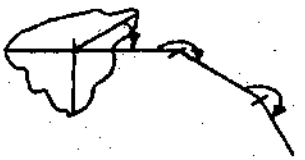	4
$R_1R_2R_2$	rotated 90° first link contracted	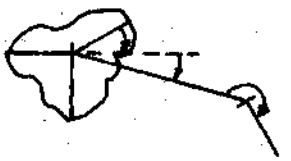	5

be the inherent characteristics of the human operator. This point receives further attention in Chapter IV.

The man-machine interface is important in achieving the best performance

possible from the accumulator and operator. The least sophisticated interface would be one in which a single lever controlled the position or rate of a single actuator in the refuse accumulator mechanism. A great deal of operator skill would be required to relate the desired motion of the accumulator to such inputs. A second and more desirable man-machine interface alternative would be a "joy-stick," similar to that used in small airplanes. In these systems motion of the accumulator would be related to motion of the joy stick in an intuitively acceptable manner. For instance, rocking the joy stick forward might cause the accumulator to move in a path parallel to the centerline of the refuse vehicle and toward the front.

Both of these man-machine interfaces have been employed in the design of manipulators for various purposes, among them an underseas electrohydraulic unilateral manipulator built by General Dynamics which uses single switches to control each actuator and another designed for use in the Deep Sea Rescue Vehicle (DSRV-1) which incorporates a "joy-stick" control interface (14).

A further improvement in the man-machine interface and the system chosen for investigation here is the slave-master system. With this system the operator moves a model of the accumulator mounted in the cab in the manner in which he desires the full scale accumulator to move. Kinematic relationships between tip position and joint rotations or extensions are automatically "computed" by the scale model and appropriate signals transmitted to the full scale system actuators. Of the interfaces discussed so far, this system requires the operator to devote the least attention to the task of translating desired motions into control inputs,

and therefore has the highest likelihood of success in non-stop accumulation operations.

Master-slave systems are not unusual and are often used in nuclear research facilities to handle radioactive materials (15). In this application the scale factor between the master and slave is often one with input signals transmitted to the slave through direct mechanical linkages.

A final degree of sophistication in the man-machine interface, most applicable to the control of anthropomorphic manipulators, is the exoskeleton. This device serves essentially to instrument a human being so that he becomes the master portion of a master-slave manipulator. Applications of these devices have been made to such diverse control problems as an arm prosthesis for amputees and a high mobility walking truck for the military (15). The exoskeletal control system is incompatible with automated refuse accumulators primarily because the operator directs his attention to the control of the accumulator only during short periods.

Other interesting applications of man-machine systems are surveyed in a very readible manner in references 14 and 15.

Major Considerations Affecting Feasibility and Performance

In this section we explore the question of which design decisions have the greatest effect on the feasibility and performance of the refuse accumulator. Once identified these design alternatives must be investigated and the questions regarding them answered before other less significant design details are given consideration. The investigation of the most significant design alternatives was

the primary object of this thesis.

One primary design consideration is selection of the dynamic characteristics of the convey subsystem. Indeed, with the exception of obstacle avoidance capability and ease of loading refuse into the vehicle, all of the kinematic chains would perform equally well if they had the same dynamic characteristics, i.e. mass, stiffness and damping ratio. A major concern then is the determination of the best combination of realizable kinematic chain stiffness, mass and damping ratio. Once these are determined, the detailed design of a specific kinematic chain with specified realizable dynamic characteristics is time consuming but not technically difficult.

Another major design alternative, especially important to the performance of non-stop refuse accumulators and also concerned with the dynamics of the mechanical system, is whether or not to equip the collection vehicle with an automated ride augmentation system. Such a system could free the operator from concern with normal road induced oscillations of the accumulator and might be a necessity, especially in areas where unpaved alleys are used for refuse collection.

Regarding capture subsystem alternatives, the most significant parameter is the error radius from the refuse container to the accumulator which can be tolerated by the alternative while maintaining a high probability for successful capture.

Other important considerations which place constraints on system performance are the dynamic response and strategy generating capabilities of the human operator.

In succeeding chapters the mathematical analysis necessary to study these questions is carried out and answers to them formulated from the analytical results.

CHAPTER IV

DYNAMIC MODELING OF THE MECHANICAL SYSTEM

Introduction

The feasibility of performing the refuse accumulation operation while in motion is heavily dependent on the dynamics of the kinematic chain, the vehicle suspension, and the signals transmitted to the accumulator through the vehicle in the form of road noise. Complete understanding of the system performance and of the task required of the operator can only be achieved if realistic information is available beginning with the road profile.

The approach that was used in this analysis was first to determine the equation of typical road roughness power spectra from readily available data, then the spectral equation was modified to reflect filtering effect of the tire patch and the resulting spatial power spectrum converted to a temporal spectrum reflecting the effect of vehicle speed on signal frequency. The temporal spectrum was filtered by the vehicle tire stiffness and unsprung mass and a resulting road noise power spectrum derived which is applied to the springs and dampers of the vehicle at the axles. For practical considerations in the analysis, a filter was designed which subject to a gaussian white noise input produces an output with the power spectrum of the road noise at the axle.

The vehicle dynamics were then investigated assuming a model with non-uniformly distributed mass mounted on springs and parallel dampers at four

suspension points and disturbed by an independent road noise at each wheel at the axle. The resulting vehicle motions are used as disturbance inputs to the refuse accumulator. (It was assumed that motion of the low inertia manipulator did not affect the vehicle dynamics, however. This assumption is investigated further in Appendix III.)

The refuse accumulator was modeled in a rather general manner to a degree of detail consistent with the objectives of the analysis and the dimensionality constraints on the numerical solution. The idealized model consists of an amorphus body with complex internal force versus displacement and displacement rate relationships. Specific alternative kinematic chains were then analyzed and the force-displacement and force-displacement rate relationships in each reformulated in a manner compatible with the more general kinematic chain dynamic model. This approach permitted the use of only one mathematic model for all of the kinematic configurations considered.

Finally, an analysis was made of the master-slave interface dynamics. The resulting complete model is the "plant" which the human operator is called on to control. His dynamics and control strategy are discussed in Chapter V.

Road Noise

In order to facilitate analysis of the system, it is necessary that all noise inputs to the plant are white gaussian and of zero mean. This requirement can be met if a shaping filter is incorporated in the plant equations which produces correctly colored noise from white noise input. The first step in the design of such a filter is the determination of the power spectrum of the colored output.

Statistical roadway roughness measurements have been made by the Michigan Department of State Highways using the "Rapid Travel Profilometer" developed by the General Motors Corporation. The profilometer, described in detail by Darlington (16), consists of an instrumented vehicle which records the roadway profile accurately over wavelengths from 3 inches to 1200 feet. This raw data is then digitized for analysis in the laboratory. Holbrook (17) reported power spectra for sixteen road profiles which had been modified to remove elevation changes. Tests for stationarity, randomness, and normalcy of amplitude distribution were performed on each test section. It was concluded (18) that the profiles were random, stationary, normally distributed and lost power at 20 decibles per decade from 100 to 4 foot waves.

Power spectra are even, real, positive functions of frequency (19). Such a function which loses power at 20 db per decade is

$$S(\underline{\omega}) = \frac{\hat{K}}{1+\lambda_1^2 \underline{\omega}^2} \tag{1}$$

where λ_1 is the wavelength at which the asymptote to the power spectrum drops at 20 db/decade. For the conditions typical of roadway profiles, $\lambda_1 = 100$ ft. The spectra reported in (17) were examined and the power at $\lambda = 10$ ft. averaged for the 16 profiles. The result was that at $\lambda = 10$, ($\underline{\omega} = 0.1$) the average profile power was 8.6×10^{-4} ft^2/cycle/ft. Substitution of these values into equation 1 yields a value for $\hat{K}$ of 0.08686.

Since the vehicle model does not include the tire parameters or suspension

mass, the road noise input must be modified to reflect the high frequency damping effect these elements have on the signal before it reaches the vehicle suspension. The tire will envelop profile components of very short wavelength. Reference 20 reports successful simulation of this tire enveloping effect by the use of two cascaded first order lag circuits where the corner frequency was set to correspond to λ_2 = 10 inch wavelengths, the longest waves enveloped by the tire patch.

If the linear transfer function $H(j\underline{\omega})$ of a system is known, the power spectrum of the system output $S_{yy}(\omega)$ is related to the power spectrum of the system input $S_{xx}(\underline{\omega})$ by (19)

$$S_{yy}(\underline{\omega}) = S_{xx}(\underline{\omega}) \left| H(j\underline{\omega}) \right|^2 \tag{2}$$

The tire enveloping function previously described has

$$H(j\underline{\omega}) = \frac{1}{(1+j\underline{\omega}\lambda_2)^2} \tag{3}$$

so that

$$\left|H(j\underline{\omega})\right| = \frac{1}{1+\underline{\omega}^2\lambda_2^2} \tag{4}$$

and

$$S_{yy}(\omega) = \left(\frac{\hat{K}}{1+\lambda_1^2\underline{\omega}^2}\right)\left(\frac{1}{1+\lambda_2^2\underline{\omega}^2}\right)^2 \tag{5}$$

So far it has been totally accurate to discuss the road profile in spatial coordinates. We now must differentiate between the road profile as a random

variable in space and the road noise transmitted to the vehicle as a random variable in time. The frequency of this noise is related to the frequency of the road profile (cycles/ft) and the vehicle speed along the road by

$$\omega \text{ rad/sec} = \left(\underline{\omega} \frac{\text{cycles}}{\text{ft}}\right)\left(\frac{2\pi \text{rad}}{\text{cycle}}\right)\left(\frac{5280 \text{ ft}}{\text{mile}}\right) r \left(\frac{\text{miles}}{\text{hour}}\right)\left(\frac{1 \text{ hour}}{3600 \text{ sec}}\right) \tag{6}$$

or

$$\omega = 2.933\, \pi\, r\, \underline{\omega} = 9.215\, r\, \underline{\omega}$$

As it is assumed that the vehicle speed r remains constant during the pick-up operation, this introduces no new difficulty.

The road noise power spectrum becomes

$$S_{yy}(\omega) = \frac{\hat{K}}{\left(1 + \frac{a^2}{r^2}\omega^2\right)\left(1 + \frac{b^2}{r^2}\omega^2\right)^2} \tag{7}$$

where

$$a^2 = \frac{\lambda_1^2}{(2.933\pi)^2} = 117.8$$

$$b^2 = \frac{\lambda_2^2}{(2.933\pi)^2} = 0.00818$$

To investigate the filtering effect of the suspension mass and tire spring constant, the vehicle body is fixed and the system shown in Figure 4 is examined.

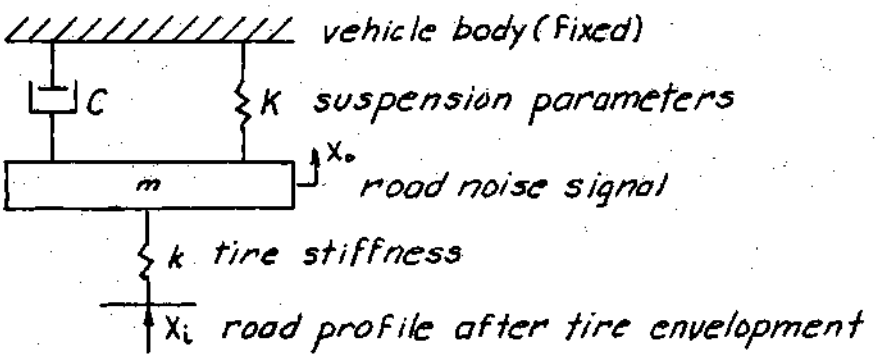

Figure 4. Suspension Unsprung Mass

The equation of motion for this system is

$$\ddot{X}_o + \frac{C}{m}\dot{X}_o + \frac{K+k}{m}X_o = \frac{k}{m}X_i \tag{8}$$

and its Laplace transform yields

$$\frac{X_o(s)}{X_i(s)} = \frac{k/m}{s^2 + \frac{C}{m}s + \frac{K+k}{m}} = H(s) \tag{9}$$

Applying equation 2 to find the power spectrum of the road noise X_o,

$$H(j\omega) = \frac{k/m}{\left(-\omega^2 + \frac{K+k}{m}\right) + \frac{C}{m}j\omega} \tag{10}$$

$$|H(j\omega)| = \frac{k/m}{\sqrt{\frac{C^2}{m^2}\omega^2 + \left(\frac{K+k}{m} - \omega^2\right)^2}} \tag{11}$$

and

$$S_{X_o X_o}(\omega) = \frac{\hat{K}}{\left(1 + \frac{a^2}{r^2}\omega^2\right)\left(1 + \frac{b^2}{r^2}\omega^2\right)^2} \frac{(k/m)^2}{\left\{\omega^4 + \left[\frac{C^2}{m^2} - 2\left(\frac{K+k}{m}\right)\right]\omega^2 + \left(\frac{K+k}{m}\right)^2\right\}} \tag{12}$$

This last term imposes additional second order filtration with a corner frequency of

$$\omega_c = \sqrt{\frac{K+k}{m}} \text{ radians/second} \tag{13}$$

For values of K, k, and m which occur in trucks of the capacity required for refuse collection, this corner frequency is about 99 radians/second, Table 6, while the modal natural frequencies of the system are on the order of 1 to 3 radians per second, or about two frequency decades lower. Therefore it is possible to approximate this last term by its value at $\omega = 0$ for all ω without great compromise in accuracy. This is highly desirable since such a term would require the definition of two additional state variables in the road noise filter for each of the four wheels. With this approximation the power spectrum becomes

$$S_{nn}(\omega) = \frac{\hat{K}\left(\frac{K}{K+k}\right)^2}{\left(1 + \frac{a^2}{r^2}\omega^2\right)\left(1 + \frac{b^2}{r^2}\omega^2\right)^2} \tag{14}$$

Table 6. Comparison of Corner Frequency for Road Noise Attenuation Due to Unsprung Mass with Sprung Mass Resonant Frequencies

Empty Vehicle:

Corner Frequencies:

	K+k	m	$\sqrt{\frac{K+k}{m}}$ rad/sec	$\sqrt{\frac{K+k}{m}}$ cy/sec	Average
Front	(750+4770)(12)	$\frac{15.73}{2}$	91.77	14.61	15.21
Rear	(1714+9540)(12)	$\frac{27.41}{2}$	99.27	15.80	

Resonant Frequencies:

	K	I, m	ω_n rad/sec	ω_n cy/sec
Pitch	12[(115.27)(750)+(34.58)(1714)]	19300	9.52	1.99
Roll	(12)(30)(1714+750)	5349	12.88	2.05
Heave	(2)(1714+750)(12)	380	12.47	1.51

Table 6 (Continued). Comparison of Corner Frequency for Road Noise Attenuation Due to Unsprung Mass with Sprung Mass Resonant Frequencies

Filled Vehicle:

Corner Frequencies:

	K+k	m	$\sqrt{\frac{K+k}{m}}$ rad/sec	$\sqrt{\frac{K+k}{m}}$ cy/sec	Average
Front	(1000 + 4770)(12)	$\frac{15.73}{2}$	93.83	14.93	15.97
Rear	(3500 + 9540)(12)	$\frac{27.41}{2}$	106.85	17.01	

Resonant Frequencies:

	k	I, m	ω_n rad/sec	ω_n cy/sec
Pitch	(12)[(147.63)(1000) + (19.95)(3500)]	28231	9.61	1.53
Roll	(12) (30) (3500 + 1000)	8071	14.17	2.25
Heave	(2) (3500 + 1000) (12)	659	12.80	2.04

$S_{X_o X_o}(\omega)$ was normalized and plotted in Figure 5 for several vehicle speeds. Also plotted in the figure are the modal resonant frequencies for the vehicle, and an approximation to $S_{X_o X_o}(\omega)$ which admits only slight inaccuracies over the range of frequencies to which the system is sensitive. The approximation $S^*_{nn}(\omega)$ also has the advantage of being of second order while $S_{nn}(\omega)$ is of third order and therefore permits the dimensions of the total system to be reduced by four state variables.

The road noise power spectrum used in the dynamic analysis of the vehicle is

$$S^*_{nn}(\omega) = \frac{K\left(\frac{k}{K+k}\right)^2}{\left(1 + \frac{a^2}{r^2}\omega^2\right)\left(1 + \frac{c^2}{r^2}\omega^2\right)} \tag{15}$$

where $c^2 = \frac{2.0409}{(2.933\pi)^2}$

To determine the state equations of a filter which will produce a signal with power spectrum $S^*_{nn}(\omega)$ when subjected to a white noise input, equation 2 is again applied. Since $S_{xx}(\omega) = 1$ for white noise, this equation becomes

$$S^*_{nn}(\omega) = 1\left|H(j\omega)\right|^2 \tag{16}$$

where $H(j\omega)$ is the transfer function of the linear filter to be specified. If H has the form

$$H(j\omega) = \frac{\alpha}{(1 + \beta j\,\omega)(1 + \gamma j\,\omega)} \tag{17}$$

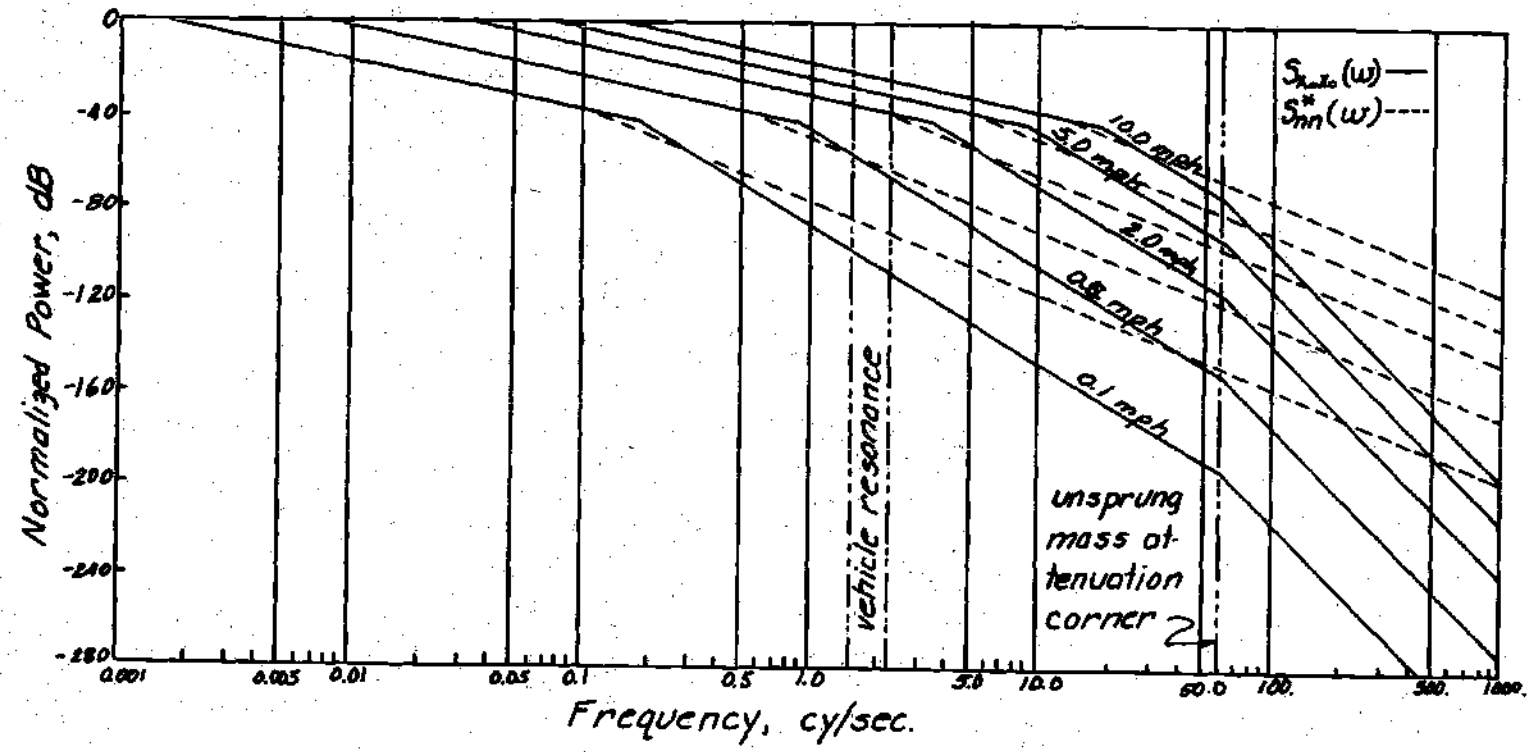

Figure 5. Ideal and Approximate Road Noise Power Spectra

then

$$|H(j\omega)| = \frac{\alpha}{\sqrt{1+\beta^2\omega^2}\sqrt{1+\gamma^2\omega^2}} \tag{18}$$

and

$$|H(j\omega|^2 = \frac{\alpha^2}{(1+\beta^2\omega^2)(1+\gamma^2\omega^2)} \tag{19}$$

so that

$$\alpha = \sqrt{\hat{K}}\left(\frac{k}{K+k}\right), \ \beta=\frac{a}{r}, \ \gamma=\frac{c}{r} \tag{20}$$

describe a filter which will produce noise with power spectrum $S^*_{nn}(\omega)$ when subjected to a white noise input. In the Laplace domain

$$H(s) = \frac{\alpha}{(1+\beta s)(1+\gamma s)} = \frac{\theta_o(s)}{\theta_i(s)} \tag{21}$$

or

$$\theta_o(s)\left[1+(\gamma+\beta)s+\gamma\beta s^2\right] = \alpha\theta_i(s) \tag{22}$$

Transforming to the time domain yields

$$\ddot{\theta}_o(t) + \frac{\gamma+\beta}{\gamma\beta}\dot{\theta}_o(t) + \frac{1}{\gamma\beta}\theta_o(t) = \frac{\alpha}{\gamma\beta}\theta_i(t) \tag{23}$$

In this application $\theta_i(t) = w$, a gaussian, zero mean white noise with variance 1.

Define filter state variables

$$\begin{aligned} X_1 &= \theta_o(t) \\ X_2 &= \dot{X}_1 = \dot{\theta}_o(t) \end{aligned} \tag{24}$$

The state equation form for equation 23 is then

$$\begin{bmatrix} \dot{X}_1 \\ \dot{X}_2 \end{bmatrix} = \begin{bmatrix} 0 & 1 \\ \frac{-1}{\gamma\beta} & \left(\frac{\gamma+\beta}{\gamma\beta}\right) \end{bmatrix} \begin{bmatrix} X_1 \\ X_2 \end{bmatrix} + \begin{bmatrix} 0 \\ \frac{\alpha}{\gamma\beta} \end{bmatrix} w \qquad (25)$$

Equation 25 defined the desired road noise filter for a single wheel; therefore eight state variables are required to model the four road noise inputs to the vehicle.

Dynamic Model of the Collection Vehicle

There are numerous vehicle dynamic models in the literature, each developed for a specific purpose. Among these are models of passenger cars in which the analysis is aimed at predicting vehicle motion and steering forces in turning and braking maneuvers. Such models, excellent examples of which are given by Sharp and Goodall (21) and Bergman, Fox and Saibel (22), assume that the wheels remain in a "wheel plane" which, though it undergoes displacement, roll, pitch, and yaw, moves as a rigid body. Other models are concerned with the detailed description of a specific suspension, again with regard to handling characteristics, in the design of new vehicles, as is the paper by Maeda and Vemura (23). Cornell Aeronautical Laboratories have developed a very sophisticated model for predicting vehicle dynamics in crash situations (24). Finally there are numerous efforts in the direction of designing wheeled and tracked vehicles for maximum mobility in rough terrain, with primary interest in the development of high flotation high traction suspensions, as reported in the series

of conferences beginning with reference 25. Other efforts in the direction of ride quality on rough terrain have been carried out, as is evidenced by the ride augmentation system recently introduced for the American M60 battle tank. No reports of the dynamic modeling techniques used are generally available however.

The nomenclature used in this analysis of the vehicle dynamics is illustrated in Figure 6. The direction of travel of the vehicle in normal operation is along the x axis and vertical displacements of the center of gravity are measured along z. Roll θ_x takes place about the x axis and pitch θ_y about the y axis. Yaw and transverse motion y are not considered as they are assumed to be constrained by the vehicle suspension while in straight travel. It is further assumed that the vehicle moves at a constant velocity throughout the accumulation process.

Examination of the figure will verify that the displacement of the vehicle suspension points in terms of body coordinates are given by

$$\begin{aligned} z_{\ell f} &= z + \frac{w_f}{2}\theta_x - a\theta_y \\ z_{rf} &= z - \frac{w_f}{2}\theta_x - a\theta_y \\ z_{\ell r} &= z + \frac{w_r}{2}\theta_x + b\theta_y \\ z_{rr} &= z - \frac{w_r}{2}\theta_x + b\theta_y \end{aligned} \tag{26}$$

The force at the ith suspension point is then given by

$$F_i = K_i(Z_i - z_i) + C_i(\dot{Z}_i - \dot{z}_i) \tag{27}$$

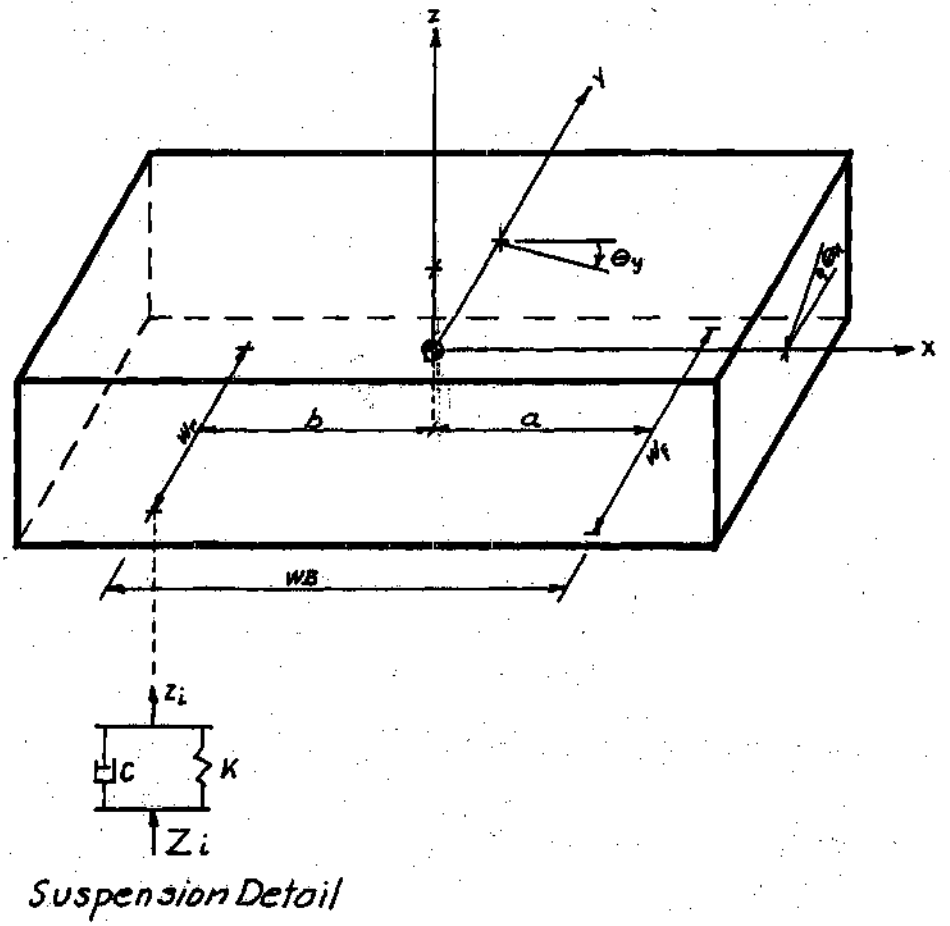

Figure 6. Vehicle Dynamics Nomenclature

where Z_i is the road noise input to the axle at the ith wheel, K_i is the suspension stiffness and C_i is the suspension damping at the ith wheel, and z_i the suspension point displacement given by equations 26. The dot notation is used to signify differentiation with respect to time. Substitution of equations 26 into equation 27 yields an expression for the force at the body due to road noise at each wheel.

$$
\begin{aligned}
F_{\ell f} &= K_f(Z_{\ell f} - z - \frac{w_f}{2}\theta_x + a\theta_y) + C_f(\dot{Z}_{\ell f} - \dot{z} - \frac{w_f}{2}\dot{\theta}_x + a\dot{\theta}_y) \\
F_{rf} &= K_f(Z_{rf} - z + \frac{w_f}{2}\theta_x + a\theta_y) + C_f(\dot{Z}_{rf} - \dot{z} + \frac{w_f}{2}\dot{\theta}_x + a\dot{\theta}_y) \\
F_{\ell r} &= K_r(Z_{\ell r} - z - \frac{w_r}{2}\theta_x - b\theta_y) + C_r(\dot{Z}_{\ell r} - \dot{z} - \frac{w_r}{2}\dot{\theta}_x - b\dot{\theta}_y) \\
F_{rr} &= K_r(Z_{rr} - z + \frac{w_r}{2}\theta_x - b\theta_y) + C_r(\dot{Z}_{rr} - \dot{z} + \frac{w_r}{2}\dot{\theta}_x - b\dot{\theta}_y)
\end{aligned}
\tag{28}
$$

Here the subscripts or suspension parameters, f and r, mean "front" and "rear" respectively, and the subscripts on the forces indicate "left front," ℓf, "left rear," ℓr, etcetera.

Summation of forces in the vertical direction yields

$$M\ddot{z} = F_{\ell f} + F_{rf} + F_{\ell r} + F_{rr} \tag{29}$$

Let the state variables X_1 through X_{14} be defined as in Table 7, then equation 28 may be substituted into equation 29 to yield

$$\dot{X}_1 = X_2$$

Table 7. State Variables for Vehicle Dynamics

Variable	Notation	Definition
X_1	z	Vertical displacement of vehicle CG
X_2	$\dot{z}$	Vertical diplacement rate of vehicle CG
X_3	θ_x	Vehicle rotation about x axis
X_4	$\dot{\theta}_x$	Vehicle rotational velocity about x axis
X_5	θ_y	Vehicle rotation about y axis
X_6	$\dot{\theta}_y$	Vehicle rotational velocity about y axis
X_7	$z_{\ell f}$	Axle displacement at left front
X_8	$\dot{z}_{\ell f}$	Axle displacement rate at left front
X_9	z_{rf}	Axle displacement at right front
X_{10}	$\dot{z}_{rf}$	Axle displacement rate at right front
X_{11}	$z_{\ell f}$	Axle displacement at left front
X_{12}	$\dot{z}_{\ell r}$	Axle displacement rate at left rear
X_{13}	z_{rr}	Axle displacement at right rear
X_{14}	$\dot{z}_{rr}$	Axle displacement rate at right rear

$$\dot{X}_2 = \frac{-2}{M}(K_f + K_r)X_1 - \frac{2}{M}(C_f + C_r)X_2 + \frac{2}{M}(K_f a - K_r b)X_5$$

$$+ \frac{2}{M}(C_f a - C_r b)X_6 + \frac{K_f}{M}X_7 + \frac{C_f}{M}X_8 + \frac{K_f}{M}X_9 \qquad (30)$$

$$+ \frac{C_f}{M}X_{10} + \frac{K_r}{M}X_{11} + \frac{C_r}{M}X_{12} + \frac{K_r}{M}X_{13} + \frac{C_r}{M}X_{14}$$

The inertial moments of the vehicle body about its center of gravity are (26)

$$\Sigma M_{CG} = \left[\dot{\omega}_x I_{xx} + \omega_y \omega_z (I_{zz} - I_{yy}) + I_{xy}(\omega_z \omega_x - \omega_y)\right.$$

$$\left. -I_{xz}(\dot{\omega}_z + \omega_x \omega_y) - I_{yz}(\omega_y^2 - \omega_z^2)\right] \bar{i} + \left[\dot{\omega}_y I_{yy} + \right.$$

$$\left. \omega_z \omega_x (I_{xx} - I_{zz}) + I_{yz}(\omega_x \omega_y - \dot{\omega}_z) - I_{yx}(\dot{\omega}_x + \omega_y \omega_z)\right.$$

$$\left. -I_{zx}(\omega_z^2 - \omega_x^2)\right] \bar{j} + \left[\omega_z I_{zz} + \omega_x \omega_y (I_{yy} - I_{xx})\right.$$

$$\left. + I_{zx}(\omega_y \omega_z - \dot{\omega}_x) - I_{zy}(\dot{\omega}_y + \omega_z \omega_x) - I_{xy}(\omega_x^2 - \omega_y^2)\right] \bar{k} \qquad (31)$$

Neglecting second order terms and requiring $\omega_z = \dot{\omega}_z = 0$ results in a simplified expression for equation 31:

$$\Sigma M_{CG} = (\dot{\omega}_x I_{xx} - I_{xy}\dot{\omega}_y)\bar{i} + (\dot{\omega}_y I_{yy} - I_{yx}\dot{\omega}_x)\bar{j}$$

$$+ (-I_{zx}\dot{\omega}_x - I_{zy}\dot{\omega}_z)\bar{k} \qquad (32)$$

which in terms of the state variables previously defined becomes

$$\Sigma M_{CG} = (I_{xx}\dot{X}_4 - I_{xy}\dot{X}_6)\bar{i} + (I_{yy}\dot{X}_6 - I_{yx}\dot{X}_4)\bar{j}$$

$$- (I_{zx}\dot{X}_4 + I_{zy}\dot{X}_6)\bar{k} \qquad (33)$$

Summing moments about the x axis yields

$$I_{xx}\dot{X}_4 - I_{xy}\dot{X}_6 = \frac{w_f}{2}\left[K_f(X_7 - X_9 - w_f X_3) + C_f(X_8 - X_{10} - w_f X_4)\right]$$

$$+ \frac{w_r}{2}\left[K_r(X_{11} - X_{13} - w_r X_3) + C_r(X_{12} - X_{14} - w_r X_4)\right] \quad (34)$$

and summing moments about the y axis yields

$$I_{yy}\dot{X}_6 - I_{xy}\dot{X}_4 = b\left[K_r(X_{11} + X_{13} - 2X_1 - 2bX_5)\right.$$

$$\left. + C_r(X_{12} + X_{14} - 2X_2 - 2bX_6)\right] - a\left[K_f(X_7 + X_9 - 2X_1 + 2aX_5)\right. \quad (35$$

$$\left. + C_f(X_8 + X_{10} - 2X_2 + 2aX_6)\right]$$

Equations 34 and 35 may be manipulated to give expressions for $\dot{X}_4$ and $\dot{X}_6$ which together with the state variable definitions yield

$$\dot{X}_3 = X_4$$

$$\dot{X}_4 = \left(\frac{-2I_{xy}}{I_{xx}I_{yy} - 1}\right)\left(bK_r - aK_f\right)X_1 - \left(\frac{2I_{xy}}{I_{xx}I_{yy} - 1}\right)$$

$$\left(bC_r - aC_f\right)X_2 - \frac{1}{2}\left(\frac{I_{yy}}{I_{xx}I_{yy} - 1}\right)\left(w_f^2 K_f + w_r^2 K_r\right)X_3$$

$$-\frac{1}{2}\left(\frac{I_{yy}}{I_{xx}I_{yy} - 1}\right)\left(w_f^2 C_f + w_r^2 C_r\right)X_4 - \left(\frac{2I_{xy}}{I_{xx}I_{yy} - 1}\right)\left(b^2 K_r + a^2 K_f\right)X_5$$

$$- \left(\frac{2I_{xy}}{I_{xx}I_{yy} - 1}\right)\left(b^2 C_r + a^2 C_f\right)X_6 + \left[-\left(\frac{I_{xy}aK_f}{I_{xx}I_{yy} - 1}\right)\right.$$

$$\left. + \frac{1}{2}\left(\frac{I_{yy}w_f K_f}{I_{xx}I_{yy} - 1}\right)\right]X_7 + \left[\left(\frac{-I_{xy}aC_f}{I_{xx}I_{yy} - 1}\right) + \frac{1}{2}\left(\frac{I_{yy}w_f C_f}{I_{xx}I_{yy} - 1}\right)\right]X_8$$

$$+\left[-\left(\frac{I_{xy}aK_f}{I_{xx}I_{yy}-1}\right)-\frac{1}{2}\left(\frac{I_{yy}w_fK_f}{I_{xx}I_{yy}-1}\right)\right]X_9+\left[-\left(\frac{I_{xy}aC_f}{I_{xx}I_{yy}-1}\right)\right.$$

$$\left.-\frac{1}{2}\left(\frac{I_{yy}w_fC_f}{I_{xx}I_{yy}-1}\right)\right]X_{10}+\left[\left(\frac{I_{xy}bK_r}{I_{xx}I_{yy}-1}\right)+\frac{1}{2}\left(\frac{I_{yy}w_rK_r}{I_{xx}I_{yy}-1}\right)X_{11}\right. \tag{36}$$

$$+\left[\left(\frac{I_{xy}bC_r}{I_{xx}I_{yy}-1}\right)+\frac{1}{2}\left(\frac{I_{yy}w_rC_r}{I_{xx}I_{yy}-1}\right)\right]X_{12}+\left[\left(\frac{I_{xy}bK_r}{I_{xx}I_{yy}-1}\right)\right.$$

$$-\frac{1}{2}\left(\frac{I_{yy}w_rK_r}{I_{xx}I_{yy}-1}\right)X_{13}+\left[\left(\frac{I_{xy}bC_r}{I_{xx}I_{yy}-1}\right)-\frac{1}{2}\left(\frac{I_{yy}w_rC_r}{I_{xx}I_{yy}-1}\right)\right]X_{14}$$

and

$$\dot{X}_5 = X_6$$

$$\dot{X}_6 = -2\left[\frac{I_{xy}^2+I_{xx}I_{yy}-1}{I_{yy}(I_{xx}I_{yy}-1)}\right](bK_r - aK_f)X_1$$

$$-2\left[\frac{I_{xy}^2+I_{xx}I_{yy}-1}{I_{yy}(I_{xx}I_{yy}-1)}\right](bC_r - aC_f)X_2$$

$$-\frac{1}{2}\left[\frac{I_{xy}}{I_{xx}I_{yy}-1}\right]\left(w_f^2K_f + w_r^2K_r\right)X_3$$

$$-\frac{1}{2}\left[\frac{I_{xy}}{I_{xx}I_{yy}-1}\right]\left(w_f^2C_f+w_r^2C_r\right)X_4$$

$$-2\left[\frac{I_{xy}^2+I_{xx}I_{yy}-1}{I_{yy}(I_{xx}I_{yy}-1)}\right]\left(b^2K_r + a^2K_f\right)X_5$$

$$-2\left[\frac{I_{xy}^2 + I_{xx}I_{yy} - 1}{I_{yy}(I_{xx}I_{yy} - 1)}\right]\left(b^2C_r + a^2C_f\right)X_6$$

$$-\left[\frac{aK_f}{I_{yy}} + \frac{I_{xy}^2 aK_f}{I_{yy}(I_{xx}I_{yy} - 1)} - \frac{1}{2}\left(\frac{I_{xy}w_f K_f}{I_{xx}I_{yy} - 1}\right)\right]X_7$$

$$-\left[\frac{aC_f}{I_{yy}} + \frac{I_{xy}^2 aC_f}{I_{yy}(I_{xx}I_{yy} - 1)} - \frac{1}{2}\left(\frac{I_{xy}w_f C_f}{I_{xx}I_{yy} - 1}\right)\right]X_8$$

$$-\left[\frac{aK_f}{I_{yy}} + \frac{I_{xy}^2 aK_f}{I_{yy}(I_{xx}I_{yy} - 1)} + \frac{1}{2}\left(\frac{I_{xy}w_f K_f}{I_{xx}I_{yy} - 1}\right)\right]X_9 \qquad (37)$$

$$-\left[\frac{aC_f}{I_{yy}} + \frac{I_{xy}^2 aC_f}{I_{yy}(I_{xx}I_{yy} - 1)} + \frac{1}{2}\left(\frac{I_{xy}w_f C_f}{I_{xx}I_{yy} - 1}\right)\right]X_{10}$$

$$+\left[\frac{bK_r}{I_{yy}} + \frac{I_{xy}^2 bK_r}{I_{yy}(I_{xx}I_{yy} - 1)} + \frac{1}{2}\left(\frac{I_{xy}w_r K_r}{I_{xx}I_{yy} - 1}\right)\right]X_{11}$$

$$+\left[\frac{bC_r}{I_{yy}} + \frac{I_{xy}^2 bC_r}{I_{yy}(I_{xx}I_{yy} - 1)} + \frac{1}{2}\left(\frac{I_{xy}w_r C_r}{I_{xx}I_{yy} - 1}\right)\right]X_{12}$$

$$+\left[\frac{bK_r}{I_{yy}} + \frac{I_{xy}^2 bK_r}{I_{yy}(I_{xx}I_{yy} - 1)} - \frac{1}{2}\left(\frac{I_{xy}w_r K_r}{I_{xx}I_{yy} - 1}\right)\right]X_{13}$$

$$+\left[\frac{bC_r}{I_{yy}} + \frac{I_{xy}^2 bC_r}{I_{yy}(I_{xx}I_{yy} - 1)} - \frac{1}{2}\left(\frac{I_{xy}w_r C_r}{I_{xx}I_{yy} - 1}\right)\right]X_{14}$$

In addition, equations of the form of equation 25 are required to model the road

noise at each wheel. Letting noise inputs be w_1 at the left front, w_2 at the right front, w_3 at the left rear and w_4 at the right rear, we have at the left front:

$$\dot{X}_7 = X_8$$

$$\dot{X}_8 = \frac{-1}{\gamma\beta} X_7 - \frac{\gamma+\beta}{\gamma\beta} X_8 + \frac{\alpha}{\gamma\beta} w_1 \tag{38}$$

and similarly at the other wheels:

$$\dot{X}_9 = X_{10}$$

$$\dot{X}_{10} = \frac{-1}{\gamma\beta} X_9 - \frac{\gamma+\beta}{\gamma\beta} X_{10} + \frac{\alpha}{\gamma\beta} w_2 \tag{39}$$

$$\dot{X}_{11} = X_{12}$$

$$\dot{X}_{12} = \frac{-1}{\gamma\beta} X_{11} - \frac{\gamma+\beta}{\gamma\beta} X_{12} + \frac{\alpha}{\gamma\beta} w_3$$

$$\dot{X}_{13} = X_{14}$$

$$\dot{X}_{14} = \frac{-1}{\gamma\beta} X_{11} - \frac{\gamma+\beta}{\gamma\beta} w_4$$

These equations complete the dynamic model of the vehicle subject to random road noise inputs at each wheel.

Dynamic Model of the Accumulator

In the design process it is often desirable to perform whatever analysis is necessary in as general a manner as possible. This helps to avoid making

design decisions in the analysis which preclude the investigation of unforseen potential design solutions. With this in mind, and noting that the dynamic model has already grown to include fourteen differential equations, a general dynamic model of the accumulator mechanism was visualized as shown in Figure 7a. The model consists of an amorphus body which reacts with rather general internal forces to externally or internally applied displacements and displacement rates. The mass of the body is lumped at its end and the dynamic relationship between vehicle attachment point displacement $\bar{X}_v$, actuator displacement $\bar{E}_a$, and accumulator tip displacement $\bar{X}_a$ in any direction is as shown in Figure 7b, where K is the stiffness of a linear spring and C the damping coefficient of a viscous damper.

To derive the equations of motion for the mass at the tip of the idealized accumulator, Newton's law is applied:

$$\bar{F}_a = m\ddot{\bar{X}}_a \tag{40}$$

The relationship between forces $\bar{F}_a$ and spring deflection ϵ is given by

$$\begin{bmatrix} F_x \\ F_y \\ F_z \end{bmatrix} = \begin{bmatrix} K_{11} & C_{11} & K_{12} & C_{12} & K_{13} & C_{13} \\ K_{21} & C_{21} & K_{22} & C_{22} & K_{23} & C_{23} \\ K_{31} & C_{31} & K_{32} & C_{32} & K_{33} & C_{33} \end{bmatrix} \begin{bmatrix} \epsilon_x \\ \dot{\epsilon}_x \\ \epsilon_y \\ \dot{\epsilon}_y \\ \epsilon_z \\ \dot{\epsilon}_z \end{bmatrix} \tag{41}$$

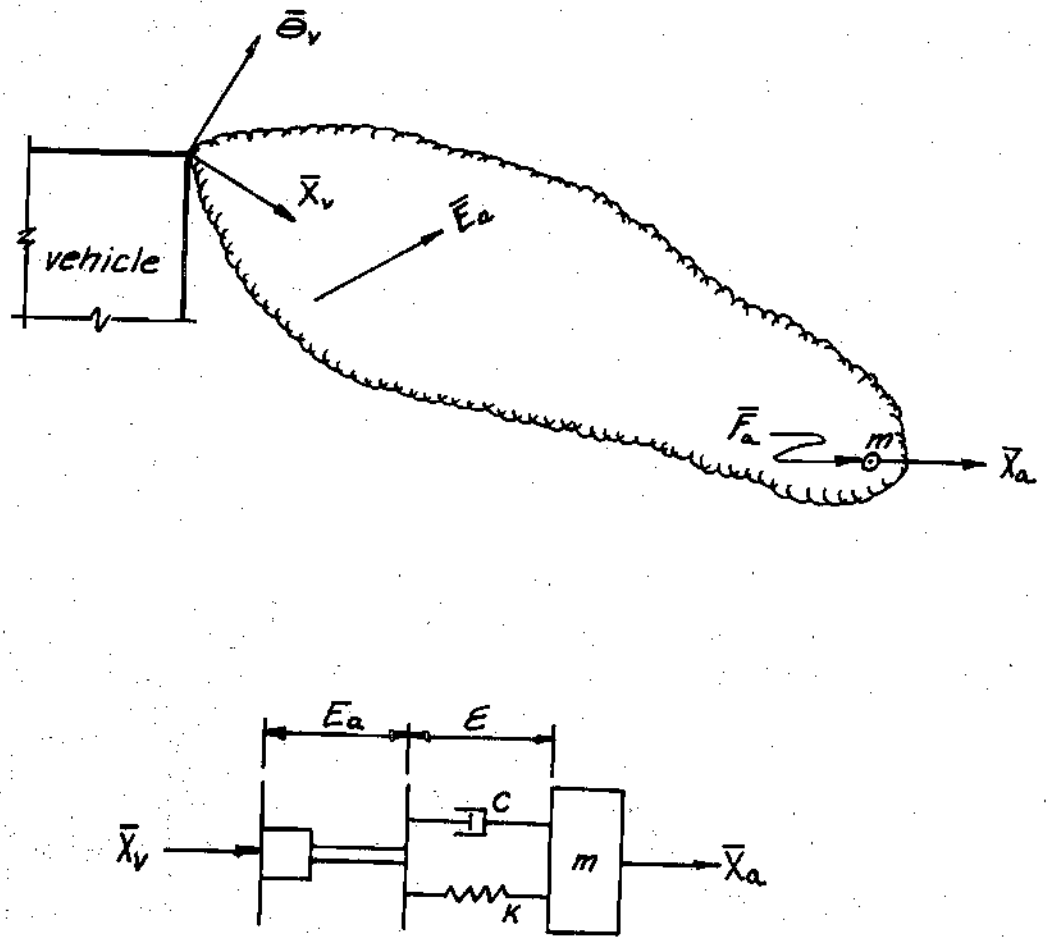

Figure 7. Accumulator Dynamic Model

Additional forces exerted on the accumulator by rotation of the vehicle are

$$\begin{bmatrix} F_x \\ F_y \\ F_z \end{bmatrix} = \begin{bmatrix} KT_{11} & CT_{11} & KT_{12} & CT_{12} \\ KT_{21} & CT_{21} & KT_{22} & CT_{22} \\ KT_{31} & CT_{31} & KT_{32} & CT_{32} \end{bmatrix} \begin{bmatrix} \theta_x \\ \dot{\theta}_x \\ \theta_y \\ \dot{\theta}_y \end{bmatrix} \tag{42}$$

The total force on the accumulator is given by the sum of equations 41 and 42, that that is

$$\bar{F}_a = \bar{F}_\epsilon + \bar{F}_\theta \tag{43}$$

The spring deflection is generally defined by

$$\bar{\epsilon} = \bar{X}_v + \bar{E}_a - \bar{X}_a \tag{44}$$

If the accumulator attachment point on the vehicle is located at a vector distance $\bar{r}_a$ from the vehicle center of gravity, $\bar{X}_v$ is given by

$$\begin{aligned} X_v\bar{i} &= r_{az}\theta_y = r_{az}X_5 \\ X_v\bar{j} &= -r_{az}\theta_x = r_{az}X_3 \\ X_v\bar{k} &= z_{CG} - r_{ax}\theta_y + r_{ay}\theta_x = X_1 + r_{ay}X_3 - r_{ax}X_5 \end{aligned} \tag{45}$$

Equations 45 may be differentiated once with respect to time to yield

$$\dot{X}_v \tilde{i} = r_{az} X_6$$

$$\dot{X}_v \tilde{j} = r_{az} X_4 \qquad (46)$$

$$\dot{X}_v \tilde{k} = X_2 + r_{ay} X_4 - r_{ax} X_6$$

If state variables are defined for the accumulator as in Table 8, equation 44 may be written

$$\epsilon_x = r_{az} X_5 + X_{17} - X_{15}$$

$$\epsilon_y = -r_{az} X_3 + X_{20} - X_{18} \qquad (47)$$

$$\epsilon_z = X_1 + r_{ay} X_3 - r_{ax} X_5 + X_{23} - X_{21}$$

Equations 47 may be differentiated once with respect to time to yield

$$\dot{\epsilon}_x = r_{az} X_6 - X_{16} + K_s U_1$$

$$\dot{\epsilon}_y = - r_{az} X_4 - X_{19} + K_s U_2 \qquad (48)$$

$$\dot{\epsilon}_z = X_2 + r_{ay} X_4 - r_{ax} X_6 - X_{22} + K_s U_3$$

Where K_s is the gain between the in-cab master accumulator and the slave and

U_1 is the extension rate of the master in the x direction.

U_2 is the extension rate of the master in the y direction and U_3 is the

Table 8. Accumulator State Variables

Variable	Notation	Definition
X_{15}	$X_a\bar{i}$	x displacement of accumulator tip
X_{16}	$\dot{X}_a\bar{i}$	x displacement rate of accumulator tip
X_{17}	$E_a\bar{i}$	x displacement of actuator
X_{18}	$X_a\bar{j}$	y displacement of accumulator tip
X_{19}	$\dot{X}_a\bar{j}$	y displacement rate of accumulator tip
X_{20}	$E_a\bar{j}$	y displacement of actuator
X_{21}	$X_a\bar{k}$	z displacement of accumulator tip
X_{22}	$\dot{X}_a\bar{k}$	z displacement rate of accumulator tip
X_{23}	$E_a\bar{k}$	z displacement of actuator

extension rate of the master in the z direction. (It will be shown in the next section that the accumulator may be designed so that the master-slave relationship is a simple gain.)

Substitution of equations 47 and 48 into equations 41 yields a result which when substituted along with equation 42 into equation 43 fully defines the force $\bar{F}_a$. Finally, equation 40 then yields

$$\dot{X}_{15} = X_{16}$$

$$\dot{X}_{16} = \frac{K_{11}}{m}\left[r_{az}X_5 + X_{17} - X_{15}\right] + \frac{C_{11}}{m}\left[r_{az}X_6 - X_{16}\right]$$

$$+ \frac{K_{12}}{m}\left[- r_{az}X_3 + X_{20} - X_{18}\right] + \frac{C_{12}}{m}\left[- r_{az}X_4 - X_{19}\right]$$

$$+ \frac{K_{13}}{m}\left[X_1 + r_{ay}X_3 - r_{ax}X_5 + X_{23} - X_{21}\right]$$

$$+ \frac{C_{13}}{m}\left[X_2 + r_{ay}X_4 - r_{ax}X_6 - X_{22}\right] + K_s \frac{C_{11}}{m} U_1$$

$$+ K_s \frac{C_{12}}{m} U_2 + K_5 \frac{C_{13}}{m} U_3 + \frac{KT_{11}}{m} X_3 + \frac{CT_{11}}{m} X_4$$

$$+ \frac{KT_{12}}{m} X_5 + \frac{CT_{12}}{m} X_6$$

$$\dot{X}_{17} = K_s U_1$$

$$\dot{X}_{18} = X_{19}$$

$$\dot{X}_{19} = \frac{K_{21}}{m}\left[r_{az}X_5 + X_{17} - X_{15}\right] + \frac{C_{21}}{m}\left[r_{az}X_6 - X_{16}\right]$$

$$+ \frac{K_{22}}{m}\left[- r_{az}X_3 + X_{20} - X_{18}\right] + \frac{C_{22}}{m}\left[- r_{az}X_4 - X_{19}\right]$$

$$+ \frac{K_{23}}{m}\left[X_1 + r_{ay}X_3 - r_{ax}X_5 + X_{23} - X_{21}\right]$$

$$+ \frac{C_{23}}{m}\left[X_2 + r_{ay}X_4 - r_{ax}X_6 - X_{22}\right] + K_s \frac{C_{21}}{m} U_1$$

$$+ K_s \frac{C_{22}}{m} U_2 + K_s \frac{C_{23}}{m} U_3 + \frac{KT_{21}}{m} X_3 + \frac{CT_{21}}{m} X_4$$

$$+ \frac{KT_{22}}{m} X_5 + \frac{CT_{22}}{m} X_6$$

$$\dot{X}_{20} = K_s U_2$$

$$\dot{X}_{21} = X_{22}$$

$$\dot{X}_{22} = \frac{K_{31}}{m}\left[r_{az}X_5 + X_{17} - X_{15}\right] + \frac{C_{31}}{m}\left[r_{az}X_6 - X_{16}\right]$$

$$+ \frac{K_{32}}{m}\left[-r_{az}X_3 + X_{20} - X_{18}\right] + \frac{C_{32}}{m}\left[-r_{az}X_4 - X_{19}\right]$$

$$+ \frac{K_{33}}{m}\left[X_1 + r_{ay}X_3 - r_{ax}X_5 + X_{23} - X_{21}\right]$$

$$+ \frac{C_{33}}{m}\left[X_2 + r_{ay}X_4 - r_{ax}X_6 - X_{22}\right] + K_s \frac{C_{31}}{m} U_1$$

$$+ K_s \frac{C_{32}}{m} U_2 + K_s \frac{C_{33}}{m} U_3 + \frac{KT_{31}}{m} X_3 + \frac{CT_{31}}{m} X_4$$

$$+ \frac{KT_{32}}{m} X_5 + \frac{CT_{32}}{m} X_6$$

$$\dot{X}_{23} = K_s U_3$$

These accumulator state equations will be referred to as equations 49.

Analysis of the Man-Machine Interface

The man-machine interface is an inertialess scale model of the accumulator which the operator moves as he wishes the full scale accumulator to move. The dynamics of the model itself are very simple:

$$\bar{E}_m = \int_0^t \dot{\bar{E}}_m \, dt \tag{50}$$

where $\bar{E}_m$ is the extension of the model and $\dot{\bar{E}}_m$ is its extension rate. Since $\dot{\bar{E}}_m = \bar{U}$, an input to the accumulator master-slave system, (see the discussion following equation 48), we see that the model is a simple integrator of the operator control input $\bar{U}$.

There are of course some additional dynamic effects associated with the control system interconnecting the master and the slave. The actuator control signals are decoded from operator inputs automatically by the kinematic similarity of the master and slave, and are transmitted through a control system which seeks to maintain a direct relationship between master position and velocity and slave position and velocity. Such a control system is shown schematically in Figure 8 for a single actuator controlling a single degree of freedom in the kinematic chain, perhaps the rotation of one link relative to another about a revolute pair. The rotation of a joint in the master unit θ_{in} is converted to an electrical signal e_{in} by a transducer with gain K_t. Another transducer measures the rotation of the corresponding joint on the slave unit θ_{out} and generates signal $-e_{out}$, proportional to rotation θ_{out} by gain K_t. Signals $-e_{out}$ and e_{in} are summed to yield a signal e_{error}

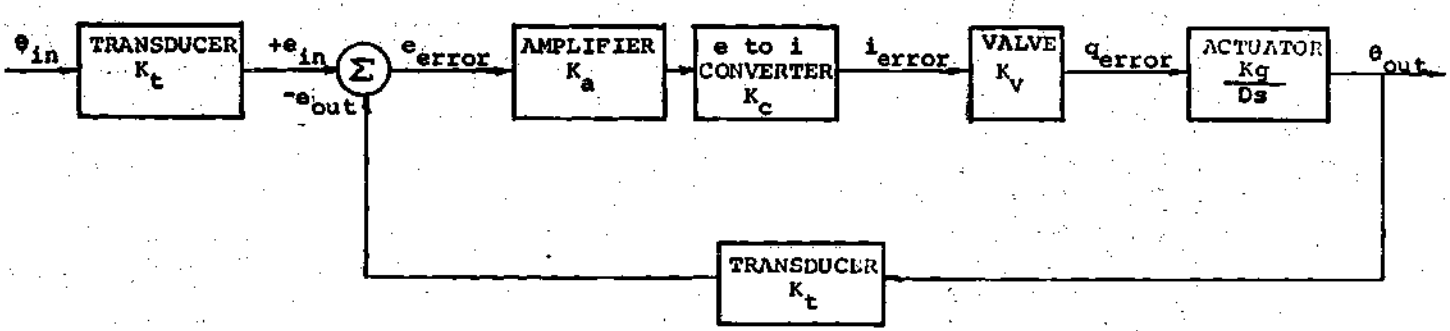

Figure 8. Master-Slave Control Dynamics

proportional to the difference in rotations θ_{out} and θ_{in}. This error signal is amplified by a power amplifier with gain K_a to produce a higher voltage signal which is then converted by a voltage to current converter of gain K_c to a current signal proportional to the rotational error. The current signal is applied to a linear valve of gain K_v which opens to permit a flow rate q_{error} to the actuator. The flow to the actuator is integrated by the actuator displacement D to produce a rotation proportional to the rotational error sensed by the transducers. Where a gear train is used, the actuator signal is further modified by gear ratio K_g. Thus the slave actuator is controlled to follow its master.

The system described above has closed loop transfer function of the form

$$\frac{\theta_o}{\theta_i} = \frac{1}{1 + Ks} \tag{51}$$

where $K = \frac{D}{K_t K_a K_c K_g}$ and s is the Laplace operator.

This system can be designed so that over the frequency range to which it will be subjected by the human operator, equation 51 may be replaced by a unit gain. To show this we first balance torques at the actuator. The torque generated at the actuator is given by

$$T_g = DP_L \tag{52}$$

where D is the actuator displacement and P_L is the pressure drop across the load. The torque transmitted to the joint through gear train K_g is given by

$$T_t = T_{g/K_g} = \frac{DP_L}{K_g} \tag{53}$$

Equating the maximum applied torque at the joint (directly related to the maximum acceleration imposed on the accumulator) to the torque transmitted to the joint, permits the required actuator displacement to be determined by

$$\frac{D}{K_g} = \frac{T_{max}}{P_L} \tag{54}$$

Substitution of equation 54 into the expression for K in equation 51 yields

$$K = \frac{T_{max}}{K_t K_a K_c K_v P_L} \tag{55}$$

Systems with transfer function 51 exhibit zero signal attenuation up to a "corner" frequency of $\omega_c = 1/K$ radians per second, at which point input signals are attenuated with increasing severity at the rate of 20 decibels per frequency decade. To avoid signal attentuation between the master and slave it is only necessary to ensure that K is sufficiently small to make the corner frequency ω_c much greater (at least one decade) than the highest frequency signal anticipated in the system. In particular one might require that

$$\frac{K_t K_a K_c K_v P_L}{T_{max}} >> \omega_{max} \tag{56}$$

where ω_{max} is the highest frequency input signal anticipated. Then over the

frequency range of interest equation 51 would reduce to

$$\frac{\theta_o}{\theta_i} = 1 \tag{57}$$

and the proportion between displacements in the slave and displacements in the master would simply be the scale factor K_s.

Examples of electrohydraulically controlled machines which successfully contend with input signals of much higher frequency than those to be anticipated in the automated refuse accumulator, such as the automatic pilot and stability augmentation systems in aircraft and the target acquisition control systems of anti-missile missiles, demonstrate the feasibility of obtaining the design condition specified by Equation 56.

Reduction of a Kinematic Chain to the General Form

In order to model a specific kinematic chain with the general dynamic model developed in this chapter, it is necessary to reduce the dynamic relationships of the chain to the form of the force-displacement and force-displacement rate relationships used in the general model. The techniques employed to do this will be developed here for the simplest of the alternative chains of Table 5, alternative configuration number 2, the contracted $R_1R_2P_3$ chain. The same approach is used for the other kinematic chains in the table and the details of the results are included in Appendix IV.

Figure 9 describes the nomenclature to be used in this development.

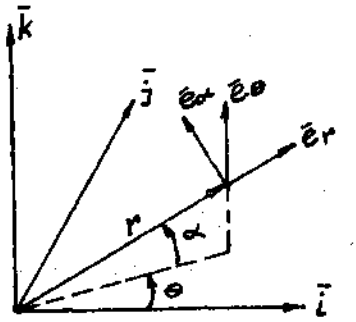

Figure 9. Nomenclature for Generalization of Contracted $R_1R_2R_3$ Chain.

Unit vector triad $\bar{i}$, $\bar{j}$, $\bar{k}$ forms the cartesian base used in the general model. Unit vector triad $\bar{e}_r$, $\bar{e}_\theta$, $\bar{e}_\alpha$ form the spherical base in which this kinematic chain is most readily analyzed. Coordinates θ and α correspond to rotations of the chain about its contracted revolute pairs while coordinate r is the instantaneous length of the extension through the prismatic link.

The position of the tip of the accumulator in the cartesian coordinates is

$$\bar{R}_c = r\cos\alpha\cos\theta\bar{i} + r\cos\alpha\sin\theta\bar{j} + r\sin\alpha\bar{k} \tag{58}$$

and the change in $\bar{R}_c$ due to incremental joint displacements $\Delta\alpha$, $\Delta\theta$, Δr is given by

$$\Delta\bar{R}_a = \frac{\partial\bar{R}_c}{\partial r}\Delta r + \frac{\partial\bar{R}_c}{\partial\theta}\Delta\theta + \frac{\partial\bar{R}_c}{\partial\alpha}\Delta\alpha \tag{59}$$

where

$$\frac{\partial \bar{R}_c}{\partial r} = \cos\alpha\cos\theta\,\bar{i} + \cos\alpha\sin\theta\,\bar{j} + \sin\alpha\,\bar{k}$$

$$\frac{\partial \bar{R}_c}{\partial \theta} = -r\sin\alpha\cos\theta\,\bar{i} + r\cos\alpha\cos\theta\,\bar{j} \tag{60}$$

$$\frac{\partial \bar{R}_c}{\partial \alpha} = -r\sin\alpha\cos\theta\,\bar{i} + r\sin\alpha\sin\theta\,\bar{j} + r\cos\alpha\,\bar{k}$$

If $\bar{\Delta}_c$ and $\bar{\Delta}_s$ are defined as

$$\bar{\Delta}_c = \begin{bmatrix} \Delta x \\ \Delta \dot{x} \\ \Delta y \\ \Delta \dot{y} \\ \Delta z \\ \Delta \dot{z} \end{bmatrix} \quad \text{and} \quad \bar{\Delta}_s = \begin{bmatrix} \Delta r \\ \Delta \dot{r} \\ \Delta \theta \\ \Delta \dot{\theta} \\ \Delta \alpha \\ \Delta \dot{\alpha} \end{bmatrix} \tag{61}$$

then an expression for $\bar{\Delta}_c$ is

$$\bar{\Delta}_c = \bar{T}\,\bar{\Delta}_s \quad \text{or} \quad \bar{\Delta}_s = \bar{T}^{-1}\,\bar{\Delta}_c \tag{62}$$

where $\bar{T}$ is the matrix

$$\begin{bmatrix} \cos\alpha\cos\theta & 0 & -r\cos\alpha\sin\theta & 0 \\ 0 & \cos\alpha\cos\theta & 0 & -r\cos\alpha\sin\theta \\ \cos\alpha\sin\theta & 0 & r\cos\alpha\cos\theta & 0 \\ 0 & \cos\alpha\sin\theta & 0 & r\cos\alpha\cos\theta \\ \sin\alpha & 0 & 0 & 0 \\ 0 & \sin\alpha & 0 & 0 \end{bmatrix}$$

$$\begin{bmatrix} -r\sin\alpha\cos\theta & 0 \\ 0 & -r\sin\alpha\cos\theta \\ -r\sin\alpha\sin\theta & 0 \\ 0 & -r\sin\alpha\sin\theta \\ r\cos\alpha & 0 \\ 0 & r\cos\alpha \end{bmatrix} \tag{63}$$

Equation 62 relates displacements in the spherical (chain oriented) coordinates to displacements in the cartesian (model oriented) coordinates.

The cartesian and spherical bases are also related by equations of the form

$$\bar{e}_s = \bar{\phi}\,\bar{e}_c \text{ and } \bar{e}_c = \bar{\phi}^{-1}\bar{e}_s \tag{64}$$

where $\bar{\phi}$ is the matrix

$$\begin{bmatrix} \cos\alpha\cos\theta & \cos\alpha\sin\theta & \sin\alpha \\ -\sin\theta & \cos\theta & 0 \\ -\sin\alpha\cos\theta & -\sin\alpha\sin\theta & \cos\alpha \end{bmatrix} \tag{65}$$

The force at the tip of the accumulator is easily expressed in spherical coordinates in terms of rotational stiffnesses and damping coefficients K_α, K_θ, C_α, C_θ and the axial stiffness and damping coefficients K_ℓ and C_ℓ, of the kinematic chain by

$$\bar{F}_s = (K_\ell \Delta r + C_\ell \dot{\Delta} r)\bar{e}_r + \left(\frac{K_\theta}{r\cos\alpha}\Delta\theta + \frac{C_\theta}{r\cos\alpha}\dot{\Delta\theta}\right)\bar{e}_\theta + \left(\frac{K_\alpha}{r}\Delta\alpha + \frac{C_\alpha}{r}\dot{\Delta\alpha}\right)\bar{e}_\alpha \tag{66}$$

which may be written

$$\bar{F}_s = \bar{K}\,\bar{\Delta}_s \tag{67}$$

where $\bar{K}$ is the matrix

$$\begin{bmatrix} K_\ell & C_\ell & 0 & 0 & 0 & 0 \\ 0 & 0 & \frac{K_\theta}{r\cos\alpha} & \frac{C_\theta}{r\cos\alpha} & 0 & 0 \\ 0 & 0 & 0 & 0 & \frac{K_\alpha}{r} & \frac{C_\alpha}{r} \end{bmatrix} \tag{68}$$

Substituting equation 62 into equation 67 yields

$$\bar{F}_s = \bar{K}\,\bar{T}^{-1}\,\bar{\Delta}_c \tag{69}$$

Equation 64 requires that

$$\bar{F}_c = \bar{\phi}^{-1}\,\bar{F}_s \tag{70}$$

so that equation 69 may be written

$$\bar{F}_c = \bar{\phi}^{-1} \bar{K} \bar{T}^{-1} \bar{\Delta}_c \tag{71}$$

and the matrix $\bar{\phi}^{-1} \bar{K} \bar{T}^{-1}$ is precisely the coefficient matrix required for equation 41 of the general model.

The vehicle rotation-force relationship given by equation 42 must now be investigated. Figure 10 shows how rotations θ_x and θ_y produce displacements Δx, Δy and Δz in the kinematic chain. Consider a vehicle rotation θ_x. Initially

$$\hat{R} = \sqrt{z_o^2 + y_o^2} = r\sqrt{\sin^2 \alpha + \cos^2 \alpha \sin^2 \theta} \tag{72}$$

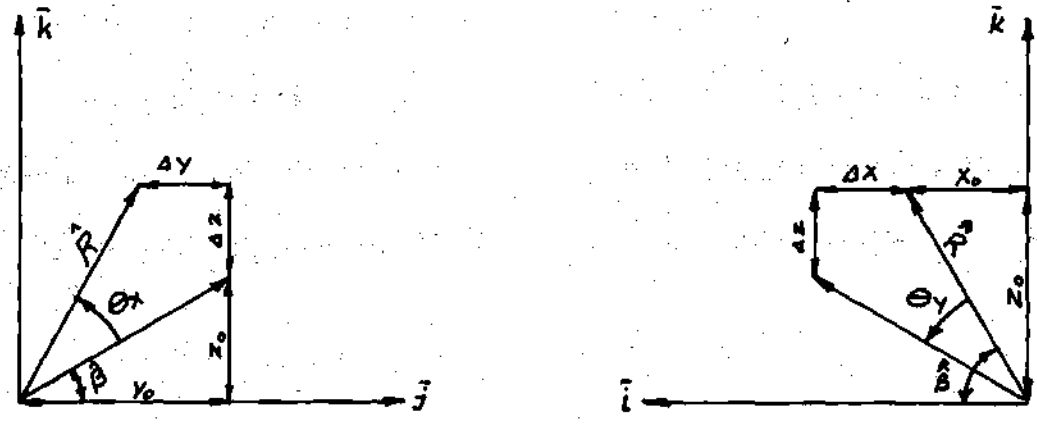

Figure 10. Effect of Vehicle Rotations θ_y and θ_x

but

$$\Delta z_{\theta_x} = \hat{R} \sin(\hat{\beta} + \theta_x) - z_o \tag{73}$$

thus

$$\Delta z_{\theta_x} = r\sqrt{\sin^2\alpha + \cos^2\alpha \sin^2\theta} \left[\frac{\sin\alpha}{\sqrt{\sin^2\alpha + \cos^2\alpha \sin^2\theta}} \cos\theta_x + \frac{\cos\alpha \sin\theta}{\sqrt{\sin^2\alpha + \cos^2\alpha \sin^2\theta}} \sin\theta_x \right] - r\sin\alpha \tag{74}$$

or

$$\Delta z_{\theta_x} = r[\sin\alpha \cos\theta_x + \cos\alpha \sin\theta \sin\theta_x - \sin\alpha] \tag{75}$$

For small θ_x, $\cos\theta_x = 1$, $\sin\theta_x = \theta_x$, yields

$$\Delta z_{\theta_x} = (r \cos\alpha \sin\theta)\, \theta_x \tag{76}$$

Similarly

$$\begin{aligned} \Delta y_{\theta_x} &= (-r \sin\alpha)\, \theta_x \\ \Delta z_{\theta_y} &= (-r \cos\alpha \cos\theta)\, \theta_y \\ \Delta x_{\theta_y} &= (r \sin\alpha)\, \theta_y \end{aligned} \tag{77}$$

The combined deflections due to rotations θ_x and θ_y are then

$$\begin{aligned} \Delta_x &= (r \sin\alpha)\, \theta_y \\ \Delta_y &= (-r \sin\alpha)\, \theta_x \\ \Delta_z &= r[(\cos\alpha \sin\theta)\, \theta_x - (\cos\alpha \cos\theta)\, \theta_y] \end{aligned} \tag{78}$$

The equivalent $\bar{\Delta}_c$ due to vehicle rotations is therefore

$$\bar{\Delta}_c = \bar{S}\,\bar{\theta} \tag{79}$$

where

$$\bar{\theta} = \begin{bmatrix} \theta_x \\ \dot{\theta}_x \\ \theta_y \\ \dot{\theta}_y \end{bmatrix} \tag{80}$$

and $\bar{S}$ is the matrix

$$\begin{bmatrix} 0 & 0 & r\sin\alpha & 0 \\ 0 & 0 & 0 & r\sin\alpha \\ -r\sin\alpha & 0 & 0 & 0 \\ 0 & -r\sin\alpha & 0 & 0 \\ r\cos\alpha\sin\theta & 0 & -r\cos\alpha\cos\theta & 0 \\ 0 & r\cos\alpha\sin\theta & 0 & -r\cos\alpha\cos\theta \end{bmatrix} \tag{81}$$

By equation 71

$$\bar{F}_c = \bar{\phi}^{-1}\bar{K}\bar{T}^{-1}\bar{\Delta}_c = \bar{\phi}^{-1}\bar{K}\bar{T}^{-1}\bar{S}\bar{\theta} \tag{82}$$

and $\bar{\phi}^{-1}\bar{K}\bar{T}^{-1}\bar{S}$ corresponds to the coefficient matrix in equation 42 of the general dynamic model.

By evaluating $\bar{\phi}^{-1}\bar{K}\bar{T}^{-1}$ and $\bar{\phi}^{-1}\bar{K}\bar{T}^{-1}\bar{S}$ for a specific alternative of the contracted $R_1R_2P_3$ chain, data may be obtained which is compatible with the general dynamic model. A similar analysis could be performed on any other chain, and

the results of such analyses for the other four alternatives which have been considered are included in the appendix.

CHAPTER V

MODELING OF THE HUMAN OPERATOR

Introduction

The vast quantity of work which is currently being carried out in an effort to model the human operator in various control tasks, attests to two basic facts about the current state of the art in this area. First, the necessity for including an analysis of the human being as an integral part of the control system of complex manually operated machines is widely recognized, and second a good general model of the human in control situations has yet to be developed.

One approach currently being used to achieve a better understanding of human control behavior is involved with system identification. Briefly, in these investigations human performance is monitored in a control task and the input-output data used to construct an equivalent circuit which would have produced the same output as the human. This technique has been made more effective by the development of such mathematical tools as the modified fast fourier transform (27) and the polarity coincidence correlation technique (28), both of which reduce the computational time required to determine the human transfer function, and therefore permit almost real time transfer function analysis. The results of such investigations are, however, unique human transfer functions for specific complex tasks. The technique is often used to investigate the changes which occur in the operator's performance under the influence of such variables as atmospheric pressure,

temperature and relative humidity, and is applied primarily by the aerospace industry.

Other efforts are more psychologically and physiologically oriented. These investigations attempt to measure reaction time, manipulation time and movement time (29), examine the importance of the order in which instrument readings are made (30) or are concerned with design details, such as the arrangement of instrument panels.

There is also a large area of endeavor in which transfer functions for simple tasks are proposed and experiments carried out to test the validity of the model. One of the earliest efforts at writing a human transfer function, due to Tustin (31), appeared in 1947. Various models have been suggested since, usually for the control of a simple linear dynamic object through a simple interface. A review of much of the work done in this area is given by Gaines (32) and a rather extensive bibliography of the manual control literature is provided by McRuer and Weir (33). Perhaps the latest published work which broadly treats manual control is that of Heer (34).

An idea advanced by Baron and Kleinman in 1968 has potential for developing into a relatively general model of human behavior in complex control tasks and is the basis for the human dynamic model used in this thesis. References 35, 36, 37, and 38 give detailed information on the development of this approach, which is based on assumptions about the general nature of human performance and human limitations in control tasks. The model is best applied to a well trained operator who is familiar with his task and with the characteristics of the machine which he

controls, is aware of the criterion against which his performance will be measured, and is well motivated to achieve a good score.

The premise for the model is that a well-trained well-motivated operator behaves in a near optimal manner subject to certain inherent constraints. No apriori structure of the controller is assumed, a significant step toward generality, which is true only of this model. In the development by Baron et al, the limitations on human performance appear as a combination neuro-physiological and perceptual delay and the imposition of gaussian white observation noise on the visual feedback signal. It is possible, therefore, to account for greater or lesser degrees of operator motivation and physical aptitude by varying the time delay and the power of the observational noise.

The mathematical development requires that a quadratic performance index be minimized. This is the scoring method by which the operator judges his performance and it has a significant effect on the results achieved. The performance index places relative weights on integrated system error and integratrated control effort and is therefore another factor which may be used to reflect varying degrees of operator motivation.

In the Baron model the human receives delayed noisy information about the state of the control object, uses his knowledge of the system dynamics to construct a "best estimate" of the true delayed state of the system, compensates for his time delay by "predicting" the present system state (again based on knowledge of the system dynamics), and then acts on this information to control the object in a near optimal manner.

The greatest limitation of the Baron model is the computational formidability of the analysis required to determine the gains of the controller and the state estimator. (The systems to which the model had been applied in the references had at maximum four state variables while the refuse accumulator model investigated here has 23.)

Modified Near Optimal Human Operator Model

The assumption that a well-trained and highly motivated human operator performs in a near optimal manner subject to inherent limitations has been advanced and tested in the literature (35, 36, 37). The assumption makes no apriori judgements on the structure of the equivalent mechanical controller and provides for varying degrees of operator capability and motivation. As presented in the literature, however, the model is limited by formidable computational requirements which preclude its use for systems with a large number of state equations. In this section, a technique is developed which retains the optimal controller concepts but which is more readily applied to the large scale refuse accumulation system, especially as a design tool.

The computational difficulties with the Baron model arise in part from the necessity to solve two sets of matrix Riccati equations of the order of the system in determining the optimal controller and state estimator gains. In the current application this would require the solution of two sets of 529 simultaneous nonlinear differential equations for each alternative accumulation configuration!

Another computational difficulty arises from the imposition of a time delay on the system which precludes the use of a probablistic "expected value" approach

to performance, desirable in design, and would require instead that a series of deterministic simulations be executed.

The modified human operator model retains the optimal-controller concept but relies on the selection of an appropriate weighting scheme for the system performance index to account for human neuro-physiological limitations. The imposition of gaussian white noise on the visual feedback path used by the Baron model to account for observational error is eliminated and in its place the dimensions of the operator's state space "target" are reduced. The modified model is more readily applied to large systems and its adaptability to this application is enhanced by a fortuitous uncoupling of the controller Riccati equation.

The system state equations presented in Chapter IV may be written in matrix form as

$$\dot{\bar{X}} = \bar{A}\,\bar{X} + \bar{B}\,\bar{U} + \bar{Q}\,\bar{W} \tag{83}$$

where $\bar{A}$, $\bar{B}$ and $\bar{Q}$ are constant coefficient matrices, $\bar{X}$ is the system state vector, $\bar{U}$ is the operator's control input vector, and $\bar{W}$ is the gaussian white noise vector input to the road noise simulation portion of the model. The operator's observation of the system state is a subset of the state variables $\bar{Y}$, given by

$$\bar{Y} = \bar{C}\,\bar{X} \tag{84}$$

where $\bar{C}$ is a diagonal matrix with diagonal elements C_{ii} equal to either 1 or 0. Thus the operator's estimate of unobserved states is zero. Near the critical operating point, which occurs when the accumulator is performing its "capture"

function, the operator's task is to keep the accumulator within range of the target in the face of random road noise inputs. He must regulate the position and velocity of the accumulator within tolerances prescribed by the capture subsystem in order that pick up can occur.

The optimal regulator problem has been investigated rather extensively in the literature and is given excellent treatment in references 39 and 40. The plant described by equation 83 to be controlled optimally so as to minimize a quadratic performance index of the form

$$J = \int_0^T (\bar{X}^T \bar{F}_x \bar{X} + \bar{U}^T \bar{F}_u \bar{U}) dt \tag{85}$$

where T is the (unspecified) end time and $\bar{F}_x$ and $\bar{F}_u$ place relative weights on the penalty associated with system state $\bar{X}$ and control input $\bar{U}$. The optimal control law which minimizes the performance index J is given by

$$\bar{U}_o = -\bar{G}\,\bar{X} \tag{86}$$

but in this application $\bar{X}$ may not be fully known and is therefore approximated by

$$\hat{\bar{X}} = \bar{Y} \tag{87}$$

$\bar{G}$ is the optimal controller gain matrix given by

$$\bar{G} = \bar{F}_u^{-1} \bar{B}^T \bar{H} \tag{88}$$

where $\bar{H}$ is defined as the positive definite symmetric steady state solution to the

matrix Riccati equation

$$\frac{d}{dt}\bar{H}(t) = -\bar{A}^T \bar{H}(t) - \bar{H}(t)\bar{A} + \bar{H}(t)\bar{B}\,\bar{F}_u^{-1}\bar{B}^T\bar{H}(t) - \bar{F}_x \tag{89}$$

with the boundary condition that $\bar{H}(T)$ is the null matrix.

Equation 84 may be substituted into equation 87 and the result substituted into equation 86 to yield

$$\bar{U}_o = -\bar{G}\,\bar{C}\,\bar{X} \tag{90}$$

which combined with equation 83 yields the state equations for the closed loop plant, including the human operator:

$$\dot{\bar{X}} = \bar{A}\,\bar{X} - \bar{B}\,\bar{G}\,\bar{C}\,\bar{X} + \bar{Q}\,\bar{W} \tag{91}$$

or

$$\dot{\bar{X}} = (\bar{A} - \bar{B}\,\bar{G}\,\bar{C})\,\bar{X} + \bar{Q}\,\bar{W} \tag{92}$$

By an appropriate choice of $\bar{F}_x$ and $\bar{F}_u$ in equation 85, the human operator gains $\bar{G}$ (equation 88) can be determined so that the control inputs $\bar{U}_o$ (equation 86) are within the range of human capability. The effect of observational noise can be accounted for in the time solution of equation 92 by requiring that tolerances on acceptable accumulator to refuse range and range rate, as required by a specific "capture" sub-system alternative, are equivalently reduced. For example, the simulation of a capture alternative tolerant of range and range rate error e could account for observational noise with standard deviation σ by engaging a state space target of dimension $e-2\sigma$.

Mathematical Details Critical to the Computational Success of the Model

As indicated previously, solution of the matrix Riccati equation in the form given as equation 89 is highly impractical, and if no alternative were found to the straight forward time solution of this equation, the mathematical model of the human operator presented in the last section would have to be abandoned. There are in the literature (38, 41) alternative solution techniques for the Riccati equation but their application is limited either by computer storage requirements or the necessity to reconstitute the entire problem including the plant equations in a special form.

The approach that was used takes advantage of the fact that in the solution sought is the positive definite symmetric steady state solution for which

$$\frac{d}{dt}\bar{H}(t) = \bar{0} \tag{93}$$

This might lead one to look at equation 89 as a set of 529 non-linear simultaneous algebraic equations, but the computational difficulties attendant to that approach are also severe. The following derivation has little intuitive motivation but a fortuitous conclusion.

The system matrix $\bar{A}$ which describes the refuse accumulator may be partitioned as follows:

$$\bar{A} = \begin{bmatrix} \bar{A}_{vv}(6,6) & \bar{A}_{rv}(6,8) & \bar{0}(6,9) \\ \bar{0}(8,6) & \bar{A}_{rr}(8,8) & \bar{0}(8,9) \\ \bar{A}_{va}(9,6) & \bar{0}(9,8) & \bar{A}_{aa}(9,9) \end{bmatrix} \tag{94}$$

The dynamic coupling which occurs between the elements of the system are indicated by the subscripts and the numbers in parentheses are the row, column dimensions of the partitioned matrices. For example, $\bar{A}_{rv}$ refers to the term of the $\bar{A}$ matrix which couple the vehicle and the road, while $\bar{A}_{va}$ contains terms coupling the vehicle and the accumulator.

Also appearing in equation 89 is $\bar{A}$ transpose,

$$\bar{A}^T = \begin{bmatrix} \bar{A}^T_{vv}(6,6) & \bar{0}(6,8) & \bar{A}^T_{va}(6,9) \\ \bar{A}^T_{rv}(8,6) & \bar{A}^T_{rr}(8,8) & \bar{0}(8,9) \\ \bar{0}(9,6) & \bar{0}(9,8) & \bar{A}^T_{aa}(9,9) \end{bmatrix} \tag{95}$$

and $\bar{B}$ which may be partitioned into

$$\bar{B} = \begin{bmatrix} \bar{0}(6,3) \\ \bar{0}(8,3) \\ \bar{B}_a(9,3) \end{bmatrix} \tag{96}$$

with transpose $\bar{B}^T = [\, \bar{0}(3,6) \;\; \bar{0}(3,8) \;\; \bar{B}^T_a(3,9) \,]$ (97)

$\bar{F}_u$ is a diagonal matrix with equal weights F_u on all inputs so that

$$\bar{F}_u^{-1} = \begin{bmatrix} \frac{1}{F_u} & 0 & 0 \\ 0 & \frac{1}{F_u} & 0 \\ 0 & 0 & \frac{1}{F_u} \end{bmatrix} \tag{98}$$

The operator has no control over the vehicle oscillations or road noise, so the state weighting matrix $\bar{F}_x$ is null except for the terms which relate to the accumulator states, and therefore may be partitioned thus:

$$\bar{F}_x = \begin{bmatrix} \bar{0}(6,6) & \bar{0}(6,8) & \bar{0}\ (6,9) \\ \bar{0}(8,6) & \bar{0}(8,8) & \bar{0}\ (8,9) \\ \bar{0}(9,6) & \bar{0}(9,8) & \bar{F}_{x_a}(9,9) \end{bmatrix} \tag{99}$$

The $\bar{H}$ which is the steady state solution to equation 89 is symmetric and may be partitioned as follows:

$$\bar{H} = \begin{bmatrix} \bar{H}_{11}(6,6) & \bar{H}_{12}(6,8) & \bar{H}_{13}(6,9) \\ \bar{H}_{12}^T(8,6) & \bar{H}_{22}(8,8) & \bar{H}_{23}(8,9) \\ \bar{H}_{13}^T(9,6) & \bar{H}_{23}^T(9,8) & \bar{H}_{33}(9,9) \end{bmatrix} \tag{100}$$

If equations 94 through 100 are substituted into equation 89 the result is

$$\dot{\bar{H}}_{11} = -\bar{A}_{vv}^T\bar{H}_{11} - \bar{A}_{va}^T\bar{H}_{13}^T - \bar{H}_{11}\bar{A}_{vv} - \bar{H}_{13}\bar{A}_{va} + \bar{H}_{13}\bar{B}_a\bar{F}_u^{-1}\bar{B}_a^T\bar{H}_{13}^T \tag{101}$$

$$\dot{\bar{H}}_{12} = -\bar{A}_{vv}^T\bar{H}_{12} - \bar{A}_{va}^T\bar{H}_{23}^T - \bar{H}_{11}\bar{A}_{rv} - \bar{H}_{12}\bar{A}_{rr} + \bar{H}_{13}\bar{B}_a\bar{F}_u^{-1}\bar{B}_a^T\bar{H}_{23}^T \tag{102}$$

$$\dot{\bar{H}}_{13} = -\bar{A}_{vv}^{T}\bar{H}_{13} - \bar{A}_{va}^{T}\bar{H}_{33} - \bar{H}_{13}\bar{A}_{aa} + \bar{H}_{13}\bar{B}_{a}\bar{F}_{u}^{-1}\bar{B}_{a}^{T}\bar{H}_{33} \tag{103}$$

$$\dot{\bar{H}}_{22} = -\bar{A}_{rv}^{T}\bar{H}_{12} - \bar{A}_{rr}^{T}\bar{H}_{22} - \bar{H}_{12}^{T}\bar{A}_{rv} - \bar{H}_{22}\bar{A}_{rr} + \bar{H}_{23}\bar{B}_{a}\bar{F}_{u}^{-1}\bar{B}_{a}^{T}\bar{H}_{23}^{T} \tag{104}$$

$$\dot{\bar{H}}_{23} = -\bar{A}_{rv}^{T}\bar{H}_{13} - \bar{A}_{rr}^{T}\bar{H}_{23} - \bar{H}_{23}\bar{A}_{aa} + \bar{H}_{23}\bar{B}_{a}\bar{F}_{u}^{-1}\bar{B}_{a}^{T}\bar{H}_{33} \tag{105}$$

$$\dot{\bar{H}}_{33} = -\bar{A}_{aa}^{T}\bar{H}_{33} - \bar{H}_{33}\bar{A}_{aa} + \bar{H}_{33}\bar{B}_{a}\bar{F}_{u}^{-1}\bar{B}_{a}^{T}\bar{H}_{33} - \bar{F}_{x} \tag{106}$$

Equation 106 is a matrix Riccati equation exactly the same form as equation 89, however $\bar{H}_{33}$ is a nine by nine matrix while $\bar{H}$ is 23 by 23. By initiating the integration of equation 106 with $\bar{H}_{33} = \bar{0}$ and proceeding backwards in time, the steady state solution may be found in approximately 20 seconds on the Univac 1108.

With the steady state solution for $\bar{H}_{33}$ in hand, equations 101 through 105 may be solved for their steady state symmetric solutions by equating the right hand side of these equations to the null matrix. Fortuitously equation 103 becomes linear in $\bar{H}_{13}$ with $\bar{H}_{33}$ known, and similarly equation 101 becomes linear in $\bar{H}_{11}$ given $\bar{H}_{13}$. Further, equation 105 is linear in $\bar{H}_{23}$ when $\bar{H}_{13}$ and $\bar{H}_{33}$ are known, and equation 102 becomes linear in $\bar{H}_{12}$ given $\bar{H}_{13}$ and $\bar{H}_{23}$. Finally equation 104 becomes linear in $\bar{H}_{22}$ given $\bar{H}_{12}$ and $\bar{H}_{23}$. The symmetry of the $\bar{H}$ matrix may be used to reduce the number of algebraic equations which must be solved still further. Table 9 summarizes the computational requirements for obtaining a solution to equation 89. Full solutions of the differential and algebraic equations require approximately 30 seconds of central processor time on the Univac 1108. By comparison, a direct solution of equation 89, initiating the integration at

$\bar{H} = \bar{0}$ and proceeding backwards in time, is estimated to require approximately 20 minutes of computation time.

Table 9. Summary of Computational Requirements of Solving Equation 85

Partition	Dimension Row	Dimension Column	Symmetry Yes	Symmetry No	Differential Equations	Algebraic Equations
H_{33}	9	9	x		45	0
H_{13}	6	9		x	0	54
H_{11}	6	6	x		0	21
H_{23}	8	9		x	0	72
H_{12}	6	8		x	0	48
H_{22}	8	8	x		0	36
				Total	45	231

CHAPTER VI

ADAPTATION OF THE MODELS TO COMPUTER SIMULATION

Introduction

The refuse accumulator system with its human operator, described by equation 92, is stochastic due to the random nature of the road noise disturbance. Two approaches are available for evaluating the performance of alternative configurations of this system.

A series of deterministic simulations of the system operating over roads which had been mathematically generated so as to have the same power spectrum as a real road could be conducted. To achieve good matching of the road profile power spectrum at the longer wavelengths, each simulated road would have to be quite long (approximately 200 feet) and several simulations would have to be run over different roads to obtain information on the average performance to be expected on any road. This is the approach which would have been required had a neurophysiological delay been explicitly included in the human operator model.

Another approach, more ideally suited to the design situation, treats equation 92 entirely from a stochastic viewpoint. This approach permits the "expected value" of the system state to be determined in a single time domain solution of the state equation. The expected value of a random variable is the mean value of the variable which would be approached if a sufficiently large number of experimental trials were conducted. In the application at hand the expected

value of the system state variables can be thought of as the most likely value which would be measured in a trial run of the refuse accumulator. The advantage of this approach in the design situation is obvious and its desirability is further enhanced by the reduction in computation time required. The computer programs used in this investigation implement the expected value approach and are documented in Appendix V.

Adaptation of the State Equation to Digital Computation

Digital computation is inherently a discrete time process and its application to continuous equations requires some special considerations which are investigated in this section.

For convenience define

$$\bar{A}^* = \bar{A} - \bar{B}\,\bar{G}\,\bar{C} \tag{107}$$

so that equation 92 may be written

$$\dot{\bar{X}} = \bar{A}^*\,\bar{X} + \bar{Q}\,\bar{W} \tag{108}$$

Equation 108 has a well known general solution in terms of the matrix exponential and the convolution integral (39):

$$\bar{X}(t - t_o) = e^{\bar{A}^*(t-t_o)}X(t_o) + \int_{t_o}^{t} e^{\bar{A}^*(t-\tau)}\bar{Q}\,\bar{W}(\tau)d\tau \tag{109}$$

To discretize equation 108, equation 109 is applied over the interval

$$KT < t \leq (K+1)\,T \tag{110}$$

where T is the integration step size:

$$\bar{X}_{K+1} = e^{\bar{A}^* T}\bar{X}_K + e^{\bar{A}^* T}\int_{KT}^{(K+1)T} e^{-\bar{A}^*\tau}\bar{Q}\,\hat{\bar{W}}(\tau)d\tau \qquad (111)$$

Since $\bar{W}(\tau)$ is a random variable we must use its average value $\hat{\bar{W}}$ in each step of the discretized state equations. The average noise $\hat{\bar{W}}$ is also a random variable with covariance $\underline{W}_d$ related to the covariance of the continuous noise $\bar{W}$, $\underline{W}_c$ by (39)

$$\underline{W}_d = \frac{1}{T}\underline{W}_c \qquad (112)$$

As $\hat{\bar{W}}(\tau)$ is a constant, $\hat{\bar{W}}_K$, over the interval 110, equation 111 may be integrated:

$$\begin{aligned}\bar{X}_{K+1} &= e^{\bar{A}^* T}\bar{X}_K + e^{\bar{A}^* T}(\bar{I} - e^{-\bar{A}^* T})\bar{A}^{*-1}\bar{Q}\,\hat{\bar{W}}_K \\ &= e^{\bar{A}^* T}\bar{X}_K + (e^{\bar{A}^* T} - \bar{I})\bar{A}^{*-1}\bar{Q}\hat{\bar{W}}_K\end{aligned} \qquad (113)$$

where $\bar{I}$ is the identity matrix. If new matrices are defined

$$\begin{aligned}\bar{P} &= e^{\bar{A}^* T} \\ \bar{R} &= (\bar{P} - \bar{I})\bar{A}^{*-1}\bar{Q}\end{aligned} \qquad (114)$$

equation 113, the discretized system state equations, may be written

$$\bar{X}_{K+1} = \bar{P}\bar{X}_K + \bar{R}\,\hat{\bar{W}}_K \qquad (115)$$

Determination of a Relation for Successive State Covariances

The transpose of equation 115 is

$$\bar{X}_{K+1}^{T} = \bar{X}_{K}^{T}\bar{P}^{T} + \hat{\bar{W}}_{K}^{T}\bar{R}^{T} \tag{116}$$

which when right multiplied on each side of equation 115, followed by taking the expectation of each term, yields:

$$E\left[\bar{X}_{K+1}\bar{X}_{K+1}^{T}\right] = \bar{P}\,E\left[\bar{X}_{K}\bar{X}_{K}^{T}\right]\bar{P}^{T} + \bar{R}\,E\left[\hat{\bar{W}}_{K}\hat{\bar{W}}_{K}^{T}\right]\bar{R}^{T} \tag{117}$$

since

$$E\left[\bar{X}_{K}\hat{\bar{W}}_{K}^{T}\right] = E\left[\hat{\bar{W}}_{K}\bar{X}_{K}^{T}\right] = \bar{0} \tag{118}$$

Equation 118 simply implies that the system state and the road noise are uncorrelated. Since the road profile is stationary:

$$E\left[\hat{\bar{W}}_{K}\hat{\bar{W}}_{K}^{T}\right] = \underline{W}_{d}\,, \tag{119}$$

the constant road noise covariance matrix defined by equation 112. Equation 117 is therefore a recursion formula for successive state covariance matrices $\underline{X}_{K}$.

$$\underline{X}_{K} = E\left[\hat{\bar{X}}_{K}\hat{\bar{X}}_{K}^{T}\right] \tag{120}$$

which may be written

$$\underline{X}_{K+1} = \bar{P}\,\underline{X}_{K}\bar{P}^{T} + \bar{R}\,\underline{W}_{d}\bar{R}^{T} \tag{121}$$

Equation 121 provides a great deal of information about the system, obtained primarily from the definition of some scaler (in particular any of the state variables of interest) by the equation

$$S_K = \bar{c}\ \bar{X}_K \tag{122}$$

where $\bar{c}$ is a row vector. The expected value of S_K^2 is given by

$$E\left[S_K^2\right] = \bar{c}\,\underline{X}_K\,\bar{c}^T \tag{123}$$

Control Effort and State Weighting Matrices

The control effort and state weighting matrices $\bar{F}_u$ and $\bar{F}_x$ which are used in the performance index J (equation 85) of the human operator model must be constructed so that the index measures those characteristics of the system performance which should be minimized. The relative magnitude of the terms in $\bar{F}_x$ and $\bar{F}_u$ determine the extent to which the operator expends his effort to improve system performance, and the relative magnitudes of weights within the matrices place greater or lesser importance on one state or one input over another.

In the master-slave control situation there is no justification for placing greater weight on control effort in one direction over another, and relative weighting between control and state variables could be achieved by adjustment of the state weighting matrix $\bar{F}_x$, so that the control matrix $\bar{F}_u$ may be equated to the identity matrix with no sacrifice in generality:

$$\bar{F}_u = \bar{I} \tag{124}$$

The control problem was stated in terms of an optimal regulator problem where the desired regulated state is zero position error of the accumulator tip when situated directly over the refuse. Where very flexible accumulators are employed, the operator might modify his strategy to avoid excessive deflections, and provisions for this can also be made in the performance index.

The quadratic inside the integral of equation 85 which would accomplish the weighting objectives described above is of the form

$$u^2 + ar^2 + bd^2 \tag{125}$$

where u is the magnitude of the control vector, r the magnitude of the position error of the accumulator tip from the refuse, and d the accumulator deflections. Weights a and b place relative emphasis on position error, deflections, and control effort.

In order to achieve a weighting scheme, equation 125, which is comparable with the control problem formulation, a state weighting matrix $\bar{F}_x$ must be found such that

$$\bar{X}^T \bar{F}_x \bar{X} = ar^2 + bd^2 \tag{126}$$

The squared position error is given in terms of the state variables defined in Table 8 by

$$r^2 = X_{15}^2 + X_{18}^2 + X_{21}^2 \tag{127}$$

and the squared deflection by

$$d^2 = (X_{15} - X_{17})^2 + (X_{18} - X_{20})^2 + (X_{21} - X_{23})^2 \tag{128}$$

Substitution of equations 127 and 128 into equation 126 gives

$$\begin{aligned} \bar{X}^T \bar{F} \bar{X} = {} & (a+b)X_{15}^2 + (a+b)X_{18}^2 + (a+b)X_{21}^2 - 2bX_{15}X_{17} \\ & - 2bX_{18}X_{20} - 2bX_{21}X_{23} + bX_{17}^2 + bX_{20}^2 + bX_{23}^2 \end{aligned} \tag{129}$$

Equation 99, the partitioned form of the $\bar{F}_x$ matrix, shows that the only non zero terms of $\bar{F}_x$ are in the nine by nine partition $\bar{F}_{x_a}$. If $\bar{F}_{x_a}$ is the matrix

$$\begin{bmatrix} a+b & 0 & -b & 0 & 0 & 0 & 0 & 0 & 0 \\ 0 & 0 & 0 & 0 & 0 & 0 & 0 & 0 & 0 \\ -b & 0 & b & 0 & 0 & 0 & 0 & 0 & 0 \\ 0 & 0 & 0 & a+b & 0 & -b & 0 & 0 & 0 \\ 0 & 0 & 0 & 0 & 0 & 0 & 0 & 0 & 0 \\ 0 & 0 & 0 & -b & 0 & b & 0 & 0 & 0 \\ 0 & 0 & 0 & 0 & 0 & 0 & a+b & 0 & -b \\ 0 & 0 & 0 & 0 & 0 & 0 & 0 & 0 & 0 \\ 0 & 0 & 0 & 0 & 0 & 0 & -b & 0 & b \end{bmatrix} \tag{130}$$

then $\bar{X}^T \bar{F}_x \bar{X}$ is precisely defined by equation 129. In the computer programs used to evaluate alternative configurations, matrix 130 is generated automatically when a and b are specified.

Extraction of System Performance Information From the State Covariance Matrix

In this section the necessary mathematical analysis is made to extract from the state covariance matrix $\underline{X}$, defined at any point in time by equation 121, the system performance indicators listed in Table 10.

Table 10. System Performance Indicators

- Expected value of actuator extension
- Expected value of actuator extension rate
- Expected value of accumulator tip position
- Expected value of accumulator tip position rate
- Expected value of accumulator deflection
- Expected value of accumulator deflection rate
- Expected value of operator's movement
- Expected value of operator's movement rate
- Relative control effort expended
- Average control effort expended
- System performance index

Equation 123 may be applied to extract the expected value of the square of any state variable X_i from $\underline{X}$ by defining the row vector $\bar{c}$ by

$$c_j = \begin{cases} 1 & j = i \\ 0 & j \neq i \end{cases} \tag{131}$$

The recursive use of equation 123 permits the expected value of the actuator extension squared to be determined as

$$E\left[E_a^2\right] = E\left[X_{17}^2 + X_{20}^2 + X_{23}^2\right] \tag{132}$$

and the expected value of the refuse accumulator tip position squared as

$$E\left[\bar{X}_a^2\right] = E\left[X_{15}^2 + X_{18}^2 + X_{21}^2\right] \tag{133}$$

Similarly the expected value of the accumulator tip displacement rate squared may be found:

$$E\left[\dot{\bar{X}}_a^2\right] = E\left[\dot{X}_{16}^2 + X_{19}^2 + X_{22}^2\right] \tag{134}$$

The operator's control movement is related to the actuator extension through the master-to-slave scale factor K_s by

$$E\left[E_m^2\right] = E\left[E_a^2\right]/K_s^2 \tag{135}$$

and may therefore be found from equation 132.

The rate at which the operator moves the master unit is a control input, related to the state of the entire system by the control strategy, equation 90:

$$\bar{U} = -\overline{GCX}$$

The covariance matrix $\underline{U}$ of the control input $\bar{U}$ at any time may be found by right multiplying equation 90 by its transpose and taking the expected value of both sides,

with the result:

$$\underline{U} = E\left[\bar{U}\,\bar{U}^T\right] = \bar{G}\,\bar{C}\;E\left[\bar{X}\,\bar{X}^T\right]\bar{C}^T\,\bar{G}^T$$

or (136)

$$\underline{U}_K = \bar{G}\,\bar{C}\,\underline{X}_K\,\bar{C}^T\,\bar{G}^T$$

The expected value of the control input (operator's movement rate) squared is then

$$E\left[\dot{E}_m^2\right] = \text{Trace}\,\{\underline{U}_K\} \tag{137}$$

and the actuator extension rate squared has expected value

$$E\left[\dot{E}_a^2\right] = K_S^2\;E\left[\dot{E}_m^2\right] \tag{138}$$

by the same argument as used for equation 135.

The relative control effort is the integrated control rate, ideally defined by

$$\text{relative control effort} = \int_o^t E\left[\dot{E}_m^2\right] dt \tag{139}$$

and computed as

$$\text{relative control effort} = \sum_{K=1}^{N} E\left[\dot{E}_m^2\right]_K T \tag{140}$$

where T is the step size. The practice an interpolation is used at the first and last steps to set initial conditions and determine capture time, and equation 140

appropriately modified to account for this. The average control effort is the relative control effort evaluated at the end of the operating period divided by the duration of operation T_c.

The expected value of the squared accumulator deflections may be determined by successive application of equation 123 with row vectors

$$c_{xj} = \begin{cases} 1 & j = 15 \\ -1 & j = 17 \\ 0 & \text{elsewhere} \end{cases}$$

$$c_{yj} = \begin{cases} 1 & j = 18 \\ -1 & j = 20 \\ 0 & \text{elsewhere} \end{cases} \qquad (141)$$

$$c_{zj} = \begin{cases} 1 & j = 21 \\ -1 & j = 23 \\ 0 & \text{elsewhere} \end{cases}$$

and is given by

$$E\left[d^2\right] = E\left[(X_{15} - X_{17})^2 + (X_{18} - X_{20})^2 + (X_{21} - X_{23})^2\right] \qquad (142)$$

To determine deflection rate expectations:

$$E\left[d^2\right] = E\left[(X_{16} - K_S U_1)^2 + (X_{19} - K_S U_2)^2 + (X_{22} - K_S U_3)^2\right] \qquad (143)$$

equation 143 is expanded:

$$E\left[\dot{d}^2\right] = E\left[X_{16}^2 + K_S^2 U_1^2 + K_S^2 U_2^2 + X_{22}^2 + K_S^2 U_3^2 \right.$$

$$\left. - 2K_S X_{16} U_1 - 2K_S X_{19} U_2 - 2K_S X_{22} U_3 \right] \tag{144}$$

The first six terms of the right hand side of equation 144 are readily available by the techniques previously described and are given by equations 134 and 137. To obtain the cross product terms define a dummy output vector

$$\bar{S}_K = \bar{D}\bar{X}_K \tag{145}$$

This equation is a vector form of equation 123. If 145 is transposed and right multiplied on the control strategy (equation 90) and the expection of both sides executed, the result is

$$E\left[\bar{U}_K \bar{S}_K^T\right] = -\bar{G}\,\bar{C}\,E\left[\bar{X}_K \bar{X}_K^T\right]\bar{D}^T \tag{146}$$

$\bar{D}$ may be chosen so that

$$E\left[\bar{U}_K \bar{S}_K^T\right] = E\begin{bmatrix} U_1X_{16} & U_1X_{19} & U_1X_{22} \\ U_2X_{16} & U_2X_{19} & U_2X_{22} \\ U_3X_{16} & U_3X_{19} & U_3X_{22} \end{bmatrix} \tag{147}$$

Equation 123 may now be employed to extract $E\left[U_1X_{16}\right]$, $E\left[U_2X_{19}\right]$, and $E\left[U_3X_{22}\right]$ from covariance matrix 147.

Evaluation of the system performance index is most easily accomplished by integrating equation 125, using appropriate expected values:

$$J = \int_0^t E\left[u^2 + ar^2 + bd^2\right] dt \qquad (148)$$

where $E\left[u^2\right]$ is given by equation 137, $E\left[r^2\right]$ is given by equation 133 and $E\left[d^2\right]$ is given by equation 142. The discrete time nature of digital simulation requires that equation 148 be computed in a manner similar to that given for equation 139.

Establishment of Initial Conditions

The human operator has been modeled by an optimal regulator in the vicinity of the target, where the performance of the system is most critical. The quadratic nature of the performance index results in little discrimination between target sizes if too large an initial error is assumed, due to the dominant effect on the penalty function of the initial portion of the state space path. To avoid this difficulty the idea of a "critical radius" is introduced, within which the operator is assumed to behave near optimally and external to which his behavior is not considered in evaluating alternatives.

For consistent comparison of the penalty function between alternatives, the accumulator is assumed to begin operation from this critical radius with zero initial velocity. In estimating "capture time," defined as the time required by the system to move from the critical radius to the state space target, it is reasonable to assume that the accumulator is moving toward the target at some initial velocity when the critical radius is reached. This corresponds to the assumption that the operator directs the accumulator toward the target initially without giving

the task his fullest concentration but begins to behave in an optimal manner when the critical radius is reached.

In order to establish non-zero initial velocity at the critical radius as an initial condition for estimating capture time, the optimal control system was initiated at zero velocity from a radius 3.5 times the critical radius. This has the advantage of providing a correlation between the quality of the alternative considered and the initial velocity at the critical radius, a feature to be expected in the operating system.

In practice it is necessary to interpolate to determine when the critical radius has been reached, and at this point the control effort and capture time are set at zero. Therefore the terms capture time time, relative control effort, and average control effort discussed in the analysis of the data, refer to these quantities measured from the critical radius to the target.

CHAPTER VII

ANALYSIS OF SIMULATION RESULTS

Introduction

In this chapter the data obtained from the computer simulation of the refuse accumulator will be presented and analyzed with the objective of formulating answers to the following questions:

1. What accumulator dynamic characteristics are most desirable for use in non-stop collection?
2. What is the relationship between non-stop collection feasibility and traveling speed?
3. Might modification of the collection vehicle suspension be desirable; in particular, is the installation of a ride augmentation system indicated?
4. How does alternative capture subsystem positional tolerance relate to system performance?

In preparation for an effective analysis of these questions preliminary consideration was given to the establishment of a benchmark system against which other alternatives could be measured. The first step in this process was the determination of a realistic road profile power spectrum as described in Chapter IV. As the road noise simulation filter described by Equation 25 involves vehicle suspension parameters, the identification of realistic vehicle dynamic

characteristics was necessary in order to simulate the road noise signal as well as to provide data for the vehicle dynamic model.

The vehicle for the benchmark system was selected from commercially available refuse bodies and truck chassis and is a 20 cubic yard "E-Z-Pack Side Loader" refuse body mounted on a Dodge L-700 cab-over-engine chassis. The side loading body type was chosen for its ready adaptability to automated refuse collection, as was the cab-over-engine chassis. A discussion of alternative packer body types and a detailed analysis of the dynamic characteristics of the benchmark chassis-body combination are included as Appendix VI.

Also of importance to the objectives of this investigation was the determination of the range of accumulator dynamic characteristics which were realizable in a physical system. To this end, Appendices VII and VIII are included. It was concluded from the study presented in Appendix VII that an accumulator with a 12 foot reach, weighing as little as 43 pounds and with a stiffness of up to 85 pounds per inch could be built. The accumulator design presented in the appendix also demonstrates the type of joint actuation and power transmission concepts which are necessary to the design of accumulators with little overhung weight.

The final effort necessary prior to the evaluation of potential alternatives was the determination of human operator performance index weights a and b (Equation 125) which would produce control inputs within the range of human capability. As a point of design philosophy it was decided that the accumulator should be constructed in such a way that the deflection of links in the kinematic chain would not enter the operator's control strategy, and therefore weight b was

equated to zero.

Several weights for tip position error were tested in the model with the benchmark vehicle and a relatively flexible lightly damped accumulator (m = 3 slugs, K = 10 lbs/in, ζ = .06) operating on a normally rough road at one mile per hour. Initial trials with a = 6, 18, 36 all resulted in excessively large control inputs (on the order of 5 to 10 feet per second). A more appropriate range for performance index weights proved to be a = 0.01, 0.1, 1.0, which resulted in maximum control inputs of 0.25, 0.82, and 1.91 feet per second respectively. Figure 11 shows the expected value of the tip position, tip velocity and actuator extension versus time for these values of position error weight a.

As may be seen from the figure, the lowest weight (a = .01) resulted in rather sluggish response, while the highest weight (a = 1.0) resulted in erratic tip velocity indicative of the large deflections also produced by this weighting scheme (0.67 feet).

The 0.82 feet per second control input required of the operator by the strategy in which a = 0.1 is not excessive and the resulting response is smooth and quick. For the reasons described in the previous paragraphs, the human operator model was fixed with the position error weight a = 0.1 and the deflection error weight b = 0.0 for evaluation of the alternative systems.

Kinematic Chain Dynamic Characteristics

To investigate the effect of varying kinematic chain dynamic characteristics on system performance, the accumulator alternative with the highest stiffness to

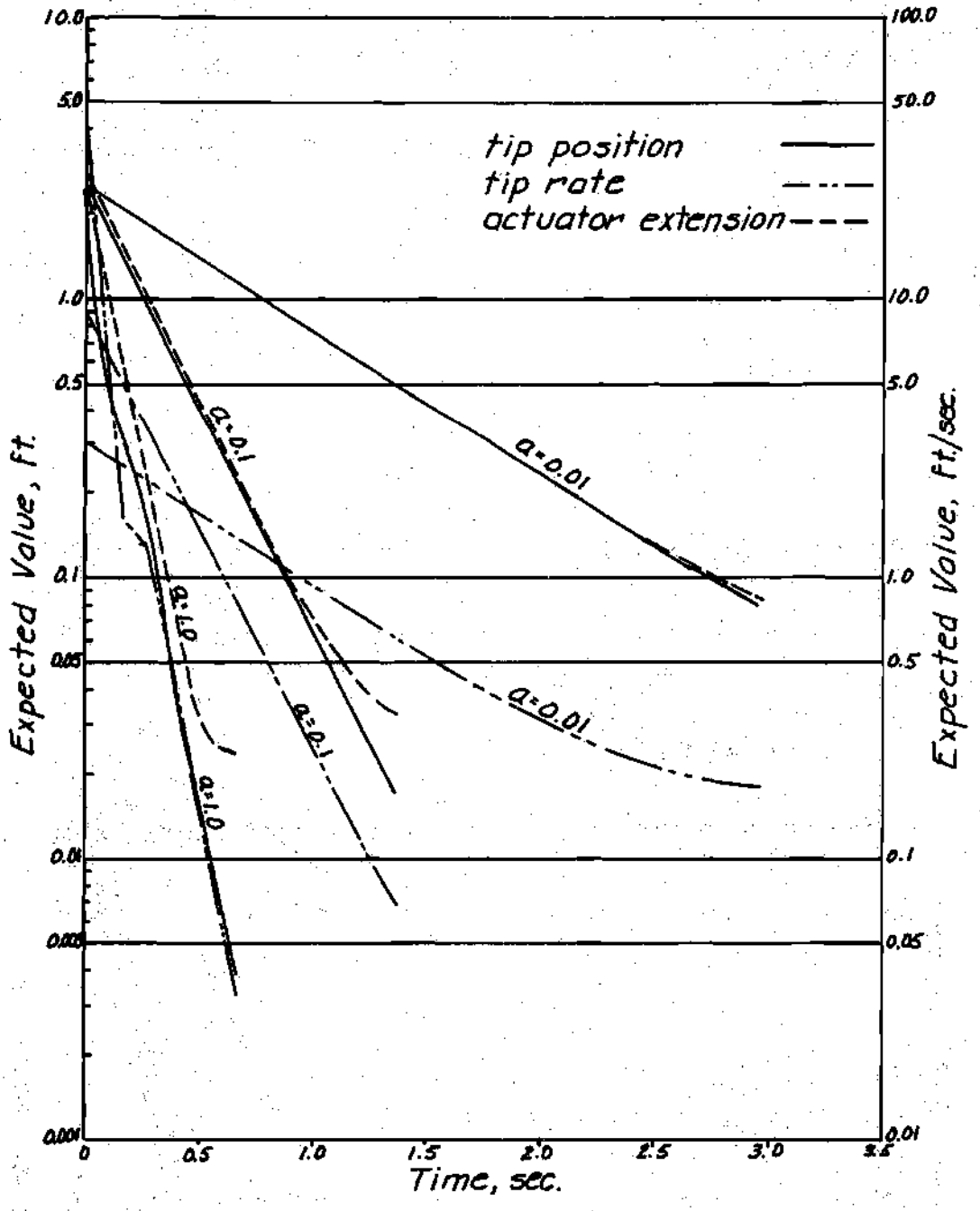

Figure 11. Performance at 1.0 MPH for AW = 1.0, 0.1, 0.01

weight ratio designed in Appendix VII was used in the system model. For fixed accumulator mass, trials were run on the benchmark vehicle with the accumulator stiffness varying between 85.4 and 20 pounds per inch and its damping ratio varying between 0.25 and 3.0. This series was conducted at both 0.25 and 0.50 miles per hour and the resulting values for the operator's penalty function are plotted in Figures 12 and 13. The higher boundary of each band in the figures represent the penalty associated with reaching a state space target for which the expected value of the accumulator range to the center of the refuse is 0.1 feet and the expected value of the extension rate is 0.1 feet per second. The lower boundary of each band is associated with a target permitting a 1.0 foot positional error and a 1.0 foot per second velocity at capture.

These data indicate that the operator's penalty function is reduced when chain stiffness is increased, or equivalently when the mass of the accumulator is reduced. The penalty function is also reduced with increased damping for the less rigid alternatives. The stiffer alternatives exhibit a reverse in this phenomena and the most rigid alternative displays a minimum penalty function for damping ratio $\zeta = 0.50$, which is an absolute minimum for all of the mass, stiffness, and damping ratio combinations tested. This agrees very well with empirical design rules which favor damping ratios of $\zeta = .7$ for "well designed" control systems.

Comparison of Figures 12 and 13 shows very little change in the penalty function versus accumulator dynamics relationship with vehicle speed in this narrow range. This is to be expected since small changes in vehicle speed

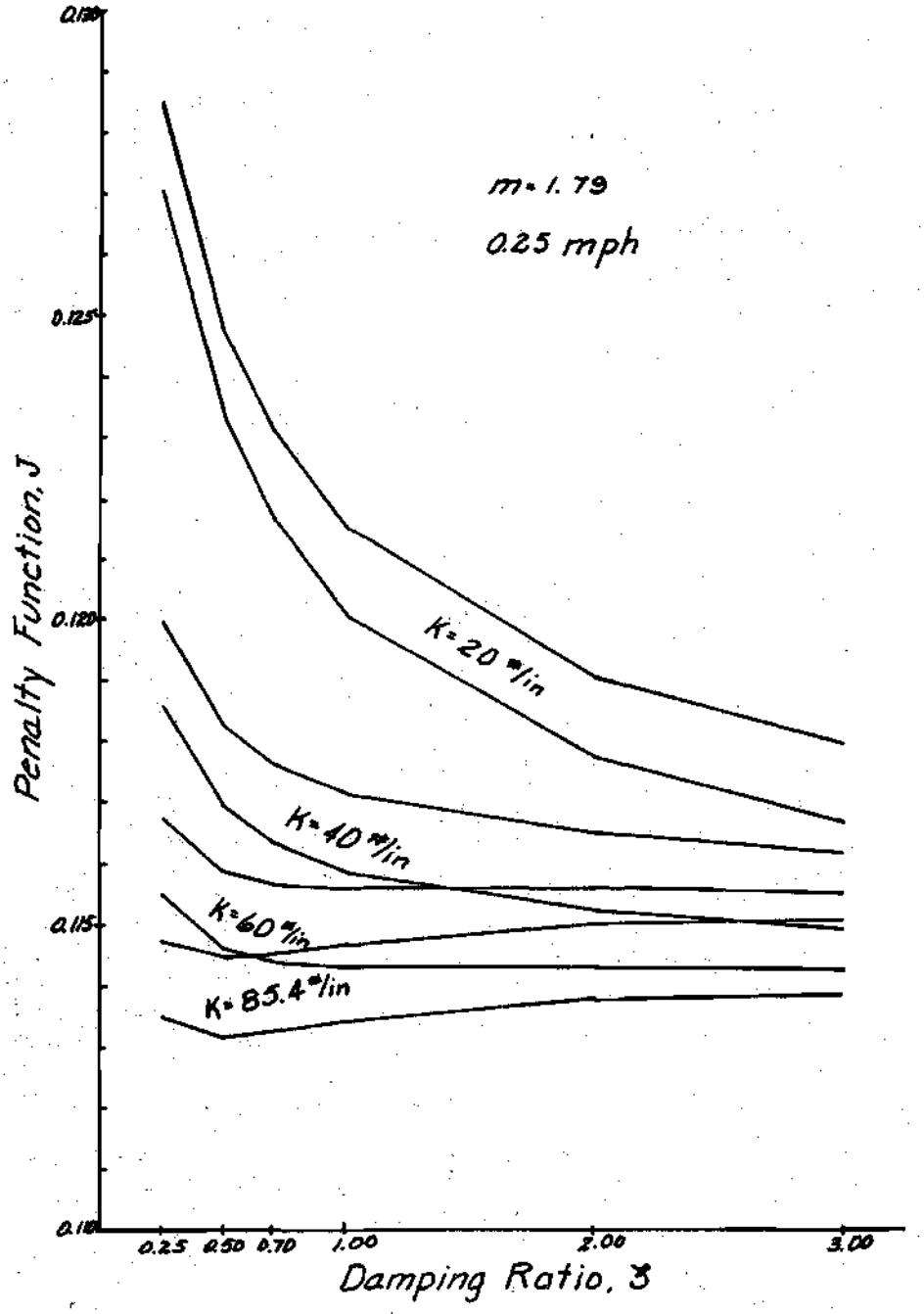

Figure 12. Variation in Penalty Function with Accumulator Dynamic Characteristics - 0.25 Miles per Hour

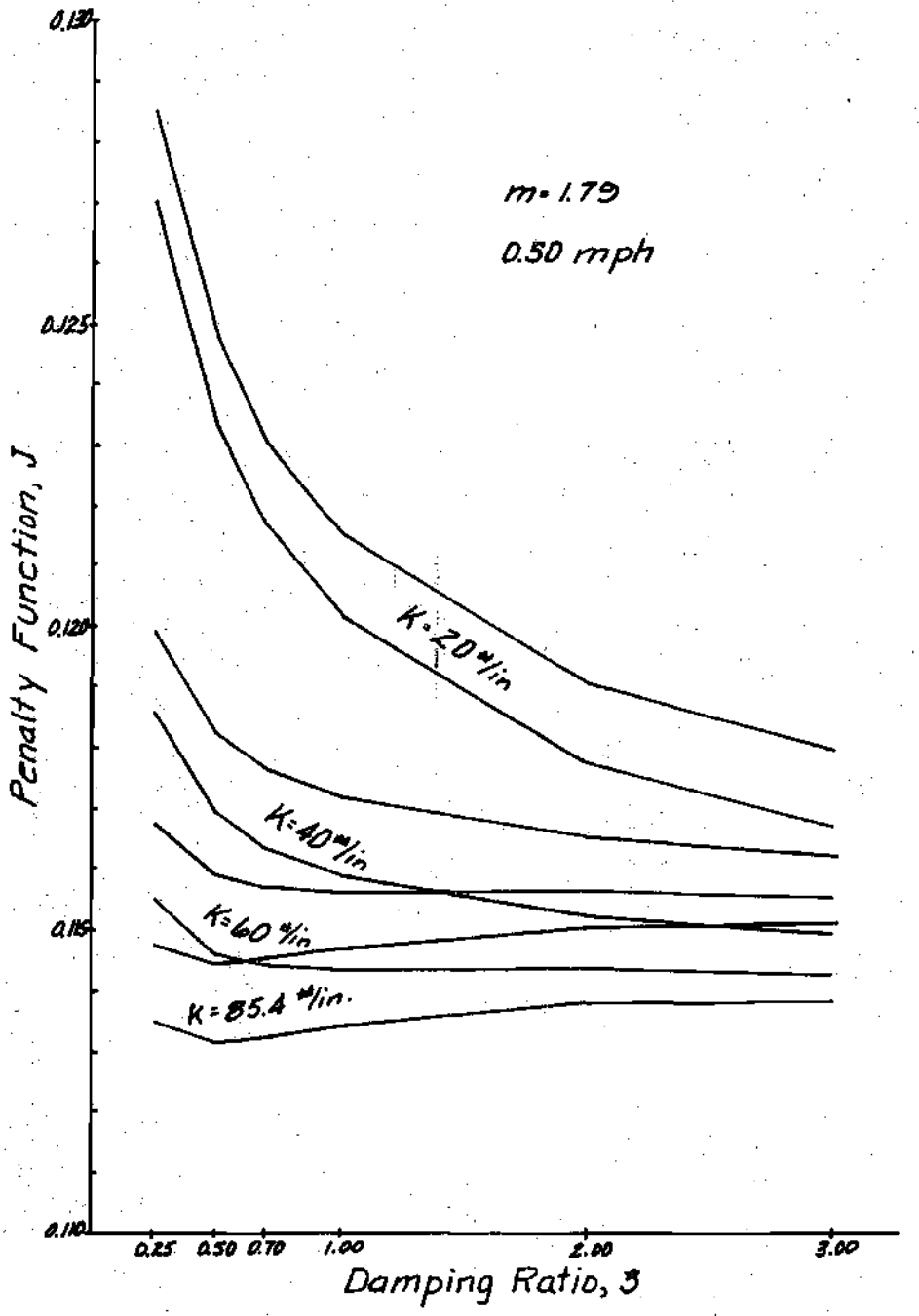

Figure 13. Variation in Penalty Function with Accumulator Dynamic Characteristics - 0.50 Miles per Hour

produce only small variations in the road noise power spectra.

The effect of damping ratio on capture time* is displayed in Figures 14 and 15, both of which are taken from data for the series of simultations discussed above. These results reinforce the conclusions drawn previously, showing the capture time to be more sensitive to damping ratio for the more flexible kinematic chain, where a large damping ratio is desirable. Significantly, however, the beneficial effect of increased damping ratio is less pronounced when smaller targets are engaged. Again the more rigid chain is superior in performance, and the relative insensitivity of capture time to damping ratio for this chain supports basing its damping ratio on the operator's penalty function.

Traveling Speed and Collection Feasibility

From the data presented in the last section, little variation in system performance is indicated when vehicle speed is varied over a narrow range. To investigate the effect of vehicle speed on system performance the kinematic chain with K = 40 pounds per inch $\zeta = 0.25$ and m = 1.79 slugs was simulated in operation on the benchmark vehicle at speeds ranging from 0.25 to 1.25 miles per hour. The accumulator tip position and actuator extension rate plotted versus time for this set of data are shown in Figure 16.

At 0.25 and 0.75 miles per hour the curves stop abruptly when the

---

*Capture time is the time required for the operator to move the accumulator from an initial state, 2.55 feet from the refuse and moving toward it, to the specified state space target. The 2.55 foot radius is the "critical radius" referred to in Chapter VI.

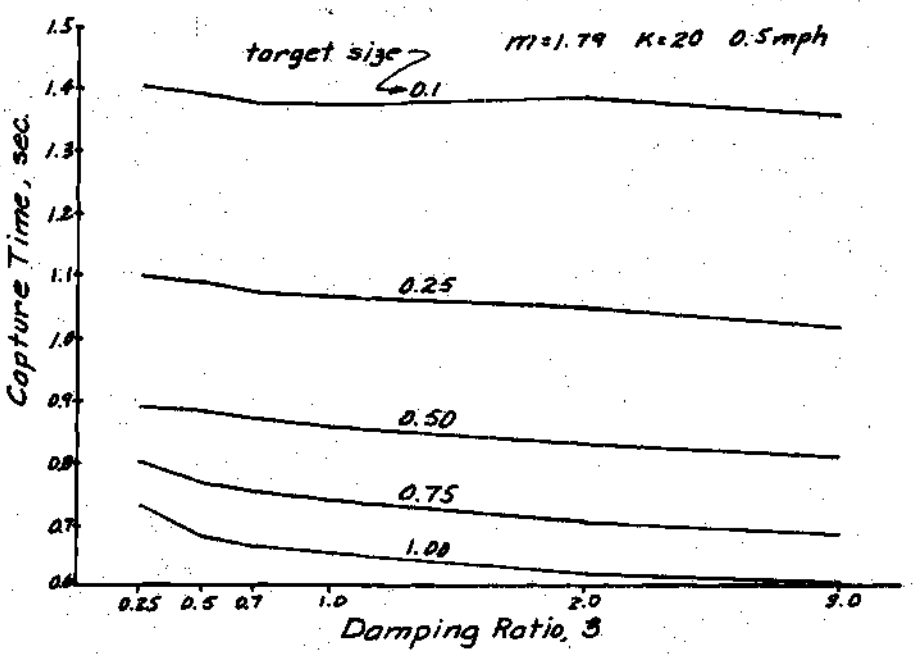

Figure 14. Capture Time Versus Damping Ratio and Target Size for m = 1.79, and K = 20

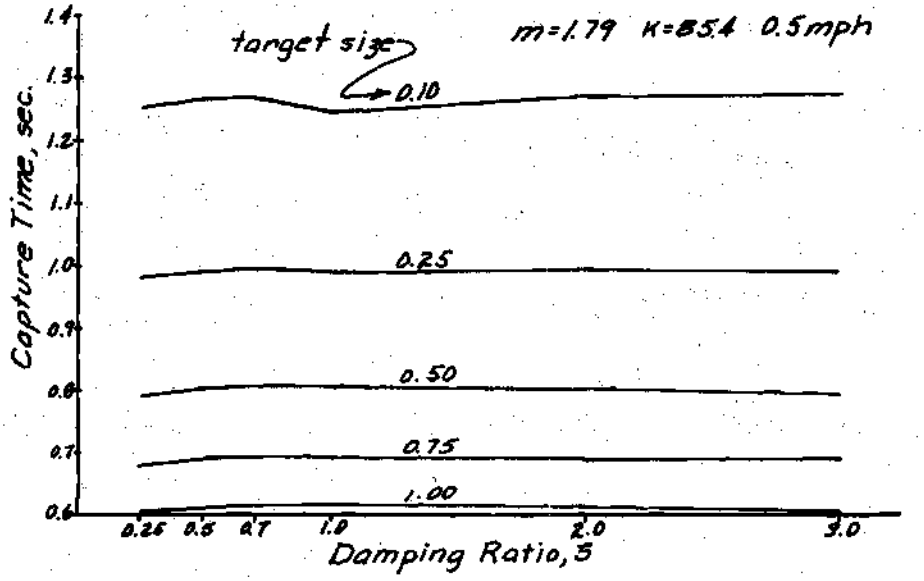

Figure 15. Capture Time Versus Damping Ratio and Target Size for m = 1.79 and K = 85.4

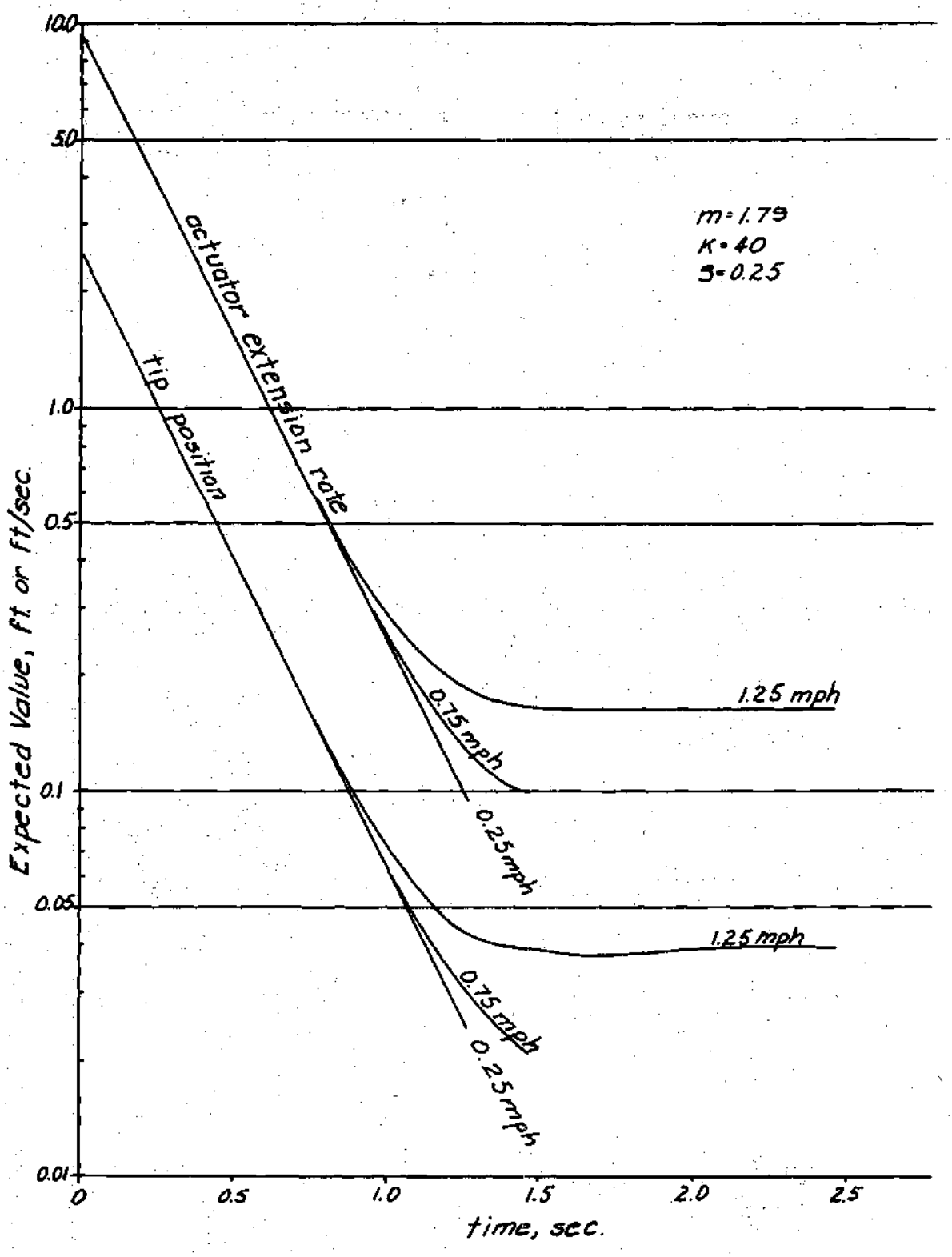

Figure 16. System Performance Versus Vehicle Speed

0.1 foot per second target is reached, determined in this case by the actuator extension rate. At 1.25 miles per hour this smallest target is never engaged and a steady state position error of 0.04 feet and steady state actuator rate of 0.162 feet per second are exhibited. These errors correspond roughly to the amplitude of oscillation about zero of the indicated variables. The frequency of the oscillation may be estimated if a sinusoidal form is assumed:

$$X = 0.04 \sin \omega t \tag{149}$$

The velocity is then given by

$$\dot{X} = 0.04\, \omega \cos \omega t \tag{150}$$

from which

$$\omega = \frac{.162}{(.04)(2\pi)} = .637 \text{ cycles per second.}$$

This frequency is well within the capability of the human operator and the steady state actuator rate is indicative of his continuing effort to overcome the road noise induced oscillations.

Presented in Figure 17 is a graph showing the time required to reach a state space target of specified size for the same data set. It is of interest that the time to target is more a function of target size than vehicle speed for those targets which are accessible, and that for fixed accumulator dynamic characteristics and road profile, accessibility is determined by vehicle speed.

Another consideration directly related to vehicle speed is the distance

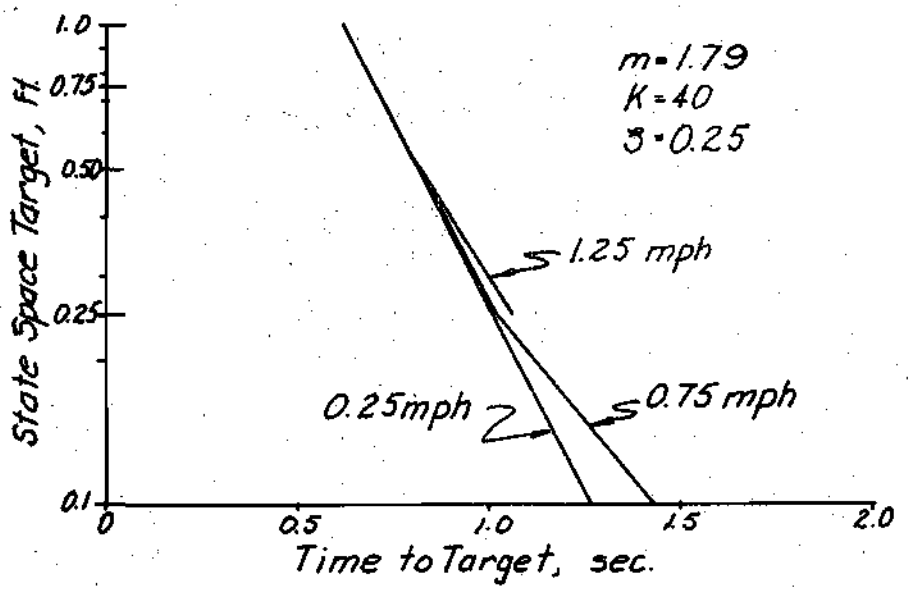

Figure 17. Capture Time Versus Target Size at Various Vehicle Speeds

traveled while the operator is attempting to achieve capture. He will of course use the forward motion of the vehicle to assist him in placing the accumulator on target, but to allow him maneuvering time it is felt that the vehicle should not travel further during the capture operation than one half the critical radius. In this analysis the "critical point," beyond which the operator is assumed to behave near optimally, was 2.55 feet from the target center, a distance consistently covered in approximately 1.5 seconds. The imposition of this constraint therefore limits travel during capture to approximately 1.3 feet and traveling speed to 0.5 miles per hour. Significantly, the 0.1 foot state space target is accessible to all of the potential accumulator chains tested when operated on the benchmark vehicle at 0.5 miles per hour over a road of normal roughness.*

Design Implications of Abnormally Rough Roads

The road of normal roughness referred to previously was generated by the procedure described in Chapter IV and is matched to the average of 16 profiles for well paved roads reported by Holbrook (17). The road profile under the left front tire is precisely this average profile, while the profile under the right front tire has 14 percent more power at all wavelengths than the left. This was done to simulate pavement degradation near the shoulders which is common in residential areas where curbs are not employed. Since the rear wheels carry dual tires, the

*The data discussed here was derived from simulations in which the benchmark vehicle was carrying a full payload. Due to the variable rate suspension with which the vehicle is equipped, very little difference in performance is noted in simulations conducted with an empty vehicle.

tire patch effect in averaging out the road roughness is more pronounced, so the profile power at each rear wheel was reduced somewhat from that at the front, eight percent at the left side and three percent at the right.

Not all areas where refuse is collected are blessed with well paved roads, so it is of interest to know how the automated refuse accumulator would perform under adverse road roughness conditions. To this end a simulation was conducted in which the benchmark vehicle and the $m = 1.79$, $K = 85.4$, $\zeta = 0.5$ kinematic chain were required to operate at 0.5 miles per hour over a poor quality unpaved surface with a profile exhibiting 34 times the power of the normal road at all wavelengths. In terms of profile amplitude, this corresponds to waves with 5.85 times the amplitude of those in a normal road.

The tip position and the actuator extension rate expectations for this case are shown versus time in Figure 18. The 0.5 foot state space target is the smallest engaged, leaving little room to compensate for observation error. It is therefore likely that the operator would be required to stop the vehicle in order to operate on such a roadway unless a form of ride augmentation were incorporated into the suspension system or a capture subsystem tolerant of larger errors in position and velocity were developed.

Design Considerations for the Capture Subsystem

Little has been said to characterize the capture subsystem except in Appendix VII where a grasp type capture alternative was considered in estimating the accumulator weight. The heavy dependence of capture time on target size shown

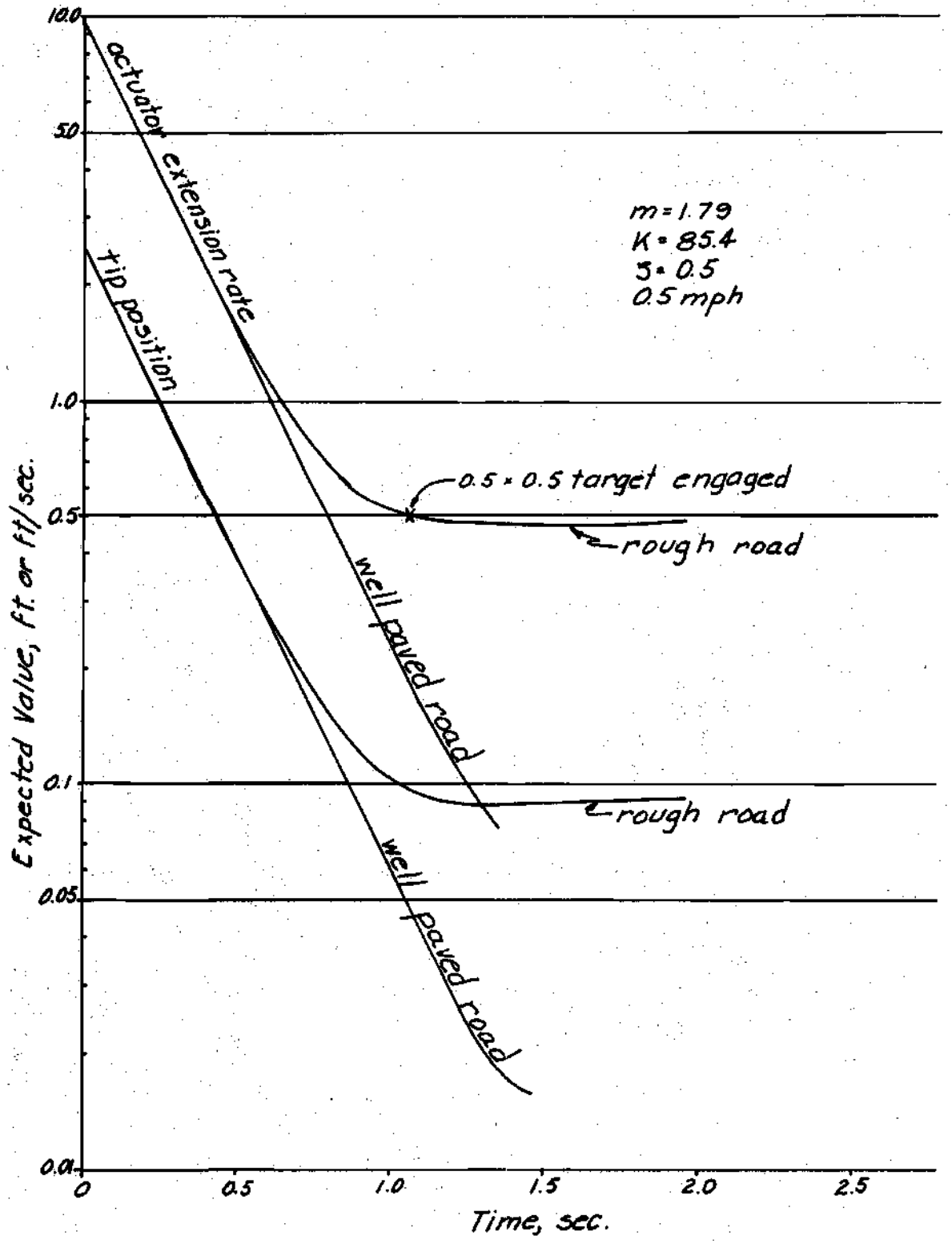

Figure 18. Operation on an Unpaved Road

in Figures 14, 15 and 17, and the necessity for large target tolerances for operation at higher speeds or over rough roads, shown in Figures 16 and 18 respectively, certainly demonstrate the desirability of a capture subsystem which can perform well in spite of large errors in position or velocity. It is likely that such systems would also have the capability to capture larger or more numerous refuse containers, presumably however, with a concomitant loss in error tolerance.

The data presented previously in this chapter should not be taken to mean that capture subsystems requiring position and velocity accuracy within 0.1 foot and 0.1 foot per second are acceptable for use in automated refuse accumulation systems. An important point in the development of the human operator model used in the simulation was that observation error could be accounted for by requiring the simulation to reach a proportionally smaller state space target than otherwise required by the capture subsystem. If, for instance, the operator's errors in judging range and range rate to the refuse have a standard deviation σ of 0.075 feet, the time required to achieve capture with a capture alternative tolerant of errors e up to 0.25 feet is best estimated by the time required for the simulation to reach a state space target with dimension

$$e - 2\sigma = 0.25 - 0.15 = 0.10 \text{ feet}$$

Also significant to system performance is the actuation time required by the capture subsystem to secure the refuse once on target. It is probable, though not necessarily unavoidable, that systems with larger target tolerance will also require additional time on target for actuation, so that a trade off between the

desirability of these two attributes may be necessary.

Power Requirements

The greatest actuator displacement rate found in any of the simulations was less than 10 feet per second. If it is assumed that an emergency maneuver requiring an instantaneous acceleration of three g is imposed on the system when it is operating at this rate,* and if the mass of the accumulator and refuse is 3 slugs, the instantaneous peak power requirement is

$$\frac{(3)\ (3)\ (3.2)\ (10)}{550} = 5.24 \text{ horsepower}$$

If the mechanical components of the accumulator (cables, pulleys, bearings and gears) are 80 percent efficient, a hydraulic system capable of delivering 6.60 horsepower to this load is required. Servovalve controlled actuators powered by variable displacement pumps have peak efficiencies on the order of 67 percent when the pressure drop across the load is two thirds of the supply pressure. A system designed for these operating conditions would therefore require a 10 horsepower hydraulic power supply. Such a power supply is capable of supplying 8.55 gallons per minute at 2000 psi.

Since the refuse accumulator is operated intermittently, it would be possible to reduce the pump size requirement by adding an appropriately sized hydraulic accumulator (surge tank) to the system. In any event, the power requirement of

*For systems designed to meet this requirement, the maximum acceleration achievable would be greater than three g if the accumulator were moving at less than 10 feet per second.

the accumulator is well within the feasible range for truck mounted equipment.

Performance of Automated Refuse Accumulators

Ralph Stone and Company (8) have investigated rather extensively the effect of crew size on solid waste collection costs in systems where only manual labor was employed to perform the "accumulation" function. Their conclusions regarding one-man crews are significant to this discussion:

> For curbside collection of refuse, one-man crews were more efficient than multi-man crews; the productivity of the one-man crew was greater than that of the multi-man crew when measured in terms of route man-hours per ton.
>
> The one-man crew was similarly more efficient than the multi-man crew for alley collection of refuse. . . .
>
> Under specified assumptions for important route factors and costs of equipment and labor, the unit cost of refuse collection by the one-man crew was 25 to 45 percent less than the two-man crew and 35 to 50 percent less than the three-man crew.
>
> Although multi-man crews required less equipment of equal size than one-man crews, this had negligible effect on unit collection costs when the combined equipment operating, amortization, and labor costs were compared for one-man and multi-man collection.
>
> In residential or light commercial curb or alley collection the work load was not excessive for one-man operation. . . .
>
> As the cost-benefits associated with the one-man crew are sensitive to excessive absenteeism and poor work habits, the one-man collection system generally requires a higher level of responsibility, performance, and loyalty on the part of both collection and supervisory personnel.
>
> Successful implementation of a one-man collection system will probably require: higher personnel standards; higher salary rates; potential upward mobility in the job structure; employees with a sense of personal pride and responsibility; and engineering evaluation of route structure and equipment requirements.
>
> There is an immediate need for improvement in the design and application of specific equipment for refuse collection tasks. The combination of packer body and conventional truck chassis does not provide for an optimum man-machine relationship.

The automated refuse accumulators discussed in this thesis obviously achieve no further reduction in crew size over the manual systems reported on by

Stone, and since he has shown one-man crews to be the most efficient for curb-side collection, it is against these crews that the performance of automated equipment must be compared.

Stone reports a mean collection time per stop* for a one-man crew of 0.68 minutes in an area where only once-a-week collection is provided and where the mean quantity of refuse collected is 77 pounds per stop and 3.4 containers per stop. For disposable containers of the type being considered for use with the automated refuse collection system, Stone reports collection time per stop for a one-man crew versus the number of items at the stop as a linear relationship between 0.3 minutes for one container and 0.65 minutes for 8 containers. The mean travel time per stop in the area from which this data was taken was 0.153 minutes and the distance between collection points was 50 feet.

The average vehicle speed through the collection area surveyed by Stone, assuming the use of 3.4 disposable containers per stop (resulting in a collection time per stop of 0.42 minutes), is

$$\left(\frac{50}{0.42 + 0.153}\right)\left(\frac{60}{5280}\right) = 0.99 \text{ miles per hour}$$

As a limiting case of automated refuse accumulator performance, suppose the operator comes to a complete stop with the accumulator in its traveling position. The accumulation cycle might then require that the tip of the accumulator travel 12.55 feet to the pick-up point and return. If the initial acceleration of the

---

*This is the average time per stop when a mixture of disposable and nondisposable containers is used.

accumulator from its rest position is a modest 10 ft/sec^2 up to a maximum speed of 10 feet per second, the time required to reach the "critical radius" would be 1.5 seconds and the time required to reach the "critical radius" would be 1.5 seconds and the time required to move the remaining 2.55 feet has been shown to be typically on the order of 1.25 seconds. Allowing 0.1 for the capture subsystem to actuate at both ends of the cycle, the entire cycle would require 5.7 seconds.

Even if the capture subsystem could only accommodate one container, the time required to accumulate the average 3.4 containers per stop would be 19.4 seconds or 0.32 minutes, a time savings of 23.8 percent over the manual system. If the capture subsystem could accommodate all 3.4 containers, not an unlikely prospect, especially for a system in which the vehicle comes to rest before accumulation begins, the collection time per stop would be reduced to 0.095 minutes, a 77.4 percent reduction over the time required for the manual system, and the average speed through the collection area would be

$$\left(\frac{50}{0.095 + 0.153}\right)\left(\frac{60}{5280}\right) = 2.29 \text{ miles per hour}$$

The time required to collect the same amount of refuse from the same collection area would therefore be reduced by 56.8 percent over the manual system.

To estimate the average speed through the collection area of an automated refuse accumulator capable of capturing the 3.4 items per pick up point while moving at 0.5 miles per hour, it is assumed that the vehicle travels at this speed for the duration of the accumulation cycle and then averages the 3.71 miles per

hour for the remainder of the trip between pick up points. During the 0.095 minute accumulation cycle the vehicle travels

$$\frac{(0.095)(0.5)(5280)}{60} = 4.2 \text{ feet}$$

For the remaining 45.8 feet the vehicle travels 3.71 miles per hour, arriving at the start of the next accumulation cycle in

$$\frac{(45.8)(60)}{(3.71)(5280)} = 0.140 \text{ minutes}$$

The average speed through the collection area of the automated refuse accumulator operating in the non-stop mode is therefore

$$\left(\frac{50}{0.140 + 0.095}\right)\left(\frac{60}{5280}\right) = 2.42 \text{ miles per hour}$$

and the reduction in total collection time over the manual system is 59.1 percent.

CHAPTER VIII

CONCLUSIONS AND RECOMMENDATIONS

Feasibility and Performance of Automated Refuse Accumulators

Regarding the feasibility and expected performance of truck mounted manually controlled refuse accumulators, the results of the simulation conducted in this investigation support the following general conclusions.

1. Truck mounted manually controlled refuse accumulators designed for non-stop operation are feasible for curb side pick up operations where standardized disposable containers are used.

2. In a collection area where pick up points were closely spaced (50 feet), the reduction in total collection time estimated for a non-stop automated refuse accumulator compared to the most cost-effective manual system was 59.1 percent.

3. The time saving benefits associated with automated refuse accumulation are not entirely dependent on non-stop operation, in fact the incremental benefit due to non-stop operation over stop to stop automated operation is quite small. Therefore automated refuse accumulation may also be desirable in congested areas where non-stop operation is not possible.

4. A potential reduction in average loading time of 77.4 percent has been estimated for the automated system when compared to the most cost effective manual system in a specific collection area. Still greater savings in loading time

may be possible.

The following conclusions, also supported by the results of the simulation, are more specifically related to the mechanical performance and design of automated refuse accumulators.

5. On well paved roads, the speed at which truck mounted refuse accumulators may be operated is limited more severely by the range of the linkage than by dynamic effects due to road noise, even when mounted on a conventional truck chassis.

6. Successful non-stop operation of automated refuse accumulators on unpaved roads may require that an active ride augmentation system or a kinematically constrained low stiffness suspension be built for the refuse collection vehicle.

7. The volumetric capacity and tolerance for errors in position and velocity of the capture subsystem are important factors in determining pick up cycle time (both the number of cycles required per stop and the time required to achieve capture) and operator effort expended in achieving capture. Large values of these parameters could also facilitate operation on poorly paved roads.

8. Low weight and high stiffness are desirable characteristics for the accumulator mechanism. Special actuation techniques, suggested in Appendix VII, may be required to achieve these characteristics.

9. The most desirable damping ratio for use in a specific accumulator is a function of the stiffness to weight ratio achieved. An active damping system may be necessary to realize desirable damping ratios.

10. Estimated power requirements for the automated refuse accumulator are well within the range suitable for mobile equipment.

Additional observations not specifically related to the simulation are the following.

1. The beneficial effect on total collection time (average speed through the collection area) due to non-stop operation is inversely related to the distance between pick up points.

2. The additional capital cost for automated vehicles is likely to be more than offset by the reduction in the number of vehicles required; therefore, the savings due to reduced collection man hours provided by the automated system will be available to fund other services.

3. Wise choise of route structure can reduce the number of vehicles required and special routing considerations may be necessary for automated collection.

4. High personnel standards will be necessary in systems using automated equipment, and as a result the quality of service provided the consumer should improve. In addition, improved working conditions should reduce employee turnover.

5. In the author's opinion, automated refuse accumulation should be an economically desirable alternative in spite of the increased cost of the individual collection vehicle.

Development of Alternative Subsystems

Potential three degree of freedom kinematic chains for use as refuse

accumulation mechanisms have been identified and alternative capture subsystems classified by the physical mechanisms employed. Actuators suitable for low weight linkages have been suggested, a prototype RRP chain designed, and a scheme for active damping of the kinematic chain proposed.

To further the development of an automated refuse accumulator, it is recommended that effort be first directed to the design and testing of alternative capture subsystems with emphasis on obtaining large capacity, high position and velocity error tolerance, and rapid actuation time. A second or concurrent investigation could be directed toward the design and testing of a low inertia master-slave accumulator with good obstacle avoidance characteristics and an active damping system.

It is recommended that a prototype accumulator be constructed and tested in various collection areas before a great deal of effort is expended in the development of an active vehicle suspension system. This recommendation is based on the excellent performance obtained in the simulation with the benchmark vehicle on well paved roads and on the relatively small incremental reduction in collection time achieved by non-stop operation over stop-to-stop operation of an automated accumulator.

On Broader Application of the Results

One objective of the dissertation was to demonstrate the potential utility of modern technology in a low technology industry. The rate at which new technology is applied to the solution of a problem sometimes seems inversely related to the age of the problem. This is especially true of the public sector where the

only conspicuous exception is rapid application of advanced technology by the military. It is hoped that the savings in collection costs, reduction in refuse worker injury rates, improved working conditions for collection personnel and improved service which seem to be possible with automated refuse accumulators will hurry their development and spur the application of state of the art technology to other areas which have felt little recent technical impact.

More directly related to the analysis and simulation of the refuse accumulator, the conclusions regarding dynamic characteristics of the linkage and target tolerance of the capture subsystem could be generalized to other applications of manually controlled manipulators where rapid response is a primary concern.

Finally, the simplified near optimal model of the human operator used in the simulation resulted in control inputs of magnitude and frequency well within the range of human capability. The use of the performance index weights to achieve acceptable control inputs and the reduction of state space target size to account for observational noise may be techniques helpful in other efforts at modeling human operators in design situations.

APPENDIX I

SUMMARY OF CURRENT OR PROPOSED AUTOMATED REFUSE COLLECTION DEVICES

Among the most common automated refuse collection devices are those produced by Dempster Brothers and others for the collection of commercial refuse from large volume standardized containers. This type of unit is not of interest here as the concern is with the design of systems for residential collection.

Possibly the first attempt at automated vehicular residential refuse collection was made in Scottsdale, Arizona under a grant from the Bureau of Solid Waste Management in 1969-70 (42). The equipment used in this project consisted of a conventional 30 cubic yard top loader fitted with a fork life mechanism across the arms. The fork lift mechanism, Figure 19, carried a single-lever clamping device which gripped 80 gallon residential containers. As the truck approached a container the fork lift mechanism moved the clamp horizontally to an intersecting path, the clamp closed on the container and the conventional loading arms raised the container off the ground. The fork lift mechanism then moved the container to the center of the truck where the lifting arms emptied it overhead in the usual manner. To replace the container on the curb, the lifting arms were brought down in front of the cab, the fork lift device moved horizontally to the curb and the clamp released. Then the fork lift mechanism was

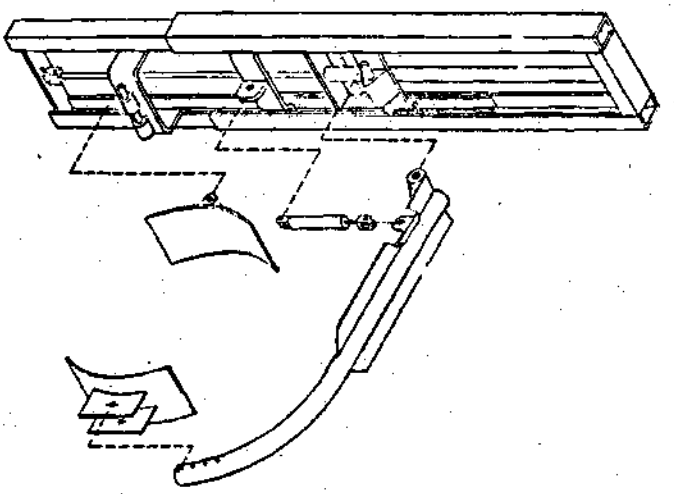

Figure 19. Scottsdale, Arizona's Fork Lift Adaptation

retracted to clear the container and the truck proceeded to the next stop.

Through a continuation of the federal grant a modified rear loader was designed as well as a refined automated front loader. The rear loader consisted of a device into which the container was fed by hand. The device then emptied the container into the vehicle and returned it to the pavement. The refined front loader used a single telescoping arm which was gree to pivot in the horizontal and vertical planes. This device, shown in Figure 20, was also designed to use standardized containers and, like its predecessor, took advantage of the unobstructed alleys of Scottsdale for efficient operation.

As an outgrowth of these experiments, a corporation, Government Innovators, was formed which, in a licensing agreement with Western Body and Hoist Company, has plans of producing other refuse collection equipment. Their Barrel Snatcher is the improved front loader described above. In addition they are designing a device called the Litter Pig, which has the capability of avoiding obstacles, and is shown in Figure 21. Also shown in this figure is their transfer vehicle, the Trash Hog, designed to couple with the Litter Pig and act as a mobile transfer station. Government Innovators also plans to design a non-stop collection vehicle.

Another automated refuse accumulation unit, developed and marketed by Gulf Oil Chemicals Company, was designed to enhance the marketability of their plastic refuse bags. The Mechanical Bag Retriever, as the device is called, consists of a basket like clam shell attached to telescoping two arm boom and uses a belt conveyor to transport the refuse from a front hopper to the compactor. The

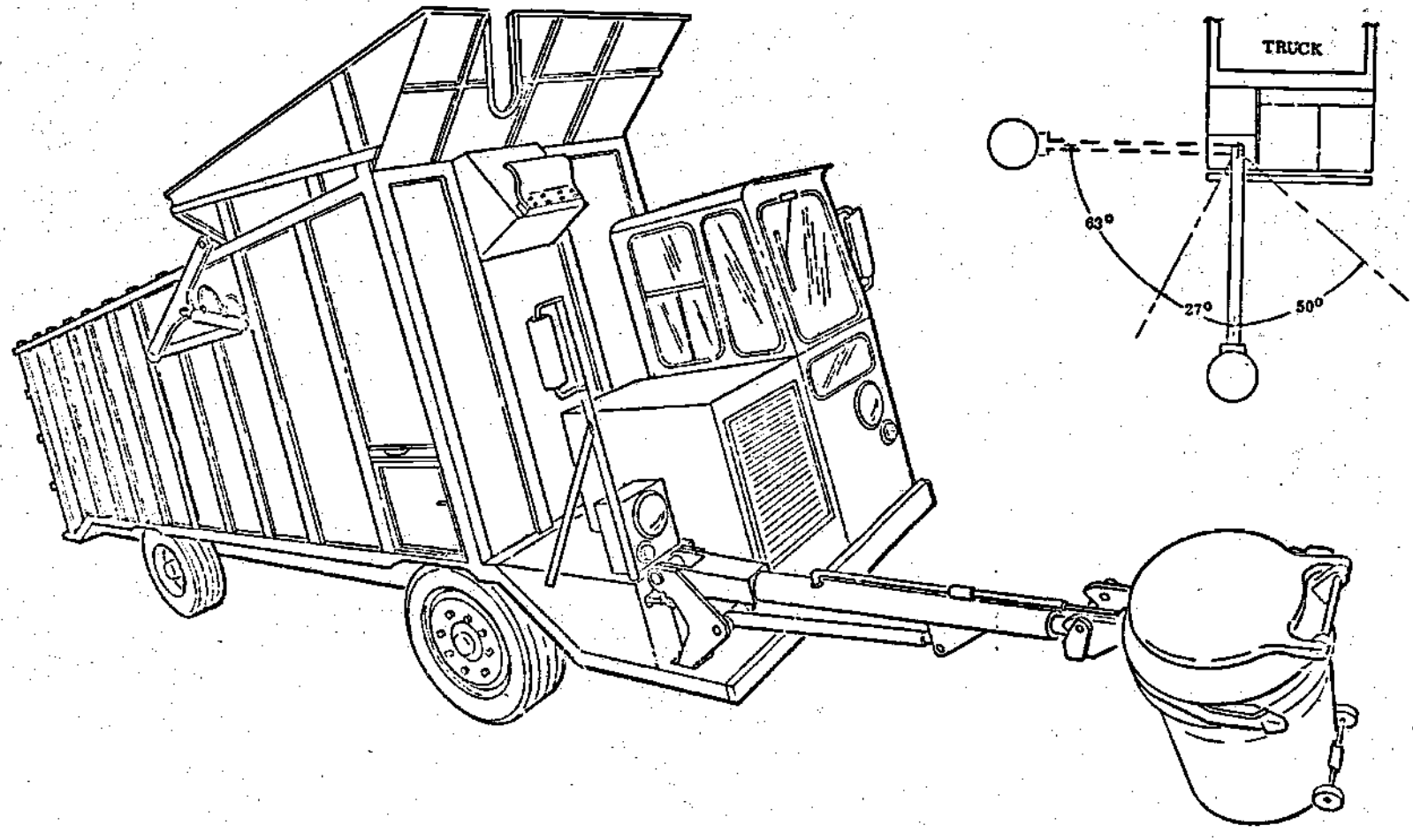

Figure 20. Scottsdale, Arizona's "Barrel Snatcher"

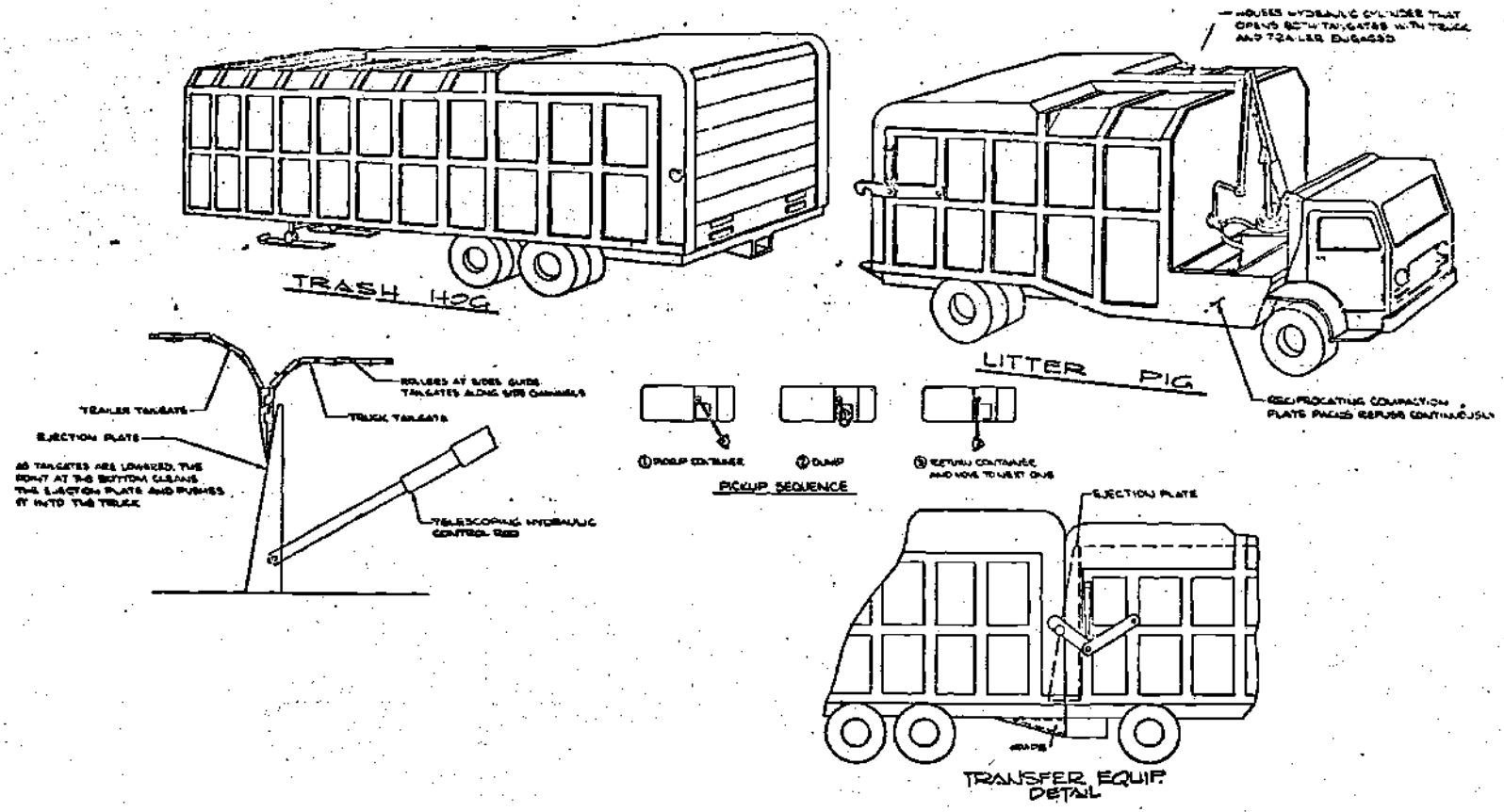

Figure 21. Government Innovator's Proposed "Litter Pig" and "Trash Hog"

device, Figure 22, has a 270 degree rotation capability of both the main boom and the basket and has a maximum reach of 21 feet. It is mechanically very similar to the Litter Pig and is leased for $10,000 per year (43).

A few continuous loading automated devices are in the planning stages, among them the Government Innovators' non-stop truck and three concepts from Glenn Meyers of Phoenix, Arizona for which patents are pending (44). Mr. Meyers' vehicles, shown in Figures 23, 24, and 25 are in the conceptual stages of development. None of these vehicles has an obstacle avoidance capability and two of the designs require that the containers be mounted on fixed poles at the curb.

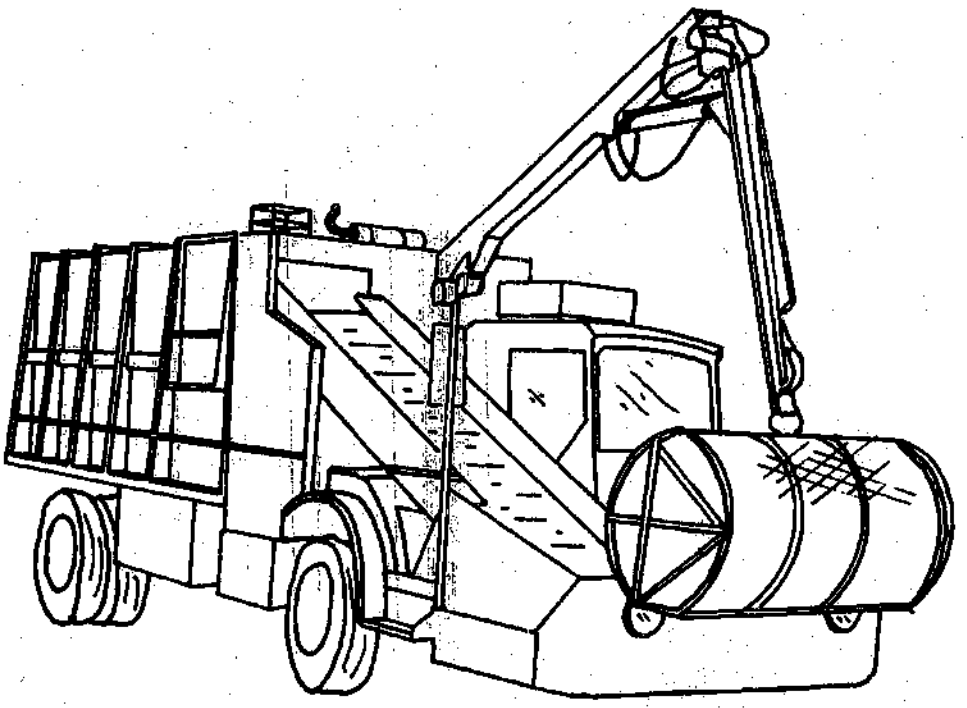

Figure 22. Gulf Oil's "Mechanical Bag Retriever"

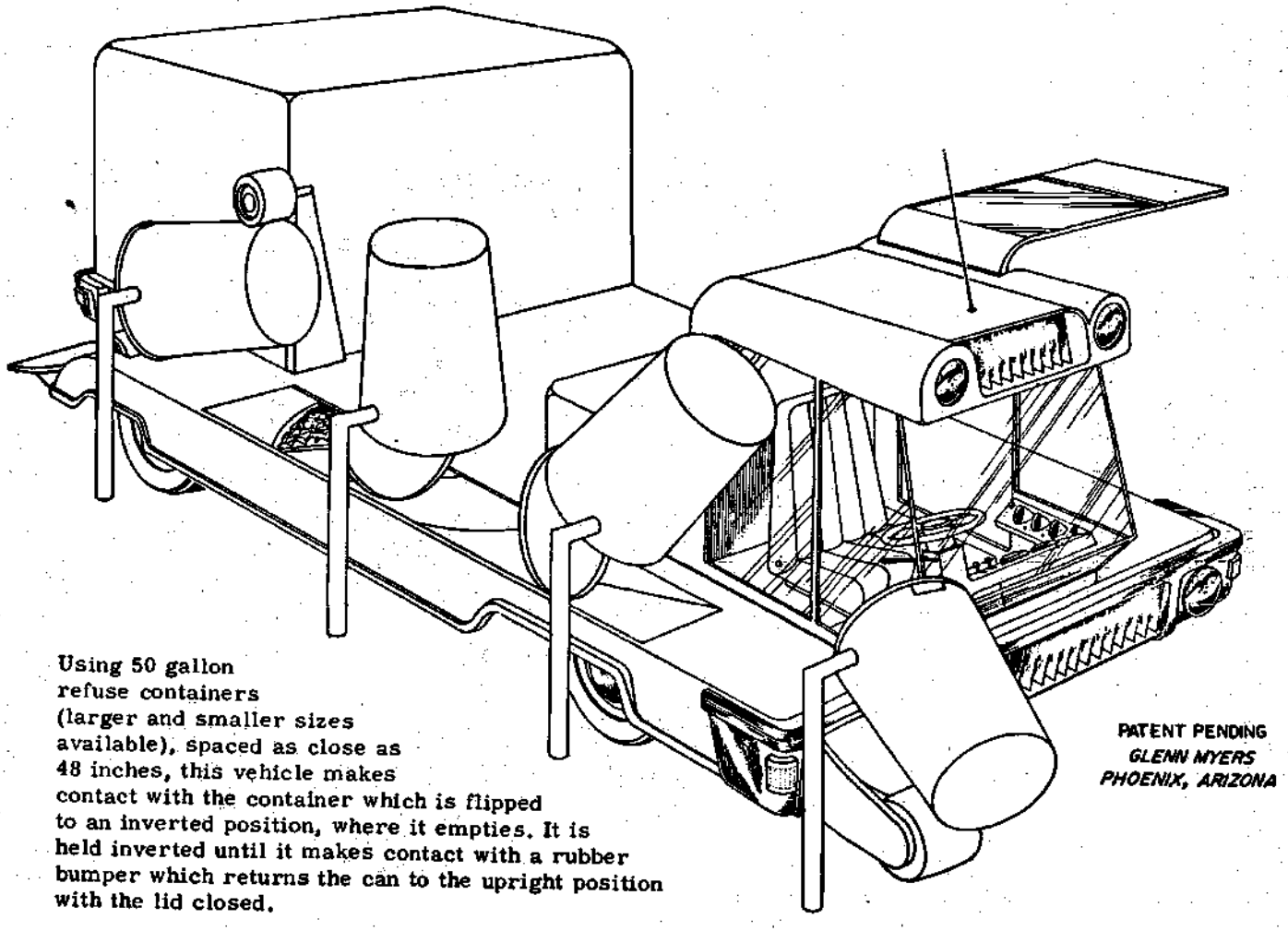

Figure 23. One of Meyers' Proposed Vehicles

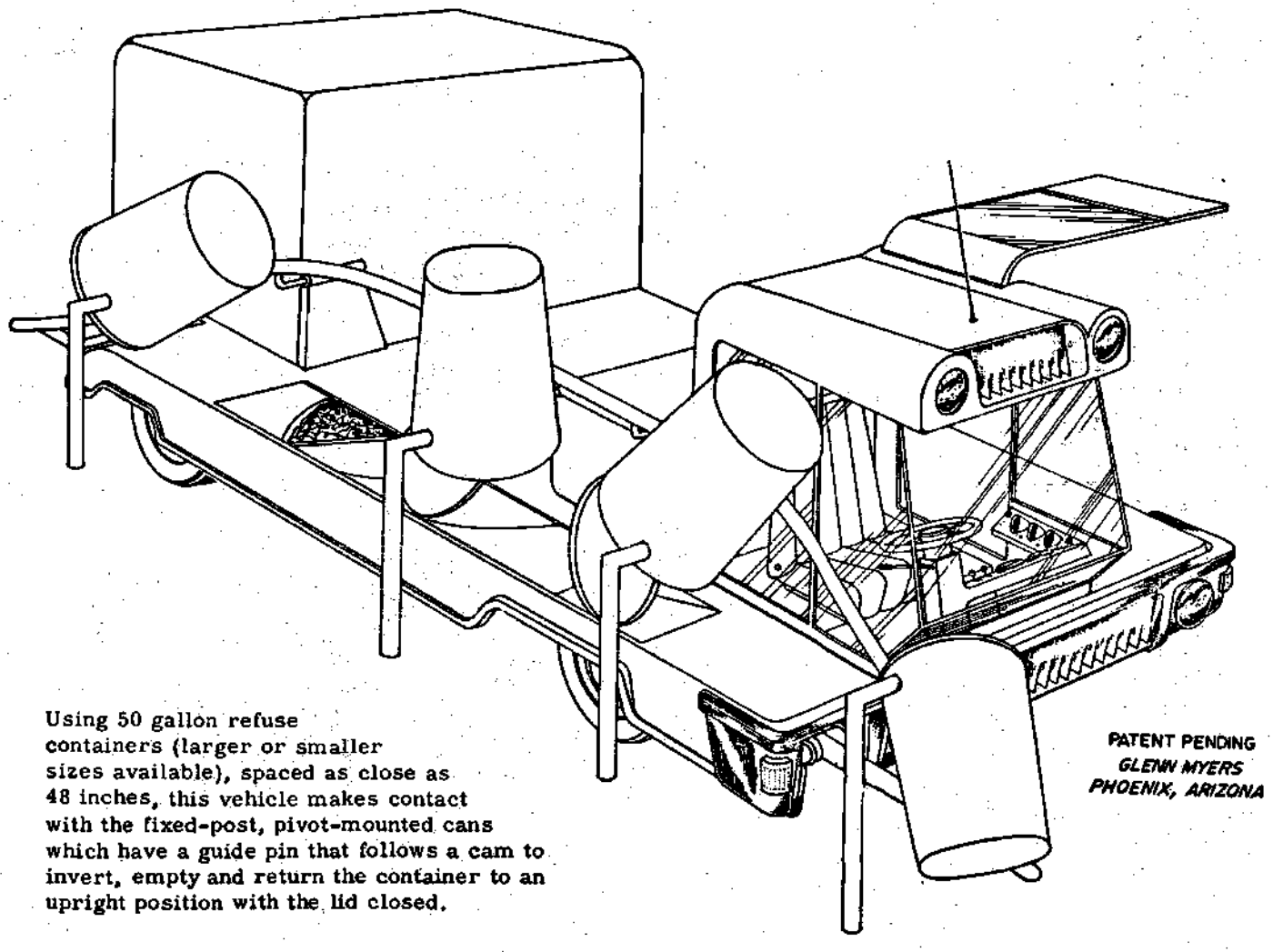

Figure 24. One of Meyers' Proposed Vehicles

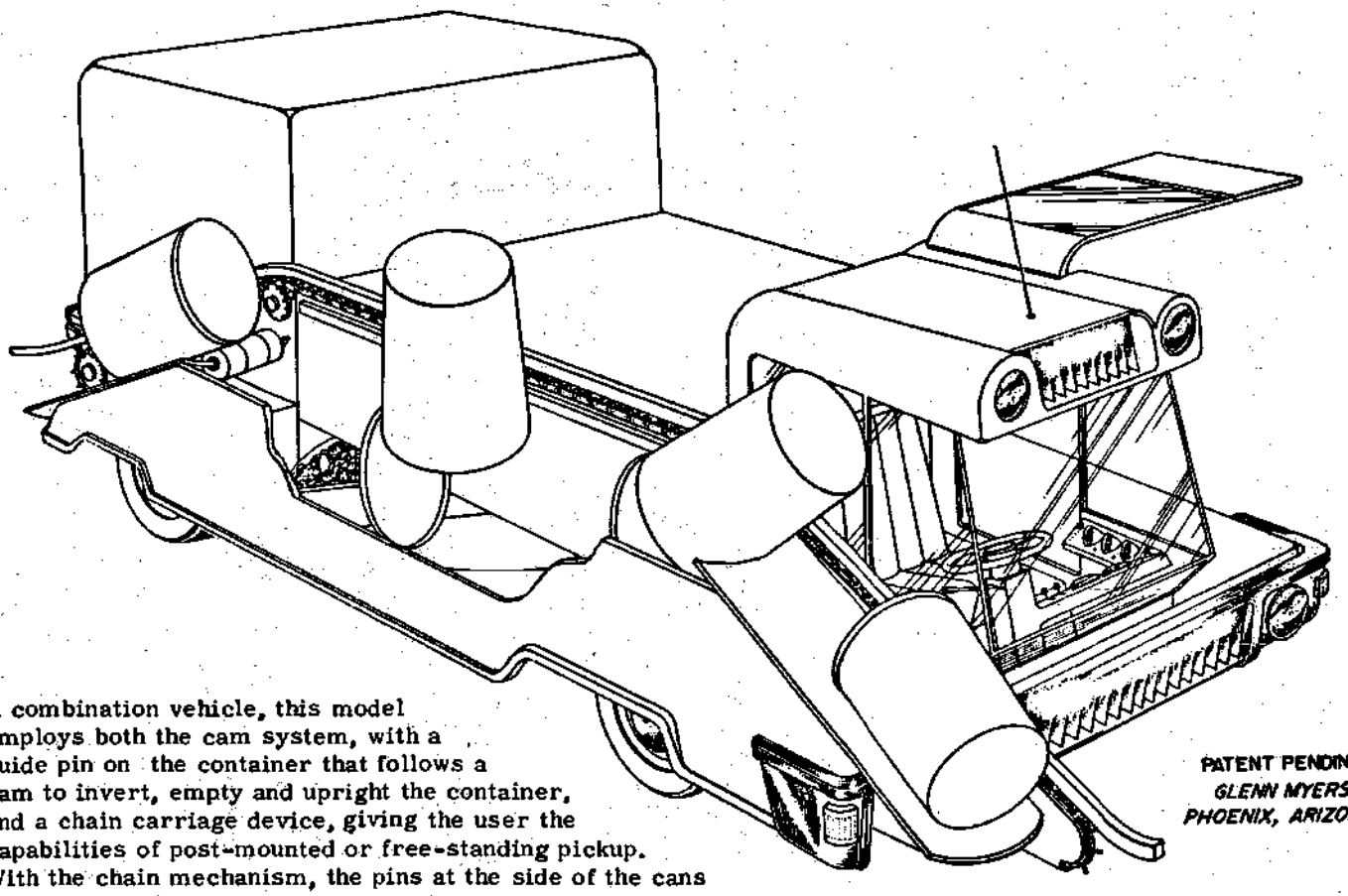

A combination vehicle, this model employs both the cam system, with a guide pin on the container that follows a cam to invert, empty and upright the container, and a chain carriage device, giving the user the capabilities of post-mounted or free-standing pickup. With the chain mechanism, the pins at the side of the cans engage with the chain pins, pulling the can up an angled trough. It is inverted, emptied and moves along the chain to a second trough which rights the can to a near vertical position and gently deposits it at the site of pickup in an upright position with the lid closed.

Figure 25. One of Meyers' Proposed Vehicles

APPENDIX II

SYSTEMATIC GENERATION OF ALTERNATIVE KINEMATIC CHAINS

Following the procedure of Chapter III, the kinematic chains with three degrees of freedom using revolute and prismatic pairs were systematically identified. The results are given in Table 11, where the numbers refer to the axis about which the pair moves 1, 2, 3 corresponding to x, y z respectively. The symbol R represents a revolute pair and P a prismatic pair. In the column labeled REJECT, a blank indicates that the chain is a viable alternative, $\not{P}$ indicates a planar chain, $\not{C}$ indicates a chain with a cylindrical equivalent, that is a prismatic pair along an axis followed by a revolute pair about the same axis, and $\not{R}$ indicates a redundancy of prismatic pairs, that is two prismatic pairs along the same axis in direct succession. The conventions used in interpreting the results are:

1. The first pair in the chain (left most in the table) is considered the ground link.
2. The ground link is held in the 1-3 plane to identify the next link.
3. If an R2 follows the ground link, it is aligned with the ground link. to identify the last link.

The chains which were considered to have high likelihood of success in this application are indicated by an alternative number.

Table 11. Results of Systematic Kinematic Chain Generation

Chain	Reject	Alternative Number	Chain	Reject	Alternative Number	Chain	Reject	Alternative Number
R1 R1 R1	✗		R1 P2 R3			P1 R3 P2	✗	
R1 R1 R2			R1 P2 P1			P1 R3 P3		
R1 R1 R3			R1 P2 P2	✗		P1 P1 R1	✗	
R1 R1 P1			R1 P2 P3	✗		P1 P1 R2	✗	
R1 R1 P2	✗		R1 P3 R1	✗		P1 P1 R3	✗	
R1 R1 P3	✗		R1 P3 R2		3	P1 P1 P1	✗	
R1 R2 R1			R1 P3 R3	✓		P1 P1 P2	✗	
R1 R2 R2		4,5	R1 P3 P1			P1 P1 P3	✗	
R1 R2 R3			R1 P3 P2	✗		P1 P2 R1		
R1 R2 P1			R1 P3 P3	✗		P1 P2 R2	✓	
R1 R2 P2			P1 R1 R1	✓		P1 P2 R3	✗	
R1 R2 P3		1,2	P1 R1 R2	✓		P1 P2 P1	✗	
R1 R3 R1			P1 R1 R3	✓		P1 P2 P2	✗	
R1 R3 R2			P1 R1 P1	✓		P1 P2 P3		
R1 R3 R3			P1 R1 P2	✓		P1 P3 R1		
R1 R3 P1			P1 R1 P3	✓		P1 P3 R2	✗	
R1 R3 P2			P1 R2 R1			P1 P3 R3	✓	
R1 R3 P3			P1 R2 R2	✗		P1 P3 P1	✗	
R1 P1 R1	✓		P1 R2 R3			P1 P3 P2		
R1 P1 R2			P1 R2 P1	✗		P1 P3 P3	✗	
R1 P1 R3			P1 R2 P2					
R1 P1 P1	✗		P1 R2 P3	✗				
R1 P1 P2			P1 R3 R1					
R1 P1 P3			P1 R3 R2					
R1 P2 R1	✗		P1 R3 R3	✗				
R1 P2 R2	✓		P1 R3 P1	✗				

APPENDIX III

INVESTIGATION OF ACCUMULATOR TO VEHICLE DYNAMIC COUPLING

In the analysis of the combined vehicle–accumulator dynamics (Chapter IV), it was assumed that motions of the accumulator had negligibly small effect on the motions of the vehicle. To investigate the adequacy of this assumption, the undamped response of the vehicle in the roll mode to a suddenly applied torque equivalent to a two g acceleration of the accumulator and refuse mass at a radius of ten feet from the vehicle center of gravity was considered.

Figure 26 describes schematically the physical arrangement, I_v being the roll moment of inertia of the vehicle, k the sum of front and rear spring stiffnesses, 2d the distance between the springs on the axle, δ the angular displacement of the vehicle from its position of equilibrium and T the suddenly applied torque.

The deflection of each spring due to a small rotation of the body is seen to be

$$\delta = d\theta .$$

The force in each spring is then given by

$$f = k\delta = kd\theta$$

and the couple applied to the vehicle by its suspension is therefore

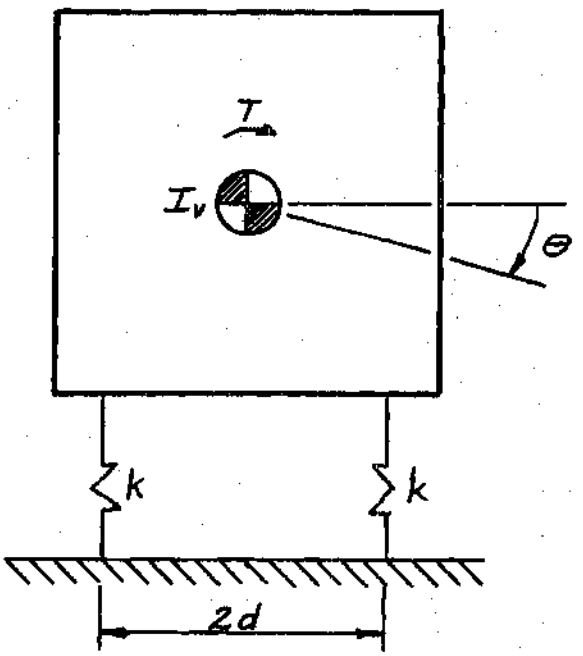

Figure 26. Vehicle Roll Mode Dynamics Model

$$C = 2kd^2\theta$$

Applying Newton's law to the vehicle body gives

$$I_V\ddot{\theta} + 2kd^2\theta = T$$

with initial conditions $\theta_o = 0$, $\dot{\theta}_o = 0$, implying that the roll mode is initially undisturbed. The solution to this equation of motion is

$$\theta = \frac{T}{2kd^2}\left[1 - \cos\left(d\sqrt{\frac{2k}{I_v}}\,t\right)\right]$$

from which the maximum rotation may be determined by setting

$$t = \frac{\pi}{d}\sqrt{\frac{I_v}{2k}}$$

and is

$$\theta_{max} = \frac{T}{kd^2}$$

Using the mechanical parameters given in Appendix VI for the empty Ford L700 vehicle,

$$K = 1714 + 750 = 2464 \text{ lbs/in}$$

and $d = 20$ in.

For a three slug accumulator-refuse mass subjected to a two g acceleration at 120 inches from the vehicle center of gravity, the disturbance torque is

$$T = (3)\,(32.2)\,(2)\,(120) = 23184 \text{ in-lb}$$

The maximum rotation of the body under these conditions is then

$$\theta \text{ max} = \frac{23184}{(2464)\,(20)^2} = 0.235 \text{ rad} = 1^{o}21'$$

As two g accelerations are unlikely to be experienced in operation and because some damping is present in the vehicle suspension, it may be concluded that the vehicle rotations caused by the accumulator will be well below one degree, and the assumption of negligibility is justified. The vehicle is even less sensitive to such disturbances in the heave and pitch modes.

APPENDIX IV

GENERAL FORM STIFFNESS-DAMPING MATRICES FOR ADDITIONAL KINEMATIC ALTERNATIVES

Introduction

The approach used to reduce the dynamic equations of a specified kinematic chain to the general form required by the automated refuse accumulator model was shown in Chapter IV for kinematic alternative number two, the contracted RRP chain. In this appendix the results of similar derivations for the other kinematic chains shown in Table 5 are presented. For simplicity the coefficient matrices in equations 41 and 42 will be referred to as $\bar{K}_{41}$ and $\bar{K}_{42}$ respectively. An ℓ subscript on stiffness or damping term always refers to the prismatic pair.

Kinematic Alternative Number One

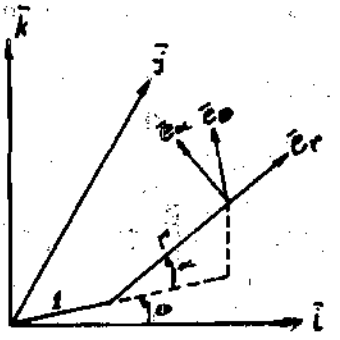

Figure 27. Nomenclature for Kinematic Alternative Number One.

$$\bar{K}_{41} = \bar{\phi}^{-1} \bar{K} \bar{T}^{-1}$$

$$\bar{K}_{42} = \bar{\phi}^{-1} \bar{K} \bar{T}^{-1} \bar{S}$$

$$\bar{\phi} = \begin{bmatrix} \cos\alpha\cos\theta & \cos\alpha\sin\theta & \sin\alpha \\ -\sin\theta & \cos\theta & 0 \\ -\sin\alpha\cos\theta & -\sin\alpha\sin\theta & \cos\alpha \end{bmatrix}$$

$$\bar{T} = \begin{bmatrix} \cos\alpha\cos\theta & 0 & -(\ell + r\cos\alpha)\sin\theta \\ 0 & \cos\alpha\cos\theta & 0 \\ \cos\alpha\sin\theta & 0 & (\ell + r\cos\alpha)\cos\theta \\ 0 & \cos\alpha\sin\theta & 0 \\ \sin\alpha & 0 & 0 \\ 0 & \sin\alpha & 0 \end{bmatrix}$$

$$\begin{bmatrix} 0 & -r\sin\alpha\cos\theta & 0 \\ -(\ell + r\cos\alpha)\sin\theta & 0 & -r\sin\alpha\cos\theta \\ 0 & -r\sin\alpha\sin\theta & 0 \\ (\ell + r\cos\alpha)\cos\theta & 0 & -r\sin\alpha\sin\theta \\ 0 & r\cos\alpha & 0 \\ 0 & 0 & r\cos\alpha \end{bmatrix}$$

$$\bar{K} = \begin{bmatrix} K_\ell & C_\ell & 0 & 0 & 0 & 0 \\ 0 & 0 & \dfrac{K_\theta}{\ell + r\cos\alpha} & \dfrac{C_\theta}{\ell + r\cos\alpha} & 0 & 0 \\ 0 & 0 & 0 & 0 & \dfrac{K_\alpha}{r} & \dfrac{C_\alpha}{r} \end{bmatrix}$$

$$\bar{S} = \begin{bmatrix} 0 & 0 & \sin\alpha & 0 \\ 0 & 0 & 0 & r\sin\alpha \\ -r\sin\alpha & 0 & 0 & 0 \\ 0 & -r\sin\alpha & 0 & 0 \\ (\ell + r\cos\alpha)\sin\theta & 0 & -(\ell + r\cos\alpha)\cos\theta & 0 \\ 0 & (\ell + r\cos\alpha)\sin\theta & 0 & -(\ell + r\cos\alpha)\cos\theta \end{bmatrix}$$

Kinematic Alternative Number Three

$$\bar{K}_{41} = \bar{\phi}^{-1}\,\bar{K}\,\bar{T}^{-1}$$

$$\bar{K}_{42} = \bar{\phi}^{-1}\,\bar{K}\,\bar{T}^{-1}\bar{S}$$

$$\bar{\phi} = \begin{bmatrix} \cos\alpha\cos\theta & \cos\alpha\sin\theta & \sin\alpha \\ -\sin\theta & \cos\theta & 0 \\ -\sin\alpha\cos\theta & -\sin\alpha\sin\theta & \cos\alpha \end{bmatrix}$$

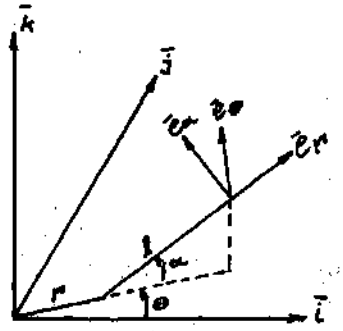

Figure 28. Nomenclature for Kinematic Alternative Number Three.

$$\bar{T} = \begin{bmatrix} \cos\theta & 0 & -(r + \ell\cos\alpha)\sin\theta & 0 \\ 0 & \cos\theta & 0 & -(r + \ell\cos\alpha)\sin\theta \\ \sin\theta & 0 & (r + \ell\cos\alpha)\cos\theta & 0 \\ 0 & \sin\theta & 0 & (r + \ell\cos\alpha)\cos\theta \\ 0 & 0 & 0 & 0 \\ 0 & 0 & 0 & 0 \end{bmatrix}$$

$$\begin{bmatrix} -\ell\sin\alpha\cos\theta & 0 \\ 0 & -\ell\sin\alpha\cos\theta \\ -\ell\sin\alpha\sin\theta & 0 \\ 0 & -\ell\sin\alpha\sin\theta \\ \ell\cos\alpha & 0 \\ 0 & \ell\cos\alpha \end{bmatrix}$$

$$\bar{K} = \begin{bmatrix} \frac{K_\ell}{\cos\alpha} & \frac{C_\ell}{\cos\alpha} & 0 & 0 & \frac{K_\alpha \sin\alpha}{\ell\cos\alpha} & \frac{C_\alpha \sin\alpha}{\ell\cos\alpha} \\ 0 & 0 & \frac{K_\theta}{r + \ell\cos\alpha} & \frac{C_\theta}{r + \ell\cos\alpha} & 0 & 0 \\ 0 & 0 & 0 & 0 & \frac{K_\alpha}{\ell} & \frac{K_\alpha}{\ell} \end{bmatrix}$$

$$\bar{S} = \begin{bmatrix} 0 & 0 & \ell\sin\alpha & 0 \\ 0 & 0 & 0 & \ell\sin\alpha \\ -\ell\sin\alpha & 0 & 0 & 0 \\ 0 & -\ell\sin\alpha & 0 & 0 \\ (r + \ell\cos\alpha)\sin\theta & 0 & -(r + \ell\cos\alpha)\cos\theta & 0 \\ 0 & (r + \ell\cos\alpha)\sin\theta & 0 & -(r + \ell\cos\alpha)\cos\theta \end{bmatrix}$$

Kinematic Alternatives Number Four and Five

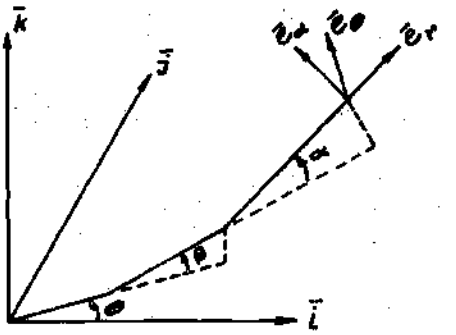

Figure 29. Nomenclature for Kinematic Alternatives Numbers Four and Five.

$$\bar{K}_{41} = \bar{\phi}^{-1} \bar{K} \bar{T}^{-1}$$

$$\bar{K}_{42} = \bar{\phi}^{-1} \bar{K} \bar{T}^{-1} \bar{S}$$

$$\phi = \begin{bmatrix} \cos(\alpha+\beta)\cos\theta & \cos(\alpha+\beta)\sin\theta & \sin(\alpha+\beta) \\ -\sin\theta & \cos\theta & 0 \\ -\sin(\alpha+\beta)\cos\theta & -\sin(\alpha+\beta)\sin\theta & \cos(\alpha+\beta) \end{bmatrix}$$

Define

$$G_1 = \ell_2 \sin\beta + \ell_3 \sin(\alpha+\beta)$$

$$G_2 = \ell_1 + \ell_2 \cos\beta + \ell_3 \cos(\alpha+\beta)$$

$$\bar{T} = \begin{bmatrix} -G_1 \cos\theta & 0 & -G_2 \sin\theta & 0 \\ 0 & -G_1 \cos\theta & 0 & -G_2 \sin\theta \\ -G_1 \sin\theta & 0 & G_2 \cos\theta & 0 \\ 0 & -G_1 \sin\theta & 0 & G_2 \cos\theta \\ G_2 - \ell_1 & 0 & 0 & 0 \\ 0 & G_2 - \ell_1 & 0 & 0 \end{bmatrix}$$

$$\begin{bmatrix} -\ell_3 \sin(\alpha+\beta) \cos\theta & 0 \\ 0 & -\ell_3 \sin(\alpha+\beta) \cos\theta \\ -\ell_3 \sin(\alpha+\beta) \sin\theta & 0 \\ 0 & -\ell_3 \sin(\alpha+\beta) \sin\theta \\ \ell_3 \cos(\alpha+\beta) & 0 \\ 0 & \ell_3 \cos(\alpha+\beta) \end{bmatrix}$$

$$\bar{K} = \begin{bmatrix} \frac{K_\beta}{\ell_2 \sin\alpha} & \frac{C_\beta}{\ell_2 \sin\alpha} & 0 & 0 & \frac{-K_\alpha(\ell_3 + \ell_2 \cos\alpha)}{\ell_2 \ell_3 \sin\alpha} \\ 0 & 0 & \frac{K_\theta}{G_2} & \frac{C_\theta}{G_2} & 0 \\ 0 & 0 & 0 & 0 & \frac{K_\alpha}{\ell_3} \end{bmatrix}$$

$$\begin{bmatrix} \frac{-C_\alpha(\ell_3 + \ell_2 \cos\alpha)}{\ell_2 \ell_3 \sin\alpha} \\ 0 \\ \frac{C_\alpha}{\ell_3} \end{bmatrix}$$

$$\bar{S} = \begin{bmatrix} 0 & 0 & G_1 & 0 \\ 0 & 0 & 0 & G_1 \\ -G_1 & 0 & 0 & 0 \\ 0 & -G_1 & 0 & 0 \\ G_2 \sin\theta & 0 & -G_2 \cos\theta & 0 \\ 0 & G_2 \sin\theta & 0 & -G_2 \cos\theta \end{bmatrix}$$

APPENDIX V

COMPUTER PROGRAM DOCUMENTATION

The symbolics of the digital computer programs used to simulate the automated refuse accumulator are included in this appendix. The algorithmic language used is FORTRAN V, available on most large computer systems. In addition to subroutines written exclusively for use with the programs, the symbolics of which are presented here, several standard matrix manipulation subroutines and a linear algebraic equation solving subroutine are called in these programs. Equivalent subroutines are available in the libraries of any large scale computer facility.

The first program listed (FIN.ALTSTFNO) takes as input data the kinematic alternative number, operating position, and chain stiffness and damping coefficients of any of the five alternative convey subsystems listed in Table 5 and outputs the general form stiffness-damping matrices for use in the model of the refuse accumulator. This program requests information of the user during execution in a conversational manner and is heavily commented in the listing. FIN.ALTSTFNO calls subroutine OPTLIB.ALTNO which actually carries out the computation of the general form stiffness-damping matrices. The listing of OPTLIB.ALTNO is also heavily commented to show the logical procedure involved.

The program FIN.PRP takes as input the dynamic characteristics of the refuse collection vehicle, the road roughness, and the accumulator. These

inputs are requested of the user in a conversational manner along with the vehicle traveling speed, the performance index weights for the human operator model, and the integration step size to be used. Several options are incorporated permitting the use of previously computed values for the $\bar{H}_{33}$ matrix or the controller gains $\bar{G}$. Output is $\bar{H}_{33}$ written to file 10 and $\bar{G}$, $\bar{P}$, and $\bar{R}$ written to file 9.

FIN.PRP calls OPTLIB.GAIN3 which computes the controller gain $\bar{G}$ by the method described in Chapter V. OPTLIB.GAIN3 calls several additional subroutines; OPTLIB.SYMFIX which corrects round off errors in a symmetric matrix, a whole series of subroutines such as OPTLIB.HA6999 which form the linear algebraic equations required in the solution of the Riccati equation and OPTLIB.DZ which zeros a matrix. OPTLIB.PQ3, which computes the matrix exponential and the discrete system matrices $\bar{P}$ and $\bar{R}$, is also called by FIN.PRP. OPTLIB.PQ3 uses an algorithm given by Takahashi (39) to determine the number of terms required in the computation of the matrix exponential for an interval 0.001T, where T is the step size to be used in the computation of the system states. The resulting matrix exponential is then raised to the 1000th power.

The programs FIN.TRANS/H33 and FIN.TRANS/GAIN are used to translate the data stored by FIN.PRP in files 10 and 9 respectively into a form compatible with the input requirements of FIN.PRP, and store their outputs in file 7. This permits the use of precomputed values for $\bar{H}_{33}$ and $\bar{G}$ in later runs of FIN.PRP. Files 7 and 9 must be copied to permanent storage files after each run of FIN.PRP, FIN.TRANS/H33 and FIN.TRANS/GAIN.

FIN.POSDEF determines the positive definateness of any matrix by principal

minors and may be used to check $\bar{H}_{33}$ for this property. FIN.XPCT takes as input the contents of file 9 as returned by FIN.PRP and produces the expected values of the system state variables, the capture time to each target and the average and relative control effort expended in engaging each target. This program is also conversational in requesting needed data from the user. FIN.XPCT initiates the modeling process with the accumulator 3.5 times the critical radius from the refuse and interpolates to determine when the critical radius is reached and when each target is engaged. FIN.XPCT calls OPTLIB.INIT, which forms the initial state covariance matrix, and OPTLIB.EVAL which evaluates the state covariance at each step in time.

SIM.J is very similar to FIN.XPCT but evaluates the system penalty function at each target rather than the average or relative control effort and initiates the modeling process with the accumulator at the critical radius. SIM.J uses the same inputs as FIN.XPCT plus the state weighting value a, and requests these inputs in a conversational manner. SIM.J also calls OPTLIB.INIT and OPTLIB.EVAL.

The extent to which a change in system parameters requires the computation of new values for $\bar{H}_{33}$, $\bar{G}$, $\bar{P}$ and $\bar{R}$ and re-evaluation of system performance is indicated below. In program FIN.PRP, $\bar{H}_{33}$ must be recomputed for: (use $\bar{H}_{33} = \bar{0}$)

a. changes to arm dynamics, neutral position, or attachment point

b. changes in master to slave scale factor

c. changes in penalty weighting

$\bar{G}$ must be recomputed for: (use appropriate $\bar{H}_{33}$)

a. all of the above

b. changes in vehicle parameters

c. changes in traveling speed.

$\bar{P}$ and $\bar{R}$ must be recomputed for: (use appropriate $\bar{G}$)

a. all of the above

b. changes in observability

c. changes in roadway roughness

d. changes in integration step size.

In programs FIN.XPCT and SIM.J a new run is required for: (use appropriate $\bar{G}$, $\bar{P}$, $\bar{R}$)

a. all of the above

b. changes in initial position or critical radius.

```
 *FIN,ALTSTEND
 1              DIMENSION PF(3,6),ATR(3,4),T(6,6),RK(3,6),DJM(3,6),P(3,3),S(6,4)
 2              COMMON /BLOCK6/S,P,DJM,RK,T
 3        1     FORMAT()
 4        2     FORMAT('0ARM STIFFNESS-DAMPING MATRIX'//3(1X,6(E10.3,2X)//))
 5        3     FORMAT('0ARM TORSIONAL RESISTANCE MATRIX'//3(1X,4(E10.3,2X)//))
 6        4     FORMAT('1INPUT DATA ALTERNATIVE CONFIGURATION NUMBER ',I4//
 7             A1X,'KINEMATIC CONFIGURATION NUMBER ',I4//
 8             A2(1X,6(E10.3,1X)//))
 9        5     FORMAT('0ENTER NO,EL1,EL2,EL3,RL,ALPHA,THETA,ALK,ALC,THK,THC,'
10             A'RLK,RLC'/1X,'FOR CONFIGURATIONS 4&5 BETA,BETAK,BETAC '
11             A'ARE ENTERED AS RL,RLK,RLC'/1X,'CAUTION, ALPHA=0.0 '
12             A'CAUSES OVERFLOW IN CONFIGURATIONS 4&5'//)
13              CALL QUOTE('ENTER NUMBER OF ALTERNATIVES TO BE CONSIDERED')
14              READ 1, NNNNNN
15              DO 300 IKJLMN=1,NNNNNN
16              PRINT 5
17        C *** NO IS ALTERNATIVE KINEMATIC CHAIN NUMBER FROM THESIS ***
18        C *** EL1, EL2, EL3 ARE FIXED LENGTH LINKS, SEE THESIS FIGURES ***
19        C *** RL IS THE LENGHT OF THE LINK CONTAINING THE PRISMATIC PAIR ***
20        C *** ALPHA, THETA, BETA ARE JOINT ANGLES, SEE THESIS FIGURES ***
21        C *** REMAINING INPUTS ARE STIFFNESS AND DAMPING TERMS ***
22              READ 1, (NO,EL1,EL2,EL3,RL,AL,TH,ALK,ALC,THK,THC,RLK,RLC)
23              PRINT 4, (IKJLMN,NO,EL1,EL2,EL3,RL,AL,TH,ALK,ALC,THK,THC,RLK,RLC)
24              CALL ALTNO(NO,EL1,EL2,EL3,RL,AL,TH,ALK,ALC,THK,THC,RLK,RLC,PF,ATR)
25              PRINT 2, ((PF(I,J),J=1,6),I=1,3)
26        300   PRINT 3, ((ATR(I,J),J=1,4),I=1,3)
27              STOP
28              END
 *OPTLIB,ALTNO
 1              SUBROUTINE ALTNO(NO,EL1,EL2,EL3,RL,ALPHA,THETA,ALK,ALC,THK,THC,
 2             ARLK,RLC,PF,ATR)
 3              DIMENSION PF(3,6),ATR(3,4),T(6,6),RK(3,6),DJM(3,6),P(3,3),S(6,4)
 4              COMMON /BLOCK6/S,P,DJM,RK,T
 5        C *** FOR CONFIGURATIONS 4&5, BETA,BETAK,BETAC=RL,RLK,RLC
 6        C *** PF=(PHI**-1)*K*(T**-1)
 7        C *** ATR=(PHI**-1)*K*(T**-1)*S
 8        C *** P=(PHI**-1)
 9        C *** T=(T**-1)
10        C *** PRELIMINARY COMPUTATION OF REPEATED TERMS
11              ALPHA=ALPHA*3.14159/180
12              THETA=THETA*3.14159/180
13              SA=SIN(ALPHA)
14              CA=COS(ALPHA)
15              ST=SIN(THETA)
16              CT=COS(THETA)
17              CACT=CA*CT
18              SACT=SA*CT
19              CAST=CA*ST
20              SAST=SA*ST
21        C *** ONLY CHAINS 4 AND 5 CONTAIN THE FOLLOWING TERMS
22              IF(NO.LT.4) GO TO 901
23              RL=RL*3.14159/180
24              SB=SIN(RL)
25              CB=COS(RL)
26              SAB=SIN(ALPHA+RL)
27              CAB=COS(ALPHA+RL)
28        C *** PHI INVERSE FOR CHAINS 4 AND 5
29              P(1,1)=CAB*CT
30              P(1,3)=-SAB*CT
31              P(2,1)=CAB*ST
32              P(2,3)=-SAB*ST
33              P(3,1)=SAB
34              P(3,3)=CAB
35              GO TO 902
```

```
      C *** PHI INVERSE FOR CHAINS 1 THROUGH 3
  901 P(1,1)=CACT
      P(1,3)=-SACT
      P(2,1)=CAST
      P(2,3)=-SAST
      P(3,1)=SA
      P(3,3)=CA
  902 P(1,2)=-ST
      P(2,2)=CT
      P(3,2)=0.0
      IF(ND.GE.4) GO TO 4
      IF(ND.EQ.3) GO TO 3
      C *** T INVERSE, S AND K FOR CHAINS 1 AND 2
      DO 21 I=1,2
      J=I+2
      K=I+4
      T(I,I)=CACT
      T(J,J)=CT/(EL1+RL*CA)
      T(K,K)=CA/RL
      T(K,J)=-SAST/RL
      S(K,J)=-(EL1+RL*CA)*CT
      T(J,I)=-ST/(EL1+RL*CA)
      S(J,I)=-RL*SA
      T(K,I)=-SACT/RL
      S(K,I)=(EL1+RL*CA)*ST
      T(I,J)=CAST
      S(I,J)=RL*SA
   21 T(I,K)=SA
      RK(1,1)=RLK
      RK(1,2)=RLC
      RK(2,3)=THK/(EL1+RL*CA)
      RK(2,4)=THC/(EL1+RL*CA)
      RK(1,5)=0.0
      RK(1,6)=0.0
      RK(3,5)=ALK/RL
      RK(3,6)=ALC/RL
      GO TO 500
      C *** T INVERSE, S AND K FOR CHAIN 3
    3 DO 23 I=1,2
      J=I+2
      K=I+4
      T(I,I)=CT
      T(J,J)=CT/(RL+EL1*CA)
      T(K,K)=1.0/(EL1*CA)
      T(K,J)=0.0
      S(K,J)=-(RL+EL1*CA)*CT
      T(J,I)=-ST/(RL+EL1*SA)
      S(J,1)=-EL1*SA
      T(K,I)=0.0
      S(K,1)=(RL+EL1*CA)*ST
      T(I,J)=ST
      S(I,J)=EL1*SA
   23 T(I,K)=SA/CT
      RK(1,1)=RLK/CA
      RK(1,2)=RLC/CA
      RK(2,3)=THK/(RL+EL1*CA)
      RK(2,4)=THC/(RL+EL1*CA)
      RK(1,5)=ALK*SA/(EL1*CA)
      RK(1,6)=ALC*SA/(EL1*CA)
      RK(3,5)=ALK/EL1
      RK(3,6)=ALC/EL1
      GO TO 500
      C *** T INVERSE, S AND K FOR CHAINS 4 AND 5
    4 A=EL2*S3+EL3*SA3
      B=EL1+EL2*C4+EL3*CA3
      C *** SIN(ALPHA)=0.0 CAUSES OVERFLOW
```

```
102             C=B*EL2*EL3*SA
103             DO 24 I=1,2
104             J=I+2
105             K=I+4
106             T(I,I)=R*EL3*CA3*CT/C
107             T(J,J)=EL2*EL3*SACT/C
108             T(K,K)=-A*B/C
109             T(I,J)=D*EL3*CAB*ST/C
110             T(I,K)=D*EL3*SAB/C
111             T(J,I)=-EL2*EL3*SAST/C
112             T(K,I)=-R*(R-EL1)*CT/C
113             T(K,J)=-R*(R-EL1)*ST/C
114             S(I,J)=A
115             S(J,I)=-A
116             S(K,I)=D*ST
117      24     S(K,J)=-R*CT
118             RK(1,1)=RLK/(EL2*SA)
119             RK(1,2)=RLC/(EL2*SA)
120             RK(2,3)=THK/B
121             RK(2,4)=THC/B
122             RK(1,5)=-ALK*(EL3+EL2*CA)/(EL2*EL3*SA)
123             RK(1,6)=-ALC*(EL3+EL2*CA)/(EL2*EL3*SA)
124             RK(3,5)=ALK/EL3
125             RK(3,6)=ALC/EL3
126      500    CONTINUE
127      C *** COMPUTATION OF PF=(PHI**-1)*K*(T**-1)
128             CALL MXMLT(P,RK,DUM,3,3,6,3,3)
129             CALL MXMLT(DUM,T,PF,3,6,6,3,6)
130      C *** COMPUTATION OF ATR=PF*S
131             CALL MXMLT(PF,S,ATR,3,6,4,3,6)
132      C *** EQUATE VERY SMALL TERMS TO 0.0
133             DO 935 III=1,3
134             DO 930 JJJI=1,4
135             IF(ABS(ATR(III,JJJI)).LE.1.E-3) ATR(III,JJJI)=0.0
136      930    IF(ABS(PF(III,JJJI)).LE.1.E-3) PF(III,JJJI)=0.0
137             DO 935 KKKL=5,6
138      935    IF(ABS(PF(III,KKKL)).LE.1.E-3) PF(III,KKKL)=0.0
139             RETURN
140             END
```

```
*FIN,PRP
  1              DIMENSION A(23,23),DJ(23,3),D(4),FJ(3),FX(9,9),G(3,23),
  2             AB(4),S(4),R(3),AK(3,3),AC(3,3),ATR(3,4),DW(23,4),
  3             AP(23,23),PG(23,4),H33(9,9)
  4       C*****DIM(WB,A,WF,WR) . . . USE D
  5       C*****STIF(KF,CF,KR,CR) . . . USE S
  6       C*****BODY(M,IAX,IYY,IXY) . . . USE B
  7       C*****R(RAX,RAY,RAZ)
  8       1      FORMAT()
  9              CALL QUOTE('*** ARE FILES 7,9,10 ASSIGNED AND/OR ERASED ***')
 10              MOPT=IO('TO ENTER TRUCK DATA IN DETAIL ENTER 1, ELSE 0 ...')
 11              IF(MOPT.EQ.1) GO TO 2
 12              CALL QUOTE('ENTER TRUCK DATA FILE')
 13              READ 1, (D(I),I=1,4)
 14              READ 1, (S(I),I=1,4)
 15              READ 1, (B(I),I=1,4)
 16              READ 1, (TKF,TKR)
 17              CALL QUOTE('ENTER ROAD NOISE DATA FILE')
 18              READ 1, (RDKLF,RDKRF,RDKLR,RDKRR)
 19              CALL QUOTE('ENTER ARM DATA FILE')
 20              READ 1, (R(I),I=1,3)
 21              READ 1, ((AK(I,J),J=1,3),I=1,3)
 22              READ 1, ((AC(I,J),J=1,3),I=1,3)
 23              READ 1, ((ATR(I,J),J=1,4),I=1,3)
 24              READ 1, RAM
 25              GO TO 3
 26       2      CALL QUOTE('ENTER TRUCK DIMENSIONS WB,A,WF,WR')
```

```
27            READ 1, (D(I),I=1,4)
28            CALL QUOTE('ENTER SUSPENSION PARAMETERS KF,CF,KR,CR')
29            READ 1, (S(I),I=1,4)
30            CALL QUOTE('ENTER BODY PARAMETERS M,IXX,IYY,IXY')
31            READ 1, (B(I),I=1,4)
32            CALL QUOTE('ENTER TIRE STIFFNESS, FRONT,REAR')
33            READ 1, (TKF,TKR)
34            CALL QUOTE('ENTER ROAD ROUGHNESS FACTORS, LF,RF,LR,RR')
35            READ 1, (RDKLF,RDKRF,RDKLR,RDKRR)
36            CALL QUOTE('ENTER ARM ATTACHMENT POINT RAX,RAY,RAZ')
37            READ 1, (R(I),I=1,3)
38            CALL QUOTE('ENTER ARM STIFFNESS MATRIX AK')
39            READ 1,((AK(I,J),J=1,3),I=1,3)
40            CALL QUOTE('ENTER ARM DAMPING MATRIX AC')
41            READ 1, ((AC(I,J),J=1,3),I=1,3)
42            CALL QUOTE('ENTER ARM TORSIONAL RESISTANCE MATRIX ATR')
43            READ 1, ((ATR(I,J),J=1,4),I=1,3)
44            RAM=XIO('ENTER ARM MASS, LB-SEC2/FT ...')
45      3     BB=D(1)-D(2)
46            RKPROP=XIO('ENTER CONTROL TO ARM PROPORTIONALTY (GAIN) ...')
47            RT=XIO('ENTER VEHICLE SPEED, MPH ...')
48      C *** COMPUTE A MATRIX ***
49            DO 10 I=1,15,2
50            J=I+1
51      10    A(I,J)=1.0
52            A(18,19)=1.0
53            A(21,22)=1.0
54            A(2,1)=-2.0*(S(1)+S(3))/B(1)
55            A(2,2)=-2.0*(S(2)+S(4))/B(1)
56            A(2,5)=2.0*(D(2)*S(1)-BB*S(3))/B(1)
57            A(2,6)=2.0*(D(2)*S(2)-BB*S(4))/B(1)
58            A(2,7)=S(1)/B(1)
59            A(2,8)=S(2)/B(1)
60            A(2,9)=A(2,7)
61            A(2,10)=A(2,8)
62            A(2,11)=S(3)/B(1)
63            A(2,12)=S(4)/B(1)
64            A(2,13)=A(2,11)
65            A(2,14)=A(2,12)
66            RI1=B(4)/(B(2)*B(3)-1.0)
67            RI2=B(3)/(B(2)*B(3)-1.0)
68            A(4,1)=-2.0*RI1*(BB*S(3)-D(2)*S(1))
69            A(4,2)=-2.0*RI1*(BB*S(4)-D(2)*S(2))
70            A(4,3)=-0.5*RI2*(S(1)*D(3)**2+S(3)*D(4)**2)
71            A(4,4)=-0.5*RI2*(S(2)*D(3)**2+S(4)*D(4)**2)
72            A(4,5)=-2.0*RI1*(S(3)*BB**2+S(1)*D(2)**2)
73            A(4,6)=-2.0*RI1*(S(4)*BB**2+S(2)*D(2)**2)
74            A(4,7)=S(1)*(0.5*D(3)*RI2-D(2)*RI1)
75            A(4,8)=S(2)*A(4,7)/S(1)
76            A(4,9)=-S(1)*(0.5*D(3)*RI2+D(2)*RI1)
77            A(4,10)=S(2)*A(4,9)/S(1)
78            A(4,11)=S(3)*(0.5*D(4)*RI2+BB*RI1)
79            A(4,12)=S(4)*A(4,11)/S(3)
80            A(4,13)=S(3)*(BB*RI1-0.5*D(4)*RI2)
81            A(4,14)=S(4)*A(4,13)/S(3)
82            RI3=(B(4)**2+S(2)*B(3)-1.0)/(B(3)*(B(2)*B(3)-1.0))
83            A(6,1)=-2.0*RI3*(BB*S(3)-D(2)*S(1))
84            A(6,2)=-2.0*RI3*(BB*S(4)-D(2)*S(2))
85            A(6,3)=-0.5*RI1*(S(1)*D(3)**2+S(3)*D(4)**2)
86            A(6,4)=-0.5*RI1*(S(2)*D(3)**2+S(4)*D(4)**2)
87            A(6,5)=-2.0*RI3*(S(1)*D(2)**2+S(3)*BB**2)
88            A(6,6)=-2.0*RI3*(S(2)*D(2)**2+S(4)*BB**2)
89            A(6,7)=-S(1)*(D(2)/B(3)+D(2)*B(4)*RI1/B(3)-0.5*D(3)*RI1)
90            A(6,8)=S(2)*A(6,7)/S(1)
91            A(6,9)=-S(1)*(D(2)/B(3)+D(2)*B(4)*RI1/B(3)+0.5*D(3)*RI1)
92            A(6,10)=S(2)*A(6,9)/S(1)
```

```
      A(6,11)=S(3)*(BB/B(3)+BB*B(4)*RI1/B(3)+0.5*)(4)*RI1)
      A(6,12)=S(4)*A(6,11)/S(3)
      A(6,13)=S(3)*(BB/B(3)+BB*B(4)*RI1/B(3)-0.5*)(4)*RI1)
      A(6,14)=S(4)*A(6,13)/S(3)
      A(8,7)=-0.5945*RT**2
      A(8,8)=-0.5428*RT
      A(10,9)=A(8,7)
      A(10,10)=A(8,8)
      A(12,11)=A(8,7)
      A(12,12)=A(8,8)
      A(14,13)=A(8,7)
      A(14,14)=A(8,8)
      A(16,1)=AK(1,3)/RAM
      A(16,2)=AC(1,3)/RAM
      A(16,3)=(R(2)*AK(1,3)-R(3)*AK(1,2)+ATR(1,1))/RAM
      A(16,4)=(R(2)*AC(1,3)-R(3)*AC(1,2)+ATR(1,2))/RAM
      A(16,5)=(R(3)*AK(1,1)-R(1)*AK(1,3)+ATR(1,3))/RAM
      A(16,6)=(R(3)*AC(1,1)-R(1)*AC(1,3)+ATR(1,4))/RAM
      A(16,15)=-AK(1,1)/RAM
      A(16,16)=-AC(1,1)/RAM
      A(16,17)=AK(1,1)/RAM
      A(16,18)=-AK(1,2)/RAM
      A(16,19)=-AC(1,2)/RAM
      A(16,20)=AK(1,2)/RAM
      A(16,21)=-AK(1,3)/RAM
      A(16,22)=-AC(1,3)/RAM
      A(16,23)=AK(1,3)/RAM
      A(19,1)=AK(2,3)/RAM
      A(19,2)=AC(2,3)/RAM
      A(19,3)=(R(2)*AK(2,3)-R(3)*AK(2,2)+ATR(2,1))/RAM
      A(19,4)=(R(2)*AC(2,3)-R(3)*AC(2,2)+ATR(2,2))/RAM
      A(19,5)=(R(3)*AK(2,1)-R(1)*AK(2,3)+ATR(2,3))/RAM
      A(19,6)=(R(3)*AC(2,1)-R(1)*AC(2,3)+ATR(2,4))/RAM
      A(19,15)=-AK(2,1)/RAM
      A(19,16)=-AC(2,1)/RAM
      A(19,17)=AK(2,1)/RAM
      A(19,18)=-AK(2,2)/RAM
      A(19,19)=-AC(2,2)/RAM
      A(19,20)=AK(2,2)/RAM
      A(19,21)=-AK(2,3)/RAM
      A(19,22)=-AC(2,3)/RAM
      A(19,23)=AK(2,3)/RAM
      A(22,1)=AK(3,3)/RAM
      A(22,2)=AC(3,3)/RAM
      A(22,3)=(R(2)*AK(3,3)-R(3)*AK(3,2)+ATR(3,1))/RAM
      A(22,4)=(R(2)*AC(3,3)-R(3)*AC(3,2)+ATR(3,2))/RAM
      A(22,5)=(R(3)*AK(3,1)-R(1)*AK(3,3)+ATR(3,3))/RAM
      A(22,6)=(R(3)*AC(3,1)-R(1)*AC(3,3)+ATR(3,4))/RAM
      A(22,15)=-AK(3,1)/RAM
      A(22,16)=-AC(3,1)/RAM
      A(22,17)=AK(3,1)/RAM
      A(22,18)=-AK(3,2)/RAM
      A(22,19)=-AC(3,2)/RAM
      A(22,20)=AK(3,2)/RAM
      A(22,21)=-AK(3,3)/RAM
      A(22,22)=-AC(3,3)/RAM
      A(22,23)=AK(3,3)/RAM
      IPRINT=IO('ENTER 1 TO PRINT A,BJ,BW, ELSE 0 ...')
      IF(IPRINT.NE.1) GO TO 411
      CALL QUOTE('SYSTEM RAW MATRIX ...')
      PRINT 11, ((A(I,J),J=1,23),I=1,23)
C     WRITE(9,1101) ((A(I,J),J=1,23),I=1,23)
11    FORMAT(23(10(1X,E10.5)/10(1X,E10.5)/3(1X,E10.5)/))
1101  FORMAT(23(2(8E10.5/),7E10.5/))
C *** COMPUTE 4 MATRIX ***
411   BJ(16,1)=RKPROP*AC(1,1)/RAM
```

```
159             QJ(15,2)=RKPROP*AC(1,2)/RAM
160             QJ(16,3)=RKPROP*AC(1,3)/RAM
161             QJ(17,1)=RKPROP
162             QJ(19,1)=RKPROP*AC(2,1)/RAM
163             QJ(19,2)=RKPROP*AC(2,2)/RAM
164             QJ(19,3)=RKPROP*AC(2,3)/RAM
165             QJ(20,2)=RKPROP
166             QJ(22,1)=RKPROP*AC(3,1)/RAM
167             QJ(22,2)=RKPROP*AC(3,2)/RAM
168             QJ(22,3)=RKPROP*AC(3,3)/RAM
169             QJ(23,3)=RKPROP
170             IF(IPRINT.NE.1) GO TO 412
171             CALL QUOTE('NONZERO TERMS OF SYSTEM "QJ" MATRIX ...')
172             PRINT 12, ((I,(QJ(I,J),J=1,3)),I=16,23)
173     C       WRITE(9,1201) ((QJ(I,J),J=1,3),I=16,23)
174     12      FORMAT(5(1X,I2,3(1X,E10.5)/))
175     1201    FORMAT(5(1X,E10.5)/)
176     C *** COMPUTE W MATRIX ***
177     412     QW(8,1)=RDKLF*0.5945*TKF*RT**2/(TKF+S(1))
178             QW(10,2)=RDKRF*QW(8,1)/RDKLF
179             QW(12,3)=RDKLR*0.5945*TKR*RT**2/(TKR+S(3))
180             QW(14,4)=RDKRR*QW(12,3)/RDKLR
181             IF(IPRINT.NE.1) GO TO 413
182             CALL QUOTE('NONZERO TERMS OF SYSTEM "QW" MATRIX ...')
183             PRINT 13, ((I,(QW(I,J),J=1,4)),I=8,14,2)
184     C       WRITE(9,1301) ((QW(I,J),J=1,4),I=8,14,2)
185     13      FORMAT(4(1X,I2,4(1X,E10.5)/))
186     1301    FORMAT(4(1X,E10.5)/)
187     413     IGAIN=IQ('TO USE PRECOMPUTED GAINS ENTER 1, ELSE 0 ...')
188             IF(IGAIN.EQ.1)GO TO 420
189             IH33=IQ('TO INITIATE H33 AS NULL MATRIX ENTER 1, ELSE 0 ...')
190             IF(IH33.EQ.1)GO TO 4139
191             CALL QUOTE('ENTER INITIAL VALUES FOR H33 ...')
192             READ 1, ((H33(I,J),J=1,9),I=1,9)
193     4139    CALL QUOTE('FO=J**2+AW*X**2+BW*(X-E)**2, ENTER AW,BW ...')
194             READ 1, AW,BW
195     C *** FORM FJ AND FX ***
196             DO 4140 I=1,3
197     4140    FJ(I)=1.0
198             DO 4141 L=0,6,3
199             J=L+3
200             I=L+1
201             FX(I,I)=AW+BW
202             FX(J,J)=BW
203             FX(I,J)=-BW
204     4141    FX(J,I)=-BW
205     C *** COMPUTE CONTROLLER GAINS G ***
206             CALL GAIN3(A,GU,FJ,FX,G,0,H33)
207     41301   TAU=IQ('ENTER INTEGRATION STEP SIZE, SECONDS ...')
208     C *** COMPUTE DISCRETE TIME MATRICES P AND R ***
209             CALL PQR3(A,GU,QW,G,TAU,P,PQW)
210             IF(IPRINT.NE.1) GO TO 414
211             CALL QUOTE('SYSTEM "P" MATRIX ...')
212             PRINT 11, ((P(I,J),J=1,23),I=1,23)
213             CALL QUOTE('SYSTEM "PQW" MATRIX ...')
214             PRINT 1301, ((PQW(I,J),J=1,4),I=1,23)
215             CALL QUOTE('SYSTEM CONTROLLER GAINS GC ...')
216             PRINT 111, ((G(I,J),J=1,23),I=1,3)
217     111     FORMAT(3(10(1X,E10.5)/10(1X,F10.5)/3(1X,E10.5)/))
218     C *** WRITE RESULTS TO FILE 9 ***
219     414     DO 41409 I=1,3
220             WRITE(9,12345) (G(I,J),J=1,8)
221             WRITE(9,12345) (G(I,J),J=9,16)
222     41409   WRITE(9,12346) (G(I,J),J=17,23)
223     12345   FORMAT(8E10.5)
224     12346   FORMAT(7E10.5)
```

```
225             DO 41406 I=1,23
226             WRITE(9,12345) (P(I,J),J=1,8)
227             WRITE(9,12345) (P(I,J),J=9,16)
228       41408 WRITE(9,12346) (P(I,J),J=17,23)
229             DO 41407 I=1,23
230       41407 WRITE(9,12347) (PQW(I,J),J=1,4)
231       12347 FORMAT(4E10.5)
232             STOP
233       420   CALL QUOTE('ENTER PRECOMPUTED CONTROLLER GAIN G ...')
234             READ 1, ((G(I,J),J=1,23),I=1,3)
235             GO TO 41301
236             END
C*OPTLIB.GAIN3
  1             SUBROUTINE GAIN3(A,QJ,FJ,FX,G,IPR,H33)
  2       C *** IPR=0 CAUSES G NOT TO BE WRITTEN TO A FILE BY GAIN3 ***
  3       C *** H33 IS STARTING VALUE FOR H33 - NORMALLY NULL ***
  4       C *** QJ IS THE SYSTEM 3 MATRIX FROM THE THESIS
  5             DIMENSION A(23,23),QJ(23,3),FJ(3),FX(9,9),G(3,23),
  6            AB(9,3),AAA(9,9),AAAT(9,9),AVA(9,6),AVAT(6,9),
  7            AAVV(6,6),AVVT(6,6),AFV(6,8),AFVT(8,6),AFF(8,8),
  8            AAFFT(8,8),D661(6,6),D662(6,6),D663(6,6),D664(6,6),
  9            AD991(9,9),D992(9,9),D993(9,9),D994(9,9),
 10            AASTAR(9,9),H11(6,6),H12(6,8),H13(6,9),H21(8,6),
 11            AH22(8,8),H23(8,9),H31(9,6),H32(9,8),H33(9,9),
 12            AGOMX1(36,36),
 13            AGOMX2(21,21),
 14            AGOMX3(48,48),D681(6,8),D682(6,8),D683(6,8),
 15            AD881(8,8),D882(8,8),D883(8,8),H(23,23),D3231(3,23),
 16            AD331(3,3),D391(3,9),D931(9,3),D691(6,9),D981(9,8),
 17            AGOMX4(54,54),
 18            AD721(72,72),D722(72,72),D723(72,72),
 19            AAT(23,23),BFUBT(23,23),HA(23,23),ATH(23,23),
 20            APT(23,23),HDOT(23,23),D891(8,9),EX(54),EXX(21),EXXX(72),
 21            AXEX(48),EXEX(36)
 22       1     FORMAT(1X,'ITERATION ',I4,' T=',E10.5,' RMXTRM=',E10.5,
 23            A' RNORM=',E10.5/)
 24       2     FORMAT(23(10(1X,E10.5)/10(1X,E10.5)/3(1X,E10.5)/))
 25       21    FORMAT(3(10(1X,E10.5)/10(1X,E10.5)/3(1X,E10.5)/))
 26       3     FORMAT(9(1X,E10.5))
 27       4     FORMAT()
 28       C *** PARTITIONING OF A AND QU MATRICES ***
 29             DO 9 I=1,6
 30             DO 9 J=1,6
 31             AVV(I,J)=A(I,J)
 32       9     AVVT(J,I)=AVV(I,J)
 33             DO 10 I=1,6
 34             DO 10 J=1,9
 35             JJ=J+14
 36             AVA(J,I)=A(JJ,I)
 37       10    AVAT(I,J)=AVA(J,I)
 38             DO 11 I=1,9
 39             II=I+14
 40             DO 112 K=1,3
 41       112   B(I,K)=QJ(II,K)
 42             DO 11 J=1,9
 43             JJ=J+14
 44             AAA(I,J)=A(II,JJ)
 45       11    AAAT(J,I)=AAA(I,J)
 46             DO 12 I=1,6
 47             DO 12 J=1,8
 48             JJ=J+6
 49             AFV(I,J)=A(I,JJ)
 50       12    AFVT(J,I)=AFV(I,J)
 51             DO 14 I=1,8
 52             II=I+6
 53             DO 14 J=1,8
```

```
54            JJ=J+5
55            AFF(I,J)=A(II,JJ)
56      14    AFFT(J,I)=AFF(I,J)
57      C *** COMPUTATION OF BSTAR, NONZERO TERM OF B*(FU**-1)*(B TRANSPOSE)
58            DO 25 I=1,3
59      25    D331(I,I)=1/FU(I)
60            CALL MXMLT(3,D331,D931,9,3,3,9,3)
61            CALL MXTRN(B,D391,9,3,9,3)
62            CALL MXMLT(D931,D391,BSTAR,9,3,9,9,3)
63            DO 26 I=1,9
64            II=I+14
65            DO 26 J=1,9
66            JJ=J+14
67      26    BFUIBT(II,JJ)=BSTAR(I,J)
68      C *** ITERATIVE STEPS BEGIN FOR H33 ***
69            T=0.0
70            II=0
71            CALL QUOTE('ENTER INITIAL DT,IGO, IGO=0 STOPS ...')
72      C *** ITERATION PROCEEDS IGO STEPS OF INTERVAL LENGTH DT ***
73            READ 4, DT,IGO
74            IF(IGO.EQ.0)GO TO 600
75      30    II=II+1
76      C *** NEGATIVE TERMS ***
77            CALL MXMLT(H33,AAA,D991,9,9,9,9,9)
78            CALL MXMLT(AAAT,H33,D992,9,9,9,9,9)
79            CALL MXADD(D991,D992,D993,9,9,9)
80            CALL MXADD(D993,FX,D992,9,9,9)
81      C *** POSITIVE TERMS ***
82            CALL MXMLT(BSTAR,H33,D993,9,9,9,9,9)
83            CALL MXMLT(H33,D993,D991,9,9,9,9,9)
84      C *** POSITIVE TERMS - NEGATIVE TERMS ***
85            DO 521 I=1,9
86            DO 521 J=1,9
87      521   D992(I,J)=D991(I,J)-D992(I,J)
88      C *** COMPUTE NORM OF HDOT ***
89            RMXTRM=0.0
90            RNORM=0.0
91            DO 550 I=1,9
92            DO 550 J=1,9
93            TRMABS=ABS(D992(I,J))
94            IF(TRMABS.GT.RMXTRM) RMXTRM=TRMABS
95            RNORM=RNORM+TRMABS
96      550   CONTINUE
97      C *** COMPUTATION OF NEW H33 ***
98            DO 580 I=1,9
99            DO 580 J=1,9
100     C *** SAVE OLD H33 FOR BACKUP ***
101           D994(I,J)=H33(I,J)
102     580   H33(I,J)=H33(I,J)+DT*D992(I,J)
103     C *** INVOKE SYMMETRY TO REDUCE ACCUMULATED NUMERICAL ERRORS ***
104           CALL SYMFIX(H33,9)
105           T=T+DT
106           IF((IGO-II).GT.0)GO TO 30
107     C *** PRINT RESULT SO FAR ***
108           PRINT 1, II,T,RMXTRM,RNORM
109     C *** IF RESULT IS UNDESIRABLE, BACK UP ***
110           INUTS=IO('TO BACK UP ENTER -1 ...')
111           IF(INUTS.EQ.-1)GO TO 590
112     C *** ITERATE FURTHER ***
113     585   CALL QUOTE('ENTER DT,IGO, IGO=0 STOPS ...')
114           READ 4, DT,IGO
115           IF(IGO.EQ.0)GO TO 599
116           IGOHLD=IGO
117           IGO=II+IGO
118           GO TO 30
119     C *** TO BACK UP SET EVERYTHING TO VALUE PRIOR TO LAST IGO ITERATIONS
```

```
      590   DO 591 I=1,9
            DO 591 J=1,9
      591   H33(I,J)=D994(I,J)
            T=T+DT*IGOHLD
            II=II-IGOHLD
            GO TO 585
      599   CONTINUE
      C *** WRITE FINAL H33 TO FILE 10 ***
            WRITE(10) ((H33(I,J),J=1,9),I=1,9)
      600   CONTINUE
      C *** COMPUTATION OF H13 AND H31 ***
      C *** SET UP ALGEBRAIC EQUATIONS ***
            CALL MXMLT(BSTAR,H33,D991,9,9,9,9)
            CALL MXSUB(D991,AAA,D992,9,9,9)
            CALL AHBN99(D721,D992,72)
            CALL AHBN69(D722,AVVT,72)
            CALL MXSUB(D721,D722,D723,54,54,72)
            DO 601 I=1,54
            DO 601 J=1,54
      601   GOMX4(I,J)=D723(I,J)
            CALL MXMLT(AVAT,H33,D691,6,9,9,6,9)
            DO 602 K=1,6
            DO 602 L=1,9
            I=K*L+(K-1)*(9-L)
      602   EX(I)=D691(K,L)
      C *** SOLVE ALGEBRAIC EQUATIONS ***
            CALL SIMQ(GOMX4,EX,54,IERROR)
            IF(IERROR.EQ.0)GO TO 6021
            CALL QUOTE('SIMQ RETURNS 1 AT STEP H13-H31')
            STOP
      C *** FORM H13, H31 FROM SOLUTION ***
      6021  DO 603 K=1,6
            DO 603 L=1,9
            I=K*L+(K-1)*(9-L)
            H31(L,K)=EX(I)
      603   H13(K,L)=EX(I)
      C *** ZERO DUMMY MATRICES ***
            CALL DZ(D721,54,54,72,72)
            CALL DZ(D722,54,54,72,72)
            CALL DZ(D723,54,54,72,72)
      C *** COMPUTATION OF H11 ***
      C *** SET UP ALGEBRAIC EQUATIONS ***
            CALL AHBNSS(D721,AVV,72)
            CALL AHBNSS(D722,AVVT,72)
            CALL MXADD(D721,D722,D723,21,21,72)
            DO 604 I=1,21
            DO 604 J=1,21
      604   GOMX2(I,J)=D723(I,J)
            CALL MXMLT(H13,AVA,D661,6,9,6,6,9)
            CALL MXMLT(AVAT,H31,D662,6,9,6,6,9)
            CALL MXMLT(H13,BSTAR,D691,6,9,9,6,9)
            CALL MXMLT(D691,H31,D664,6,9,6,6,9)
            CALL MXSUB(D664,D661,D663,6,6,6)
            CALL MXSUB(D663,D662,D661,6,6,6)
            DO 605 I=1,6
      605   EXX(I)=D661(1,I)
            DO 606 I=7,11
            J=I-5
      606   EXX(I)=D661(2,J)
            DO 607 I=12,15
            J=I-9
      607   EXX(I)=D661(3,J)
            DO 608 I=16,18
            J=I-12
      608   EXX(I)=D661(4,J)
            EXX(19)=D661(5,5)
```

```
      EXX(20)=D661(5,6)
      EXX(21)=D661(6,6)
C *** SOLVE ALGEBRAIC EQUATIONS ***
      CALL SIMQ(GOMX2,EXX,21,IERROR)
      IF(IERROR.EQ.0)GO TO 6081
      CALL QUOTE('SIMQ RETURNS 1 AT STEP H11')
      STOP
C *** FORM H11 FROM SOLUTION ***
6081  DO 609 I=1,6
      H11(1,I)=EXX(I)
609   H11(I,1)=H11(1,I)
      DO 700 I=7,11
      J=I-5
      H11(2,J)=EXX(I)
700   H11(J,2)=H11(2,J)
      DO 701 I=12,15
      J=I-9
      H11(3,J)=EXX(I)
701   H11(J,3)=H11(3,J)
      DO 702 I=16,18
      J=I-12
      H11(4,J)=EXX(I)
702   H11(J,4)=H11(4,J)
      H11(5,5)=EXX(19)
      H11(5,6)=EXX(20)
      H11(6,5)=H11(5,6)
      H11(6,6)=EXX(21)
C *** ZERO DUMMY MATRICES ***
      CALL DZ(D721,21,21,72,72)
      CALL DZ(D722,21,21,72,72)
      CALL DZ(D723,21,21,72,72)
C *** COMPUTATION OF H23 AND H32 ***
C *** SET UP ALGEBRAIC EQUATIONS ***
      CALL MXMLT(SSTAR,H33,D991,9,9,9,9,9)
      CALL MXSUB(D991,AAA,D992,9,9,9)
      CALL H4A999(D721,D992)
      CALL AH6H89(D722,AFFT)
      CALL MXSUB(D721,D722,D723,72,72,72)
      CALL MXMLT(AFVT,H13,D891,8,6,9,8,5)
      DO 704 K=1,8
      DO 704 L=1,9
      I=K*L+(K-1)*(9-L)
704   EXXX(I)=D891(K,L)
C *** SOLVE ALGEBRAIC EQUATIONS ***
      CALL SIMQ(D723,EXXX,72,IERROR)
      IF(IERROR.EQ.0)GO TO 7401
      CALL QUOTE('SIMQ RETURNS 1 AT STEP H23-H32')
      STOP
C *** FORM H23, H32 FROM SOLUTION ***
7401  DO 705 K=1,8
      DO 705 L=1,9
      I=K*L+(K-1)*(9-L)
      H23(K,L)=EXXX(I)
705   H32(L,K)=H23(K,L)
C *** ZERO DUMMY MATRICES ***
      CALL DZ(D721,72,72,72,72)
      CALL DZ(D722,72,72,72,72)
      CALL DZ(D723,72,72,72,72)
C *** COMPUTATION OF H12 AND H21***
C *** SET UP ALGEBRAIC EQUATIONS ***
      CALL HA6B98(D721,AFF,72)
      CALL AH6B68(D722,AVVT,72)
      CALL MXADD(D721,D722,D723,48,48,72)
      DO 706 I=1,48
      DO 706 J=1,48
706   GOMX3(I,J)=D723(I,J)
```

```
252             CALL MXMLT(SSTAR,H32,D981,9,9,8,9,9)
253             CALL MXMLT(H13,D981,D682,6,9,8,8,9)
254             CALL MXMLT(AVAT,H32,D681,6,9,8,6,9)
255             CALL MXSUB(D682,D981,D683,6,8,6)
256             CALL MXMLT(H11,AFV,D681,8,6,8,6,6)
257             CALL MXSUB(D683,D681,D682,6,8,6)
258             DO 707 K=1,6
259             DO 707 L=1,8
260             I=K*L+(K-1)*(8-L)
251     707     XEX(I)=D682(K,L)
262     C *** SOLVE ALGEBRAIC EQUATIONS ***
263             CALL SIMQ(GMX3,XEX,48,IERROR)
264             IF(IERROR.EQ.0)GO TO 7071
265             CALL QUOTE('SIMQ RETURNS 1 AT STEP H12-H21')
266             STOP
267     C *** FORM H12, H21 FROM SOLUTION ***
268     7071    DO 705 K=1,6
269             DO 708 L=1,8
270             I=K*L+(K-1)*(8-L)
271             H12(K,L)=XEX(I)
272     708     H21(L,K)=H12(K,L)
273     C *** ZERO DUMMY MATRICES ***
274             CALL DZ(D721,48,48,72,72)
275             CALL DZ(D722,48,48,72,72)
276             CALL DZ(D723,48,48,72,72)
277     C *** COMPUTATION OF H22 ***
278     C *** SET UP ALGEBRAIC EQUATIONS ***
279             CALL AMBASS(D721,AFFT,72)
280             CALL MASMSS(D722,AFF,72)
281             CALL MXADD(D721,D722,D723,36,36,72)
282             DO 709 I=1,36
283             DO 709 J=1,36
284     709     GMX1(I,J)=D723(I,J)
285             CALL MXMLT(SSTAR,H32,D981,9,9,8,9,9)
286             CALL MXMLT(H23,D981,D881,8,9,8,8,9)
287             CALL MXMLT(AFVT,H12,D882,8,6,8,8,6)
288             CALL MXSUB(D881,D882,D883,8,8,8)
289             CALL MXMLT(H21,AFV,D881,8,6,8,8,6)
290             CALL MXSUB(D883,D881,D882,8,8,8)
291             DO 710 I=1,8
292     710     XEX(I)=D882(1,I)
293             DO 711 I=9,15
294             J=I-7
295     711     XEX(I)=D882(2,J)
296             DO 712 I=16,21
297             J=I-13
298     712     XEX(I)=D882(3,J)
299             DO 714 I=22,26
300             J=I-18
301     714     XEX(I)=D882(4,J)
302             DO 715 I=27,30
303             J=I-22
304     715     XEX(I)=D882(5,J)
305             DO 716 I=31,33
306             J=I-25
307     716     XEX(I)=D882(6,J)
308             XEX(34)=D882(7,7)
309             XEX(35)=D882(7,8)
310             XEX(36)=D882(8,8)
311     C *** SOLVE ALGEBRAIC EQUATIONS ***
312             CALL SIMQ(GMX1,XEX,36,IERROR)
313             IF(IERROR.EQ.0)GO TO 7161
314             CALL QUOTE('SIMQ RETURNS 1 AT STEP H22')
315             STOP
316     C *** FORM H22 FROM SOLUTION ***
317     7161    DO 717 I=1,8
```

```
318             H22(1,I)=EXEX(I)
319       717   H22(1,1)=H22(1,I)
320             DO 718 I=9,15
321             J=I-7
322             H22(2,J)=EXEX(I)
323       718   H22(J,2)=H22(2,J)
324             DO 719 I=16,21
325             J=I-13
326             H22(J,3)=EXEX(I)
327       719   H22(3,J)=H22(J,3)
328             DO 720 I=22,26
329             J=I-18
330             H22(4,J)=EXEX(I)
331       720   H22(J,4)=H22(4,J)
332             DO 721 I=27,30
333             J=I-22
334             H22(5,J)=EXEX(I)
335       721   H22(J,5)=H22(5,J)
336             DO 722 I=31,33
337             J=I-25
338             H22(6,J)=EXEX(I)
339       722   H22(J,6)=H22(6,J)
340             H22(7,7)=EXEX(34)
341             H22(7,8)=EXEX(35)
342             H22(8,7)=H22(7,8)
343             H22(8,8)=EXEX(36)
344       C *** FORMATION OF H MATRIX ***
345             DO 810 I=1,6
346             DO 810 J=1,6
347       810   H(I,J)=H11(I,J)
348             DO 811 I=1,6
349             DO 811 J=1,8
350             JJ=J+6
351             H(I,JJ)=H12(I,J)
352       811   H(JJ,I)=H21(J,I)
353             DO 812 I=1,8
354             II=I+6
355             DO 812 J=1,8
356             JJ=J+6
357       812   H(II,JJ)=H22(I,J)
358             DO 813 I=1,9
359             II=I+14
360             DO 813 J=1,9
361             JJ=J+14
362       813   H(II,JJ)=H33(I,J)
363             DO 814 I=1,6
364             DO 814 J=1,9
365             JJ=J+14
366             H(I,JJ)=H13(I,J)
367       814   H(JJ,I)=H31(J,I)
368             DO 815 I=1,8
369             II=I+6
370             DO 815 J=1,9
371             JJ=J+14
372             H(II,JJ)=H23(I,J)
373       815   H(JJ,II)=H32(J,I)
374       C *** TEST ACCURACY IN H MATRIX BY SUBSTITUTION INTO RICCATI EQUATION
375             CALL MXTRN(A,AT,23,23,23,23)
376             CALL MXMLT(H,A,HA,23,23,23,23,23)
377             CALL MXMLT(AT,H,ATH,23,23,23,23,23)
378             CALL MXADD(HA,ATH,HA,23,23,23)
379             DO 820 I=1,9
380             II=I+14
381             DO 820 J=1,9
382             JJ=J+14
383       820   HA(II,JJ)=HA(II,JJ)+FX(I,J)
```

```
384             CALL MXMLT(SFJIBF,H,ATH,23,23,23,23,23)
385             CALL MXMLT(H,ATH,PT,23,23,23,23,23)
386             CALL MXSUB(PT,H4,HDOT,23,23,23)
387       C *** COMPUTE NORM OF HDOT ***
388             RNORM=0.0
389             RMXTRM=0.0
390             DO 825 I=1,23
391             DO 825 J=1,23
392             TRMABS=ABS(HDOT(I,J))
393             IF(TRMABS.GT.RMXTRM) RMXTRM=TRMABS
394       825   RNORM=RNORM+TRMABS
395             PRINT 826, RMXTRM,RNORM
396       826   FORMAT('0TEST OF H MATRIX ACCURACY ...'/1X,
397            A'HDOT SHOULD BE NULL MATRIX'/1X,'MAX HDOT(I,J)=',E10.5/
398            A1X,'NORM OF HDOT =',E10.5/)
399       C *** COMPUTATION OF OPTIMAL CONTROLLER GAIN G ***
400             DO 861 I=1,3
401             DO 861 J=15,23
402       861   D3231(I,J)=GU(J,I)/FJ(I)
403             CALL MXMLT(D3231,H,G,3,23,23,3,23)
404             IF(IPR.EQ.0) RETURN
405             DO 862 I=1,3
406             WRITE(IPR,863) (G(I,J),J=1,8)
407             WRITE(IPR,863) (G(I,J),J=9,16)
408       862   WRITE(IPR,864) (G(I,J),J=17,23)
409       863   FORMAT(8E10.5/)
410       864   FORMAT(7E10.5/)
411             RETURN
412             END
  *OPTLIB.SYMFIX
  1             SUBROUTINE SYMFIX(A,N)
  2             DIMENSION A(N,N)
  3             DO 10 J=2,N
  4             K=J-1
  5             DO 10 I=1,K
  6             AVG=0.5*(A(I,J)+A(J,I))
  7             A(I,J)=AVG
  8       10    A(J,I)=AVG
  9             RETURN
 10             END
  *OPTLIB.HA6999
  1             SUBROUTINE HA6999(HA54,A,NXX,XN)
  2       C *** NXXXXN MUST BE .GE. 54 ***
  3             DIMENSION HA54(NXXXXN,NXXXXN),A(9,9)
  4             DO 10 L=0,45,9
  5             DO 10 I=1,9
  6             DO 10 J=1,9
  7             M=I+L
  8             N=J+L
  9       10    HA54(M,N)=A(J,I)
 10             RETURN
 11             END
  *OPTLIB.AH6669
  1             SUBROUTINE AH6669(AH54,A,NXX,XN)
  2       C *** NXXXXN MUST BE .GE. 54 ***
  3             DIMENSION AH54(NXXXXN,NXXXXN),A(6,6)
  4             DO 10 I=1,46,9
  5             DO 10 J=1,46,9
  6             KK=(I+8)/9
  7             LL=(J+8)/9
  8             DO 10 K=0,8
  9             II=I+K
 10             JJ=J+K
 11       10    AH54(II,JJ)=A(KK,LL)
 12             RETURN
 13             END
```

```
*OPTLIB.DZ
1             SUBROUTINE DZ(A,N,M,NMX,MMX)
2             DIMENSION A(NMX,MMX)
3             DO 10 I=1,N
4             DO 10 J=1,M
5       10    A(I,J)=0.0
6             RETURN
7             END
*OPTLIB.HA66SS
1             SUBROUTINE HA66SS(HA21,A,NXXxXN)
2       C *** NXXxXN MUST BE .GE. 21 ***
3             DIMENSION HA21(NXXXXN,NXXXXN),A(6,6)
4             DO 10 I=1,6
5             DO 10 J=1,6
6       10    HA21(I,J)=A(J,I)
7             DO 11 I=7,11
8             J=I-5
9             HA21(I,2)=A(1,J)
10            DO 11 K=7,11
11            L=K-5
12      11    HA21(I,K)=A(L,J)
13            DO 12 I=12,15
14            J=I-9
15            HA21(I,3)=A(1,J)
16            HA21(I,8)=A(2,J)
17            DO 12 K=12,15
18            L=K-9
19      12    HA21(I,K)=A(L,J)
20            DO 13 I=16,18
21            J=I-12
22            HA21(I,4)=A(1,J)
23            HA21(I,9)=A(2,J)
24            HA21(I,13)=A(3,J)
25            DO 13 K=16,18
26            L=K-12
27      13    HA21(I,K)=A(L,J)
28            DO 14 I=19,20
29            J=I-14
30            HA21(I,5)=A(1,J)
31            HA21(I,10)=A(2,J)
32            HA21(I,14)=A(3,J)
33            HA21(I,17)=A(4,J)
34            HA21(I,19)=A(5,J)
35      14    HA21(I,20)=A(6,J)
36            HA21(21,6)=A(1,6)
37            HA21(21,11)=A(2,6)
38            HA21(21,15)=A(3,6)
39            HA21(21,18)=A(4,6)
40            HA21(21,20)=A(5,6)
41            HA21(21,21)=A(6,6)
42            RETURN
43            END
*OPTLIB.AH66SS
1             SUBROUTINE AH66SS(AH21,A,NXXxXN)
2       C *** NXXxXN MUST BE .GE. 21 ***
3             DIMENSION AH21(NXXXXN,NXXXXN),A(6,6)
4             DO 10 I=1,6
5       10    AH21(I,I)=A(1,1)
6             DO 11 I=7,11
7             AH21(I,I)=A(2,2)
8             K=I-5
9             AH21(I,K)=A(2,1)
10      11    AH21(K,I)=A(1,2)
11            DO 12 I=12,15
12            AH21(I,I)=A(3,3)
13            K=I-9
```

```
14              AH21(I,K)=A(3,1)
15              AH21(K,I)=A(1,3)
16              J=K+5
17              AH21(I,J)=A(3,2)
18        12    AH21(J,I)=A(2,3)
19              DO 13 I=16,18
20              AH21(I,I)=A(4,4)
21              K=I-12
22              AH21(I,K)=A(4,1)
23              AH21(K,I)=A(1,4)
24              J=K+5
25              AH21(I,J)=A(4,2)
26              AH21(J,I)=A(2,4)
27              L=K+9
28              AH21(I,L)=A(4,3)
29        13    AH21(L,I)=A(3,4)
30              DO 14 I=19,20
31              AH21(I,I)=A(5,5)
32              K=I-14
33              AH21(I,K)=A(5,1)
34              AH21(K,I)=A(1,5)
35              J=K+5
36              AH21(I,J)=A(5,2)
37              AH21(J,I)=A(2,5)
38              L=K+9
39              AH21(I,L)=A(5,3)
40              AH21(L,I)=A(3,5)
41              LL=K+12
42              AH21(I,LL)=A(5,4)
43        14    AH21(LL,I)=A(4,5)
44              AH21(21,21)=A(6,6)
45              DO 15 I=20,21
46              J=I-15
47              K=J+5
48              L=J+9
49              M=J+12
50              N=J+14
51              AH21(J,I)=A(1,6)
52              AH21(K,I)=A(2,6)
53              AH21(L,I)=A(3,6)
54              AH21(M,I)=A(4,6)
55        15    AH21(N,I)=A(5,6)
56              DO 16 I=2,6
57        16    AH21(1,I)=A(1,I)
58              DO 17 I=3,6
59              J=I+5
60              AH21(2,J)=A(1,I)
61        17    AH21(7,J)=A(2,I)
62              DO 18 I=4,6
63              J=I+9
64              AH21(3,J)=A(1,I)
65              AH21(8,J)=A(2,I)
66        18    AH21(12,J)=A(3,I)
67              DO 19 I=5,6
68              J=I+12
69              AH21(4,J)=A(1,I)
70              AH21(9,J)=A(2,I)
71              AH21(13,J)=A(3,I)
72        19    AH21(16,J)=A(4,I)
73              J=0
74              DO 20 I=1,5
75              J=J+7-I
76        20    AH21(21,J)=A(6,I)
77              RETURN
78              END
```

```
*OPTLIB.HA8999
      SUBROUTINE HA8999(HA72,A)
      DIMENSION HA72(72,72),A(9,9)
      DO 10 L=0,63,9
      DO 10 I=1,9
      DO 10 J=1,9
      M=I+L
      N=J+L
10    HA72(M,N)=A(J,I)
      RETURN
      END
*OPTLIB.AH8889
      SUBROUTINE AH8889(AH72,A)
      DIMENSION AH72(72,72),A(8,8)
      DO 10 I=1,64,9
      DO 10 J=1,64,9
      KK=(I+8)/9
      LL=(J+8)/9
      DO 10 K=0,8
      II=I+K
      JJ=J+K
10    AH72(II,JJ)=A(KK,LL)
      RETURN
      END
*OPTLIB.HA6888
      SUBROUTINE HA6868(HA48,A,NXX,XN)
C *** NXX,XN MUST BE .GE. 48 ***
      DIMENSION HA48(NXXXX,NXXXXN),A(8,8)
      DO 10 L=0,40,8
      DO 10 I=1,8
      DO 10 J=1,8
      M=I+L
      N=J+L
10    HA48(M,N)=A(J,I)
      RETURN
      END
*OPTLIB.AH6668
      SUBROUTINE AH6668(AH48,A,NXX,XN)
C *** NXX,XN MUST BE .GE. 48 ***
      DIMENSION AH48(NXXXX,NXXXXN),A(6,6)
      DO 10 I=1,41,8
      DO 10 J=1,41,8
      KK=(I+7)/8
      LL=(J+7)/8
      DO 10 K=0,7
      II=I+K
      JJ=J+K
10    AH48(II,JJ)=A(KK,LL)
      RETURN
      END
*OPTLIB.AH8SS
      SUBROUTINE AH8SS(AH36,A,NXX,XN)
C *** NXX,XN MUST BE .GE. 36 ***
      DIMENSION AH36(NXXXX,NXXXXN),A(8,8)
      DO 10 I=1,8
10    AH36(I,I)=A(I,I)
      DO 11 I=9,15
      AH36(I,I)=A(2,2)
      K=I-7
      AH36(I,K)=A(2,1)
11    AH36(K,I)=A(1,2)
      DO 12 I=16,21
      AH36(I,I)=A(3,3)
      K=I-13
      AH36(I,K)=A(3,1)
      AH36(K,I)=A(1,3)
```

```
      J=K+7
      AH36(I,J)=A(3,2)
   12 AH36(J,I)=A(2,3)
      DO 13 I=22,26
      AH36(I,I)=A(4,4)
      K=I-18
      AH36(I,K)=A(4,1)
      AH36(K,I)=A(1,4)
      J=K+7
      AH36(I,J)=A(4,2)
      AH36(J,I)=A(2,4)
      L=K+13
      AH36(I,L)=A(4,3)
   13 AH36(L,I)=A(3,4)
      DO 14 I=27,30
      AH36(I,I)=A(5,5)
      K=I-22
      AH36(I,K)=A(5,1)
      AH36(K,I)=A(1,5)
      J=K+7
      AH36(I,J)=A(5,2)
      AH36(J,I)=A(2,5)
      L=K+13
      AH36(I,L)=A(5,3)
      AH36(L,I)=A(3,5)
      LL=K+18
      AH36(I,LL)=A(5,4)
   14 AH36(LL,I)=A(4,5)
      DO 141 I=31,33
      AH36(I,I)=A(6,6)
      K=I-25
      AH36(I,K)=A(6,1)
      AH36(K,I)=A(1,6)
      J=K+7
      AH36(I,J)=A(6,2)
      AH36(J,I)=A(2,6)
      L=K+13
      AH36(I,L)=A(6,3)
      AH36(L,I)=A(3,6)
      LL=K+18
      AH36(I,LL)=A(6,4)
      AH36(LL,I)=A(4,6)
      LLL=K+22
      AH36(I,LLL)=A(6,5)
  141 AH36(LLL,I)=A(5,6)
      DO 142 I=34,35
      AH36(I,I)=A(7,7)
      K=I-27
      AH36(I,K)=A(7,1)
      AH36(K,I)=A(1,7)
      J=K+7
      AH36(I,J)=A(7,2)
      AH36(J,I)=A(2,7)
      L=K+13
      AH36(I,L)=A(7,3)
      AH36(L,I)=A(3,7)
      LL=K+18
      AH36(I,LL)=A(7,4)
      AH36(LL,I)=A(4,7)
      LLL=K+22
      AH36(I,LLL)=A(7,5)
      AH36(LLL,I)=A(5,7)
      LM=K+25
      AH36(I,LM)=A(7,6)
  142 AH36(LM,I)=A(6,7)
      AH36(36,36)=A(8,8)
```

```
      DO 15 I=35,36
      J=I-29
      K=J+7
      L=J+13
      M=J+18
      N=J+22
      MN=J+25
      MMN=J+27
      AM36(J,I)=A(1,8)
      AM36(K,I)=A(2,8)
      AM36(L,I)=A(3,8)
      AM36(M,I)=A(4,8)
      AM36(N,I)=A(5,8)
      AM36(MN,I)=A(6,8)
   15 AM36(MMN,I)=A(7,8)
      DO 16 I=2,8
   16 AM36(1,I)=A(1,I)
      DO 17 I=3,8
      J=I+7
      AM36(2,J)=A(1,I)
   17 AM36(9,J)=A(2,I)
      DO 18 I=4,8
      J=I+13
      AM36(3,J)=A(1,I)
      AM36(10,J)=A(2,I)
   18 AM36(16,J)=A(3,I)
      DO 19 I=5,8
      J=I+19
      AM36(4,J)=A(1,I)
      AM36(11,J)=A(2,I)
      AM36(17,J)=A(3,I)
   19 AM36(22,J)=A(4,I)
      DO 191 I=6,8
      J=I+22
      AM36(5,J)=A(1,I)
      AM36(12,J)=A(2,I)
      AM36(18,J)=A(3,I)
      AM36(23,J)=A(4,I)
  191 AM36(27,J)=A(5,I)
      DO 192 I=7,8
      J=I+25
      AM36(6,J)=A(1,I)
      AM36(13,J)=A(2,I)
      AM36(19,J)=A(3,I)
      AM36(24,J)=A(4,I)
      AM36(28,J)=A(5,I)
  192 AM36(31,J)=A(6,I)
      J=0
      DO 20 I=1,7
      J=J+9-I
   20 AM36(36,J)=A(8,I)
      RETURN
      END
*OPTIONS,AM8SS
      SUBROUTINE AM8SS(AM36,A,NXXXXN)
C *** NXXXXN MUST BE .GE. 36 ***
      DIMENSION AM36(NXXXXN,NXXXXN),A(8,8)
      DO 10 I=1,8
      DO 10 J=1,8
   10 AM36(I,J)=A(J,I)
      DO 101 I=9,15
      J=I-7
      AM36(I,2)=A(1,J)
      DO 101 K=9,15
      L=K-7
  101 AM36(I,K)=A(L,J)
```

```
13              DO 102 I=16,21
14              J=I-13
15              HA36(I,3)=A(1,J)
16              HA36(I,10)=A(2,J)
17              DO 102 K=16,21
18              L=K-13
19        102   HA36(I,K)=A(L,J)
20              DO 11 I=22,26
21              J=I-19
22              HA36(I,4)=A(1,J)
23              HA36(I,11)=A(2,J)
24              HA36(I,17)=A(3,J)
25              DO 11 K=22,26
26              L=K-19
27        11    HA36(I,K)=A(L,J)
28              DO 12 I=27,30
29              J=I-22
30              HA36(I,5)=A(1,J)
31              HA36(I,12)=A(2,J)
32              HA36(I,18)=A(3,J)
33              HA36(I,23)=A(4,J)
34              DO 12 K=27,30
35              L=K-22
36        12    HA36(I,K)=A(L,J)
37              DO 13 I=31,33
38              J=I-25
39              HA36(I,6)=A(1,J)
40              HA36(I,13)=A(2,J)
41              HA36(I,19)=A(3,J)
42              HA36(I,24)=A(4,J)
43              HA36(I,28)=A(5,J)
44              DO 13 K=31,33
45              L=K-25
46        13    HA36(I,K)=A(L,J)
47              DO 14 I=34,35
48              J=I-27
49              HA36(I,7)=A(1,J)
50              HA36(I,14)=A(2,J)
51              HA36(I,20)=A(3,J)
52              HA36(I,25)=A(4,J)
53              HA36(I,29)=A(5,J)
54              HA36(I,32)=A(6,J)
55              HA36(I,34)=A(7,J)
56        14    HA36(I,35)=A(8,J)
57              HA36(36,8)=A(1,8)
58              HA36(36,15)=A(2,8)
59              HA36(36,21)=A(3,8)
60              HA36(36,26)=A(4,8)
61              HA36(36,30)=A(5,8)
62              HA36(36,33)=A(6,8)
63              HA36(36,35)=A(7,8)
64              HA36(36,36)=A(8,8)
65              RETURN
66              END
  *OPTLIB.PQ3
 1              SUBROUTINE PQ3(A,JJ,QW,G,T,P,PQW)
 2              DIMENSION A(23,23),JJ(23,3),QW(23,4),P(23,23),PQW(23,4),
 3             AJC(23),DNN1(23,23),DNN2(23,23),DNN3(23,23),G(3,23),
 4             AASTAR(23,23),C(23),DNN1(3,23),
 5             ADNN4(23,23),DNN5(23,23)
 6              DOUBLE PRECISION DP4(23,23),VV(2)
 7        C *** JJ=3 FROM THESIS ***
 8        C *** QW=3 FROM THESIS ***
 9        C *** FORMATION OF ASTAR=A-BU*G*C ***
10              IOBS=IO('ENTER 1 TO CONTROL OBSERVABILITY, ELSE 0...')
11              IF(IOBS.NE.1)GO TO 8
```

```
12          CALL GJO;E('ENTER DIAGIONAL OBSERVER MATRIX ...')
13          REA) 1, (C(I),I=1,23)
14      1   FORMAT()
15          CALL MXMDIG(G,C,DMN1,3,23,3)
16          DO 7 I=1,3
17          DO 7 J=1,23
18      7   G(I,J)=DMN1(I,J)
19      C *** G NOW CONTAINS G*C ***
20      8   CALL MXMLT(GJ,G,DMN4,23,3,23,23,3)
21          CALL MXSUB(A,DMN4,ASTAR,23,23,23)
22      C *** DETERMINATION OF NECESSARY TERMS IN P EXPANSION ***
23      C901  FORMAT(2X,2(2(E10.5/),7E10.5/))
24          TMAX=0.0
25          DO 10 I=1,23
26          DO 10 J=1,23
27      10  IF(ABS(ASTAR(I,J)).GT.TMAX) TMAX=ABS(ASTAR(I,J))
28          PRINT 11, TMAX
29       11   FORMAT('0MAXIMUM ABS(ASTAR(I,J))=',E10.3/)
30      C *** INTERVAL INITIALLY DIVIDED BY 1000 ***
31          TERMT=T/1000.0
32          QZ=TMAX*TERMT
33          GO=-23*QZ-6.90776
34          NKEEP=1
35          ZKEEP=0.0
36          ZONE=0.0
37      12  NZ=IO('ENTER GUESS FOR NZ REQUIRED TERMS FOR P EXPANSION ...')
38          ZONE=NZ*ALOG(23*QZ)
39          Z=ZONE+ZKEEP
40          DO 15 I=NKEEP,NZ
41      15  Z=Z+ALOG(FLOAT(I))
42          ZKEEP=Z-ZONE
43          NKEEP=NZ+1
44          PRINT 20 Z,NZ,GO
45      20  FORMAT(1X,'Z= ',E10.3,' WITH NZ= ',I4,' TERMS'/
46         A1X,'Z SHOULD BE ',E10.3/)
47          IGO=IO('ENTER 1 TO CHANGE NZ, ELSE 2 ...')
48          IF(IGO.EQ.1) GO TO 12
49      C *** COMPUTATION OF P MATRIX ***
50          DO 30 I=1,23
51          DO 30 J=1,23
52          DMN1(I,J)=0.0
53          DMN3(I,J)=ASTAR(I,J)
54      30  P(I,J)=0.0
55          DO 31 I=1,23
56      31  P(I,I)=1.0
57          CALL MXSCA(DMN3,23,23,23,TERMT)
58          CALL MXADD(P,DMN3,P,23,23,23)
59      C   WRITE(9,901) ((P(I,J),J=1,23),I=1,23)
60          DO 32 I=1,23
61          DO 32 J=1,23
62      32  DMN1(I,J)=DMN3(I,J)
63          DO 35 I=2,NZ
64          CALL MXMLT(DMN3,DMN1,DMN2,23,23,23,23,23)
65          DO 33 KI=1,23
66          DO 33 KJ=1,23
67      33  DMN1(KI,KJ)=DMN2(KI,KJ)/I
68          CALL MXADD(P,DMN1,P,23,23,23)
69      C   WRITE(9,901) ((P(IROW,J),J=1,23),IROW=1,23)
70      35  CONTINUE
71      C *** NOW P(TERMT) IS RAISED TO THE 1000TH POWER, > P(T) ***
72          DO 3501 I=1,3
73          CALL MXMLT(P,P,DMN1,23,23,23,23,23)
74          CALL MXMLT(DMN1,DMN1,DMN2,23,23,23,23,23)
75          CALL MXMLT(P,DMN2,DMN1,23,23,23,23,23)
76          CALL MXMLT(DMN1,DMN1,P,23,23,23,23,23)
```

```
      3501  CONTINUE
C *** COMPUTATION OF  (P-I)*(ASTAR**-1) ***
            DO 35 I=1,23
            DO 35 J=1,23
            DPA(I,J)=ASTAR(I,J)
      35    DNN1(I,J)=P(I,J)
C *** COMPUTE (P-I) ***
            DO 37 I=1,23
      37    DNN1(I,I)=DNN1(I,I)-1.0
            VV(1)=1.0
C *** INVERT ASTAR ***
            CALL DGJR(DPA,23,23,23,23,$50,JC,VV)
            DO 3705 I=1,23
            DO 3705 J=1,23
      3705  DNN2(I,J)=DPA(I,J)
      38    CALL MXHOI(ASTAR,DNN2,DNN3,DNN5,23,23,10,0.005,$51,$52)
      39    CALL MXMLT(DNN1,DNN2,DNN3,23,23,23,23,23)
C *** COMPUTATION OF PQW=(P-I)*(ASTAR**-1)*QW ***
            CALL MXMLT(DNN3,QW,PQW,23,23,4,23,23)
            RETURN
      50    CALL QUOTE('OVERFLOW IN DGJR, CALLED BY PQ3')
            STOP
      51    CALL QUOTE('POOR INVERSE ACCURACY IN PQ3, ERROR FOLLOWS')
            CALL MXMLT(ASTAR,DNN2,DNN3,23,23,23,23,23)
            DO 5101 I=1,23
      5101  DNN3(I,I)=1.0
            CALL MXSUB(DNN5,DNN3,DNN5,23,23,23)
            RNORM=0.0
            RMXTRM=0.0
            DO 5102 I=1,23
            DO 5102 J=1,23
            TRMABS=ABS(DNN5(I,J))
            IF(TRMABS.GT.RMXTRM)RMXTRM=TRMABS
      5102  RNORM=RNORM+TRMABS
            PRINT 5103, TRMABS,RNORM
      5103  FORMAT('0ERROR MAXTERM = ',E10.5,5X,'ERROR NORM = ',E10.5)
            IYGO=IDI('ENTER 1 TO IMPROVE INVERSE, 2 TO GO, 3 TO STOP ...')
            IF(IYGO-2)38,39,80
       80   STOP
            END
 *FIN.TRANS/H33
            DIMENSION H(9,9)
            READ (10) ((H(I,J),J=1,9),I=1,9)
            DO 100 I=1,9
            WRITE(7,2) (H(I,J),J=1,5)
      100   WRITE(7,3) (H(I,J),J=6,9)
      2     FORMAT(4(E14.9,','),E14.9)
      3     FORMAT(3(E14.9,','),E14.9)
            STOP
            END
 *FIN.TRANS/GAIN
            DIMENSION G(3,23)
            CALL QUOTE('ENTER APPROPRIATE GPW ELEMENT')
            DO 10 I=1,3
            READ 1, (G(I,J),J=1,8)
            READ 1, (G(I,J),J=9,16)
      10    READ 2, (G(I,J),J=17,23)
      1     FORMAT(8E10.5)
      2     FORMAT(7E10.5)
            DO 20 I=1,3
            WRITE(7,3) (G(I,J),J=1,7)
            WRITE(7,3) (G(I,J),J=8,14)
            WRITE(7,3) (G(I,J),J=15,21)
      20    WRITE(7,4) (G(I,J),J=22,23)
      3     FORMAT(6(E10.5,','),E10.5)
      4     FORMAT(E10.5,',',E10.5)
```

```
      STOP
      END
*FIN.POSDEF
      DIMENSION H(23,23),GOMX(23,23),JC(23),V(2)
C *** INVESTIGATION OF POSITIVE DEFINATENESS BY PRINCIPAL MINORS ***
1     FORMAT()
C2    FORMAT(1X,'MINOR= ',I2,' DET= ',E10.5/)
      NEID('ENTER MATRIX DIMENSION N ...')
      CALL QUOTE('ENTER MATRIX ...')
      READ 1, ((H(I,J),J=1,N),I=1,N)
      MINOR=1
      IF(H(1,1).LE.0.)GO TO 1000
      DO 900 MINOR=2,N
      DO 10 I=1,MINOR
      DO 10 J=1,MINOR
10    GOMX(I,J)=H(I,J)
      V(1)=2.0
      CALL GJR(GOMX,23,23,MINOR,MINOR,$1900,JC,V)
C     PRINT 5,V(1)
C     DET=V(1)*EXP(V(2))
C     PRINT 2, MINOR,DET
      IF(V(1).LE.0.)GO TO 1000
900   CONTINUE
      CALL QUOTE('H IS POSITIVE DEFINATE !!!')
      STOP
1000  PRINT 3,MINOR
3     FORMAT('0H FAILS POSITIVE DEFINATENESS TEST AT MINOR ',I2)
      STOP
1900  PRINT 4,MINOR
4     FORMAT('0OVERFLOW IN GJR AT MINOR ',I2)
C5    FORMAT(1X,'V(1)=',E10.5)
      STOP
      END
*FIN.XPCT
      DIMENSION P(23,23),PQW(23,4),PQWT(4,23),DWL1(23,4),
     &W(4),FTRW(23,23),RJK(23,23),PT(23,23),G(3,23),
     &AJJW(23,23),DWM1(3,23),DWM1(23,3),DWM1(3,3),II(2)
1     FORMAT()
      IOPT=IDI('ENTER 1 FOR DATA BY KEYBOARD, 2 IF BY FILE ...')
      IF(IOPT.NE.1) GO TO 10
      CALL QUOTE('ENTER OPTIMAL CONTROLLER GAIN G ...')
      READ 1, ((G(I,J),J=1,23),I=1,3)
      CALL QUOTE('ENTER P,PQW ...')
      READ 1, ((P(I,J),J=1,23),I=1,23),
     &((PQW(I,J),J=1,4),I=1,23)
10    CALL QUOTE('ENTER DATA FILE ...')
      DO 11 I=1,3
      READ 12, (G(I,J),J=1,8)
      READ 12, (G(I,J),J=9,16)
11    READ 13, (G(I,J),J=17,23)
12    FORMAT(8E10.5)
13    FORMAT(7E10.5)
      DO 14 I=1,23
      READ 12,(P(I,J),J=1,8)
      READ 12,(P(I,J),J=9,16)
14    READ 13,(P(I,J),J=17,23)
      DO 15 I=1,23
15    READ 16,(PQW(I,J),J=1,4)
16    FORMAT(4E10.5)
      TAU=XIO('ENTER INTEGRATION STEP SIZE, SECONDS ...')
      AKPROP=XIO('ENTER CONTROL TO ARM PROPORTIONALITY (GAIN) ...')
      VSPD=XIO('ENTER VEHICLE SPEED, MPH ...')
      DO 7 I=1,4
7     W(I)=1.0/TAU
      CALL MXTXN(PQW,PQWT,23,4,23,4)
      CALL MXMDIG(PQW,W,DWL1,23,4,23)
```

```
      CALL MXMLT(ONE,1,PHIT,FTRM,23,4,23,23,4)
      CALL SYMFIX(FTRM,23)
      CALL QUOTE('ENTER ARM NEUTRAL POSITION XN,YN,ZN')
      READ 1,ARMXN,ARMYN,ARMZN
      RMAXR=SQRT(ARMXN**2+ARMYN**2+ARMZN**2)
      VSFPS=1.4566667*VSPD
      TMX=RMAXR/VSFPS
      IF(TMX.GT.3.5)TMX=3.5
      CALL QUOTE('ENTER ARM CRITICAL POSITION XO,YO,ZO')
      READ 1, (ARMXO,ARMYO,ARMZO)
C *** I.C.'S START AT 3.5*CRITICAL RADIUS ***
      ARMDX=(ARMXO-ARMXN)*3.5
      ARMDY=(ARMYO-ARMYN)*3.5
      ARMDZ=(ARMZO-ARMZN)*3.5
      START=SQRT((ARMXO-ARMXN)**2+(ARMYO-ARMYN)**2+(ARMZO-ARMZN)**2)
C *** FORM INITIAL STATE COVARIANCE MATRIX ***
      CALL INIT(RJK,ARMDX,ARMDY,ARMDZ)
      CALL MXTRN(S,DMM1,3,23,3,23)
      CALL MXTRN(P,PT,23,23,23,23)
C *** INITIALIZE RESPONSES ***
      ISET=0
      CNTEFT=0.0
      ISTEP=0
      TIME=0.0
      ETP=3.5*START
      EAE=ETP
      EAEDT=0.0
      ETPDT=0.0
      EDL=0.0
      EDLDT=0.0
      EME=EAE/RATPROP
      EMEDT=0.0
      TCAP=XIO('ENTER CORRESPONDING CAPTURE TIME ...')
      YGOAL=1.0
30    ISTEP=ISTEP+1
      TIME=TIME+TAU
      ETPK=ETP
      EAEK=EAE
      EAEDTK=EAEDT
      ETPDTK=ETPDT
      EDLK=EDL
      EDLDTK=EDLDT
      EMEK=EME
      EMEDTK=EMEDT
C *** PROCEED ONE STEP IN TIME ***
      CALL EVAL(RJK,P,PT,FTRM,23,DUM)
C *** INVOKE SYMMETRY TO REDUCE ACCUMULATED NUMERICAL ERRORS ***
      CALL SYMFIX(RJK,23)
C *** ETP=SQRT(EC(ARM TIP POSITION MEASURED FROM NEUTRAL POSITION)**2))
C *** EME=SQRT(EC(MODEL EXTENSION MEASURED FROM NEUTRAL POSITION)**2))
C *** EAE=SQRT(EC(ARM EXTENSION MEASURED FROM NEUTRAL POSITION)**2))
C *** EDL=SQRT(EC(ARM DEFLECTIONS)**2))
C *** SUFFIX DT ON THE ABOVE INDICATES FIRST TIME DERIVATIVE ***
C *** SUFFIX S ON THE ABOVE REMOVES SQRT() ***
      ETPS=0.0
      ETPDTS=0.0
      DO 31 I=15,21,3
      J=I+1
      ETPDTS=ETPDTS+RJK(J,J)
31    ETPS=ETPS+RJK(I,I)
      CALL MXMLT(S,RJK,DMM1,3,23,23,3,23)
      CALL MXMLT(DMM1,DMM1,DMM1,3,23,3,3,23)
      EAES=0.0
      EMEDTS=0.0
      DO 34 I=1,3
34    EMEDTS=EMEDTS+DMM1(I,I)
```

```
      DO 35 I=17,23,3
   35 EAES=EAES+RJK(I,I)
      EDLS=ETPS+EAES
      DO 36 I=15,21,3
      J=I+2
   36 EDLS=EDLS-2.0*RJK(I,J)
      EDLDTS=EMEDTS*RKPROP**2+ETPDTS
      DO 37 I=1,3
      J=13+I*3
   37 EDLDTS=EDLDTS-2.0*RKPROP*DMN1(I,J)
      SIGN=1.0
      IF(ETPS.LT.0.)SIGN=-1.0
      ETP=SQRT(ABS(ETPS))
      ETP=SIGN*ETP
      SIGN=1.0
      IF(ETPDTS.LT.0.)SIGN=-1.0
      ETPDT=SQRT(ABS(ETPDTS))
      ETPDT=SIGN*ETPDT
      SIGN=1.0
      IF(EAES.LT.0.)SIGN=-1.0
      EAE=SQRT(ABS(EAES))
      EAE=EAE*SIGN
      SIGN=1.0
      IF(EMEDTS.LT.0.)SIGN=-1.0
      EMEDT=SQRT(ABS(EMEDTS))
      EMEDT=SIGN*EMEDT
      SIGN=1.0
      EAEDT=RKPROP*EMEDT
      EME=EAE/RKPROP
      IF(EDLS.LT.0.)SIGN=-1.0
      EDL=SQRT(ABS(EDLS))
      EDL=SIGN*EDL
      SIGN=1.0
      IF(EDLDTS.LT.0.)SIGN=-1.0
      EDLDT=SQRT(ABS(EDLDTS))
      EDLDT=SIGN*EDLDT
C *** HAS CRITICAL RADIUS BEEN CROSSED ***
C *** IF SO CONTINUE ***
      IF(ISET.NE.0)GO TO 399
C *** IF NOT DO NOT COUNT TIME OR PENALTY ***
      IF(ETP.GT.START)GO TO 38
C *** IF THIS IS THE FIRST TIME ETP.LT.START INTERPOLATE FOR TO ***
      ISET=1
      GO TO 39
   38 TIME=0.0
      ISTEP=0
      GO TO 30
C *** LINEAR INTERPOLATION FOR STARTING CONDITIONS ***
   39 TS=(START-ETP)*TAU/(ETPX-ETP)
      SETP=START
      SEAE=EAE+(EAEX-EAE)*TS/TAU
      SEDL=EDL+(EDLX-EDL)*TS/TAU
      SEME=EME+(EMEX-EME)*TS/TAU
      SETPDT=ETPDT+(ETPDTX-ETPDT)*TS/TAU
      SEAEDT=EAEDT+(EAEDTX-EAEDT)*TS/TAU
      SEDLDT=EDLDT+(EDLDTX-EDLDT)*TS/TAU
      SEMEDT=EMEDT+(EMEDTX-EMEDT)*TS/TAU
      CNTEFT=SEMEDT**2*TS
      TIME=0.0
      IS=0
      PRINT 80, TIME,IS,SEAE,SEAEDT,SETP,SETPDT,SEDL,SEDLDT,SEME,SEMEDT
      TIME=TS
  399 CNTEFT=CNTEFT+EMEDTS*TAU
      PRINT 80, TIME,ISTEP,EAE,EAEDT,ETP,ETPDT,EDL,EDLDT,EME,EMEDT
C *** IF TARGET HAS NOT BEEN REACHED CONTINUE ***
      IF(((ETP.GT.YGOAL).OR.(EAEDT.GT.YGOAL)).AND.(TIME.LT.TMX))GO TO 30
```

```
      C *** IF TARGET HAS BEEN REACHED INTERPOLATE FOR CAPTURE TIME ***
            IF((ETP.LE.YGOAL).AND.(EAEDT.LE.YGOAL))GO TO 401
      C *** IF NOT TIME MUST BE UP SO ...
            STOP
      C *** LINEAR INTERPOLATION FOR TIME OF CAPTURE ***
      401   TI(1)=TAU*(ETPK-YGOAL)/(ETPK-ETP)
            IF(ETP.GT.ETPK)TI(1)=0.0
            TI(2)=TAU*(EAEDTK-YGOAL)/(EAEDTK-EAEDT)
            IF(EAEDT.GT.EAEDTK)TI(2)=0.0
            ISLOW=0
            TINC=0.0
            DO 40 I=1,2
            IF((TI(I).LT.TINC).OR.(TI(I).GT.TAU))GO TO 40
            TINC=TI(1)
            ISLOW=I
      40    CONTINUE
            CTIME=TIME-TAU+TINC
            CETPE=ETPK-(ETPK-ETP)*TINC/TAU
            CEAEDT=EAEDTK-(EAEDTK-EAEDT)*TINC/TAU
            CONTEF=CONTEFT-EMEDTS*(TAU-TINC)
            ACNTEF=CONTEF/CTIME
            TTOT=TCAP+CTIME
      C *** PRINT RESULTS AT CAPTURE ***
            PRINT 91, (YGOAL,CETP,YGOAL,CEAEDT,TTOT,TCAP,CTIME,CONTEF,
           &ACNTF)
            IF(ISLOW**2-2)92,95,94
      92    CALL QUOTE('TIP POSITION REQUIREMENT MET LAST')
            GO TO 95
      94    CALL QUOTE('ARM EXTENSION RATE REQUIREMENT MET LAST')
      C *** IF THIS IS THE SMALLEST TARGET STOP ***
      95    IF((YGOAL+0.05).LT.0.25)STOP
      C *** IF NOT PROCEED TO NEXT TARGET ***
            YGOAL=YGOAL-0.25
            IF(YGOAL.LT.0.05)YGOAL=0.1
            IF((ETP.LE.YGOAL).AND.(EAEDT.LE.YGOAL))GO TO 401
            GO TO 30
      80    FORMAT('0TIME, SECONDS = ',F6.2,' STEP NUMBER    = ',1X,I2/
           &' EXPECTED VALUE OF ARM EXTENSION = ',E10.5,' RATE = ',E10.5/
           &' EXPECTED VALUE OF TIP POSITION  = ',E10.5,' RATE = ',E10.5/
           &' EXPECTED VALUE OF DEFLECTIONS   = ',E10.5,' RATE = ',E10.5/
           &' EXPECTED VALUE OF CONTROL INPUT = ',E10.5,' RATE = ',E10.5)
      91    FORMAT('0*** TARGET HAS BEEN REACHED ***'/1X,
           &'REQUIRED MAXIMUM CAPTURE RADIUS ',1X,F5.2,4X,
           &'ACTUAL CAPTURE RADIUS ',F5.2/1X,
           &'REQUIRED MAXIMUM CAPTURE SPEED  ',1X,F5.2,4X,
           &'ACTUAL CAPTURE SPEED  ',F5.2/1X,
           &'TOTAL TIME TO CAPTURE, SECONDS  ',F7.3/1X,
           &'CAPTURE ACTUATION TIME, SECONDS ',F7.3/1X,
           &'CONVEY ACTUATION TIME, SECONDS  ',F7.3/1X,
           &'RELATIVE CONTROL EFFORT ',10X,E10.5/1X,
           &'AVERAGE CONTROL EFFORT  ',10X,E10.5/)
            END
*OPILIB.INIT
      1     SUBROUTINE INIT(RJK,ARX,ARY,ARZ)
      2     DIMENSION ROW(23),COL(23),RJK(23,23)
      3     DO 10 I=1,23
      4  10 ROW(I)=0.0
      5     ROW(15)=ARX
      6     ROW(17)=ARX
      7     ROW(19)=ARY
      8     ROW(20)=ARY
      9     ROW(21)=ARZ
     10     ROW(23)=ARZ
     11     DO 20 I=1,23
     12  20 COL(I)=ROW(I)
     13     CALL MXMLT(COL,ROW,RJK,23,1,23,23,1)
```

```
14              RETURN
15              END
 *OPTLIB.EVAL
1               SUBROUTINE EVAL(RJK,PI,PIT,FTERM,NN,DUM)
2               DIMENSION RJK(NN,NN),PI(NN,NN),PIT(NN,NN),FTERM(NN,NN),DUM(NN,NN)
3               CALL MXMLT(PI,RJK,DUM,NN,NN,NN,NN,NN)
4               CALL MXMLT(DUM,PIT,RJK,NN,NN,NN,NN)
5               CALL MXADD(RJK,FTERM,RJK,NN,NN,NN)
6               RETURN
7               END
 *SIM.J
1               DIMENSION P(23,23),PQW(23,4),PQWT(4,23),DNL1(23,4),
2              &W(4),FTRM(23,23),RJK(23,23),PT(23,23),G(3,23),
3              &DUM(23,23),DNM1(3,23),DNM1(23,3),DNM1(3,3),TI(2)
4        1      FORMAT()
5               IOPT=IQ('ENTER 1 FOR DATA BY KEYBOARD, 2 IF BY FILE ...')
6               IF(IOPT.NE.1) GO TO 10
7               CALL QUOTE('ENTER OPTIMAL CONTROLLER GAIN G ...')
8               READ 1, ((G(I,J),J=1,23),I=1,3)
9               CALL QUOTE('ENTER P,PQW ...')
10              READ 1, ((P(I,J),J=1,23),I=1,23),
11             &((PQW(I,J),J=1,4),I=1,23)
12       10     CALL QUOTE('ENTER DATA FILE ...')
13              DO 11 I=1,3
14              READ 12, (G(I,J),J=1,8)
15              READ 12, (G(I,J),J=9,16)
16       11     READ 13, (G(I,J),J=17,23)
17       12     FORMAT(8F10.5)
18       13     FORMAT(7F10.5)
19              DO 14 I=1,23
20              READ 12,(P(I,J),J=1,8)
21              READ 12,(P(I,J),J=9,16)
22       14     READ 13,(P(I,J),J=17,23)
23              DO 15 I=1,23
24       15     READ 16,(PQW(I,J),J=1,4)
25       16     FORMAT(4E10.5)
26              TAU=XIQ('ENTER INTEGRATION STEP SIZE, SECONDS ...')
27              RKPROP=XIQ('ENTER CONTROL TO ARM PROPORTIONALITY (GAIN) ...')
28              VSPD=XIQ('ENTER VEHICLE SPEED, MPH ...')
29              AW=XIQ('ENTER AW ...')
30              DO 7 I=1,4
31       7      W(I)=1.0/TAU
32              CALL MXTRN(PQW,PQWT,23,4,23,4)
33              CALL MXMDIG(PQW,W,DNL1,23,4,23)
34              CALL MXMLT(DNL1,PQWT,FTRM,23,4,23,23,4)
35              CALL SYMFIX(FTRM,23)
36              CALL QUOTE('ENTER ARM NEUTRAL POSITION XN,YN,ZN')
37              READ 1,ARMXN,ARMYN,ARMZN
38              RMAXRESQRT(ARMXN**2+ARMYN**2+ARMZN**2)
39              VSFPS=1.466666667*VSPD
40              TMX=RMAXR/VSFPS
41              IF(TMX.GT.3.5)TMX=3.5
42              CALL QUOTE('ENTER ARM CRITICAL POSITION XO,YO,ZO')
43              READ 1, (ARMXO,ARMYO,ARMZO)
44              ARMDX=(ARMXO-ARMXN)
45              ARMDY=(ARMYO-ARMYN)
46              ARMDZ=(ARMZO-ARMZN)
47              START=SQRT((ARMXO-ARMXN)**2+(ARMYO-ARMYN)**2+(ARMZO-ARMZN)**2)
48       C ***  FORM INITIAL STATE COVARIENCE ***
49              CALL INIT(RJK,ARMDX,ARMDY,ARMDZ)
50              CALL MXTRN(G,DNVI,3,23,3,23)
51              CALL MXTRN(P,PT,23,23,23,23)
52       C ***  INITIALIZE RESPONSES ***
53              ISET=0
54              CNTEFT=0.0
55              ISTEP=0
```

```
      TIME=0.0
      ETP=START
      EAE=ETP
      EAEDT=0.0
      ETPDT=0.0
      EDL=0.0
      EDLDT=0.0
      EME=EAE/RKPROP
      EMEDT=0.0
      TCAP=XIO('ENTER CORRESPONDING CAPTURE TIME ...')
      YGOAL=1.0
30    ISTEP=ISTEP+1
      TIME=TIME+TAU
      ETPK=ETP
      EAEK=EAE
      EAEDTK=EAEDT
      ETPDTK=ETPDT
      EDLK=EDL
      EDLDTK=EDLDT
      EMEK=EME
      EMEDTK=EMEDT
C *** PROCEED ONE STEP IN TIME ***
      CALL EVAL(RJK,P,PT,ETRM,23,DUM)
C *** INVOKE SYMMETRY TO REDUCE ACCUMULATION OF NUMERICAL ERRORS ***
      CALL SYMFIX(RJK,23)
C *** ETP=SQRT(EC(ARM TIP POSITION MEASURED FROM NEUTRAL POSITION)**2))
C *** EME=SQRT(EC(MODEL EXTENSION MEASURED FROM NEUTRAL POSITION)**2))
C *** EAE=SQRT(EC(ARM EXTENSION MEASURED FROM NEUTRAL POSITION)**2))
C *** EDL=SQRT(EC(ARM DEFLECTIONS)**2))
C *** SUFFIX DT ON THE ABOVE INDICATES FIRST TIME DERIVATIVE ***
C *** SUFFIX S ON THE ABOVE REMOVES SQRT() ***
      ETPS=0.0
      ETPDTS=0.0
      DO 31 I=15,21,3
      J=I+1
      ETPDTS=ETPDTS+RJK(J,J)
31    ETPS=ETPS+RJK(I,I)
      CALL MXMLT(S,RJK,DMN1,3,23,23,3,23)
      CALL MXMLT(DMN1,DMN1,DMM1,3,23,3,3,23)
      EAES=0.0
      EMEDTS=0.0
      DO 34 I=1,3
34    EMEDTS=EMEDTS+DMM1(I,I)
      DO 35 I=17,23,3
35    EAES=EAES+RJK(I,I)
      EDLS=ETPS+EAES
      DO 36 I=15,21,3
      J=I+2
36    EDLS=EDLS-2.0*RJK(I,J)
      EDLDTS=EMEDTS*RKPROP**2+ETPDTS
      DO 37 I=1,3
      J=13+I*3
37    EDLDTS=EDLDTS-2.0*RKPROP*DMN1(I,J)
      SIGN=1.0
      IF(ETPS.LT.0.)SIGN=-1.0
      ETP=SQRT(ABS(ETPS))
      ETP=SIGN*ETP
      SIGN=1.0
      IF(ETPDTS.LT.0.)SIGN=-1.0
      ETPDT=SQRT(ABS(ETPDTS))
      ETPDT=SIGN*ETPDT
      SIGN=1.0
      IF(EAES.LT.0.)SIGN=-1.0
      EAE=SQRT(ABS(EAES))
      EAE=EAE*SIGN
```

```
      SIGN=1.0
      IF(EMEDTS.LT.0.)SIGN=-1.0
      EMEDT=SQRT(ABS(EMEDTS))
      EMEDT=SIGN*EMEDT
      SIGN=1.0
      EAEDT=RKPROP*EMEDT
      EME=EAE/RKPROP
      IF(EDL.LT.0.)SIGN=-1.0
      EDL=SQRT(ABS(EDLS))
      EDL=SIGN*EDL
      SIGN=1.0
      IF(EDLDTS.LT.0.)SIGN=-1.0
      EDLDT=SQRT(ABS(EDLDTS))
      EDLDT=SIGN*EDLDT
399   CNTEFT=CNTEFT+EMEDTS*TAU+ETPS*TAU*AW
      PRINT 80, TIME,ISTEP,EAE,EAEDT,ETP,ETPDT,EDL,EDLDT,EME,EMEDT
C *** HAS TARGET BEEN ENGAGED ***
C *** IF NOT CONTINUE UNLESS TIME IS OUT ***
      IF(((ETP.GT.YGOAL).OR.(EAEDT.GT.YGOAL)).AND.(TIME.LT.TMX))GO TO 30
C *** IF TARGET HAS BEEN ENGAGED INTERPOLATE FOR CAPTURE TIME ***
      IF((ETP.LE.YGOAL).AND.(EAEDT.LE.YGOAL))GO TO 401
C *** IF NOT TIME MUST BE UP SO ...
      STOP
C *** LINEAR INTERPOLATION FOR TIME OF CAPTURE ***
401   TI(1)=TAU*(ETPK-YGOAL)/(ETPK-ETP)
      IF(ETP.GT.ETPK)TI(1)=0.0
      TI(2)=TAU*(EAEDTK-YGOAL)/(EAEDTK-EAEDT)
      IF(EAEDT.GT.EAEDTK)TI(2)=0.0
      ISLOW=0
      TINC=0.0
      DO 40 I=1,2
      IF((TI(1).LT.TINC).OR.(TI(I).GT.TAU))GO TO 40
      TINC=TI(I)
      ISLOW=I
40    CONTINUE
      CTIME=TIME-TAU+TINC
      CETP=ETPK-(ETPK-ETP)*TINC/TAU
      CEAEDT=EAEDTK-(EAEDTK-EAEDT)*TINC/TAU
      CONTEF=CNTEFT-EMEDTS*(TAU-TINC)-ETPS*(TAU-TINC)*AW
      TTOT=TCAP+CTIME
C *** PRINT RESULTS AT CAPTURE ***
      PRINT 91, (YGOAL,CETP,YGOAL,CEAEDT,TTOT,TCAP,CTIME,CONTEF)
      IF(ISLOW**2-2)92,95,94
92    CALL QUOTE('TIP POSITION REQUIREMENT MET LAST')
      GO TO 95
94    CALL QUOTE('ARM EXTENSION RATE REQUIREMENT MET LAST')
C *** IF THIS IS SMALLEST TARGET STOP ***
95    IF((YGOAL+0.05).LT.0.25)STOP
C *** IF NOT CONTINUE TOWARD NEXT TARGET ***
      YGOAL=YGOAL-0.25
      IF(YGOAL.LT.0.05)YGOAL=0.1
      IF((ETP.LE.YGOAL).AND.(EAEDT.LE.YGOAL))GO TO 401
      GO TO 30
80    FORMAT('0TIME, SECONDS = ',F6.2/' STEP NUMBER   = ',1X,I2/
     A' EXPECTED VALUE OF ARM EXTENSION = ',E10.5,' RATE = ',E10.5/
     A' EXPECTED VALUE OF TIP POSITION  = ',E10.5,' RATE = ',E10.5/
     A' EXPECTED VALUE OF DEFLECTIONS   = ',E10.5,' RATE = ',E10.5/
     A' EXPECTED VALUE OF CONTROL INPUT = ',E10.5,' RATE = ',E10.5)
91    FORMAT('0*** TARGET HAS BEEN REACHED ***'/1X,
     A'REQUIRED MAXIMUM CAPTURE RADIUS ',1X,F5.2,4X,
     A'ACTUAL CAPTURE RADIUS ',F5.2/1X,
     A'REQUIRED MAXIMUM CAPTURE SPEED  ',1X,F5.2,4X,
     A'ACTUAL CAPTURE SPEED  ',F5.2/1X,
     A'TOTAL TIME TO CAPTURE, SECONDS  ',F7.3/1X,
     A'CAPTURE ACTUATION TIME, SECONDS ',F7.3/1X,
     A'CONVEY ACTUATION TIME, SECONDS  ',F7.3/1X,
```

```
187           A*PENALTY FUNCTION *,10X,E10.5/)
188           END
```

APPENDIX VI

MECHANICAL CHARACTERISTICS OF A COMMERCIALLY AVAILABLE REFUSE VEHICLE

Introduction

In the interest of obtaining realistic values for the mechanical parameters in the dynamic model of the refuse collection vehicle, a survey of commercially available refuse packer bodies and truck chassis was made. From these alternative configurations a packer body and truck chassis were chosen which could be readily adapted to automated refuse collection. The object of this appendix is to explain the selection process and to evaluate the mechanical parameters needed for use in the dynamic model of the collection vehicle.

Packer Body Selection and Characteristics

Of the refuse packer bodies commercially available in the United States, there are only two basic configurations: the rear-loading, rear-ejecting design and the front- (side or top) -loading, rear-ejecting design. The rear loading design features a relatively complex packing mechanism which must be hopper fed and which compresses the refuse against a movable ejection ram (45). The front loading packer body is much simpler in operation. It features an ejection ram which is used to periodically compress the refuse against the fixed rear wall of the collection body and is returned to the front wall at the end of each cycle. This

type of packer body offers a larger degree of freedom in the selection of the refuse loading point. Figures 30 and 31 describe schematically these two alternative packing cycles.

A third refuse body, which is designed to reduce the volume of the refuse during transportation, is the "Kuka Shark," manufactured in Europe and sold in the United States by the Environmental Systems Division of St. Regis Paper Company (46). This body does not compress the refuse directly but tumbles it continuously in transit, relying on this action to compress the refuse under its own weight. The "Shark" is currently available only in rear-loading rear-ejecting models, Figure 32, but could be readily adapted to a front-loading rear-ejecting design and would have the advantage for automated collection of being essentially a continuous feed rather than cyclical feed mechanism.

Of these three refuse bodies, the design which is most easily adapted to automated collection is the front-loading, rear-ejecting packer body, a representative example of which is the "E-Z-Pack Side Loader," manufactured by the Peabody Galion Company of Galion, Ohio. This body is available in three body capacities ranging from 16 to 24 cubic yards, and was chosen as the design prototype because the manufacturer's technical information sheet was more complete than those of other manufacturers surveyed. The 20 cubic yard model number SL-20 was chosen for use in the dynamic model of the collection vehicle because vehicles of larger capacity are rarely used in practice due to maneuverability problems (4). Table 12 contains the pertinent data on this packer body.

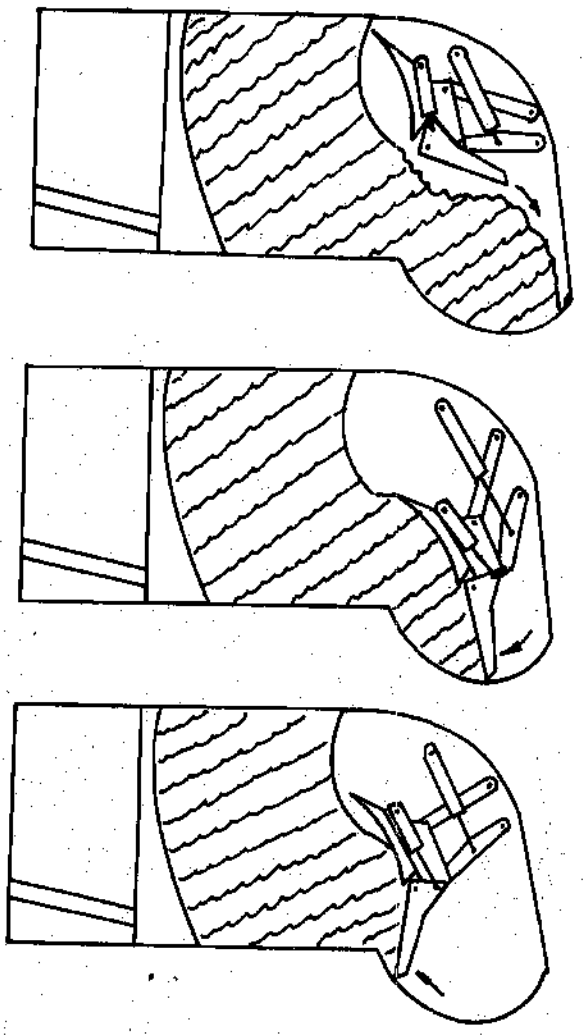

Figure 30. Packing Cycle for Rear Loading Refuse Bodies

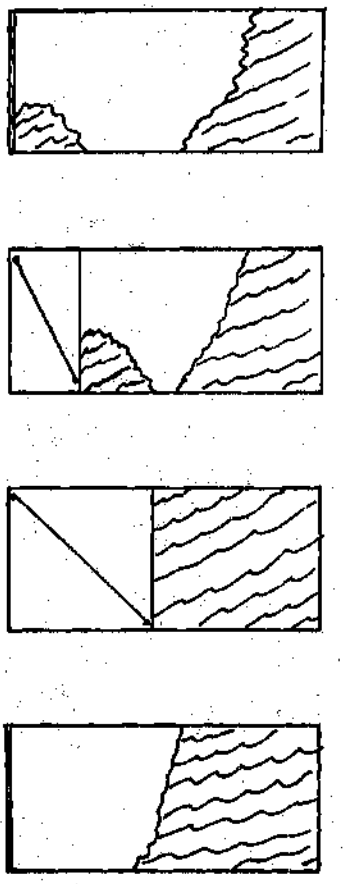

Figure 31. Packing Cycle for Front Loading Refuse Bodies

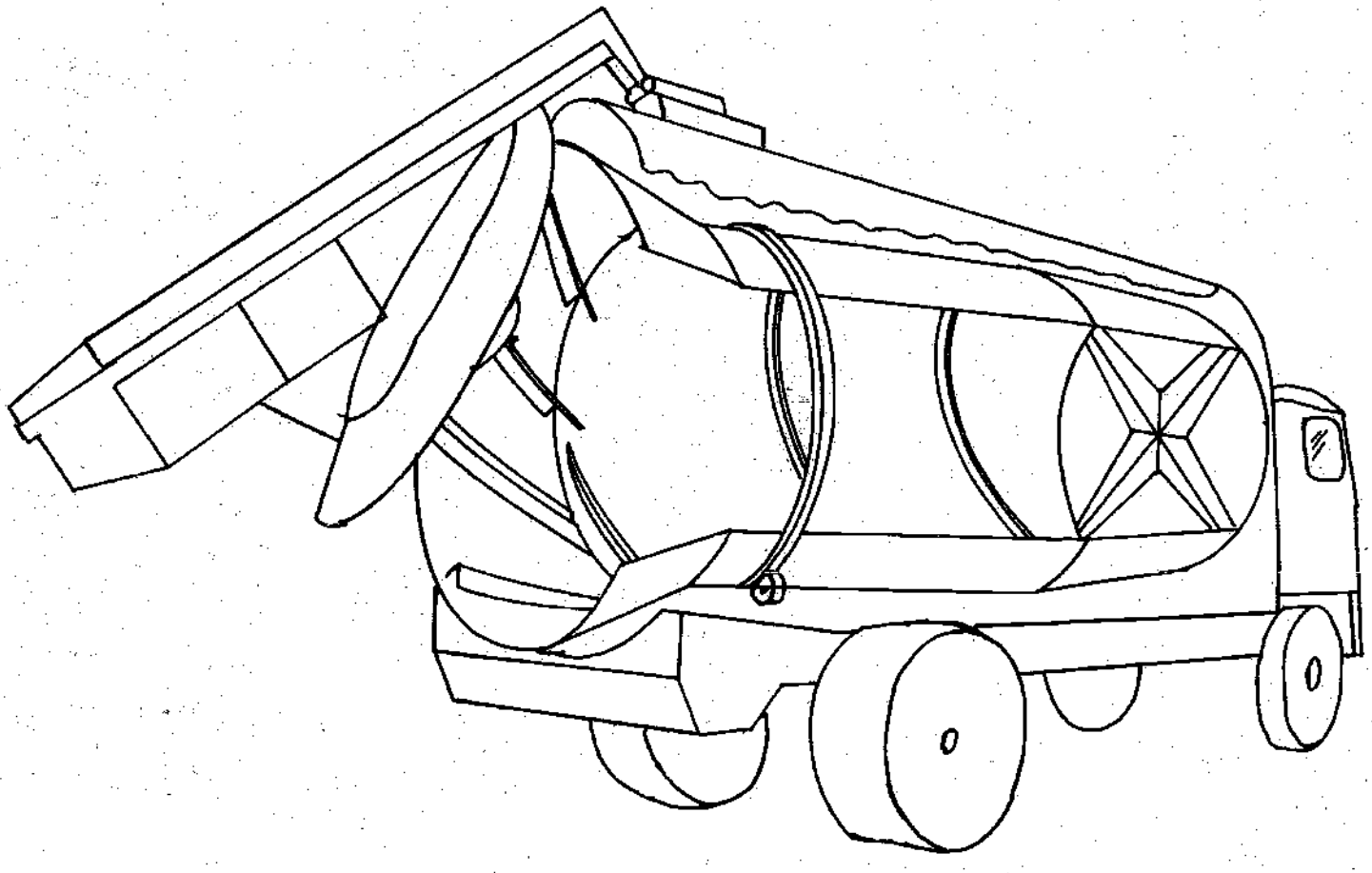

Figure 32. "Kuka Shark" Refuse Body

Table 12. Body Specifications of E-Z Pack Model SL-20 (47)

Body Capacity, cubic yard	20
Overall Length, inches	205
Overall Width, inches	95 1/2
Overall Height Above Frame, inches	81
Approximate Body Weight, pounds	7808
Weight of Oil, Pump, P.T.O., pounds	492
Required Minimum Gross Vehicle Weight Rating, pounds	24000
Required Minimum Distance, Rear of Cab to ℄ Rear Axle, inches	120

Chassis Selection and Characteristics

The cab-over engine truck chassis is particularly adaptable to automated refuse collection applications for several reasons. The shorter overall length of such a chassis as opposed to that of the conventional cab-behind-engine design aids maneuverability in congested areas and the forward observability of low objects at close range is unexcelled by any other cab configuration. The cab itself could easily be modified to a one-occupant design providing further improvement in the observability of low objects and/or a location for the attachment of the manipulator, Figure 33. The short wheel base of the cab-over-engine chassis also transfers a greater proportion of the payload to the front axle, thereby making the use of a

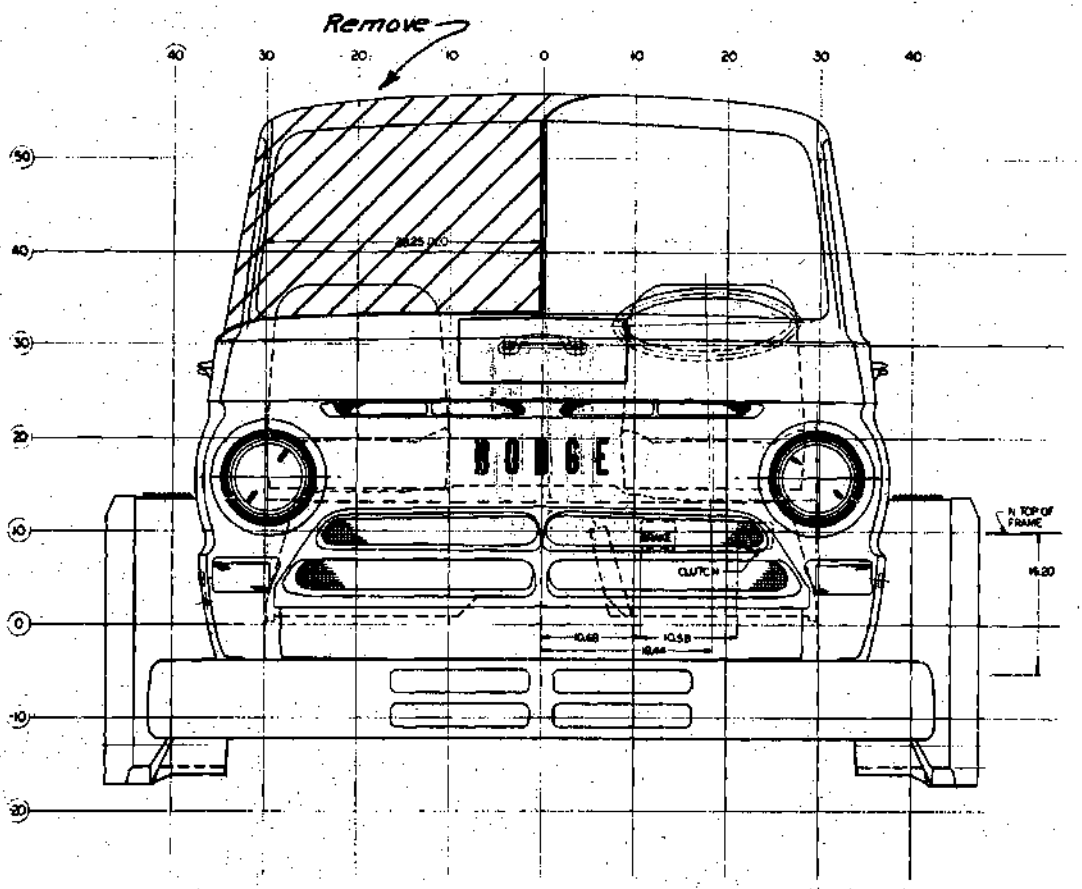

Figure 33. Cab-Over-Engine Modified for Automated Refuse Accumulation

single rear axle possible in situations where a conventional chassis would require a tandem rear axle to meet statutory maximum axle loading requirements. For these reasons, a cab-over-engine chassis was chosen for the prototype design vehicle.

Cab-over-engine chassis which meet the minimum requirements of the packer body manufacturer enumerated in Table 12 are available from every major truck manufacturer in the United States. For the purpose of dynamic modeling of the refuse collection vehicle a Dodge L700 chassis was chosen primarily because the Dodge body builder's manual (48) contained more detailed information on suspension parameters than those of the other manufacturers.

For all large trucks, the basic model number is only a partial description of the chassis, and details such as axle capacity and transmission ratios must also be determined before the vehicle may be fully described. For purposes of the dynamic model it is only necessary that suspension parameters be determined accurately and therefore only the computations required for the selection of these components are presented here. In the discussion which follows reference will be made to basic chassis characteristics enumerated in Table 13 and body characteristics enumerated in Table 12. The results of these computations are summarized in the lower half of Table 13 as "data for selected chassis components."

Selection of Axle and Spring Capacity

The load carried by each axle is greatest when the refuse body is filled to capacity. In order to determine the axle loadings under this condition the weight of the refuse body and cargo must be estimated.

Table 13. Specifications for the Dodge L-700 Chassis

Basic Data	
Wheel Base, inches	141
Distance Between Springs on an Axle, inches	40
Distance, Rear of Cab to ℄ Rear Axle, inches	124
Maximum Available Gross Vehicle Weight, pounds	27500
Maximum Allowable Payload, pounds	20775
Curb Weight, Total, pounds	6725
Curb Weight on Front Axle, pounds	4080
Curb Weight on Rear Axle, pounds	2645
Data for Selected Chassis Components	
Front Axle Capacity, pounds	7000
Front Spring Capacity, pounds	4150
Rear Axle Capacity, pounds	18000
Rear Spring Capacity, pounds	9100
Weight of Front Axle, Hubs, Brakes, Drums, and Attaching Hardware (49)	627
Weight of Rear Axle, Brakes, Drums, and Attaching Hardware (49)	993
Front Tire and Wheel Weights, pounds/axle (50)	386
Rear Tire and Wheel Weights, pounds/axle (50)	772

It is assumed that the packer body manufacturer, in specifying a minimum gross weight rating for chassis to be used with his product, made an accurate estimate of the refuse bulk density in the packer body and of the curb weight of such a chassis. An estimate of the maximum weight of the body and its cargo can therefore be obtained as the difference in the minimum gross vehicle weight specified and the curb weight of a chassis meeting this specification. The calculated weight of the body and cargo is 24000 - 6725 = 17275 pounds. Since the packer body and accessories weigh 8300 pounds (Table 1) the refuse weight at full capacity is 17275 - 83000 = 8975 pounds, which results in a refuse bulk density of approximately 450 pounds per cubic yard for the 20 cubic yard packer body. This refuse density agrees very well with the data presented in reference (4) for twenty cubic yard packer bodies.

As depicted schematically in Figure 34, the axle loadings at full capacity consist of the curb weight of the chassis alone plus the distributed weight of the body and cargo. The center of gravity of the rectangular packer body and densely packed cargo is assumed to be at the geometric center of the body. The body and cargo load on the rear axle is found by summing moments about the front axle:

Rear axle payload = 17275(141 - 124 + 102.5)/141 = 14641 pounds.

Front axle body and cargo load = 17275 - 14641 = 2634 pounds.

The required axle capacities are the sum of the axle loads due to the body and cargo and the axle loads for the chassis alone. The required capacity for the front axle is therefore

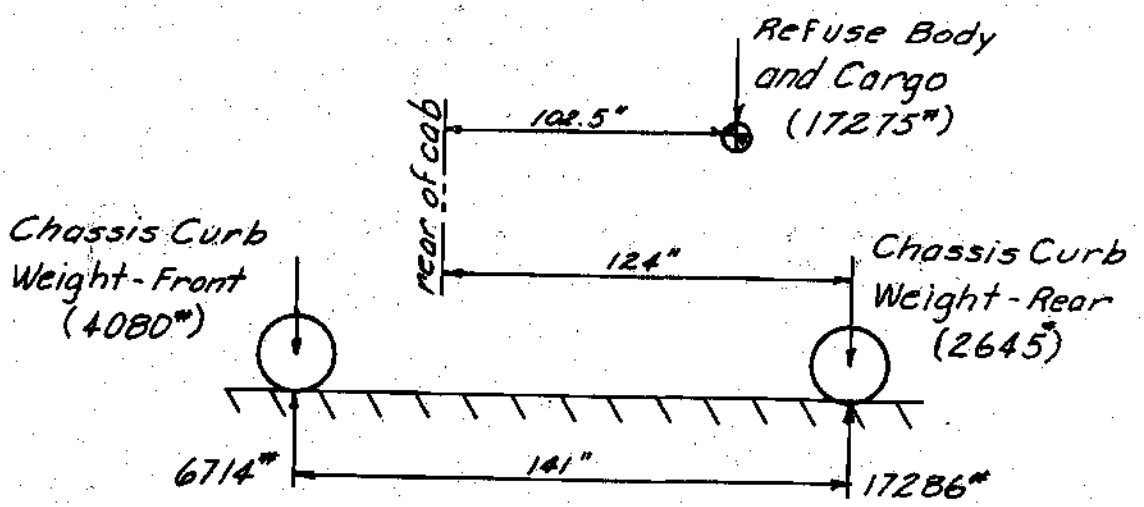

Figure 34. Axle Loadings at Full Capacity

2634 + 4080 = 6714 pounds

and for the rear axle the required capacity is

14641 + 2645 = 17286 pounds.

The axles available from the manufacturer which meet these requirements have capacities of 7000 and 18000 pounds respectively, and the springs capable of carrying equal loads are the 4150 pound capacity front springs and 9100 pound capacity rear springs, as indicated in the latter half of Table 13. The tires and wheels required for this loading are 10.00-20 bias ply tires, load range F, and 20 x 7.50 wheels, the weights of which are included in Table 13 (49, 50).

Front Axle Loading at Partial Capacity. The compacting cycle of the packer body forces the cargo to the extreme rear of the vehicle as shown in Figure 31. This results in reduced front axle loading until the face of the partial refuse load progresses beyond the rear axle. It is prudent to check the worst case, when the partial load face just reaches the rear axle, to ensure that reasonable steering forces can be applied by the front tires. Referring to Figure 35, the loads from left to right are: chassis front curb weight less unsprung weight at front axle (4080-726-386 = 3067), weight of empty packer body, chassis rear curb weight less unsprung weight at rear axle (2645 - 993 - 772 = 880), and weight of partial refuse load (8975 x 81/205 = 3546).

Summation of moments about the rear axle yields a front axle reaction of 3314 pounds. Since this exceeds the front axle loading of the chassis alone, it

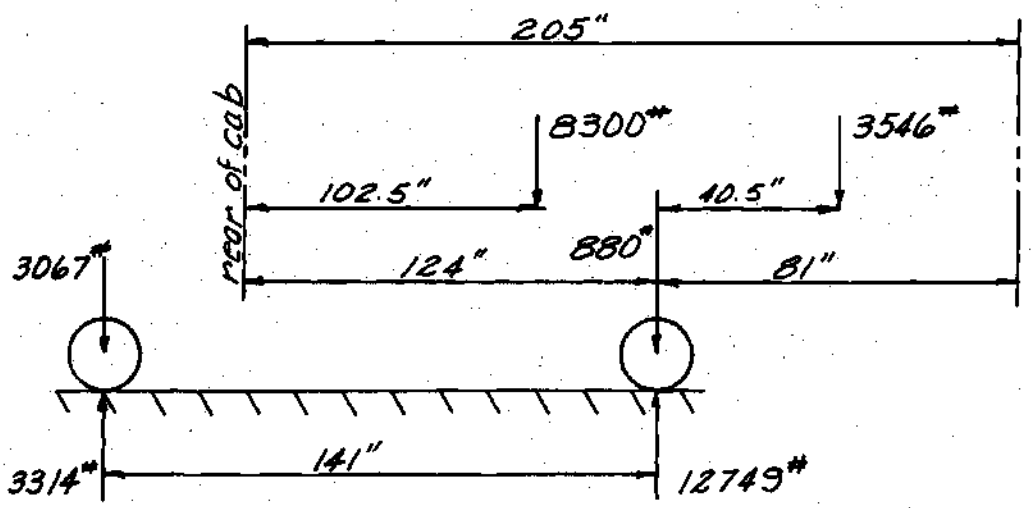

Figure 35. Axle Loadings at Partial Capacity

may be assumed safe. The rear axle load is found to be 12179 pounds by summation of forces.

Determination of Suspension Spring Constants and Damping

The Dodge L700 is equipped with variable rate front and rear springs as shown in Figures 36 and 37. For the purposes of the dynamic model the spring rates were assumed to be the tangents to the load deflection curves at the appropriate static load.

At full capacity, the front axle load is 6714 pounds, Figure 34, so that the load above curb weight is 2634 pounds. As shown in Figure 36, this results in a spring constant of 1000 pounds per inch for the front springs when fully loaded. The rear axle load at full capacity is 17286 pounds, resulting in a load above curb weight of 14641 pounds and a spring rate of 3500 pounds per inch.

When the vehicle is empty the front axle load above curb weight is 1265 pounds, found by distributing the weight of the empty packer body to the front and rear axles. This results in a spring constant of 750 pounds per inch. Similarly the load above curb weight on the rear axle is 7035 pounds, resulting in a spring constant of 1714 pounds per inch. These results are summarized in Table 14.

Table 14. Suspension Parameters for Dodge L700 Chassis

Load	Rear Spring Rate	Front Spring Rate	Front Damping Rate
Full	3500 lb/in.	1000 lb/in.	130 lb sec/in.
Empty	1714 lb/in.	750 lb/in.	130 lb sec/in.

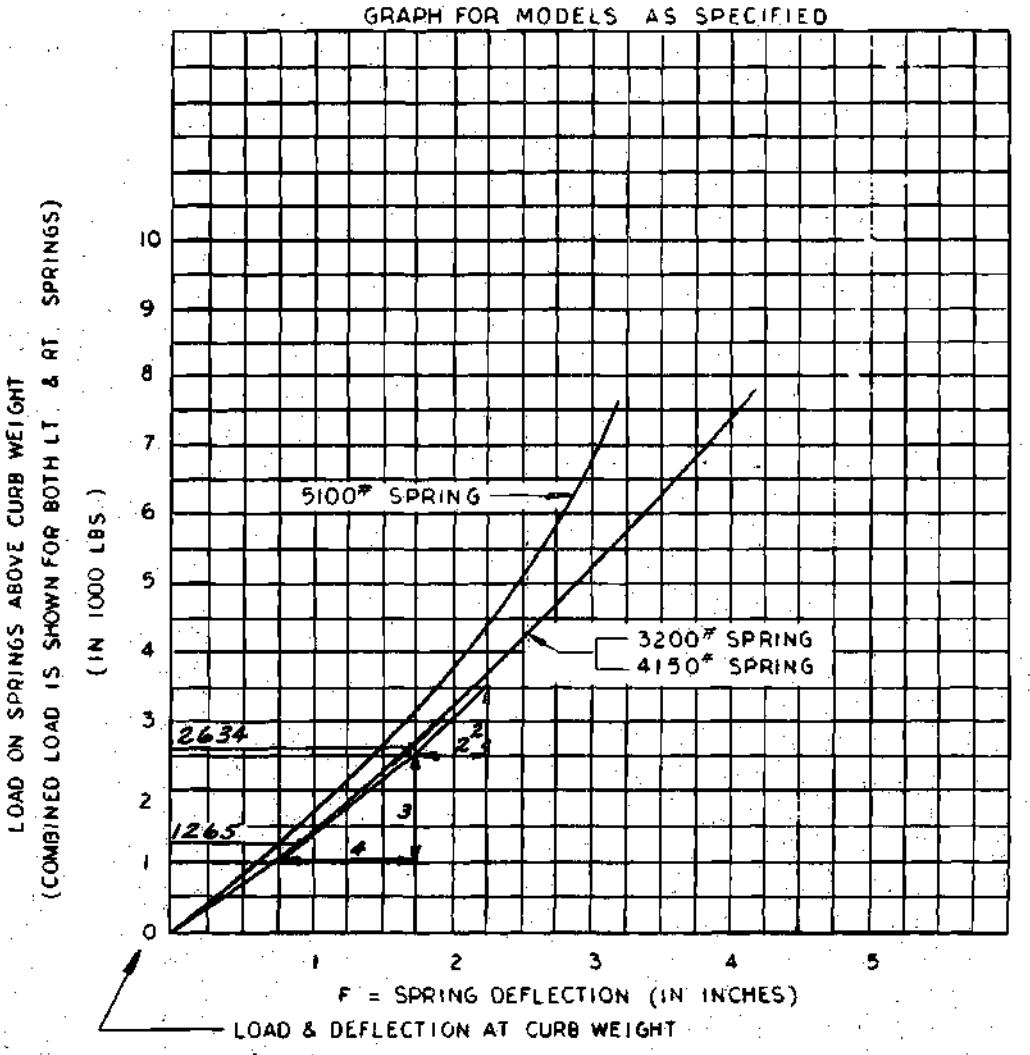

Figure 36. Front Spring Load-Deflection Curve

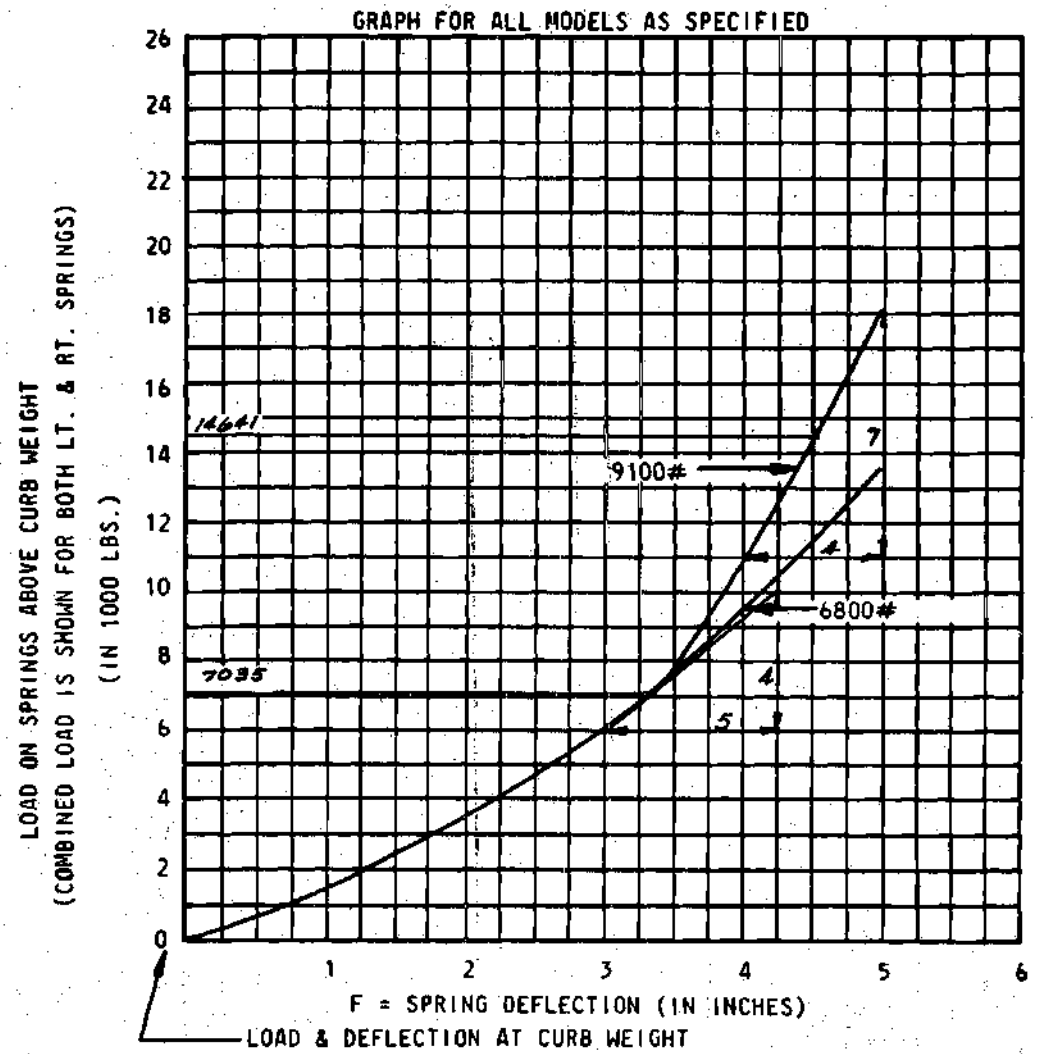

Figure 37. Rear Spring Load-Deflection Curve

The damping coefficient for the front suspension was determined by analyzing a quarter vehicle model at a front suspension point as shown in Figure 38. The damping term C for such a system is given in terms of the damping ratio by

$$C = 2\zeta\sqrt{Km}$$

Initially, suppose $\zeta = 1.0$ when the vehicle is unloaded. This gives

$$C = \frac{2}{12}\sqrt{(750 \times 12)\left(\frac{3067 + 1265}{(2)\ (32.2)}\right)} = 130 \text{ lb-sec/in}$$

where 32.2 is the acceleration due to gravity in feet per second squared. The resulting damping ratio when the vehicle is fully loaded is then given by

$$\zeta = \frac{(12)\ (130)}{2\sqrt{(1000 \times 12)\left(\frac{3067 + 2634}{(2)\ (32.2)}\right)}} = 0.757$$

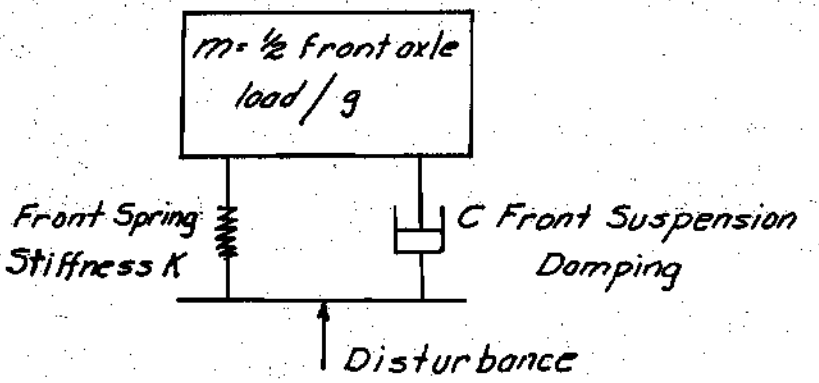

Figure 38. Quarter Vehicle Model of Front Suspension.

This is a reasonable result which provides good response over the entire load range.

The radial stiffness of 10.00-20 load range F truck tires has been measured statically at 5300 pounds/inch by Davisson (5) who states:

> Dynamic spring rates measured on rolling tires are more representative (of performance in use), but by experiment, those have not been found to differ significantly from the static values. Usually dynamic spring rates are on the order of 5 to 10 percent less.

The parenthetical phrase is the author's. Davisson also reports that the damping in truck tires is very small when determined for a rolling tire, ranging from 1 to 20 lb-sec/in.

Dynamic Characteristics of the Packer Body-Chassis Combination

Introduction

The combined packer body-chassis dynamics vary with the amount of refuse in the vehicle. For the purposes of evaluating alternative accumulator designs, the vehicle was modeled at two extreme operating states; packer body empty and packer body filled to capacity. In this section the location of the center of gravity of the combined body-chassis-cargo system, the sprung and unsprung masses, and the moments and products of inertia are estimated for these two operating conditions.

Sprung and Unsprung Masses

The unsprung mass is invariant with operating state and is given by the weight of the axles, wheels, tires, brakes, drums and attaching hardware divided by the acceleration due to gravity.

The unsprung mass at the front axle is

$$\frac{627 + 386}{32.2} = 31.46 \text{ slugs/axle or } 15.73 \text{ slugs/wheel}$$

The unsprung mass at the rear axle is

$$\frac{993 + 772}{32.2} = 54.81 \text{ slugs/axle or } 27.41 \text{ slugs/wheel}$$

The sprung mass is given by the total system weight less the unsprung weight divided by the acceleration due to gravity.

For the vehicle with full load the sprung mass is

$$\frac{17275 + 880 + 3067}{32.2} = 659 \text{ slugs}$$

When the vehicle is empty the sprung mass is

$$\frac{8300 + 880 + 3067}{32.2} = 380 \text{ slugs}$$

Location of Center of Gravity

The horizontal coordinate, X, of the center of gravity of the chassis and packer body may be found, as shown in Figure 39, by summation of the moments about an arbitrary point X of the sprung mass of the chassis and the mass of the refuse body and cargo. When X is located at the center of gravity, the summation of these moments must be zero; therefore, at the center of gravity

$$X = \frac{119.5\, W_{b+c} + 141\, F_r}{W_{b+c} + F_r + F_f}$$

When the vehicle is filled to capacity

$$X = \frac{(119.5)\ (17275)\ + (141)\ (880)}{17275 + 880 + 3067} = 103.1''$$

When the body is empty

$$X = \frac{(119.5)\ (8300) + (141)\ (880)}{8300 + 880 + 3067} = 91.1''$$

To determine the vertical coordinate, Y, of the center of gravity of the combined chassis-body-cargo system, a uniform acceleration in the horizontal direction equal to the acceleration due to gravity is assumed to act on the system as shown in Figure 40. It is assumed that the center of gravity of the cab and chassis lies at the top of the frame as shown.

Summing moments yields

$$Y = \frac{(W_{b+c})\ (40.5)}{W_c + W_{b+c}}$$

When the vehicle is filled to capacity

$$Y = \frac{(17275)\ (40.5)}{17275 + 880 + 3067} = 33''$$

When the vehicle is empty

$$Y = \frac{8300\ (40.5)}{8300 + 880 + 3067} = 27.45''$$

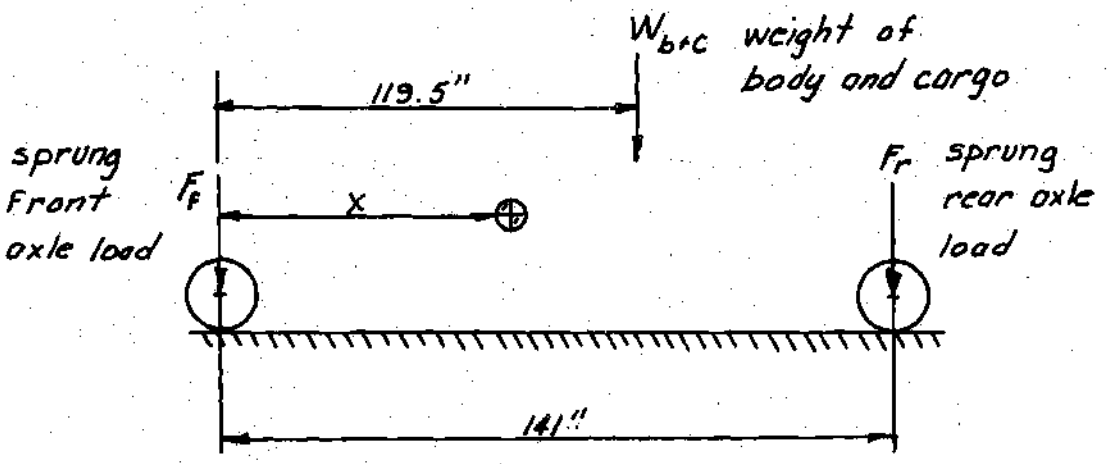

Figure 39. Horizontal Coordinate of the Center of Gravity of the Sprung Mass.

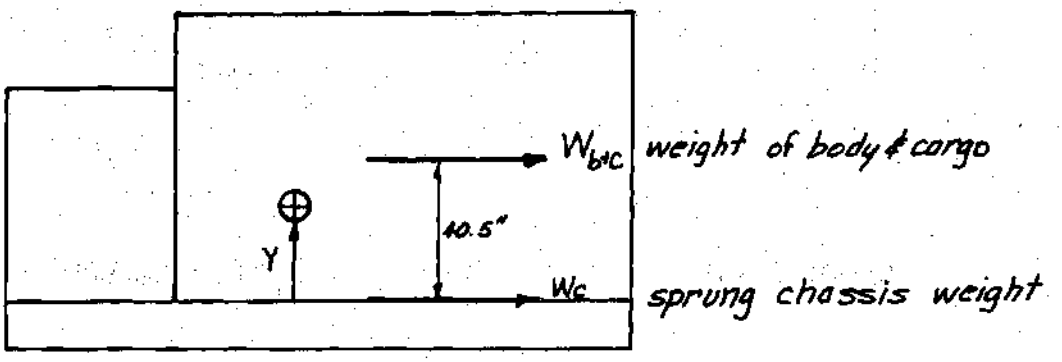

Figure 40. Vertical Coordinate of Center of Gravity of Sprung Mass.

Moments of Inertia

In order to estimate the moments of inertia of the combined chassis-body-cargo system, it is necessary to make some simplifying assumptions about the nature of the weight distribution in this complex body. First, it is assumed that the packer body with uniform bulk density, and the chassis is modeled by two rails and a homogeneous rectangular block as detailed below.

The first consideration is to determine the dimensions of the uniform masses used to represent the chassis so the center of gravity and total mass correspond to the values of these parameters for the real vehicle. The chassis frame depth is 9.5 inches, the distance between rail center lines is approximately 31 inches and the chassis overall length is 275 inches (48). The rear axle load of the unsprung chassis mass has been calculated previously to be 880 pounds. With this information the weight of the frame rails may be estimated if it is assumed that the engine-cab weight is centered over the front axle.

Summing moments about the front axle (Figure 41) yields:

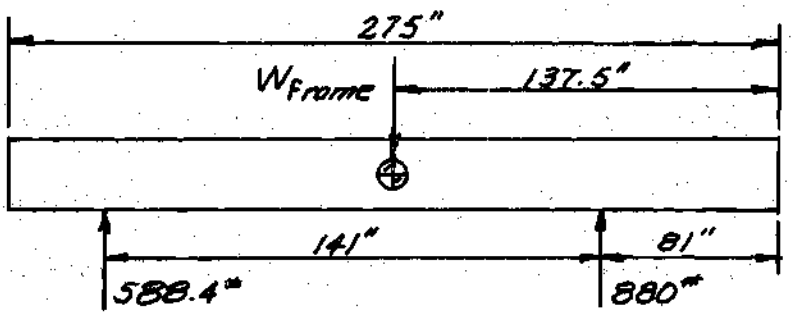

Figure 41. Idealized Frame Rails Weight Distribution.

$$(880)\,(141) = (141 + 81 - 137.5)\,W_{frame}$$

or

$$W_{frame} = 1468.4 \text{ pounds}$$

The load on the front axle due to the frame rails is then

$$1468.4 - 880 = 588.4 \text{ pounds}$$

The front axle load of the entire unsprung chassis is 3067 pounds, so the weight of the idealized engine-cab mass must be

$$3067 - 588.4 = 2478.6 \text{ pounds}$$

This mass distribution ensures that the horizontal position of the idealized chassis center of gravity corresponds to that of the real chassis.

If the frame rails are steel with weight density of 0.283 pounds per cubic inch, their width may be calculated as follows:

$$W = \frac{1468.4}{2 \times 275 \times 9.5 \times 0.283} = 1.0 \text{ inch}$$

If the engine-cab mass has a bulk density of approximately 0.1 pounds per cubic inch (35% of that of solid steel), its dimensions may be determined as follows. First the width of the mass is fixed at 30 inches by the requirement that it rest between the frame rails. Since the mass is assumed uniform, its center of gravity must be located at its geometrical center, and since the center of gravity of the entire unsprung chassis is required to lie along the top of the frame rails,

the distance from the top of the frame rails to the center of gravity of the engine-cab mass may be determined by summing moments about this point.

$$(1468.4)\left(\frac{9.5}{2}\right) = (2478.6)\ Y$$

or

$$Y = 2.8 \text{ inches.}$$

If it is assumed that the engine does not extend below the bottom of the frame rails, the height of the engine-cab mass must be

$$2 \times (9.5 + 2.8) = 24.6 \text{ inches}$$

The length of the engine cab mass is then

$$\frac{2478.6}{(24.6)\ (30)\ (.1)} = 33.6 \text{ inches}$$

which results in a cab to axle distance of exactly 124.2 inches. The idealized chassis is shown in Figure 42.

The refuse body weighs 8300 pounds (Table 12), is 95.5 inches wide by 205 inches long, and is made of steel (.283 pounds/inch^3). A uniform shell with these dimensions weighing 8300 pounds is 0.33 inches thick.

In determining the moment of inertia for the chassis-body-cargo system, the first step is to determine these parameters for the individual components about their own centers of gravity. Each component is a uniform rectangular prism, and the equations which define the moments of inertia about the center of gravity of a prism are as given in Figure 43 (52).

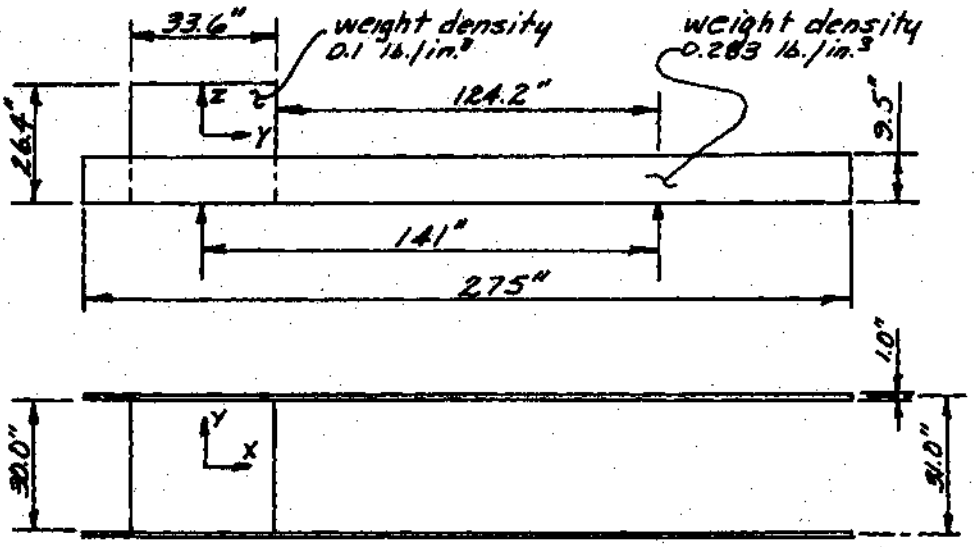

Figure 42. Idealized Chassis.

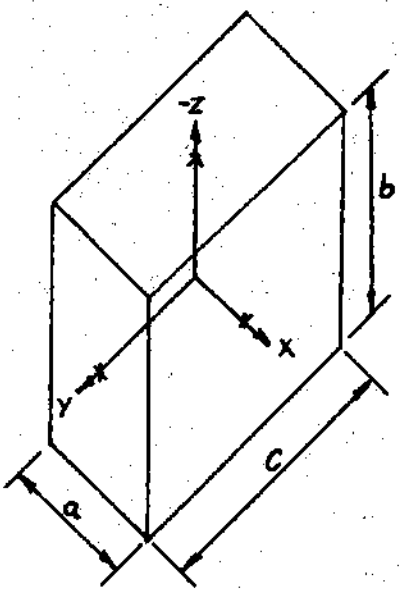

$$I_{xx} = m(b^2 + c^2)/12$$
$$I_{yy} = m(a^2 + b^2)/12$$
$$I_{zz} = m(c^2 + a^2)/12$$
$$I_{xy} = I_{yz} = I_{zx} = 0$$

Figure 43. Equations for Moments of Inertia for a Rectangular Prism.

Table 15 summarizes the calculations and results for the moments of inertia of the vehicle components about their own centers of gravity.

The moments and products of inertia of the combined system about its center of gravity may be determined by applying the parallel axis theorem to determine these parameters for each component about the system center of gravity and then summing the contribution of the individual components. For moments of inertia about parallel axes, the theorem states

$$I_z = I_{z_{cg}} + Md^2$$

and for products of inertia

$$I_{xy} = XYM + I_{xy_{cg}}$$

Where I_z and I_{xy} are properties about arbitrary axes, $I_{x_{cg}}$ and $I_{xy_{cg}}$ are properties about the component centers of gravity, d is the distance between parallel axes and X and Y are the coordinates of the component center of gravity from the origin of the arbitrary coordinate system. In application to the problem at hand these axes are centered at the center of gravity of the chassis-body-cargo system. Table 16 summarizes these calculations and the resulting values for the system moments of inertia for the filled-to-capacity and empty operating conditions.

Table 15. Summary of Calculations for Moments of Inertia of Vehicle Components About Component Centers of Gravity

Component	m	a	b	c	I_{xx}	I_{yy}	I_{zz}
Engine/Cab	$\frac{2478.6}{32.2}$	$\frac{33.6}{12}$	$\frac{24.6}{12}$	$\frac{30.0}{12}$	67.05	77.25	90.38
Frame Rail	$\frac{1468.4}{(2)(32.2)}$	$\frac{275}{12}$	$\frac{9.5}{12}$	$\frac{1}{12}$	1.20	999.08	997.90
Cargo Full	$\frac{8975}{32.2}$	$\frac{205}{12}$	$\frac{81}{12}$	$\frac{95.5}{12}$	2529.39	7836.93	8299.74
Cargo Empty	0	-	-	-	0	0	0
Body Top/ Bottom	$\frac{1850.0}{32.2}$	$\frac{205}{12}$	$\frac{.33}{12}$	$\frac{95.5}{12}$	303.24	1397.27	1700.50
Bottom End	$\frac{731.0}{32.2}$	$\frac{.33}{12}$	$\frac{81}{12}$	$\frac{95.5}{12}$	206.01	86.20	119.82
Body Side	$\frac{1569.0}{32.2}$	$\frac{205}{12}$	$\frac{81}{12}$	$\frac{133}{12}$	185.01	1370.04	1185.04

Table 16. Summary of Calculations for System Moments of Inertia

Component	Slugs	Slug Ft^2			Feet			Slug Ft^2					
	m	I_{xx_c}	$I_{yy_{cb}}$	$I_{33_{cb}}$	x	y	z	I_{xx}	I_{yy}	I_{zz}	I_{xy}	I_{yz}	I_{xz}
Filled to Capacity:													
Engine	77	67	77	90	8.59	0	-2.52	556	6248	5772	0	0	-1667
Left rail	23	1	999	998	1.55	1.29	-3.15	267	1282	1092	46	-93	- 112
Right rail	23	1	999	998	1.55	-1.29	-3.15	267	1282	1092	-46	93	- 112
Top	57	303	1397	1700	-1.37	0	4.00	1215	2416	1807	0	0	- 312
Bottom	57	303	1397	1700	-1.37	0	-2.75	734	1935	1807	0	0	215
Front	23	206	86	120	7.18	0	0.63	215	1281	1306	0	0	104
Rear	23	206	86	120	-9.91	0	0.63	215	2354	2379	0	0	- 144
Left side	49	185	1370	1185	-1.37	-3.98	0.63	981	1481	2053	267	-123	- 42
Right side	49	185	1370	1185	-1.37	3.98	0.63	981	1481	2053	-267	123	- 42
Cargo	279	2529	7837	8250	-1.37	0	0.63	2640	8471	8774	0	0	- 241
TOTAL	660							8071	28231	28135	0	0	-2353
Empty:													
Engine	77	67	77	90	7.59	0	-2.06	394	4840	4526	0	0	-1204
Left rail	23	1	999	998	0.55	1.29	-2.69	206	1172	1043	16	-80	- 34
Right rail	23	1	999	998	0.55	-1.29	-2.69	206	1172	1043	-16	80	- 34
Top	57	303	1397	1700	-2.37	0	4.46	1437	2851	2020	0	0	- 603
Bottom	57	303	1397	1700	-2.37	0	-2.29	602	2016	2020	0	0	309
Front	23	206	86	120	6.18	0	1.09	233	992	998	0	0	155
Rear	23	206	86	120	-10.91	0	1.09	233	2851	2858	0	0	- 274
Left side	49	185	1370	1185	-2.37	-3.98	1.09	1019	1703	2236	462	-213	- 127
Right side	49	185	1370	1185	-2.37	3.98	1.09	1019	1703	2236	-462	213	- 127
Cargo	0	0	0	0	-	-	-	-	-	-	-	-	-
TOTAL	381							5349	19300	18980	0	0	-1939

APPENDIX VII

DESIGN OF A PROTOTYPE LOW INERTIA ACCUMULATOR

Introduction

To demonstrate the feasibility of constructing an accumulator with good strength and stiffness, reasonable endurance life, low inertia and little cantilevered mass, an investigation of the critical design problems is presented. The kinematic configuration chosen for the design study is the contracted revolute-revolute-prismatic chain, Figure 44. However, similar solutions could be applied to the design problems inherent in any of the other alternative kinematic chains.

There are several alternative vehicle accumulator configurations to which the R-R-P chain could be adapted, three of which are outlined in Figure 45. This kinematic chain consists of the mechanical implementation of a vector from the accumulator attachment point to the target and has very little obstacle avoidance capability; however, its simplicity permits concentration on the most significant design considerations with a minimum of complicating details.

Actuator Conceptual Design

One of the most obvious problems in the design of an accumulator with a low cantilevered weight is that of providing for link extensions and/or rotations without placing heavy hydraulic or pneumatic components at each joint. If the actuators are located with their centers of gravity on or near the base of the

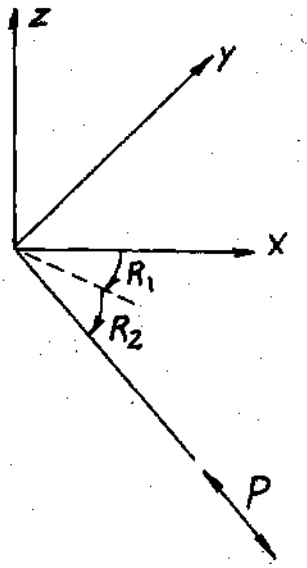

Figure 44. Contracted Revolute-Revolute-Prismatic Kinematic Chain

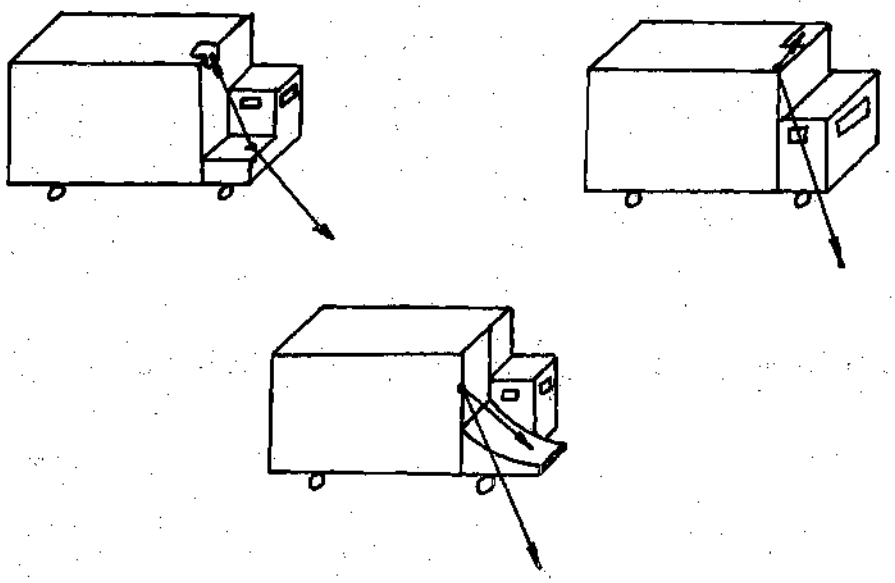

Figure 45. R-R-P Chain Implementation in Refuse Accumulation

accumulator, the problem becomes one of transmitting the actuator outputs to the joints without the use of heavy power transmission components.

For the R-R-P chain, the only joint not located directly on the base of the accumulator is the prismatic extension. Most commonly such joints are activated by hydraulic or pneumatic cylinders, an inverted rack and pinion, or a ball screw. All of these actuators feature massive components located at the joint and of a length at least as great as the extension to be produced. An alternative actuation scheme for prismatic pairs which features little overhung weight is shown schematically in Figure 46. It consists of preloaded steel bands or cables which extend or retract the moving part of the link as shown.

The cables or bands could be counter wound on a pair of motor driven drums or rigged through a pair of cylinder driven inverted block and tackle. The winding drum arrangement could include a worm gear drive to avoid the necessity of clutches and brakes to support static loads, while the cylinder driven block and tackle would support quasistatic loads (no control signal, both ports blocked) without further modification, limited only by leakage.

The revolute pairs located in the base of the accumulator could be driven by a modified version of this same arrangement by fixing the cable to a pulley on the moving part of the joint, and it is this arrangement which is proposed for the revolute pairs of other kinematic chains. It is more likely, however, that a conventional drive system would be used for the revolute pairs located in the base of the accumulator.

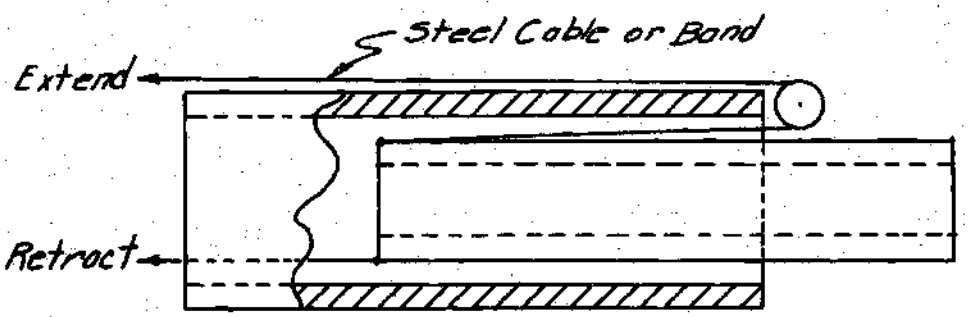

Remote Actuation of a Prismatic Pair

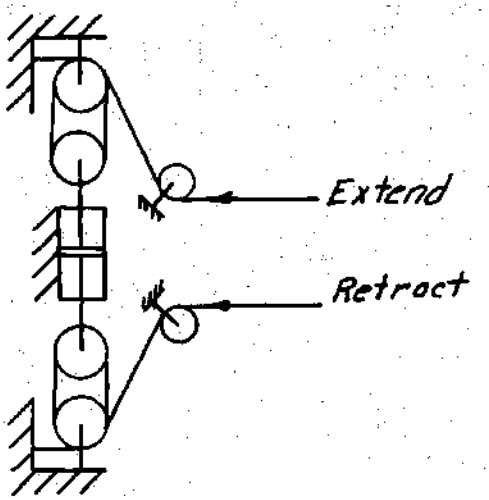

Cylinder Driven Inverted Block & Tackle

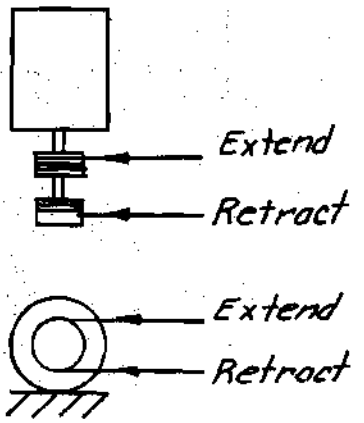

Motor Driven Winding Drum

Figure 46. Actuator for Prismatic Pairs Featuring Low Overhung Weight

Link Selection

Preliminary Discussion

In selecting members for use as prismatic pairs the first consideration must be that the sections chosen are easily "telescoped" and that rotation about the longitudinal axis of the pair is resisted. For the application at hand it is also desirable that the resulting beam have the same stiffness in bending about any of the principal axes of the section. These considerations indicate the use of square tubular sections for both the fixed and moving links in the pair. Tubular sections also have good torsional stiffness, a feature more important in some of the other kinematic chains than in the R-R-P chain.

Having determined the cross sectional shape of the links, a method of transmitting loads between them must be devised which is compatible with their kinematic function. As shown schematically in Figure 47, the use of commercially available roller bearing cam followers at the rear of the moving link and the front of the fixed link could perform this function. Hardened steel wearing surfaces would be attached to each link, and the cam followers would be stiffly spring mounted to ensure continuous contact. In addition, mechanical stops would be employed to maintain a minimum distance, ℓ_o, between rollers at full extension.

Stiffness Considerations

The accumulator could easily experience simultaneous transverse and axial loading in use and therefore the deflections to be expected under such loading are investigated in Appendix VIII. There it is shown that the axial load F may be neglected in computing transverse deflections and hence in computing transverse

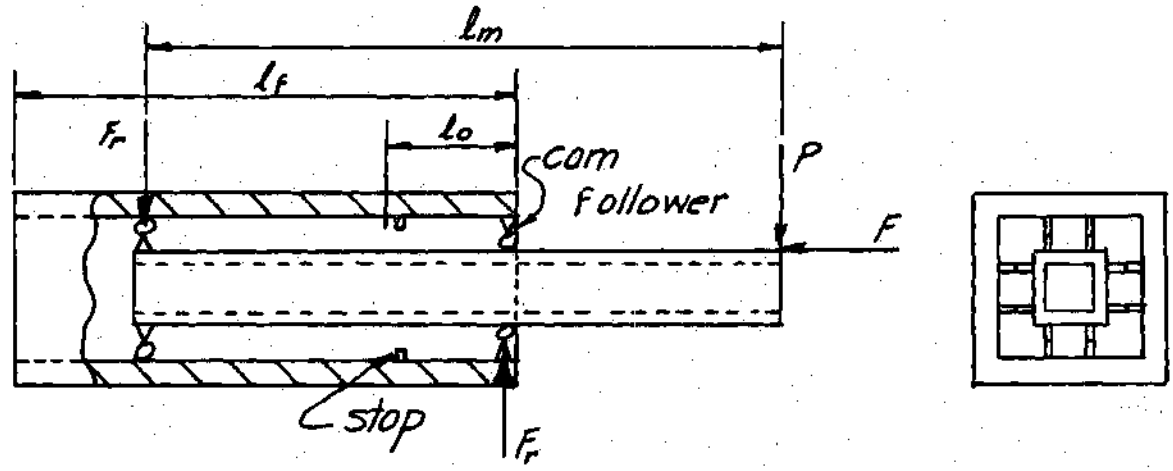

Figure 47. Method of Transmitting Loads Between Prismatic Pairs.

stiffness, with less than one percent error.

The expression for transverse stiffness derived for the prismatic pair at full extension,

$$K = \frac{3E_m E_f I_m I_f \ell_o^2}{\left\{E_f I_f \ell_m \ell_o^2 (\ell_m - \ell_o)^2 + E_m I_m \left[\ell_m^2 \ell_f^3 + (\ell_f - \ell_o)^2 \left(\ell_o(\ell_f + \ell_m) - \ell_m^2(\ell_f + \ell_o) - \ell_o(\ell_o - \ell_m)^2\right)\right]\right\}} \tag{151}$$

is a function only of the material properties and dimensions of the links. If the two revolute pairs located in the base of the accumulator are worm gear driven, and if the shaft lengths are sufficiently short, the deflections due to rotation of the revolute pairs would be negligible. Under these conditions, the transverse stiffness

of the prismatic pair, given by equation 151, could be written as an equivalent rotational stiffness at the base of the manipulator. The rotational stiffness $\hat{K}$ is related to the applied torque T and equivalent angular displacement θ_e by

$$T = \hat{K}\,\theta_e$$

For small tip deflections δ,

$$\theta_e = \frac{\delta}{(\ell_m + \ell_f - \ell_o)} \tag{153}$$

The torque is related to the transverse force P applied at the tip of the accumulator by

$$T = P(\ell_m + \ell_f - \ell_o) \tag{154}$$

The tip deflection δ and force P are related by

$$P = K\delta \tag{155}$$

Substitution of equations 5, 4, and 3 into 2 yields an expression for the equivalent rotational stiffness $\hat{K}$:

$$\hat{K} = (\ell_m + \ell_f - \ell_o)^2 K \ \frac{\text{ft-lbs}}{\text{rad}} \tag{156}$$

Since the links in the prismatic pair are square tubes, their stiffness is equal in all transverse directions and $\hat{K}$ is valid for both revolute joints.

Manufacturing and economic considerations make the use of standard

sections desirable whenever possible. Table 17 summarizes the properties of readily available square tubes in the size range applicable to accumulator design. Also included in the table is the value of $EI/Wx\ 10^{-6}$, a measure of the stiffness to weight ratio, for each section. This ratio is helpful in choosing efficient sections, it is not, however, possible to choose the most efficient prismatic pair based on this ratio alone.

The objective in selecting members for the accumulator must be that for a given required stiffness, extension length, and maximum section width, the lightest pair meeting all of these requirements is chosen. The limit on section width is necessary because the stiffness to weight efficiency objective favors larger section widths. If the section width were not restricted, the search for an "optimum section" would result in sections so thin that localized buckling would cause failure, or so large that the operator's view of the refuse would be obstructed by the accumulator.

For an accumulator of specified maximum extension length, the parameters which may be varied by the designer are the link lengths ℓ_f and ℓ_m, the overlap distance ℓ_o, section moduli I_m and I_f, and the modulus of elasticity of each link. The greatest range of possible extension lengths is provided when $\ell_f = \ell_m$ and the overlap distance ℓ_o is small. In order to achieve a good range of extension lengths, the alternatives chosen all have equal length fixed and movable links ($\ell_f = \ell_m$).

Given the materials and cross sections for the prismatic pair and a required maximum reach, the accumulator stiffness and weight increase with

Table 17. Properties of Standard Square*

Width Inches	Wall Inches	Moment of Inertia in^4 I	Material	Grade	Modulus of Elasticity 10^6 psi E	Endurance Limit 1000 psi	Weight/ft. lbs W	$\frac{EI}{W} \times 10^{-6}$
5	0.188	13.99	Steel	A36	30.0	29.0	12.290	34.15
$4\frac{1}{2}$	0.188	10.07	Steel	1010	30.3	24.0	11.010	27.71
4	0.250	8.828	Steel	A36	30.0	29.0	12.735	20.80
4	0.188	6.960	Steel	A36	30.0	29.0	9.735	20.62
4	0.125	4.854	Steel	1010	30.3	24.0	6.580	22.35
4	0.083	3.327	Steel	1010	30.3	24.0	4.416	22.83
4	0.065	2.641	Steel	1010	30.3	24.0	3.474	23.03
$3\frac{1}{2}$	0.250	5.755	Steel	A36	30.0	29.0	11.037	15.64
$3\frac{1}{2}$	0.188	4.568	Steel	A36	30.0	29.0	8.458	16.20
$3\frac{1}{2}$	0.120	3.093	Steel	1010	30.3	24.0	5.510	17.01
3	0.250	3.495	Steel	A36	30.0	29.0	9.339	11.23
3	0.203	2.977	Steel	1010	30.3	24.0	7.713	11.69
3	0.188	2.799	Steel	A36	30.0	29.0	7.181	11.69
3	0.134	2.108	Steel	1010	30.3	24.0	5.217	12.24
3	0.125	1.984	Steel	1010	30.3	24.0	4.882	12.31
3	0.109	1.758	Steel	1010	30.3	24.0	4.281	12.44

Table 17 (Continued). Properties of Standard Square*

Width Inches	Wall Inches	Moment of Inertia in^4 I	Material	Grade	Modulus of Elasticity 10^6 psi E	Endurance Limit 1000 psi	Weight/ft. lbs W	$\frac{EI}{W} \times 10^{-6}$
3	0.095	1.554	Steel	1010	30.3	24.0	3.749	12.56
3	0.083	1.375	Steel	1010	30.3	24.0	3.289	12.67
3	0.065	1.096	Steel	1010	30.3	24.0	2.591	12.82
4	0.250	8.828	Aluminum	6061-T6	10.0	14.0	4.500	19.62
4	0.156	5.917	Aluminum	6063-T52	10.0	10.0	2.878	20.56
4	0.125	4.854	Aluminum	6063-T52	10.0	10.0	2.325	20.88
$3\frac{1}{2}$	0.156	3.897	Aluminum	6063-T52	10.0	10.0	2.504	15.56
3	0.375	4.614	Aluminum	6061-T6	10.0	14.0	4.725	9.77
3	0.250	3.495	Aluminum	6061-T6	10.0	14.0	3.300	10.59
3	0.156	2.400	Aluminum	6063-T52	10.0	10.0	2.130	11.27
3	0.125	1.984	Aluminum	6063-T52	10.0	10.0	1.725	11.50
$2\frac{1}{2}$	0.250	1.922	Aluminum	6061-T6	10.0	14.0	2.700	7.12

*Data from references 53, 54, 55, and 56, endurance limit of A36 steel estimated at 50 percent of ultimate strength.

increasing overlap length ℓ_o; however, as shown in Figure 48, the stiffness to weight ratio decreases. Increasing ℓ_o also increases the minimum extension, thereby reducing the area accessible to the accumulator in operation. It should be pointed out that at $\ell_o = 0$ the pair has zero transverse stiffness and therefore the stiffness must drop off sharply at some point less than $\ell_o = 4$ inches. What would in fact happen is that as ℓ_o approached zero the reactions $P\left(\frac{\ell_m}{\ell_o} - 1\right)$ would become sufficiently great to cause failure. Since manufacturing considerations make the use of overlap lengths less than 4 inches difficult, there is no point in exploring the accumulator behavior for this range of ℓ_o.

Several alternative combinations of fixed and movable links were chosen from the sections in Table 17 to design an accumulator with a maximum reach of 12 feet. Since $\ell_o = 4$ inches is the lower limit for the overlap length, prescribed primarily by manufacturing considerations, and because the accumulator weight efficiency is greatest at this limit, all of the alternatives investigated have $\ell_f = \ell_m = 74$ inches and $\ell_o = 4$ inches. Table 18 summarizes the result of the selection process for six alternative accumulators ranging in stiffness from 77.5 to 409.4 pounds per inch. The high penalty paid in terms of weight efficiency for small section width is easily seen in the first two entries in the table. The second entry, with sections only one half inch larger than those of the first entry, is 10.2 percent more rigid and 14.6 percent lighter. The third entry in the table is less efficient than the second entry, but is the best alternative with section widths under four inches and stiffness near 110 pounds per inch. The fourth entry is the most efficient of all--a result of its five inch section width. The high weight

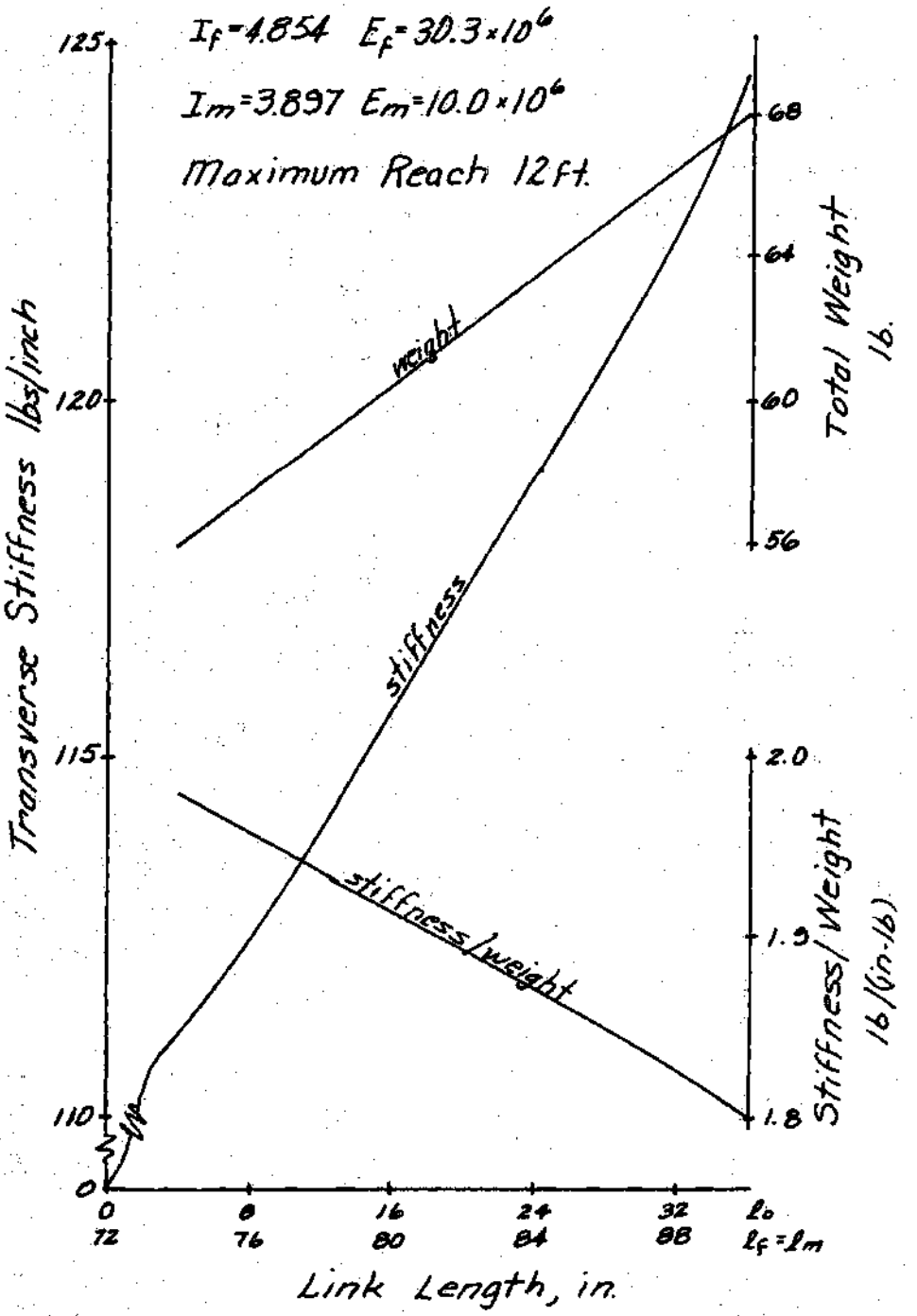

Figure 48. Effect of Overlap Length ℓ_o

Table 18. Alternative Contracted RRP Accumulator with 12 Ft Reach

Alternative	Fixed Link				Movable Link				Pair		
	I_f in^4	W_f in	Material	Grade	I_m in^4	W_m in	Material	Grade	Weight lbs.	Stiffness lbs/in	Stiffness/ Weight
1	3.093	3.5	Steel	1010	1.096	3.0	Steel	1010	50.0	77.5	1.55
2	3.327	4.0	Steel	1010	3.897	3.5	Aluminum	6063-T52	42.7	85.4	2.00
3	4.854	4.0	Steel	1010	3.897	3.5	Aluminum	6063-T52	56.0	111.1	1.98
4	13.990	5.0	Steel	A36	10.07	4.5	Steel	1010	143.7	409.4	2.85
5	8.828	4.0	Steel	A36	3.495	3.0	Steel	A36	136.1	225.8	1.66
6	2.641	4.0	Steel	1010	3.897	3.5	Aluminum	6063-T52	36.9	71.7	1.94

of this alternative and its unnecessarily large stiffness, however, make it an unlikely design solution. The fifth entry in the table is the most rigid alternative possible using the standard sections listed in Table 17 with ℓ_o = 4 inches and four inch section width. The last entry is included to demonstrate that the EI/W ratio given in Table 17 is not sufficient information to select members for the most efficient accumulator. The fixed link for entry six has EI/W = 23.03 while the fixed link for entry two has EI/W = 22.83. The overall stiffness to weight ratio of the accumulators, however, are 1.94 and 2.00 respectively. In this case, the less efficient but stiffer fixed link resulted in the greatest efficiency for the total accumulator.

Applied Stresses and Fatigue Life

In order that the desired kinematic relationship between the links of the accumulator be maintained, no permanent deformation of the parts may be allowed to occur. This can be assured if the stresses applied to the parts do not exceed the yield points of the materials. A more severe requirement, however, is that the machine have a reasonable fatigue life in the face of its continuously varying loads. A near infinite fatigue life can be assured if the stresses applied to the parts are held below the endurance limits of the materials. (It is assumed that the beneficial effect on endurance strength of thin walls and the detrimental effect of unpolished surface finishes are approximately equivalent.)

For the fixed link of the prismatic pair, the maximum bending moment occurs at the point where the accumulator is attached to the vehicle, x = 0, and has magnitude

$$M_{max_f} = P(\ell_f + \ell_m - \ell_o) + F y_{\ell_f} \tag{157}$$

while the maximum shear load occurs over the interval $\ell_f - \ell_o < x < \ell_f$ and has magnitude

$$V_{max_f} = P \frac{\ell_m}{\ell_o} \tag{158}$$

For the movable link the maximum bending moment occurs at $x = \ell_o$ and has magnitude

$$M_{max_m} = P(\ell_m - \ell_o) + F(y_{\ell_m} - y_{\ell_f}) \tag{159}$$

and the maximum shear load occurs over the interval $0 \leq x \leq \ell_o$ and has magnitude

$$V_{max_m} = P\left(\frac{\ell_m}{\ell_o} - 1\right) \tag{160}$$

Examination of equations 151 and 159 reveals that the contribution to the maximum bending moment by axial force F is a small term (on the order of one percent of M_{max} even for F = P), and may be neglected.

The equation for maximum normal stress in an elastic flexural member is well known and is (57),

$$\sigma_{max} = \frac{M_{max} c}{I} \tag{161}$$

where c is the distance from the neutral axis to the extreme fiber of the section

and I is the moment of inertia of the section. For square tubular sections c is greater when the tube is bent about an axis through its diagonal, and for this loading (Figure 49a)

$$c = \frac{b}{\sqrt{2}} \tag{162}$$

where b is the outside dimension of the section. Substituting Equation 162 into Equation 161 yields an expression for the maximum normal stress due to bending for square tubular sections

$$\sigma_{max} = \frac{M_{max} b}{\sqrt{2}\ I} \tag{163}$$

The equation for maximum shear stress in an elastic flexural member is also well known:

$$\tau_{max} = \frac{V_{max} Q_n}{wI} \tag{164}$$

Here w is the material thickness at the neutral axis, I is the moment of inertia of the section and Q_n is the static moment of the cross sectional area of the section above the neutral axis taken about the vertical axis. For square tubular section, V_{max} is greatest when the tube is bent about an axis parallel to its sides. Under this loading (Figure 49b)

$$\tau_{max} = \frac{V_{max}(b^3 - (b-2t)^3)}{16\ It} \tag{165}$$

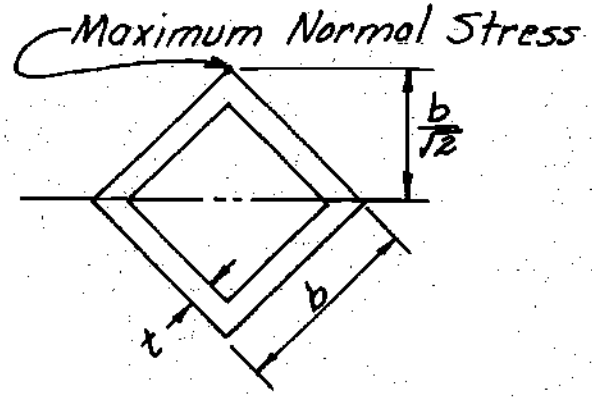

$$c = \frac{b}{\sqrt{2}}$$

$$Q_n = \frac{b^3 - (b - 2t)^3}{6\sqrt{2}}$$

$$\sigma_{max} = \frac{M_{max}\, b}{\sqrt{2}\, I}$$

$$\tau_{max} = \frac{V_{max}(b^3 - (b-2t)^3)}{24\, It}$$

(a)

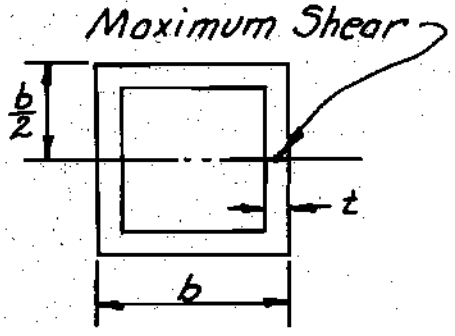

$$c = \frac{b}{2}$$

$$Q_n = \frac{b^3 - (b - 2t)^3}{8}$$

$$\sigma_{max} = \frac{M_{max}\, b}{2I}$$

$$\tau_{max} = \frac{V_{max}(b^3 - (b - 2t)^3)}{16\, It}$$

(b)

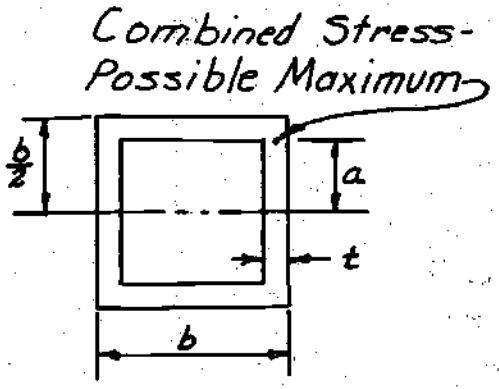

$$a = \frac{b}{2} - t$$

$$Q_a = bt\left(\frac{b - t}{2}\right)$$

$$\sigma_a = \frac{M_a\left(\frac{b}{2} - t\right)}{I}$$

$$\tau_a = \frac{V_a\, b(b - t)}{4\, I}$$

(c)

Figure 49. Critical Stress Points for Square Tubes Used as Beams.

where t is the wall thickness of the section ($w = 2t$).

It is possible that the most severe case of combined stress occurs when the beam is bent about an axis parallel to its sides, the critical point being where the sides join the top and bottom, point "a" in Figure 49c. At this point the stresses are

$$\sigma_a = \frac{M_a(\frac{b}{2} - t)}{I}$$

$$\tau_a = \frac{V_a b(b - t)}{4I} \qquad (166)$$

The normal stress due to axial load F is uniform across the section and is given by

$$\sigma_{axial} = \frac{F}{A} \qquad (167)$$

where A is the cross sectional area of the section.

For plane stress, the largest principal normal stress σ_1 is related to the applied normal and shear stresses at a point by (58),

$$\sigma_1 = \frac{\sigma_x + \sigma_y}{2} + \sqrt{\left(\frac{\sigma_x - \sigma_y}{2}\right)^2 + \tau_{xy}^2} \qquad (168)$$

Applying Equation 168 to Equations 163 and 166 results in a maximum compressive stress of

$$\sigma_1 = \frac{M_{max} b}{\sqrt{2}I} + \frac{F}{A} \qquad (169)$$

at the extreme fibers for the loading considered in Figure 49a. Equations 165 and 166 result in a maximum normal stress of

$$\sigma_1 = \frac{F}{2A} + \sqrt{\left(\frac{F}{2A}\right)^2 + \left(\frac{V_{max}(b^3 - (b-2t)^3)}{16\,I\,t}\right)^2} \qquad (170)$$

at the neutral axis for the loading considered in Figure 49b. The combined stresses at point a, Figure 49c, result in

$$\sigma_1 = \frac{\frac{F}{A} + \frac{(\frac{b}{2} - t)M_{max}}{I}}{2} + \sqrt{\left[\frac{\frac{F}{A} + \frac{(\frac{b}{2} - t)M_{max}}{I}}{2}\right]^2 + \left(\frac{V_{max}\,b(b-t)}{4I}\right)^2} \qquad (171)$$

Equation 171 must be evaluated twice for the fixed link since V_{max} and M_{max} do not occur at the same value of x.

Table 19 lists the maximum principal stresses at the three critical points in the fixed and movable links for the first five alternative prismatic pairs listed in Table 18, when subjected to a load equivalent to a two g acceleration of the accumulator and 50 pound payload. The three cases considered are P = 2g and F = 0, P = F = $\frac{2g}{\sqrt{2}}$, and P = 0, F = 2g. The values given for the stress at point "a" for the fixed link are the larger of normal stresses at point "a" when x = 0 or x = $\ell_f - \ell_o$. In every case this stress was largest at x = 0.

The stress in the extreme fiber was found to be the largest stress experienced by both the movable and fixed links and is enclosed in the blocks in Table 19. No member experiences stresses in excess of its endurance limit except the movable link of alternative number 1. By changing the material for this member

Table 19. Principal Normal Stress at Critical Points in Contracted R-R-P Accumulator Subject to 2g Load

Alternative	Fixed Link					Movable Link				
	M_{max} in-lbs	U_{max} lbs	σ_1 Extreme Fiber psi	σ_1 Neutral Axis psi	σ_1 Point "a" psi	M_{max} in-lbs	U_{max} lbs	σ_1 Extreme Fiber psi	σ_1 Neutral Axis psi	σ_1 Point "a" psi
CASE I: P = 2g load, F = 0										
1	28800	3700	23044	5127	15180	14000	3500	27097	10317	20716
2	26698	3429	22697	5932	15368	12978	3245	8242	3494	6256
3	30528	3922	17789	4551	11795	14840	3710	9424	3995	7155
4	55786	7167	14098	4450	9553	27118	6780	8569	4697	7063
5	53597	6886	17172	4119	10627	26054	6514	15814	5299	10699
CASE II: $P = F = \frac{2}{\sqrt{2}}$ g load										
1	20365	2616	16382	3669	10821	9899	2475	19345	7389	14748
2	18878	2425	16150	4245	10980	9177	2294	5891	2501	4426
3	21587	2773	12656	3257	8418	10493	2623	6736	2861	5060
4	39446	5068	10044	3185	6596	19175	4794	6144	3364	4989
5	37898	4868	12212	2948	7584	18473	4606	11278	3796	7499

Table 19 Continued. Principal Normal Stress At Critical Points in Contracted R-R-P

Accumulator Subject to 2g Load

Alternative	Fixed Link					Movable Link				
	M_{max} in-lbs	U_{max} lbs	σ_1 Extreme Fiber psi	σ_1 Neutral Axis psi	σ_1 Point "a" psi	M_{max} in-lbs	U_{max} lbs	σ_1 Extreme Fiber psi	σ_1 Neutral Axis psi	σ_1 Point "a" psi
CASE III: P = 0, F = 2g Load										
1	0	0	123	123	123	0	0	262	262	262
2	0	0	143	143	143	0	0	89	89	89
3	0	0	109	109	109	0	0	102	102	102
4	0	0	107	107	107	0	0	119	119	119
5	0	0	99	99	99	0	0	135	135	135

from 1010 to A36 steel, this situation can be corrected. With this change any of the alternative accumulators listed in Table 18 would have an infinite endurance life.

Axial Stiffness

The axial deflection of the prismatic pair is due almost entirely to extension in the control cables. The stiffness of steel cables is not normally specified by suppliers and since it is a function of the strand material, number of strands, core material, and lay, it would be very difficult to estimate without complete knowledge of the manufacturing details of each cable considered. It is reasonable to assume however, that by varying these design parameters a cable of specified stiffness could be fabricated. It is also a reasonable assumption that a steel cable of specified stiffness would have a higher yield point and ultimate strength than a single strand of the same stiffness. (Consider the superior strength properties of smaller sections and the larger net area required to give a twisted cable equivalent stiffness.) For these reasons, in this discussion reference will be made to an "equivalent cable" used for improved flexibility and ready availability, which has the stiffness of a specified steel wire and superior strength.

The deflection δ of a steel wire loaded in tension by force F is well known and is given by

$$\delta = \frac{F\ell}{AE} \tag{172}$$

where ℓ is the length of the wire, E its modulus of elasticity (30×10^6 psi) and A its cross-sectional area. The force applied and wire length ℓ are determined

by other design considerations. Thus the only variable available to the designer for controlling deflections is the cross-sectional area A.

The corresponding stress applied to the material is given by

$$\sigma = \frac{F}{A} \tag{173}$$

By requiring that the stress in the wire does not exceed the endurance limit of the material, equation 173 becomes an expression for a lower limit on allowable area A.

$$A_{min} = \frac{F_{max}}{\sigma_{en}} \tag{174}$$

Since the stiffness K of the wire if given by

$$K = \frac{AE}{\ell} \tag{175}$$

Equation 174 specifies a minimum stiffness

$$K_{min} = \frac{F_{max} E}{\sigma_{en} \ell} \tag{176}$$

below which helical tension springs would have to be used between the cable and movable link. Figure 50 relates graphically this minimum stiffness to wire length ℓ and maximum applied force F for music wire (σ_{en} = 94500 psi). As can be seen from the figure, the minimum K prescribed by stress considerations is extremely high and therefore it is likely that helical springs would be used between the movable

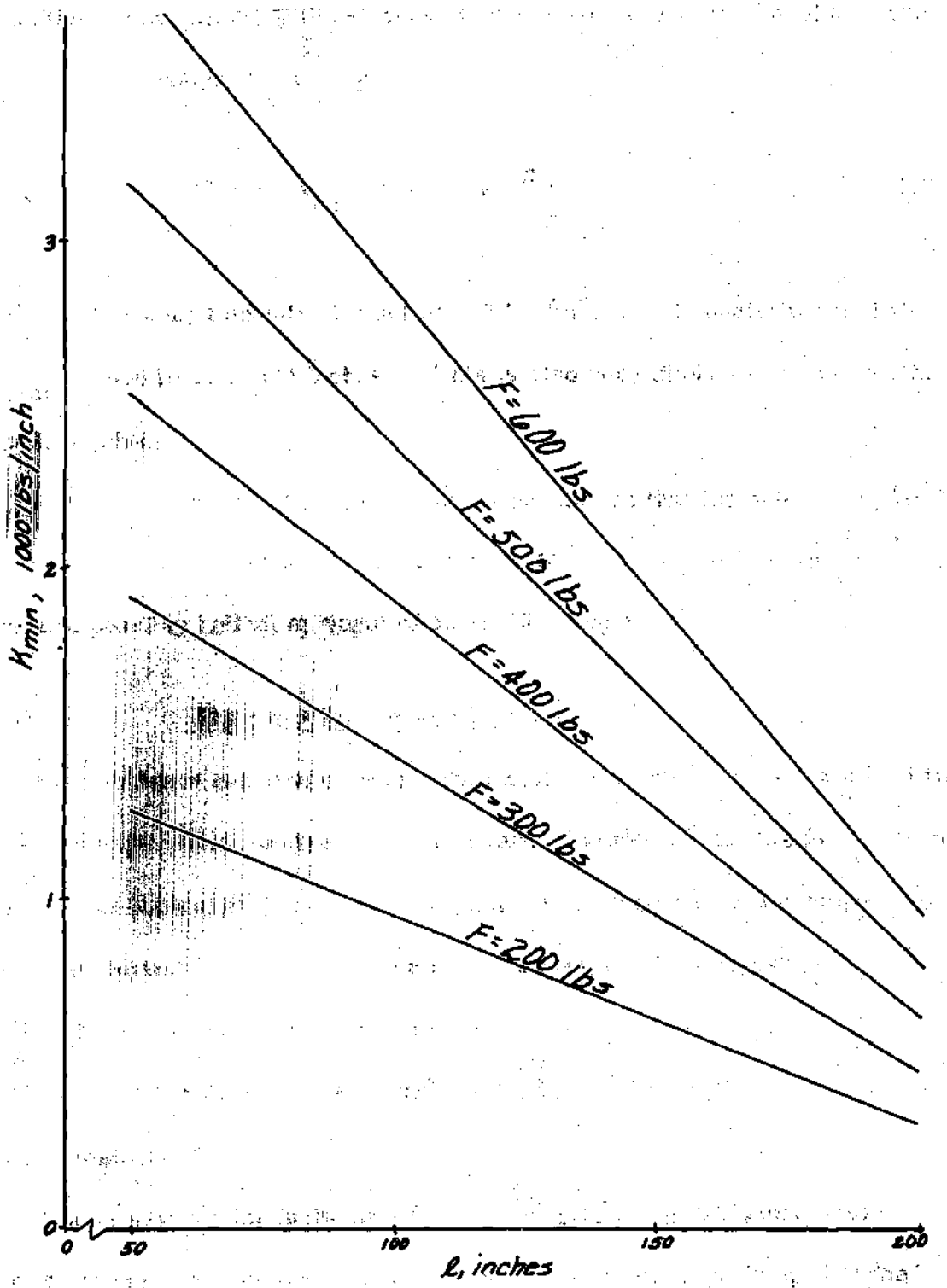

Figure 50. Minimum Axial Stiffness Versus Wire Length for Various Applied Loads

link and the cables, allowing the stiffness to be varied readily over a wide range.

The wire weight is given by

$$W = \rho \ell A_{min} = F_{max} \ell \frac{\rho}{\sigma_{en}} \tag{177}$$

where ρ is the weight density of steel (0.283 lbs/in^3), and is negligible (0.4 lbs for F_{max} = 600 lbs., ℓ 200 inches). This is also very likely to be true for the "equivalent cable."

The major result of this section is the conclusion that the prismatic pair can easily be as stiff in the axial direction as in the transverse direction using calbes (and possibly helical springs) of negligible weight.

Provision for Viscous Damping

Accumulators actuated by cables as described in this appendix exhibit little viscous damping, with a maximum damping ratio of perhaps 0.25 due to structural damping in the links and at the prismatic joint. Since higher damping ratios are typically employed in automated systems, some provision for increasing the damping effect in the accumulator may be desirable. Passive damping elements could be included in the axial direction by enclosing the helical tension springs on each cable in a dashpot.

A technique for the inclusion of active damping at the actuators would enable transverse oscillations as well as axial oscillations to be damped. The accumulator can be modeled as a mass suspended on a spring and parallel damper subject to base excitation as indicated in Figure 51, where u is the extension of

the actuator.

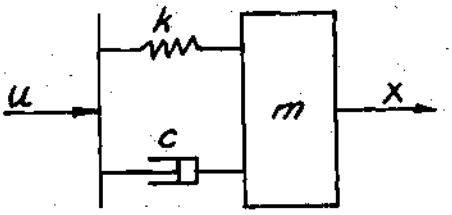

Figure 51. Accumulator Model

The equation of motion of this system is

$$m\ddot{x} + c(\dot{x} - \dot{u}) + k(x - u) = 0 \tag{178}$$

and its transfer function in Laplace notation is

$$\frac{x}{u} = \frac{cs + k}{ms^2 + cs + k} \tag{179}$$

In the problem at hand we are confronted with a system in which $c \approx 0$ so that the equation becomes

$$\frac{x}{u} = \frac{k}{ms^2 + k} \tag{180}$$

To provide damping to the accumulator a control system is proposed as shown in Figure 52 with gains G_1 and G_2 to be determined so that the overall system transfer function is identical to that of a viscously damped system, equation 179.

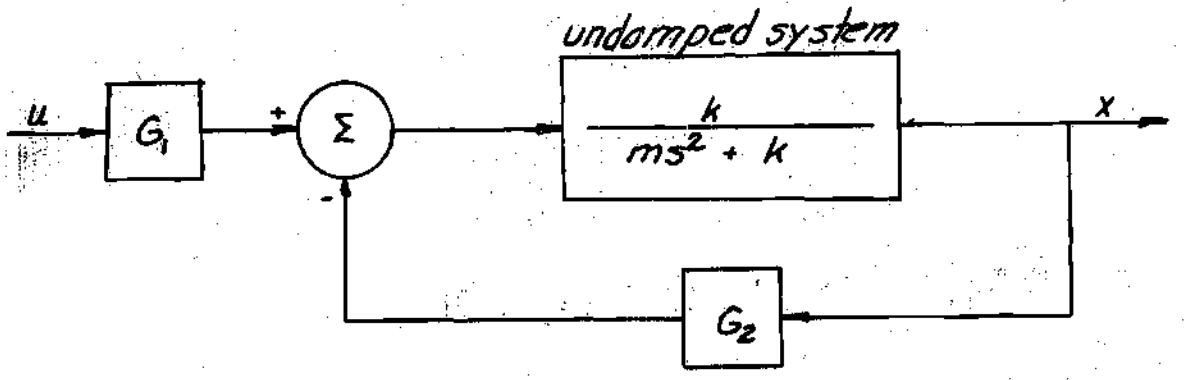

Figure 52. Active Damping System.

The closed loop transfer function of this system is

$$\frac{x}{u} = \frac{G_1 k}{ms^2 + (G_2 + 1)k} \tag{181}$$

Equating equations 179 and 181, the system gains G_1 and G_2 are found:

$$G_1 = \frac{c}{k} s + 1$$

$$G_2 = \frac{c}{k} s \tag{182}$$

Implementation of the active damping system is facilitated by the use of an equivalent block diagram shown in Figure 53. The modification in the system arrangement

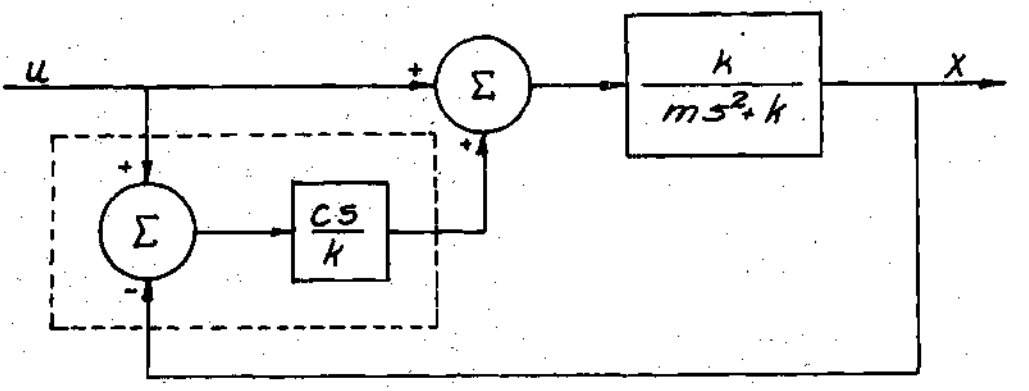

Figure 53. Active Damping System Implementation.

permits the computation of $\frac{c}{k}(\dot{u} - \dot{x})$ by placing strain gages on the accumulator to measure (u - x) and then differentiating the signal once with respect to time in an operational amplifier.

Capture Subsystem Weight Estimation

A grasping device consisting of three links as shown in Figure 54 is typical of its class of capture subsystems. The links are actuated by a pneumatic cylinder with stroke e. The angle θ which corresponds to the extreme open position of the device is related to the cylinder stroke e and lever length ℓ by

$$\theta = \sin^{-1} \frac{e}{\ell}$$

The horizontal distance d between the open end of each link and a vertical line through its pivot point is given by

$$d = r \sin \theta = r \frac{e}{\ell}$$

In the application at hand, r = 36 inches and d = 18 inches would be adequate for plastic refuse bags up to 30 gallon capacity. For these values of r and d, $\frac{e}{\ell} = 0.5$, easily accomplished with a cylinder stroke e of one inch and lever arm ℓ of two inches. Allowing an additional inch on the radius for the cylinder-to-lever attachment, the minimum closing diameter of the device is six inches and the extreme open position encloses a circle of 42 inch diameter.

In supporting a 50 pound load the three links might each exert a 10 pound side force. The required countering cylinder force, found by the summation of moments about the pivot point for each link, would be

$$F_{cyl} = \frac{(10)\ (36)\ (3)}{2} = 540 \text{ lbs.}$$

A two inch bore commercial air cylinder operating at 250 psi is capable of exerting 775 pounds force (59) and weighs approximately two pounds, while a one

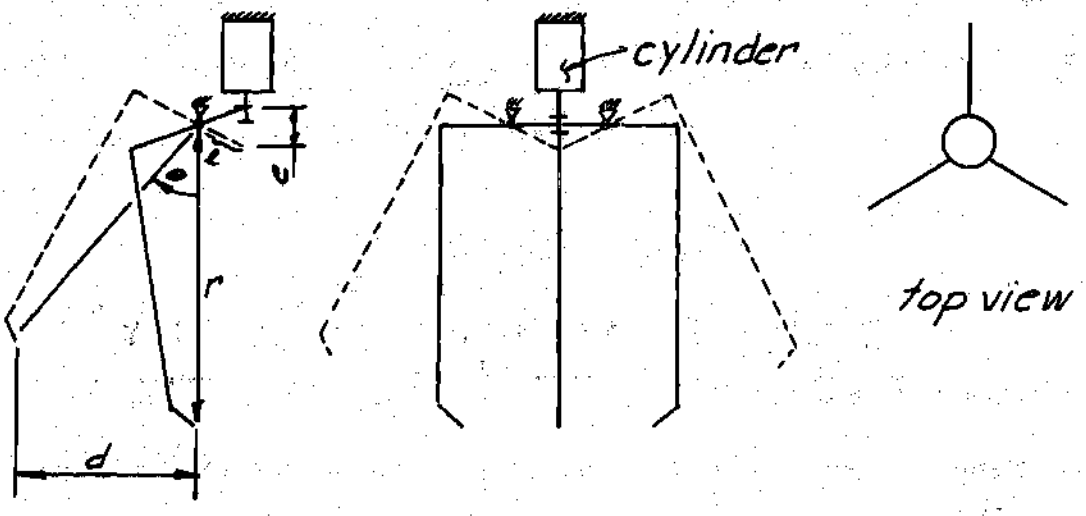

Figure 54. A Grasping Type Capture Subsystem.

inch square tube of 1010 steel with 0.060 inch wall is more than adequate for the links--an additional weight of approximately eight pounds. Including the valves and attaching hardware, the capture subsystem would weigh approximately fifteen pounds and require 3.1 cubic inches of air at 250 psi at each operation.

APPENDIX VIII

DERIVATION OF AN EXPRESSION FOR THE TIP DEFLECTION OF THE FULLY EXTENDED R-R-P ACCUMULATOR AND TRANSVERSE STIFFNESS K

Introduction

The fully extended R-R-P accumulator, loaded by a transverse force P and axial force F at its tip, and constructed as shown in Figure 46 of Appendix VII, deflects δ inches at its tip. The object of this appendix is to derive an expression for δ in terms of the link dimensions, material properties and applied loads. The linear approximation to δ which results when the axial load is neglected is also derived and an estimate is made of the error inherent in the approximation. Finally an expression for the transverse stiffness K of the beam is derived.

Combined Transverse and Axial Loading

The loads imposed on the fixed and movable links at full extension due to the application of forces P and F at the tip of the movable link are given in Figure 55 along with the reference axes and pertinent dimensions. The expression for tip deflection y_{ℓ_m} must be derived by first determining the equation of the deflected fixed link, and then the equation of the deflected movable link, using as boundary conditions the requirement that the points of application of the reactions

$$P\left(\frac{\ell_m}{\ell_o} - 1\right) \text{ and } P\,\frac{\ell_m}{\ell_o}$$

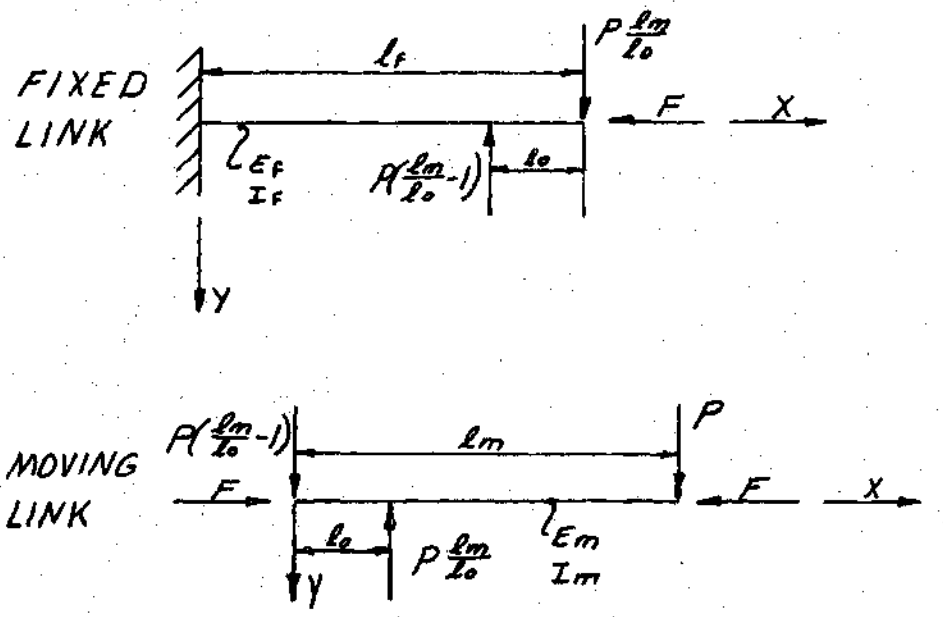

Figure 55. Loads on the Prismatic Pair Due to Forces P and F at the Tip

have the same deflection by either equation. Then y_{ℓ_m} is given by the equation for the deflected movable link evaluated at $x = \ell_m$.

Using the usual sign convention that moments producing concave-up deflections are positive, the moment at a point x on the fixed link is given by

$$M_x = P\frac{\ell_m}{\ell_o}(x - \ell_f) - P\left(\frac{\ell_m}{\ell_o} - 1\right)(x - \ell_o) - F(y_{\ell f} - y) \qquad 0 \le x \le \ell_f - \ell_0$$

$$M_x = P\frac{\ell_m}{\ell_o}(x - \ell_f) - F(y_{\ell f} - y) \qquad \ell_f - \ell_o \le x \le \ell_f \tag{183}$$

The equation of the neutral axis of a deflected elastic beam is well known (see for example reference 57) and is given by

$$\frac{d^2y}{dx^2} = -\frac{M}{EI} \tag{184}$$

The differential equations for the deflected fixed link are therefore

$$\frac{d^2y}{dx^2} + \frac{F}{E_f I_f} y = -\frac{P}{E_f I_f} x + \frac{F}{E_f I_f} y_{\ell f} + \frac{P}{E_f I_f}(\ell_f + \ell_m - \ell_o); \quad 0 \le x \le \ell_f - \ell_o$$

$$\frac{d^2y}{dx^2} + \frac{F}{E_f I_f} y = -\frac{P}{E_f I_f}\frac{\ell_m}{\ell_o} x + \frac{F}{E_f I_f} y_{\ell f} + \frac{P}{E_f I_f}\frac{\ell_m \ell_f}{\ell_o}; \qquad \ell_f - \ell_o \le x \le \ell_f \tag{185}$$

with boundary conditions

$$y(0) = 0, \quad \frac{dx}{dx}(0) = 0, \quad y(\ell_f) = y_{\ell f}, \quad y[(\ell_f - \ell_o)_-] = y[(\ell_f - \ell_o)_+]$$

$$\frac{dy}{dx}\left[(\ell_f - \ell_o)_-\right] = \frac{dy}{dx}\left[(\ell_f - \ell_o)_+\right]$$

The homogeneous equation over both intervals is

$$\frac{d^2y}{dx^2} + \frac{F}{E_f I_f} y = 0 \tag{186}$$

which has the solution

$$y = C_1 \sin \omega_f x + C_2 \cos \omega_f x \tag{187}$$

where

$$\omega_f = \sqrt{\frac{F}{E_f I_f}}$$

Over the interval $0 \leq x \leq \ell_f - \ell_o$, the particular solution to equation 105 is

$$y = -\frac{P}{F}x + y_{\ell f} + \frac{P}{F}(\ell_f + \ell_m - \ell_o) \tag{188}$$

and the equation of the elastic line on the interval is

$$y = C_1 \sin \omega_f x + C_2 \cos \omega_f x - \frac{P}{F}x + \frac{P}{F}(\ell_f + \ell_m - \ell_o) + y_{\ell f} \tag{189}$$

Application of boundary conditions $y(0) = 0$ and $\frac{dy}{dy}(0) = 0$ yields constants

$$C_1 = \frac{P}{\omega_f F}\ ;\ C_2 = -\left[\frac{P}{F}(\ell_m + \ell_f - \ell_o) + y_{\ell f}\right] \tag{190}$$

Over the interval $\ell_f - \ell_o \leq x \leq \ell_f$, the particular solution to equation 185 is

$$y = \frac{P}{F}\frac{\ell_m}{\ell_o}x + y_{\ell_f} + \frac{P}{F}\frac{\ell_m \ell_f}{\ell_o} \tag{191}$$

The equation of the elastic line over this interval is therefore

$$y = C_3 \sin \omega_f x + C_4 \cos \omega_f x - \frac{P}{F}\frac{\ell_m}{\ell_o}x + \frac{P}{F}\frac{\ell_m \ell_f}{\ell_o} + y_{\ell_f} \tag{192}$$

Application of boundary conditions $y\left[(\ell_f - \ell_o)_-\right] = y\left[(\ell_f + \ell_o)_+\right]$ and $\frac{dy}{dx}\left[(\ell_f - \ell_o)_-\right] = \frac{dy}{dx}\left[(\ell_f - \ell_o)_+\right]$ yields constants

$$\begin{aligned} C_3 &= \frac{P}{\omega_f F}\left[1 + \left(\frac{\ell_m}{\ell_o} - 1\right)\cos \omega_f (\ell_f - \ell_o)\right] \\ C_4 &= \frac{P}{\omega_f F}\left(1 - \frac{\ell_m}{\ell_o}\right)\sin \omega_f (\ell_f - \ell_o) - \frac{P}{F}(\ell_f + \ell_m - \ell_o) - y_{\ell_f} \end{aligned} \tag{193}$$

Finally application of boundary condition $y(\ell_f) = y_{\ell_f}$ yields

$$\begin{aligned} y_{\ell_f} = \frac{P}{F}\Big[&\frac{1}{\omega_f}\tan \omega \ell_f - \frac{1}{\omega_f}\left(1 - \frac{\ell_m}{\ell_o}\right)\Big(\cos \omega_f (\ell_f - \ell_o)\tan \omega_f \ell_f \\ &- \sin \omega_f (\ell_f - \ell_o)\Big) - (\ell_m + \ell_f - \ell_o)\Big] \end{aligned} \tag{194}$$

From equation 189,

$$y_{\ell_f - \ell_o} = \frac{P}{\omega_f F} \sin \omega_f(\ell_f - \ell_o) - \left(\frac{P}{F}(\ell_m + \ell_f - \ell_o) + y_{\ell_f}\right)\cos \omega_f(\ell_f - \ell_o) + \frac{P}{F}\ell_m + y_{\ell_f} \tag{195}$$

$y_{\ell_f - \ell_o} = \delta_1$ and $y_{\ell_f} = \delta_2$ are boundary conditions for the deflection equations of the movable link at $x = 0$ and $x = \ell_o$ respectively.

The moment at a point x on the movable link is given by

$$M_x = P(x - \ell_m) + P\frac{\ell_m}{\ell_o}(\ell_o - x) - F(y_{\ell_m} - y) \qquad 0 \leq x \leq \ell_o$$
$$M_x = P(x - \ell_m) - F(y_{\ell_m} - y) \qquad \ell_o \leq x \leq \ell_m \tag{196}$$

Therefore the differential equations for the deflected movable link are, by equation 184,

$$\frac{d^2y}{dx^2} + \frac{F}{E_m I_m} y = \frac{P}{E_m I_m}\left(\frac{\ell_m}{\ell_o} - 1\right)x + \frac{F}{E_m I_m} y_{\ell_m} \qquad 0 \leq x \leq \ell_o$$
$$\frac{d^2y}{dx^2} + \frac{F}{E_m I_m} y = \frac{P}{E_m I_m} x + \frac{P}{E_m I_m}\ell_m + \frac{F}{E_m I_m} y_{\ell_m} \qquad \ell_o \leq x \leq \ell_m \tag{197}$$

with boundary conditions

$$y(o) = \delta_1,\ y(\ell_o) = \delta_2,\ y(\ell_m) = y_{\ell_m},\ y(\ell_{o_+}) = (\ell_{o_-}),$$

$$\frac{dy}{dx}(\ell_{o_+}) = \frac{dy}{dx}(\ell_{o_-})$$

Equations 197 have homogeneous equations of the form of equation 186 over both intervals, for which a solution is

$$y = C_5 \sin \omega_m + C_6 \cos \omega_m x$$

$$\omega_m = \sqrt{\frac{F}{E_m I_m}}$$

Over the interval $0 \leq x \leq \ell_o$, the particular solution to equation 197 is

$$y = \frac{P}{F}\left(\frac{\ell_m}{\ell_o} - 1\right)x + y_{\ell_m} \tag{199}$$

and the equation of the elastic line on the interval is

$$y = \frac{P}{F}\left(\frac{\ell_m}{\ell_o} - 1\right)x + y_{\ell_m} + C_5 \sin \omega_m x + C_6 \cos \omega_m x \tag{200}$$

Boundary conditions $y(0) = \delta_1$, $y(\ell_o) = \delta_2$ require that

$$C_5 = \frac{\delta_2 - y_{\ell_m} - (\delta_1 - y_{\ell_m}) \cos \omega_m \ell_o - \frac{P}{F}(\ell_m - \ell_o)}{\sin \omega_m \ell_o} \tag{201}$$

$$C_6 = \delta_1 - y_{\ell_m}$$

Over the interval $\ell_o \leq x \leq \ell_m$, the particular solution is given by

$$y = -\frac{P}{F}x + y_{\ell_m} + \frac{P}{F}\ell_m \tag{202}$$

and the equation of the elastic line on this interval is

$$y = -\frac{P}{F}x + y_{\ell_m} + \frac{P}{F}\ell_m + C_7 \sin \omega_m x + C_8 \cos \omega_m x \tag{203}$$

Boundary conditions $y(\ell_{o_+}) = y(\ell_{o_-})$ and $\frac{dy}{dx}(\ell_{o_+}) = \frac{dy}{dx}(\ell_{o_-})$ require constants

$$C_7 = \left[\delta_2 - y_{\ell_m} + \frac{P}{F}(\ell_o - \ell_m)\right] \sin \omega_m \ell_o + \left[\frac{P}{F\omega_m} \frac{\ell_m}{\ell_o} - C_6 \sin \omega_m \ell_o \right.$$

$$\left. + C_5 \cos \omega_m \ell_o\right] \cos \omega_m \ell_o \tag{204}$$

$$C_8 = \frac{\delta_2 - y_{\ell_m} + \frac{P}{F}(\ell_o - \ell_m) - C_7 \sin \omega_m \ell_o}{\cos \omega_m \ell_o}$$

The final boundary condition, $y(\ell_m) = y_{\ell_m}$ results in the following equation for the deflection of the tip of the accumulator under axial load F and transverse load P:

$$y_{\ell_m} = \left[\frac{\sin \omega_m \ell_o \cos \omega_m \ell_m}{\sin \omega_m \ell_o \cos \omega_m \ell_m + (1 - \cos \omega_m \ell_o) \sin \omega_m (\ell_m - \ell_o)}\right]$$

$$\left[\delta_2 + \frac{P}{F}(\ell_o - \ell_m) + \left(\frac{\sin \omega_m (\ell_m - \ell_o)}{\cos \omega_m \ell_m}\right)\left(\frac{\delta_2}{\sin \omega_m \ell_o} - \delta_1 \cot \omega_m \ell_o\right.\right. \tag{205}$$

$$\left.\left. + \frac{P}{F\omega_m} \frac{\ell_m}{\ell_o} \cos \omega_m \ell_o + \frac{\frac{P}{F}(\ell_o - \ell_m)}{\sin \omega_m \ell_o}\right)\right]$$

Transverse Loading Only

If the axial force F is neglected, the moment at a point x in the fixed

link is given by

$$M_x = P\frac{\ell_m}{\ell_o}\left(x - \ell_f\right) - P\left(\frac{\ell_m}{\ell_o} - 1\right)\left(x - \ell_f + \ell_o\right) \qquad 0 \le x \le \ell_f - \ell_o$$

$$M_x = P\frac{\ell_m}{\ell_o}\left(x - \ell_f\right) \qquad \ell_f - \ell_o \le x \le \ell_f \qquad (206)$$

By equation 184 the neutral axis of the fixed link is described by

$$\frac{d^2y}{dx^2} = \frac{P}{E_f I_f}\left[(\ell_m + \ell_f - \ell_o) - X\right] \qquad 0 \le x \le \ell_f - \ell_o$$

$$\frac{d^2y}{dx^2} = \frac{P}{E_f I_f}\frac{\ell_m}{\ell_o}(\ell_f - x) \qquad \ell_f - \ell_o \le x \le \ell_f \qquad (207)$$

with boundary conditions

$$y(0) = 0,\ \frac{dy}{dx}(0) = 0,\ y[(\ell_f - \ell_o)_+] = y[(\ell_f - \ell_o)_-],$$

$$\frac{dy}{dx}[(\ell_f - \ell_o)_+] = \frac{dy}{dx}[(\ell_f - \ell_o)_-]$$

Equations 207 may be integrated twice, yielding the equation of the elastic line

$$y = \frac{P}{E_f I_f}\left[-\frac{x^3}{6} + (\ell_m + \ell_f - \ell_o)\frac{x^2}{2} + C_1 x + C_2\right] \qquad 0 \le x \le \ell_f - \ell_o$$

$$y = \frac{P}{E_f I_f}\frac{\ell_m}{\ell_o}\left(-\frac{x^3}{6} + \ell_f\frac{x^2}{2} + C_3 x + C_4\right) \qquad \ell_f - \ell_o \le x \le \ell_f \qquad (208)$$

Boundary conditions $y(0) = \frac{dy}{dx}(0) = 0$ require that $C_1 = C_2 = 0$ while the boundary

conditions on $y\left((\ell_f - \ell_o)_+\right)$ and $\frac{dy}{dx}\left((\ell_f - \ell_o)_+\right)$ require that

$$C_3 = \frac{a}{2}\left[\left(1 - \frac{\ell_o}{\ell_m}\right)a + 2\left(\frac{\ell_o}{\ell_m}b - \ell_f\right)\right]$$

$$C_4 = \frac{a^2}{6}\left[2\left(\frac{\ell_o}{\ell_m} - 1\right)a - 3\left(\frac{\ell_o}{\ell_m}b - \ell_f\right)\right] \qquad (209)$$

where $a = \ell_f - \ell_o$, $b = a + \ell_m$.

The deflections at $x = \ell_f - \ell_o$ and $x = \ell_f$, boundary conditions for the movable link, are

$$\delta_1 = y(\ell_f - \ell_o) = \frac{Pa^2}{6E_f I_f}(3b-a)$$

$$\delta_2 = y(\ell_f) = \frac{P}{E_f I_f}\frac{\ell_m}{\ell_o}\left(\frac{\ell_f^3}{3} + C_3\ell_f + C_4\right) \qquad (210)$$

The moment at a point x in movable link is

$$M_x = P(x - \ell_m) + P\frac{\ell_m}{\ell_o}(\ell_o - x) \qquad 0 \le x \le \ell_o$$

$$M_x = P(x - \ell_m) \qquad \ell_o \le x \le \ell_m \qquad (211)$$

and by equation 184, the neutral axis of the movable link is described by

$$\frac{d^2y}{dx^2} = \frac{P}{E_m I_m}\left(\frac{\ell_m}{\ell_o} - 1\right)x \qquad 0 \le x \le \ell_o \qquad (212)$$

$$\frac{d^2y}{dx^2} = \frac{P}{E_m I_m}(\ell_m - x) \qquad \ell_o \leq x \leq \ell_m$$

with boundary conditions

$$y(0) = \delta_1,\ y(\ell_o) = \delta_2,\ y(\ell_{o+}) = y(\ell_{o-}),\ \frac{dy}{dx}(\ell_{o+}) = \frac{dy}{dx}(\ell_{o-})$$

Integrating twice with respect to x yields the equation of the neutral axis of the movable link.

$$y = \frac{P}{E_m I_m}\left(\frac{\ell_m - \ell_o}{\ell_o}\right)\left(\frac{x^3}{6} + C_5 x + C_6\right) \qquad 0 \leq x \leq \ell_o$$

$$y = \frac{P}{E_m I_m}\left(-\frac{x^3}{6} + \ell_m \frac{x^2}{2} + C_7 x + C_8\right) \qquad \ell_o \leq x \leq \ell_o \tag{213}$$

Boundary conditions $y(0) = \delta_1$, $y(\ell_o) = \delta_2$ yield constants

$$C_5 = \frac{E_m I_m(\delta_2 - \delta_1)}{P(\ell_m - \ell_o)} - \frac{\ell_o^2}{6}$$

$$C_6 = \frac{E_m I_m \ell_o \delta_1}{P(\ell_m - \ell_o)} \tag{214}$$

The boundary conditions at $x = \ell_o$ require

$$C_7 = \left(\frac{\ell_m - \ell_o}{\ell_o}\right)C_5 - \frac{\ell_m \ell_o}{2}$$

$$C_8 = \left(\frac{\ell_m - \ell_0}{\ell_o}\right)C_6 + \frac{\ell_m \ell_o^2}{6} \tag{215}$$

The deflection of the tip of the accumulator under transverse load P and neglecting the effects of axial force F is given by

$$y_{\ell_m} = \delta_1 + \frac{\ell_m}{\ell_o}(\delta_2 - \delta_1) + \frac{P\ell_m}{3E_m I_m}(\ell_m - \ell_o)^2 \qquad (216)$$

Error in y_{ℓ_m} When Axial Force is Neglected

The error which results when the axial force F is neglected in computing y_{ℓ_m} (equation 216) rather than including its effect (equation 205), is greatest for long flexible beams subject to large transverse and axial loads. The exact relationship is rather complex as may be seen by examination of equation 205 in which ω_m, δ_1 and δ_2 are functions of F. Rather than investigate this relationship in a general way it will suffice, for the purposes of achieving a reasonable dynamic model of the accumulator, to determine if the simplifying assumption is valid for the class of beams of interest in this application.

Consider an alternative configuration for the prismatic pair in which the members have the properties described in Table 20.

Table 20. Properties of a Potential Prismatic Pair

Link	Dimension	Wall	Moment of Inertia	E (psi)	Wt/Ft	Length
Fixed	4 in.	.250 in.	8.828 $in.^4$	10×10^6	4.5 #	7.5 ft.
Movable	3 in.	.375 in.	4.614 $in.^4$	10×10^6	4.725#	7.5 ft.

Total length 12 ft
Overlap length 3 ft.
Total Structure weight 69.19 pounds

If the payload is 50 pounds the total overhung weight is 119.19 pounds and a 2 g load is therefore 238.38 pounds. Suppose the link is accelerating in such a way that the transverse load P and axial load F are equal and have a vector sum of 238.38 pounds, then P = F = 168.56 pounds. The deflection y_{ℓ_m} computed by equation 216 (neglecting the axial force) is 1.942 inches while by equation 205 (including the axial force) it is 1.960 inches, a difference of less than one percent.

Transverse Stiffness

As shown in the preceding section, the transverse stiffness of the contracted R-R-P accumulator may be considered independent of the axially applied loads likely to be experienced in use; therefore, equation 216 is adequate to describe the tip deflection y_{ℓ_m}. To restate equation 216 in terms of applied load P and mechanical properties of the accumulator only, δ_1 and δ_2 must be eliminated by use of equations 209 and 210 with the result

$$y_{\ell_m} = \frac{P}{3}\left\{\frac{\ell_m}{E_m I_m}(\ell_m - \ell_o)^2 + \frac{1}{E_f I_f \ell_o^2}\left[\ell_m^2 \ell_f^3 + (\ell_f - \ell_o)^2 \left(\ell_o^2(\ell_f + \ell_m) - \ell_m^2(\ell_f + \ell_o) - \ell_o(\ell_o - \ell_m)^2\right)\right]\right\} \tag{217}$$

The transverse stiffness K is defined by

$$K = \frac{P}{y_{\ell_m}}$$

from which

$$K = \frac{3E_m E_f I_m I_f \ell_o^2}{\left\{E_f I_f \ell_m \ell_o^2 (\ell_m - \ell_o)^2 + E_m I_m \left[\ell_m^2 \ell_f^3 + (\ell_f - \ell_o)^2 \left(\ell_o^2(\ell_f + \ell_m) - \ell_m^2(\ell_f + \ell_o) - \ell_o(\ell_o - \ell_m)^2\right)\right]\right\}} \tag{218}$$

expresses the transverse stiffness of the contracted R-R-P accumulator in terms of its dimensions and material properties.

REFERENCES

1. R. D. Vaughn, Foreward to Public Health Service Publication Number 1892, A Study of Solid Waste Collection Systems Comparing One-Man With Multi-Man Crews, Bureau of Solid Waste Management, Washington, D. C., 1969

2. F. Flintoff and R. Millard, Public Cleansing, MacLaren and Sons, London, England, 1969

3. R. Hering and S. Greeley, Collection and Disposal of Municipal Refuse, McGraw-Hill, New York, New York, 1921

4. American Public Works Association Committee on Solid Wastes, Refuse Collection Practice, APWA Public Administration Service, Chicago, Illinois, 1966

5. Bureau of Labor Statistics, Injury Rates by Industry, 1969, United States Department of Labor, Washington, D. C., 1970

6. C. Goulke, Comprehensive Studies of Solid Wastes Management Abstracts and Excerpts from the Literature, University of California Press, Berkeley, California, 1968

7. D. Marks and J. Liebman, Mathematical Analysis of Solid Wastes Collection, Bureau of Solid Waste Management, Washington, D. C., 1970

8. R. Stone, A Study of Solid Waste Collection Systems Comparing One-Man With Multi-Man Crews, Bureau of Solid Waste Management, Washington, D. C., 1969

9. United States Public Health Service, Solid Waste Demonstration Grant Abstracts, United States Department of Health, Education, and Welfare, Washington, D. C., Annually since 1966

10. Anon., "Grab Bag Texas Style," The Orange Disc, Gulf Oil Company, Pittsburg, Pennsylvania, July-August 1971

11. United States Public Health Service, Solid Waste/Disease Relationships, United States Department of Health, Education, and Welfare, Washington, D. C., 1967

12. D. Ecke and D. Linsdale, "Fly and Economic Evaluation of Urban Refuse Systems. Part I: Control of Green Bow Flies (Phaenicia) by Improved Methods of Residential Refuse Storage and Collection," California Vector Views, April 1967

13. F. Reuleaux, Theoretische Kinematik: Grundzuge einer Theorie des Maschinenwesens, Trans. A. Kennedy, Dover Publications, New York, New York, 1963.

14. W. Corliss and E. Johnsen, Teleoperator Controls An AEC-NASA Technology Survey, NASA Office of Technology Utilization, Washington, D. C., 1968

15. E. Johnsen and W. Corliss, Teleoperators and Human Augmentation An AEC-NASA Technology Survey, NASA Office of Technology Utilization, Washington, D. C., 1967

16. J. Darlington, "Evaluation and Application Study of the General Motors Corporation Rapid Travel Profilometer," Research Report No. R-731, Michigan State Highway Commission, Lansing, Michigan, 1970

17. L. Holbrook, "Prediction of Subjective Response to Road Roughness Using the General Motors--Michigan Department of State Highways Rapid Travel Profilometer," Research Report No. R-719, State of Michigan Department of State Highways, Lansing, Michigan, 1970

18. Private Communication, L. T. Oehler, Engineer of Research, Research Laboratory Section, State of Michigan Department of State Highways, Lansing, Michigan, April 19, 1972

19. A. Papoulis, Probability, Random Variables, and Stochastic Processes, McGraw-Hill Book Company, New York, New York, 1965

20. A. Whittemore et al, "Dynamic Pavement Loads of Heavy Highway Vehicles," National Cooperative Highway Research Program, Report 105, 1970

21. R. Sharp and J. Goodall, "A Mathematical Model for the Simulation of Vehicle Motions," Journal of Engineering Mathematics, Vol. 3, No. 3, July 1969

22. W. Bergman, E. Fox and E. Saibel, "Dynamics of an Automobile in a Cornering Maneuver On and Off the Highway," Mechanics of Soil-Vehicle Systems, Proceedings of the First International Conference on the Mechanics of Soil-Vehicle Systems, Turin and St. Vincent, Italy, 1961

23. T. Maeda and H. Vemura, "On Development of Vehicle Dynamics by Means of a Digital Computer," SAE International Automotive Engineering Congress, Detroit, Michigan,1969

24. R. McHenry, N. DeLeys and J. Eicher, "An Analytical Aid for Evaluating Highway and Roadside Geometrics," Presented for Highway Research Board Committee A3E02 Operational Effects of Geometrics, Washington, D. C., January 19, 1971

25. J. Siddall and P. Southwell, eds., Proceedings of the First International Conference on the Mechanics of Soil-Vehicle Systems, Turin and St. Vincent, Italy, 1961

26. I. Shames, Engineering Mechanics Volume II, Dynamics, Prentice-Hall, Inc., Englewood Cliffs, New Jersey, 1966, p. 571

27. P. Gray, "Application of a Modified Fast Fourier Transform to Calculate Human Operator Describing Functions," IEEE Transactions on Man-Machine Systems, Volumes 10, No. 4, December 1969

28. H. Stassen, "The Polarity Coincidence Correlation Technique--A Useful Tool in the Analysis of Human-Operator Dynamics," IEEE Transactions on Man-Machine Systems, Vol. MMS-10, No. 1, March 1969

29. A. Kuttan and G. Robinson, "Models of Temporal Motor Responses--Stimulus, Movement, and Manipulation Information," IEEE Transactions on Man-Machine Systems, Vol. MMS-11, No. 2, June 1970

30. E. Poulton, "Bias in Experimental Comparisons between Equipments Due to the Order of Testing," IEEE Transactions on Man-Machine Systems, Vol. MMS-10, No. 4, December 1969

31. A. Tustin, "The Nature of the Human Operator's Response in Manual Control and the Implication for Controller Design," Journal of the Institution of Electrical Engineers, Vol. 94, No. 190, 1947

32. B. Gaines, "Linear and Nonlinear Models of the Human Controller," International Journal of Man-Machine Studies (1969), No. 1

33. D. McRuer and D. Weir, "Theory of Manual Vehicular Control," IEEE Transactions on Man-Machine Systems, Vol. MMS-10, No. 4, December 1969

34. E. Heer, ed., Remotely Manned Systems, Exploration and Operation in Space, Proceedings of the First National Conference, California Institute of Technology, 1973

35. S. Baron and D. Kleinman, "The Human as an Optimal Controller and Information Processor," IEEE Transactions on Man-Machine Systems, Vol. MMS-10, No. 1, March 1969

36. J. Elkind et al, An Optimal Control Method for Predicting Control Characteristics and Display Requirements of Manned-Vehicle Systems, Technical Report AFFDL-67-187, Air Force Flight Dynamics Laboratory, Wright-Patterson Air Force Base, Ohio, 1968

37. S. Baron and D. Kleinman, The Human as an Optimal Controller and Information Processor, NASA Contractor Report CR-1151, NASA, Washington, D. C., 1969

38. J. Senders et al, An Investigation of the Visual Sampling Behavior of Human Observers, NASA Contractor Report CR-434, NASA, Langley Research Center, Virginia, 1966

39. Y. Takahashi, M. Robins and D. Auslander, Control and Dynamic Systems, Addison-Wesley Publishing Co., Reading, Massachusetts, 1970

40. B. Anderson and J. Moore, Linear Optimal Control, Prentice-Hall, Inc., Englewood Cliffs, New Jersey, 1971

41. R. Howerton, "Computational Procedures for the Synthesis of Linear Stationary Control Systems," Unpublished Ph.D. Thesis, Georgia Institute of Technology, 1970

42. M. Stragier, Mechanized Residential Refuse Collection, Department of Public Works, Scottsdale, Arizona, 1970

43. J. Aulakh and H. Myrick, An Economic Analysis of the One-Man-Crew Mechanical Bag Retriever Truck and the Three-Man-Crew Conventional Rear Load Truck Using Take-Away Plastic Bags in the Collection of Solid Waste, University of Houston, Houston, Texas, 1971

44. Private communication from M. G. Stragier, Director of Public Works, Scottsdale, Arizona, August 9, 1971

45. Anon., Gar Wood Sales Form W-328, Gar Wood Industries, Wayne, Michigan

46. Anon., St. Regis Environmental Systems Division, Sales Form K5410M S/F, St. Regis Company, New York, New York

47. Anon., E-Z Pack Data Form No. E-Z163A-12/70-5M, E-Z Pack Company, Galion, Ohio

48. Anon., 1970 Dodge Body Builder's Book, Dodge Truck Division, Crysler Motor Corporation, Detroit, Michigan, 1969

49. Private Conversation, Mr. R. Ajac, Rockwell Standard Company, Detroit, Michigan, March 18, 1974

50. Anon., GMC Trucks 1971 Body Builder's Drawings and Supporting Data, GMC Truck & Coach Division, General Motors Corporation, Detroit, Michigan, 1970

51. Davisson, J.A., "Design and Application of Commercial Type Tires," The Fifteenth L. Ray Buchendale Lecture, Society of Automotive Engineers Special Publication SP-344, SAE, New York, New York, 1969

52. A. Higdon and W. Stiles, Engineering Mechanics, Vector Edition, Statics and Dynamics, Prentice-Hall, Englewood Cliffs, New Jersey, 1962

53. Anon., Industrial Metals, Reynolds Aluminum Supply Co., Park Ridge, Illinois, 1968

54. Anon., Tubesales Stock List No. 172, Tubesales, Inc., Los Angeles, California, 1972

55. Anon., AISC Manual of Steel Construction, American Institute of Steel Construction, New York, New York, 1967

56. Siegel et al, Mechanical Design of Machines, International Textbook Co., Saraston, Pennsylvania, 1965

57. S. Timoshenko and D. Young, Elements of Strength of Materials, P. Van Nostrand Co., Princeton, New Jersey, 1966

58. N. Polakowski and E. Ripling, Strength and Structure of Engineering Materials, Prentice-Hall, Englewood Cliffs, New Jersey, 1966

59. Anon., Bima Small Bore Air Cylinders, Catalog 1266-B, Bima Manufacturing Company, Monee, Illinois, 1966

VITA

William Edward Pugh, III, the son of Mrs. Lina Doering Pugh and the late William E. Pugh, Jr., was born and raised in Jacksonville, Florida, where he attended the public schools. He entered Georgia Tech as a freshman in 1964. In 1967 Mr. Pugh married the former Julie Lynn Vollers, also of Jacksonville. The same year he was employed by the Georgia Tech Engineering Experiment Station where he worked on a wide variety of projects throughout his undergraduate and graduate study. Upon graduation in 1968 with a Bachelor's Degree in Civil Engineering, Mr. Pugh was commissioned a Second Lieutenant in the U. S. Army Reserve. He entered graduate school in mechanical engineering at Georgia Tech in 1968 and earned his Masters Degree in 1971. In 1973 Mr. Pugh was called to active duty in the Ordnance Corps where he served as a First Lieutenant at Aberdeen Proving Ground, Maryland. Mr. Pugh joined the technical staff of Bell Telephone Laboratories in 1974 where he is currently employed. He is a member of ASME, Sigma Xi, Sigma Chi, GSPE and NSPE and was the recipient of a NASA Design Traineeship.